博士論文

Thermophysical Property of Molten Borate Systems and their Structural Factors

(ホウ酸塩系融体の熱物性とその構造的因子)

金　永宰

TABLE OF CONTENTS

Chapter I

Introduction

1.1. Borate System in the Steelmaking and Glassmaking

More than half of world production of boron minerals is used for glass and ceramic products.[1] Owing to the covalent bonding characteristic of B-O bond, B_2O_3 is famous for the strong glass forming tendency, and it is crystallized only under pressure.[2] For this reason, during the glass making, B_2O_3 has been widely adopted as glass formers along with SiO_2. In addition, during the continuous casting process in steelmaking, B_2O_3 consists of a large portion of mold flux system playing a glass former along with SiO_2, Al_2O_3 and Fe_2O_3.[3] B_2O_3 is an excellent Lewis acid, and thus molten boron oxide can dissolve most kind of metal oxide above approximately 1273 K.[4] Due to such characteristic of B_2O_3, boron oxide has been widely adopted in many metallurgical processes as a flux.[4] For instance, during the precious metal recovery process, B_2O_3 is supplied into a furnace along with impure metal and forms slag with metal oxide contaminant.[4] In this section, the industrial use of B_2O_3 in the steelmaking and glassmaking field will be briefly reviewed.

1.1.1. Borate System in the Steelmaking Process

1.1.1.1. Continuous Casting Process and Mold Flux

At the end of steelmaking process, the liquid steel in ladle transferred from tundish into water-cooled mold through a submerged entry nozzle (SEN). Below the mold, the liquid steel is cooled down by spraying water and solidified. Finally, the strand of solidified steel is transferred into a rolling mill. The series of process[5] is called a continuous casting process; linking the steelmaking with rolling process. Although continuous casting method was firstly proposed in 1856 by Sir Henry Bessemer, ingot casting process had been used as common process until 1960s.[6] However, with the breakthrough of continuous casting process, the amount of steel produced by continuous casting process has been exceeded that of conventional ingot casting process since middle of 1980s.[5] In present, 99.9 % of carbon steel and 96.4 % of specialty steel are produced by continuous casting process in Japan.[7] Figure 1-1 (a) shows the schematic diagram of continuous casting process.[8]

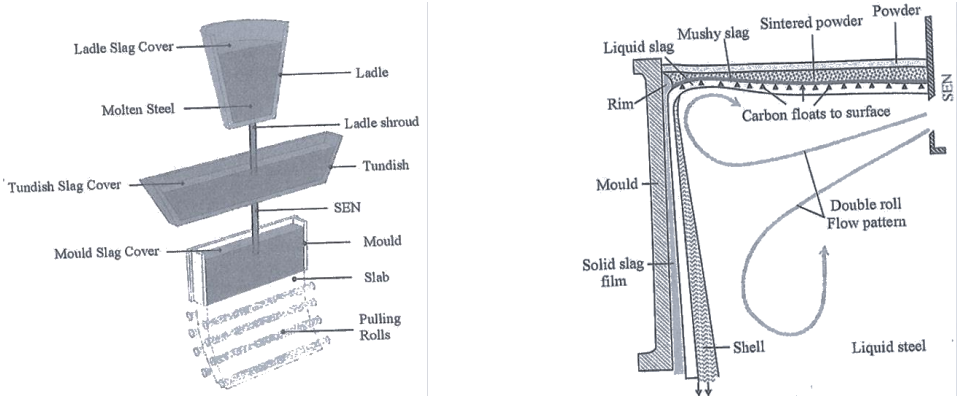

(a) **(b)**

Fig. 1-1. Schematic diagram of **(a)** the continuous casting process **(b)** the various phases of mold flux.[8]

During the continuous casting process, mold flux, which is the synthetic oxides powder, is fed through the top of the mold. As shown in Fig. 1-1(b),[8] the mold flux exists between mold and molten steel and plays important roles during the continuous casting process;[3, 9]

1) Thermal insulation
2) Prevention of oxidation of steel
3) Inclusion entrapment
4) Lubrication
5) Heat transfer control

The mold flux with inappropriate thermo-physical properties results in the various defects on the final products. For example, "longitudinal cracking" and "star cracking" are attributed to the irregular horizontal heat transfer.[3, 9] In addition, lack of lubrication results in the "sticker breakage" and "SEN erosion".[3, 9] Since it affects both operational conditions and quality of final product, control and optimization of mold flux is important.[5, 8] In order to control the thermo-physical property of mold flux, various oxides are considered as additives. The typical compositions of mold flux system and its role are listed in Table 1-1.

Table 1-1. The typical compositions of the mold flux system.[3, 10]

Role	Oxide	Composition
Network former	SiO_2	14 – 56 wt%
	Al_2O_3	0 – 13 wt%
Network breaker	CaO	22 – 45 wt%
	MgO	0 – 10 wt%
Fluxes	B_2O_3	0 – 19 wt%
	Li_2O	0 – 5 wt%
	Na_2O	0 – 25 wt%
	K_2O	0 – 2 wt%
	CaF_2	2 – 15 wt%
	FeO	0 – 6 wt%
	MnO	0 – 5 wt%
Other	Carbon	2 – 20 wt%

1.1.1.2. B_2O_3 in the mold flux system

Recently, the demand for materials with high-strength and low weight has been increased in the automobile industry owing to the strict regulation for greenhouse gas emission. TRIP (transformation-induced plasticity) and TWIP (twinning-induced plasticity) steels have been paid attention as a promising candidate for the next-generation automobile steel due to its high tensile strength along with better formability.[11, 12] However, the contained Si results in the formation of Mn_2SiO_4 oxide film on the surface of TRIP steel and it lowers galvanizability. For this reason, several studies has been carried out in order to develop the Si-free TRIP steel. Mahieu et al.[12] reported that Al can be the one of the substitution for Si. Recently, Jin and Lee[11] observed that addition of Al enhances the physical properties of TWIP steel by increasing of yield strength. As a result, TWIP and TRIP steels contain more than 1 wt% of Al. Compared to conventional Al-killed steel, the Al contained TWIP and TRIP steel results in the unexpected reaction during the continuous casting process; SiO_2 contained in mold flux is likely to react with dissolved Al in the molten steel by following equation.[13, 14]

$$4[Al] + 3SiO_2 = 2Al_2O_3 + 3[Si] \quad (1\text{-}1)$$

As a result, the concentration of SiO_2 in the mold flux gradually decreases and Al_2O_3 increases by the reaction shown in equation (1-1). In the real process, after 10 min of continuous casting of high Al TRIP steel, the concentration of Al_2O_3 in mold flux becomes

10 times of initial composition.[14] For this reason, less reactive mold flux system, which contains less SiO_2, has been paid attention. Many researchers pointed out that lime-alumina based system would be the promising candidate for the mold flux system for TWIP and TRIP steel. However, the substitution of Al_2O_3 for SiO_2 in the mold flux system results in the change of the lubrication ability and heat transfer. Especially, drastic increasing of viscosity was observed in the lime-alumina based system.[13] Although B_2O_3 is known as a typical glass forming oxide, the addition of B_2O_3 results in the decreasing of break temperature and melting temperature along with lowering viscosity.[9, 13, 15–18] Huang et al.[15] reported that the addition of B_2O_3 is necessary for stabilization of the lime-alumina based mold flux system.

On the other hands, the environmental regulation upon steelmaking field have increased for last decade due to the carbon and toxic emission.[16] Especially, fluorine emissions has been pointed out as the major environmental concern during the continuous casting process. As shown in Table 1-1, CaF_2 is one of the major component in the commercial mold flux system. During the continuous casting process, CaF_2 in mold flux decreases liquidus temperature and viscosity. In addition, CaF_2 promotes the formation of crystalline cuspidine ($Ca_4Si_2O_7F_2$) phase resulting in the drastic decreasing of heat transfer.[19, 20] However, during the process, CaF_2 in the mold flux system reacts with SiO_2 or H_2O and forms SiF_4 and HF compounds by following reaction.

$$2CaF_2 + SiO_2 = SiF_4 + 2CaO \quad (1\text{-}2)$$

$$CaF_2 + H_2O = HF + CaO \quad (1\text{-}3)$$

The fluoride reactants are easily dissolved into secondary cooling water leading to the environmental pollution.[21] In addition, emission of fluoride gases causes hazardous effect on human health.[16] For this reason, recently, development for fluorine-free mold flux has been paid attention. Na_2O, Li_2O, and B_2O_3 has been suggested as the candidates for CaF_2 substitution in the mold flux system.[16, 19, 21] Especially, Na_2O and B_2O_3 cause the lowering viscosity, breaking temperature and liquidus temperature which is the similar effect of CaF_2.[9, 17] Based on the Na_2O and B_2O_3 system, Fox et al.[16] designed the new fluoride-free mold flux system. Their fluorine-free mold flux system was successfully adopted in the real process implying the possibility of removing CaF_2 in the mold flux system. In addition, Choi et al.[22], who studied viscosity, thermal conductivity and crystallization behavior in the fluorine free mold flux system of the $CaO\text{-}SiO_2\text{-}Al_2O_3\text{-}Na_2O\text{-}B_2O_3$ system, observed that the CaB_2SiO_7 and $CaAl_4B_2[SiO_4]_8$ phases can be easily crystallized at high temperature. Similar to cuspidine phase in the CaF_2 based mold flux system, their result suggests that the heat transfer can be controlled by crystalline phase in the B_2O_3 based fluorine-free mold flux system.

However, using a large amount of B_2O_3 in the mold flux system would lead to boron pick-up by a redox reaction with SiO_2 or Al_2O_3.[13, 19, 23] In addition, higher concentration of B_2O_3 would result in the SEN erosion.[13] Recently, Sakamoto[23], who measured activity coefficient of B_2O_3 in the $CaO\text{-}SiO_2\text{-}B_2O_3$ system, calculated the boron pick-up concentration during the continuous casting process. According to his thermodynamic calculation, approximately 50, 150 and 220 ppm of boron dissolves into aluminum-killed steel when the mold flux contains 5, 10 and 15 mol% of $BO_{1.5}$, respectively. In the steel, low concentration of boron plays a role of carbide stabilizer. However, large amount of boron in steel would result in reducing elongation and tensile strength.[24] Therefore, boron concentration in steel should be controlled no more than 50 ppm. Although, B_2O_3 is the promising candidate for new environment-friendly mold flux system for high Al containing TRIP and TWIP steel, B_2O_3 concentration in the mold flux system should be optimized below certain amount in order to prevent boron pick-up.

1.1.2. Borate System in the Glass and Ceramics

The glass and ceramic fields are the largest sector consuming B_2O_3. Approximately 50 % and 70 % of B_2O_3 in Western Europe and Japan, respectively, were used in glass-related products.[25] It has been known that addition of B_2O_3 in glass system results in decreasing thermal expansion, crystallization tendency or increasing thermal conductivity, thermal shock resistance, mechanical strength, chemical durability and optical properties.[26] Due to the characteristic properties of B_2O_3 along with relatively low price, B_2O_3 has been widely adopted for the glass and ceramics products; such as fiberglass, glassware, sealing glass for Solid oxide fuel cells(SOFCs), optical glass, capacitor ceramics, filter glass, flat panel display, and nuclear waste storage glass.[4, 25, 27–34]

1.1.2.1. Boron oxide in fiber glass

Due to its low coefficient of heat transmission, fiber glass has widely used as insulator in residential and commercial instruction.[4, 35] The insulation fiber glass is the intermingled fibers withdrawn from the molten glass melt, which is soda lime borosilicate glass. In general, fiber glass contains approximately 4 – 7 % of B_2O_3,[4] and B_2O_3 plays various important roles such as improving product durability and lowering melting temperature along with preventing glass from devitrification. In addition, B_2O_3 provides resiliency to fiber glass.

Another usage of fiber glass is textile fiberglass. Textile fiber glass is continuously strand fiber glass.[4] Electronic circuit board or reinforcement for plastic and construction products are made of the textile fiber glass. In the case of electronic circuit board, a lime alumina silicate glass is used due to the good tensile strength with durability along with low electrical conductivity property. In this lime alumina silicate based textile fiberglass, B_2O_3 is added approximately 8 – 9 %[25] in order to reduce the melting and fiberizing temperature along with lowering viscosity.

1.1.2.2. Boron oxide in glassware

50 million ton of glass over approximately 115 million ton of world production is used as container glass in 2001.[35] Especially, borosilicate glass; which contains approximately 12 – 15% of B_2O_3,[25] accounts for approximately 10 % of total container glass production.[26] Compared to 8 – 9 ppm/K of thermal expansion coefficient of typical soda lime silicate glass, borosilicate glass has 3 ppm/K of thermal expansion coefficient.[35] Due to the relatively lower thermal expansion coefficient, borosilicate glass shows high resistance of thermal shock and

thus, it is suitable for the severe condition where rapid heating and cooling are occurred. In addition, borosilicate glass has high chemical resistance, aqueous durability, and physical strength.[4] For this reason, borosilicate glass is widely used for cookware or laboratory glassware.

1.1.2.3. Boron oxide in sealing glass for Solid Oxide Fuel Cells(SOFCs)

Solid Oxide Fuel Cells (SOFCs) is the electrochemical device converting chemical energy into electric power.[33] At the cathode, oxygen molecule from air is ionized and then oxygen ion is transferred into anode part. According to Nernst equation, voltage is generated due to the difference of oxygen partial pressure between cathode and anode. Compared to tubular type of SOFCs, planar SOFCs has high specific power output, volumetric power density along with low electrical resistance and manufacturing cost.[33] However, planar SOFCs requires high-temperature sealant placing between each cells and the fuel cells stack.[34, 36] Due to its severe operational conditions, the sealant requires specific physical and chemical properties. In order to prevent leakage of oxygen and fuel gas, the seal should tightly adhere to the cell component. In addition, it should be stable for long enough time (approximately more than 1000 h)[34] without degradation. Glass can form strong chemical bond with metal[32] and it is chemically stable when it contacts with fuel cell component. For this reason, glass material has been widely adopted as sealant materials for SOFCs.

When we select the appropriate glass materials for SOFCs, two factor should be considered; one is glass transition temperature, and another one is thermal expansion coefficient.[34] Glass material should have both appropriate fluidity and rigidity in order to seal adequately along with mechanical integrity.[34] The glass transition temperature is the one of the good criteria for the expectation of the fluid characteristic of glass material. On the other hand, thermal expansion coefficient of cell components (electrolyte, interconnect materials and sealant) should be similar to each other in order to avoid the mechanical stress occurred during thermal cycling.[34, 37] Borate glass is the one of the candidates satisfying the above mentioned two criteria of seal material for SOFCs. It has been known that B_2O_3 decreases viscosity along with softening temperature.[33] Also, the addition of boron oxide results in increasing thermal expansion coefficient and stabilizes amorphous structure. For this reason, barium boroaluminosilicates glass has been paid attention for sealing material of SOFCs.[34]

However, despite of the various advantage of B_2O_3, the usage of borate based glass has limitation due to its low melting temperature and phase separation resulting from the different configurational entropy between silicate and borate units. For this reason, borate based SOFCs sealant is suitable only SOFCs operated at low temperature.[33]

1.1.2.4. Boron oxide in nuclear waste immobilization

During the treatment of irradiated nuclear fuel element for the energy, the highly radioactive nuclear waste is formed. In order to storage and isolate the high level nuclear waste, material for nuclear waste immobilization is needed. The material for nuclear waste immobilization requires several properties; durability over thousands years, low melting temperature and low viscosity.[30]

Borate glass satisfies all criteria mentioned above. Borosilicate glass has high chemical and physical durability. Compared to silicate glass, borosilicate glass has low melting temperature so that even volatile radionuclides; such as cesium (Cs) and ruthenium (Ru), are not vaporized during the process. In addition, due to the low viscosity, it can be easily poured into disposal container accommodating all of nuclear wastes. For these reasons, many countries including United States, France, United Kingdom, Germany, Japan and South Korea use borosilicate glass for the high level nuclear waste storage.[26]

1.1.2.5. Boron oxide in display glass

Recently, the glass for the display device and mobile device has been paid attention as a result of breakthrough of display technology. In 2000, the growth rate of display glass market already exceeded 20 %.[27] Since the displays are getting lighter, thinner and bigger,[32] the required properties for display glass become challenging. In order to prevent the interaction between glass and semiconducting layer, addition of alkali oxide into display glass is prohibited.[26] In the case of the glass for mobile display, it requires great resistance to physical scratching and chemical contamination.[32] In addition, low thermal expansion coefficient is required in order to make thin and flat sheets. For this reason, alkali-free aluminoborosilicate glass was developed in order to fulfill the above mentioned requirement.[26, 31] In the alumino-borosilicate glass, B_2O_3; which is contained approximately 10 wt%, controls viscosity and melting temperature along with lowering thermal expansion coefficient.[4, 26]

1.2. Relationship Between Borate Structure and its Physical Properties

1.2.1. Structure of B_2O_3 and Borate System

Boron has three electrons in the outermost orbit shell and it forms three covalent bonds with oxygen leading to the boron oxide structure consists of BO_3 unit.[38] In pure B_2O_3 glass and melt, approximately 75 – 80% of boron atoms belong to the boroxol ring structure consisting of three BO_3 units in hexagonal arrangement of six B-O bond and it implies the presence of intermediate range order structure.[2, 39, 40] Boron in planar BO_3 triangle structure has 6 electron in the valence shell along with vacant p_z orbital having electron deficient.[38] As a result, it easily accepts a donor bond from oxide ion and forms covalent bond resulting in BO_4 tetrahedral structure unit. The structural change from 3-coordinated boron into 4-coordinated boron has been observed in the various B_2O_3 bearing systems; such as alkali-borate or alkali borosilicate systems. Bray and his coworkers,[41, 42] who investigated the borate structure in the binary alkali borate system (R_2O-B_2O_3 where R = Li, Na, K, Rb and Cs) using NMR, reported that the conversion proceeds until half of BO_3 units changes into BO_4 units. However, above certain amount of alkali oxide concentration; where R ratio (R_2O/B_2O_3) exceeds approximately 0.5, the BO_4 concentration decreases along with formation of BO_3 units incorporating non-bridging oxygen (NBO).

$$BO_4 \leftrightarrow BO_3 + NBO \qquad (1\text{-}4)$$

The concentration of alkali oxide affects the equilibrium of equation (1-4); an addition of alkali oxide leads to a shift in the equilibrium to the right. Recently, using high temperature Raman spectroscopy, Yano et al.[43], confirmed the temperature dependence of the relative fraction of 4-coordinated boron in the Na_2O-B_2O_3 system, which is an increase in the 4-cooridinated boron with lower temperature.

The series of structure change of B_2O_3 units is also observed in the sodium borosilicate system (Na_2O-B_2O_3-SiO_2) and the coordination change of boron can be well estimated by "Dell and Bray model".[44] According to Dell and Bray model, at the fixed K ratio; which is the fraction of SiO_2/B_2O_3, the increase in Na_2O/B_2O_3 ratio (denoted as R ratio) results in the structural change from 3- to 4- and then 4- to 3-coordinated boron attached with NBO. Below R ratio of 0.5, oxygen ion from Na_2O primary incorporates with boron ion forming 4-coordinated boron. At R = 0.5, both two 3-coordinated boron and two 4-coordinated boron is arranged in the diborate unit. Further addition of Na_2O results in the formation of

reedmergnerite groups; oxygen linked to tetrahedral boron associates with tetrahedral silicon. The reedmergnerite unit continuously forms until all the SiO_2 is used up; where is R = 1/2+K/16. Above the R ratio, all the additional oxygen provided by Na_2O form with NBO on the silicate network. However, when R ratio exceeds R = 1/2+K/4, additional Na_2O begins to combine with both diborate unit and reedmergnerite unit. The fraction (2–K/4)/(2+K) of the additional Na_2O associates with diborate unit forming pyroborate unit; boron with two NBO, and the fraction (K+K/4)/(2+K) of the additional Na_2O incorporated with reedmergnerite unit forming both pyroborate unit and silicate tetrahedral units with two NBO. Finally, when all the diborate and reedmergnerite units are exhausted, all the remained boron exists as 3-coordinated boron associated with NBO; which is also known as asymmetry boron. The overall structural change reported in Dell and Bray model is summarized in the Table 1-2. In the Na_2O-B_2O_3-SiO_2 system, recent works using ^{17}O triple quantum (3Q) NMR[45] and molecular dynamic (MD) calculation[46] revealed that the oxide from Na_2O is well mixed with both borate and silicate structure and does not have any bonding preference assumed in Dell and Bray model. However, Dell and Bray model still provides the useful structural information in the alkali borosilicate system, especially the relative fraction of 4-coordinated boron. As shown in Fig. 1-2, the relative fraction of 4-coordinated boron calculated using Dell and Bray model is excellent accordance with the calculation results by MD technique.

Table 1-2. Dominant intermediate range order structure in the Na_2O-B_2O_3-SiO_2 system at the each region; estimated by Dell and Bray model.

Region	Intermediate range order structure unit
$R < 0.5$	Diborate
$0.5 \leq R < 1/2 + K/16$	Diborate + Reedmergnerite
$1/2 + K/16 \leq R < 1/2 + K/4$	Diborate + Reedmergnerite with NBO
$1/2 + K/4 \leq R < 2 + K$	Pyroborate

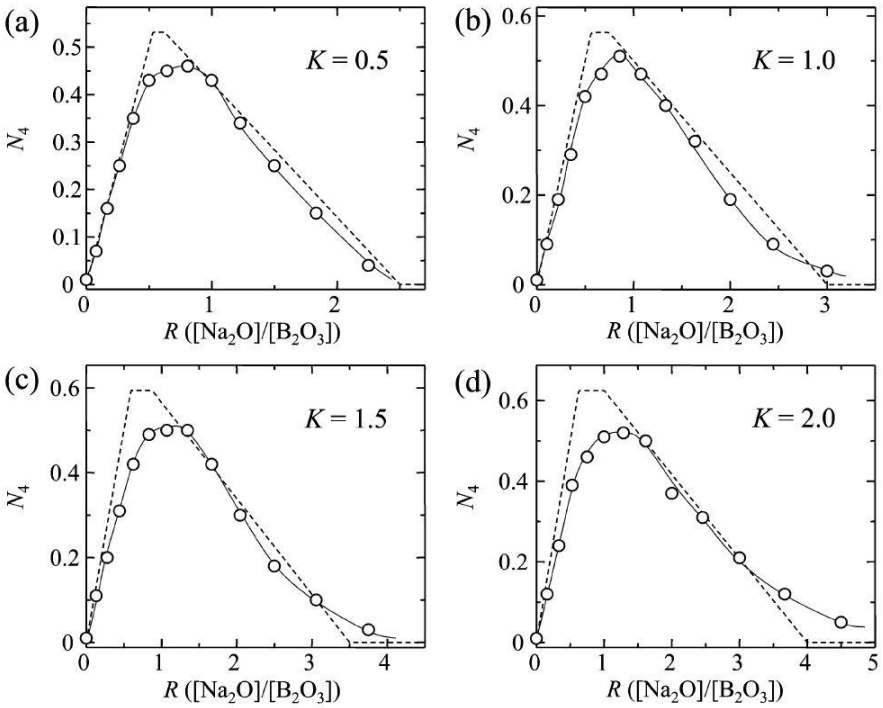

Fig. 1-2. Relationship between R ratio and the relative fraction of 4-coordinated boron (N_4) at a fixed K ratio.[46] (The dashed line is obtained by Dell and Bray model. The solid line is calculated value by MD technique) [Reprinted with permission from *The Journal of Physical Chemistry B*, Vol. 116 No. 40, pp.12325–31 (2012). Copyright (2012) American Chemical Society.]

While SiO_2 tetrahedral structure has simple network structure that is three dimensionally interconnected ring with four or more tetrahedral per ring,[47] B_2O_3 has systematic intermediate range order structure. As mentioned above, in pure B_2O_3, three BO_3 triangular unit is arranged in the boroxol ring structure where the average size of boroxol ring is approximately 20 Å.[48] In the sodium borosilicate system, 3- and 4-coordinated boron compose the various intermediate range order structure which is diborate, reedmergnerite and pyroborate units depending on the R ratio.[44] The short range order structure shows the nearest neighbor bonding of each atomic species in the range of 2 – 5 Å, whereas the intermediate range order structure provides the information of the relative atomic positions over 5 – 10 Å, or larger.[49] The intermediate range order structure consists of the covalently bonded rings or clusters forming layer-like, chain-like or isolated cluster.[50]

Such an intermediate range order structure is also known as "super-structure" in the borate system. Wright[51] defined the super-structure as "*structural units comprising well arrangement of the basic borate structural units, with no internal degrees of freedom in the form of variable bond or torsion angles*". In the borate glass and melts, various type of super-structure units exists and the larger superstructure unit consists of two three-membered ring

and one or two BO_4 tetrahedral unit.[38] Figure. 1-3 shows the various type of super-structural units observed in the potassium borate system.[52] Although direct association of BO_4 tetrahedral unit is energetically unfavorable due to the delocalized negative charge, it can be observed in the super-structural unit owing to the energy compensation by the stabilization energy.[51] Such stabilization energy of super-structural units affects the formation of BO_4 and asymmetric BO_3 units in the borate system. According to Wright et al.[38], the increasing number of external $B^{[4]}$-O-$B^{[4]}$ bond results in the formation of BO_3 unit with NBO to lower the stabilization energy of super-structural unit. Therefore, it can be inferred that in the borate system, the change of short range order structure is closely related to the change of intermediate range order structure, and vice versa.

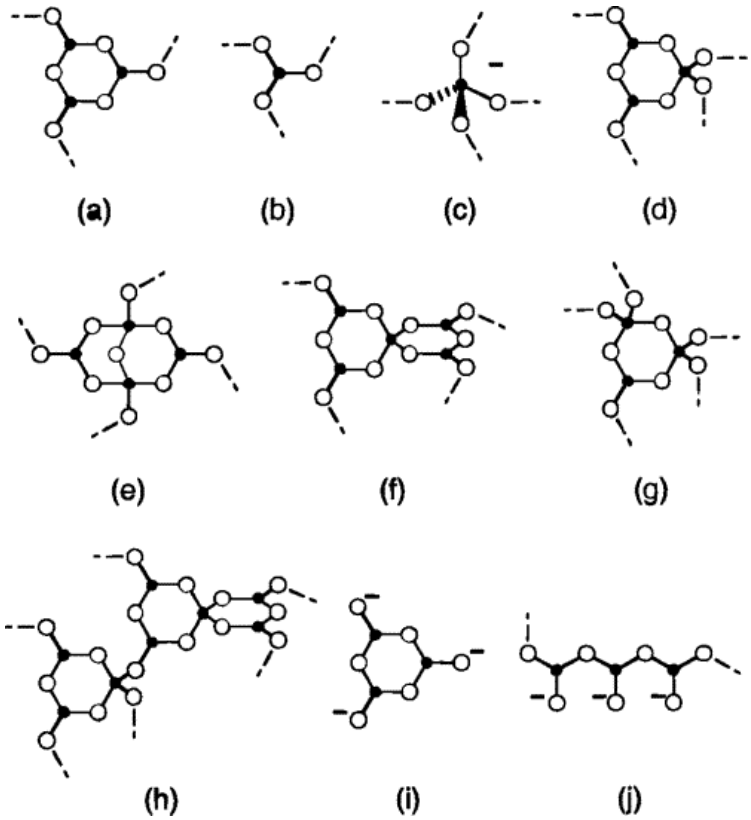

Fig. 1-3. The super-structural units observed in the K_2O-B_2O_3 glass system: (a) boroxol ring (b) non-ring BO_3 (c) non-ring BO_4^- (d) triborate (e) diborate (f) pentaborate (g) di-triborate (h) tetraborate (i) ring-type metaborate (j) chain-type metaborate.[52] [Reprinted with permission from *The Journal of Physical Chemistry*, Vol. 100 No.41 pp.16720–16728 (1996). Copyright (1996) American Chemical Society.]

1.2.2. Structural Investigation Technique for Oxide System

Although there is no long-range order structure, it has been commonly accepted that short-range order and medium-range order exist in the glass and molten oxide system. Last for decades, many researchers have studied about the network structure of glass and molten oxide system using the various experimental structural probes; such as Nuclear magnetic resonance (NMR) spectroscopy, Fourier transform-infrared (FT-IR) spectroscopy, and Raman spectroscopy. Each structural probe provides different aspects of structural information; such as interatomic distance, angle or symmetry-asymmetry of structure unit.[49] For this reason, various structural investigations should be used together in order to obtain more precise structural information of the glass system.

As previously mentioned, not only the short-range order borate structure, but also the medium-range order borate structure; so called super-structure coexist in the borate system. For this reason, in order to understand the borate network structure, both aspects should be considered, simultaneously. In this section, the principle of representative structural investigation probes for short- and intermediate-range order structure will be briefly introduced.

1.2.2.1. Nuclear magnetic resonance (NMR) spectroscopy

1.2.2.1.1. Magic angle spinning nuclear magnetic resonance (MAS-NMR) spectroscopy

NMR spectroscopy has been known as the one of the powerful probes for both short-range and medium-range order structure. For this reason, NMR techniques have been widely adopted for the purpose of investigation of the structure of glass and molten oxide system since 1950's.[53]

The NMR spectroscopy is based on the "Zeeman interaction" which is the splitting of energy level in the presence of external magnetic field. When energy transition between two split single energy level is occurred, absorption or emission of a photon is detected in radiofrequency range. NMR is the structural investigation technique measuring the radiofrequency signal.

Simply, NMR measurement consists of 3 steps; preparation, perturbation and detection.[54] At first, in the preparation step, the magnetic moment of nuclear dipoles system precesses under the circumstance of the external magnetic field of B_0. The precession of orbital magnetization (M) in an external magnetic field can be characterized by in terms of Larmor frequency (υ_L) which is the function of gyromagnetic ratio (γ) and external magnetic field (B_0);

$$\nu_L = \frac{\gamma}{2\pi} B_0 \qquad (1\text{-}5)$$

Since gyromagnetic ratio is different from each element, Larmor frequency is characterized depending on the elements under same magnetic field. At the perturbation step, the radio frequency (rf) is irradiated into sample resulting in the rotation of magnetic moment from z-direction into the x-y plane. Finally, in the detection stage, the rf radiation is turned off and signal containing information of frequency is obtained by a free induction decay (FID). Using Fourier transformation, the time dependent FID signal is converted into the frequency – amplitude plot. In Fig. 1-4, 3-steps of simple NMR analysis procedure is displayed along with its magnetization change.[54]

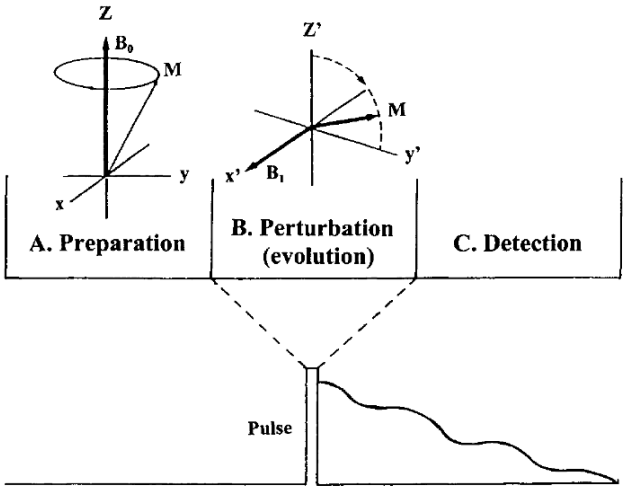

Fig. 1-4. 3-steps of simple MAS-NMR analysis.[54]
[From *Multinuclear solid-state NMR of inorganic materials* by Mackenzie, Kenneth J.D.; Smith, Mark E. Reproduced with permission of PERGAMON.]

Depending on the environments of nuclei, different magnetic field is experienced due to the shielding effects by the surrounding electrons. When B_0 of external magnetic field is applied to nuclei, only B_0^o of magnetic field affects the nuclei on account of the shielding effect. Between B_0 and B_0^o, there is the following relationship;

$$B_0^o = (1-\sigma)B_0 \qquad (1\text{-}6)$$

where σ is the shielding constant. The shielding constant can be normalized from the

difference between the resonance frequency of sample and reference Larmor frequency (υ_L) of the bare nuclei.[54] Such normalization facilitates direct comparison among the measurement data observed in different magnetic field. However, Larmor frequency of bare nuclei cannot be practically measured. For this reason, resonance frequency of the standard reference sample (ν_{ref}) is used instead of resonance of Larmor frequency of the bare nuclei. The normalized resonance frequency expressed by the resonance frequency of standard reference sample is defined as chemical shifts (δ); unit of ppm.

$$\delta_{sample} = \frac{\nu_{sample} - \nu_{ref}}{\nu_{ref}} \times 10^6 \qquad (1\text{-}7)$$

Therefore, the electrons shielding effect is reflected in the chemical shift. The information of surrounding of nuclei can be obtained from the comparison of chemical shift. From the above equation, it can be inferred that more screened nuclei by electron has lower chemical shift due to lower resonance frequency. In general, NMR spectra is plotted with change of chemical shift, as shown in Fig 1-5. The right side of x-axis is called "up-field" and left side of x-axis is called "down-field". "up-field" side indicates the electron rich shielded nuclei.

Besides "Zeeman interaction", many other interactions between the nucleus and its surroundings are occurred in the presence of external magnetic field. The interactions result in the change of Zeeman splitting energy level, and these can be expressed in terms of the internal interactions Hamiltonian.[54]

$$H_{Int} = H_Z + H_D + H_\sigma + H_J + H_P + H_Q \qquad (1\text{-}8)$$

The solid which has more than 1/2 of the nuclear spin quantum number ($I \geq 1/2$) experiences "Zeeman interaction Hamiltonian (H_Z)", "Dipolar interaction Hamiltonian (H_D)", "Chemical-shielding Hamiltonian (H_σ)", and "Spin-spin interaction Hamiltonian (H_J)". The material contains paramagnetic center, there is "Paramagnetic interaction Hamiltonian (H_P)" resulting from the interaction between unpaired electrons and nuclei. However, in the case of the nuclei spin $I > 1/2$, final term of "Quadrupolar interaction Hamiltonian (H_Q)" should be considered. It denotes the interaction between nuclear electric quadrupole moment and the gradient in the electric field at the nucleus.[54]

The above interactions result in the broadening of the NMR spectra and such a broadening effect makes analysis difficult. Mathematically, the equation of dipolar interaction and 1st

order quadrupolar interaction contains ($3\cos^2\theta$-1) term, where θ is the angle between external magnetic field and principal axis of the interaction. At the angle (θ) where ($3\cos^2\theta$-1) becomes zero, the broadening effect is cancelled out. In addition, rapid spinning of the sample (greater than the magnitude of the isotropic dipole-dipole interaction) reduces the broadening effect. For these reasons, solid-state NMR measurement is usually carried out at an angle (θ) of 54.74° along with rapid spinning rate; typically more than 10 kHz. NMR analysis performing under the tilted angle of 54.74° is called magic angle spinning (MAS) NMR. As shown in Fig. 1-5, the higher resolution of sharp peaks can be obtained under the MAS condition providing useful structural information of the sample.[54]

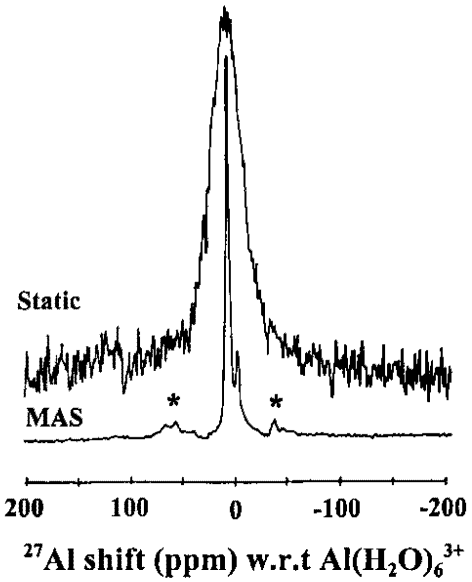

Fig. 1-5. ^{27}Al NMR spectra of solid powdered Al_2O_3-Y_2O_3 without MAS (upper) and with MAS (lower). The asterisk-marked peaks indicate spinning side bands.[54]
[From *Multinuclear solid-state NMR of inorganic materials* by Mackenzie, Kenneth J.D.; Smith, Mark E. Reproduced with permission of PERGAMON.]

1.2.2.1.2. Multiple Quantum Magic Angel Spinning (MQMAS)

When nuclear spin quantum number is larger than 1/2 ($I > 1/2$), the electric distribution is not the spherical shape and it causes nuclear quadrupole moment. Under the electric field gradient, energy of the system is changed due to the interaction between nuclear quadrupole moment and electric field. Such electric static interaction is called quadrupole interaction. As shown in Eq. (1-8), nuclear quadrupole interaction affects Zeeman interaction. Equation (1-9) shows the resonance frequency by nuclear quadrupole interaction (ν_Q) affecting Larmor

resonance (ν_L).

$$\nu_Q = \frac{3}{2I(2I-1)} C_Q \tag{1-9}$$

$$C_Q = \frac{e^2 qQ}{h} \tag{1-10}$$

C_Q is nuclear quadrupole coupling constant which sensitively reflects the circumstance around the nuclei, e is unit charge, Q is nuclear quadrupole moment and h is plank constant. Since C_Q has the order of MHz – GHz, not only the first-order but also second-order of quadrupole interaction should be considered. As previously mentioned, such quadrupole interaction results in the broadening of NMR spectra. However, the second-order interaction cannot be cancelled out by the MAS technique. For this reason, multiple quantum magic angle spinning (MQMAS) is adopted for the analysis of element which nuclear spin quantum number is larger than 1/2 ($I > 1/2$).

In the MQMAS analysis, 2-dimensional diagram is obtained by the transition of two-different magnetic quantum number (m) during time of t_1, and t_2 at a fixed magic angle. The anisotropic broadening can be related to the time-domain refocusing condition, and an isotropic signal can be solely detected at the point of (t_1,t_2).[55] Depending on the spin quantum number (I) and transition order quantum number (p), coefficient between t_1 and t_2 is determined. For this reason, the FID data obtained by MQMAS is tilted resulting in inclined spectra after Fourier transform. In order to find the genuine chemical shift, shearing transformation and scaling are carried out during MQMAS analysis. Shearing transformation is the scheme for rotating line shape. Following the shearing transformation, scaling is carried out. Through the scaling, the chemical shifts observed isoshift (vertical axis) and direct observation axis (horizontal axis) become coincidence with genuine chemical shift. After the procedure, conventional MAS-NMR spectrum is obtained on horizontal axis and isotropic spectrum is observed on vertical axis.

Figure 1-6 shows the pulse sequence of 3QMAS method along with magnetization transfer pathway. The first induced rf pulse results in the excitation of the 3Q transfer and 3Q coherence is maintained for a time of t_1. After that, 3Q coherence is converted into coherence of -1 by the second induced pulse and it is observed within a time of t_2. However, during the transfer of coherence, there is difference between echo and anti-echo path resulting in the distortion of NMR spectra. For this reason, 3QMAS including Z-filter is generally used. In this method, there is the coherence transfer from 3 to 0. After a time of τ, weak 90° pulse is induced in order to translate the coherence from 0 to –1.[56] The 3QMAS including Z-filter has

the advantage of symmetric transfer of coherence.[54]

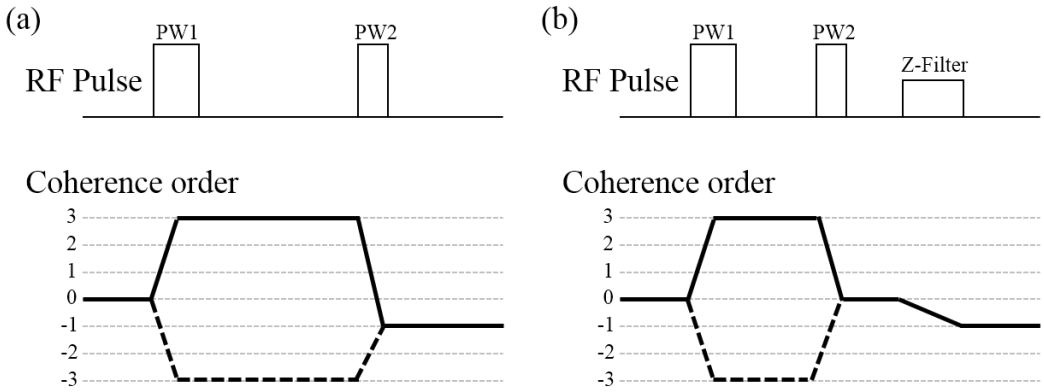

Fig. 1-6. The pulse sequence and magnetization transfer of 3QMAS method (a) without Z-filter and (b) with Z-filter

1.2.2.2. Infrared (IR) absorption spectroscopy

Infrared (IR) is the electromagnetic radiation observed from 780 nm to 1nm of wavelength. Specifically, the region from 780 nm to 2.5 μm, from 2.5 to 25μm, and from 25 μm to 1 mm is called near-IR, mid-wavelength IR, and long-wavelength IR, respectively. In the IR absorption spectroscopy, the mid-wavelength IR (frequency of 4000 – 400 cm^{-1}) is irradiated into sample and then the transparent infrared is detected. Since molecule with covalent bonds would absorb the IR radiation, IR absorption spectrum can provide the meaningful information concerning about the covalent bonds in the molecule.[57] Figure 1-7 shows the electromagnetic spectrum along with spectrometer and structural information corresponding to each range of wavelength.

The absorbed radiation results in the transfer of molecule into higher energy level along with the rotating and vibrating of molecules. There are several vibration modes when IR is irradiated; symmetrical and asymmetrical vibration, or scissoring, rocking, wagging and twisting bending. Stretching vibration results in a change of interatomic distance along with bond length. On the other hand, bending vibration results in a change of bond angle.

However, not all molecule can absorb the IR radiation. Only, a molecule which dipole moment changes with time can absorb IR radiation. For this reason, different electronegativity in a molecule, called polar, is required for structure study using IR absorption. For example, symmetric vibration cannot be detected by IR spectroscopy because it does not change the dipole moment.

A molecule consists of several atoms by chemical bonds, and each chemical bond has

characteristic vibration. Based on the kinetic and potential energy of diatomic bonds, the frequency of harmonic vibration can be expressed by following equation.[58]

$$\nu = \frac{1}{2\pi c}\sqrt{\frac{k}{\mu}} \tag{1-11}$$

Where ν is the wavenumber of the absorption maximum, c is the speed of light, k is the force constant of the bond, and μ is the reduced mass. The force constant is directly proportional to the bond order. In addition, force constant depends on the electronegativity of the vibrating atoms along with mean distance; which are physical properties of molecule.[57] Therefore, the vibration of molecule by IR absorption can provide characteristic structure information.

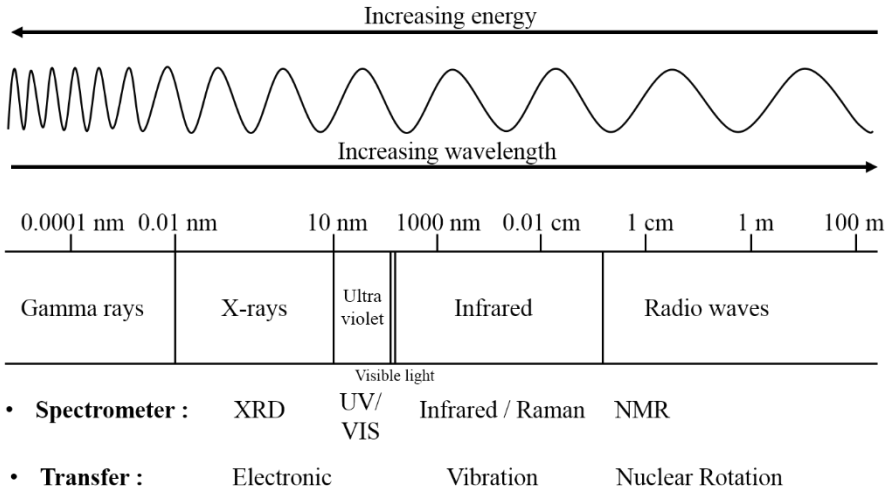

Fig. 1-7. Electromagnetic spectrum, spectrometer and structural information corresponding to each range of wavelength

1.2.2.3. Raman spectroscopy

Comparted to Rayleigh scattering based on elastic collisions, Raman scattering results from loss or gain of energy when photons are scattered. A collision of photon with a molecule leads to the excitation of energy from ground electronic state into virtual state. Following the transition of electronic state, energy of molecule returns to the ground electronic state. However, Raman scattering causes the energy level difference from its original state (ΔE) due to the loss or gain of energy. The ΔE represents the vibrational energy change of the molecules.

The energy change can be expressed in terms of frequency change; which is called shift, and the Raman shift (cm^{-1}) is identical to the IR absorption peak because both vibration result from same excitation.[57]

While IR absorption spectroscopy is only valid for the molecule with dipole moment, Raman spectrum can only observe the vibration of molecule which has polarizability. Such polarizability can be obtained by the distortion of the electron cloud around the vibrating atom.[57] Figure 1-8 shows Raman and IR spectra of benzene (C_6H_6).[59] It can be found that Raman spectroscopy can observe the symmetric stretching vibration of C-H (3082 cm^{-1}) and breathing vibration of benzene ring (980 cm^{-1}) which are not observable in IR spectroscopy due to no dipole moment change. On the other hand, the asymmetric stretching vibration (3370 cm^{-1}) and bending (667 cm^{-1}) of C-H are only IR active due to no polarizability change. The combination of Raman and IR absorption spectroscopy provides better understanding for molecule structure because both two have the complementary relationship.

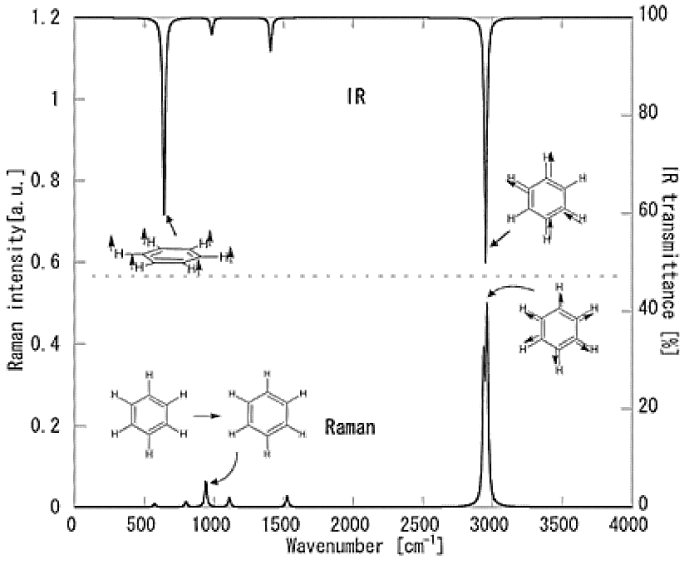

Fig. 1-8. Spectra of benzene obtained by IR absorption (up) and Raman (down) spectroscopy.[59]

The intensity of Raman spectrum is proportional to the both fourth power of the excitation frequency and number of scattering molecules. For these reasons, monochromatic light source with shorter wavelength has an advantage of better signal-to-noise (S/N) ratio and quantification of the structural unit can be obtained using Raman spectroscopy.[59] In addition using Raman spectroscopy, depolarization ratio can be calculated providing symmetry of vibration (symmetric or asymmetric vibration).

1.2.3. Effect of Borate Structure on the Physical Properties

As mentioned previously, borate is widely used over glassmaking and steelmaking field due to its characteristic features. Similar to other oxide system, the physical properties of molten borate system is closely related to its structural characteristic which is the function of composition, pressure and temperature.[60] Therefore, in order to control and optimize process, understanding of borate structure is significant from not only scientific aspect but also industrial viewpoint.

However, borate system shows complicated structure change with higher alkali or alkali-earth oxide concentration along with formation of various intermediate-range order structure and boron coordination change. For this reason, complicated physical property change is observed with varying basic oxide concentration

In this section, the physical properties of borate system bearing alkali and alkali-earth oxide will be briefly reviewed.

1.2.3.1. Density and thermal expansion coefficient

It is undoubtedly that density of molten oxide system is directly related to the molten oxide structure because volume is mainly determined by the packing condition and cation size of oxide system. Kunugi et al.[61] observed the change of volume of alkali-borate at 1273 K reporting the direct relationship between borate structure and melt volume. It can be observed that molar volume of alkali-borate binary system initially decreases with formation of 4-coordinated boron and then increases due to the structural change from 4-coordinated boron into 3-coordinated boron associated with non-bridging oxygen (NBO). Change of glass density also effects on the properties of refractive index and the hardness.

Similar to the change of density, thermal expansion coefficient change is also complicated. Figure 1-9(a) shows the change of thermal expansion coefficient of alkali-borate binary glass system with varying alkali oxide concentration.[62] As shown in this figure, addition of alkali oxide initially decreases in the thermal expansion coefficient and then, increases subsequently. In early 1930's, when such a complicated change of thermal expansion coefficient was firstly observed, reason of the complicated change was not fully understood. The anomalous behavior of thermal expansion coefficient of the alkali-borate system was called as "Boron anomaly".[26] However, owing to the breakthrough of structural investigation technique; especially NMR spectroscopy, it was found that "anomalous" behavior results from the change of borate structure along with change of boron coordination number. The structure change of borate from three-dimensional cross-linking of planar networks into less

polymerized units associated with NBO ions leads to the change of thermal expansion coefficient.[63]

1.2.3.2. Viscosity

Viscosity of molten oxide system is the physical property related to the temperature and network structure. In the SiO_2 bearing oxide melts, monotonous decrease of viscosity with higher concentration of basic oxide is commonly observed as a result of the depolymerization of silicate network structure. In the case of alumina containing oxide system, more complicated viscosity change can be observed due to the amphoteric behavior of aluminum oxide. In addition, several studies has revealed that viscosity can be affected by interaction between metal and oxygen ions as well as the cation size.[60]

Due to the complicated structure change of B_2O_3 bearing oxide melts, viscosity of borate system cannot be simply expected based on the additive rule.[64] According to Fox et al.[16], addition of B_2O_3 could result in both increasing and decreasing of the viscosity in the mold flux system due to the formation of 3-coordinated and 4-cooridnated boron. Li et al.[65], who studied viscosity in the molten alkali-borate binary system, reported that addition of alkali oxide results in the formation of 4-coorinated boron along with increasing viscosity. On the other hand, above certain concentration of alkali oxide, due to the structural change from 4-coordinated boron into 3-coordinated boron associated with NBOs, the viscosity decreases; as shown in Fig. 1-9(b). In addition, in the case of B_2O_3 and alkali-earth oxide binary system, maximum viscosity can be observed around metaborate or diborate composition region.[66] Not only the borate structure, but also the field strength of cation of alkali oxide effect on the change of viscosity resulting in higher viscosity activation energy with higher field strength of cation.

More complicated relationship between viscosity and borate structure have observed at the ternary and quaternary system. In the blast furnace slag system, Ren et al.[67] reported that even though the addition of boron oxide increases the amount of 4-coordinated boron oxide ($[BO_4]^{5-}$), viscosity is nonetheless reduced due to a lowering of the eutectic temperature. Zhang and Reddy[68], observed that the addition of B_2O_3 resulted in increasing of viscosity at low SiO_2/Na_2O ratio, but in decreasing of viscosity at high SiO_2/Na_2O ratio in the molten sodium borosilicate system. Kim and Sohn,[20] who measured viscosity in the CaO-Al_2O_3-Na_2O-B_2O_3 quaternary system along with structural investigation by Raman spectroscopy, reported that the structural change from 3 dimensional borate structure into 2 dimensional borate structure results in the lowering viscosity.

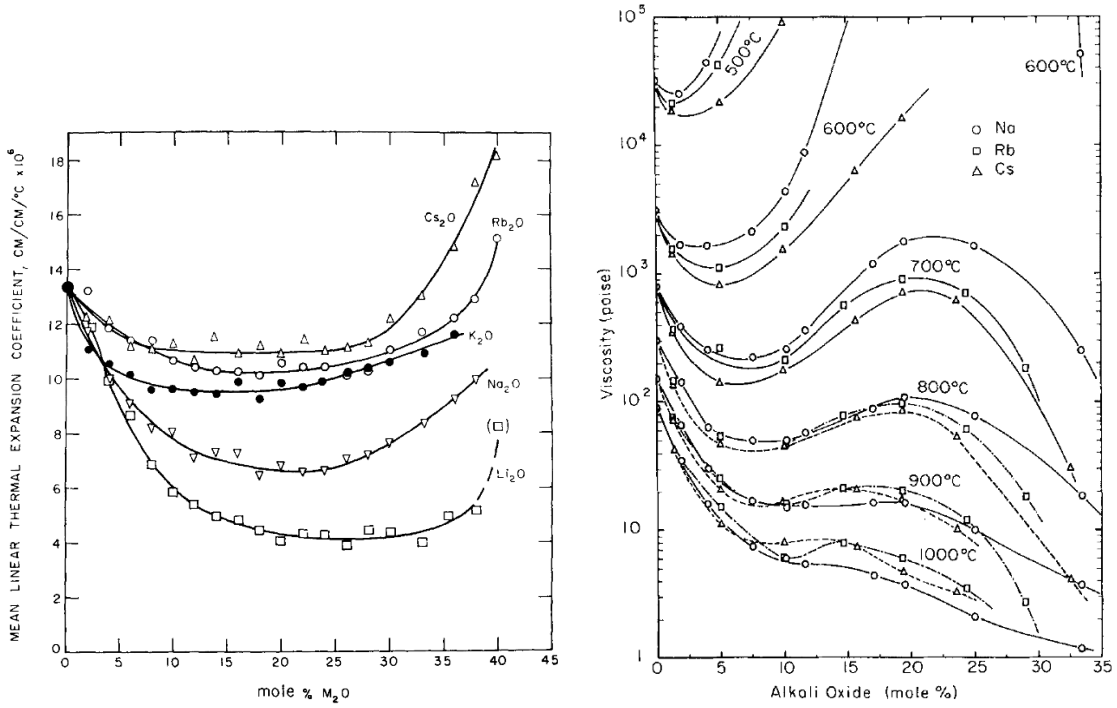

(a) **(b)**

Fig. 1-9. Change of (a) thermal expansion coefficient[62] and (b) viscosity[65] of alkali-borate glass system with varying composition. [Reprinted with permission from (a) *J. Non-Cryst. Solids* Vol. 1, pp.347–359 (1969). Copyright (1969) Elsevier (b) *J. Am. Ceram. Soc.* Vol. 45, pp.83-88 (1962). Copyright (1962) John Wiley and Sons.]

1.2.3.3. Electrical conductivity

Compared to other physical properties, electrical conductivity of borate system is related to the cation which is the metallic ions. Except for the transition metal bearing system; which shows electronic conduction by variable valence ion, electrical conductivity is based on the ionic conductivity transferred by metallic ion. In the oxide melts, the movement of borate ions is much slower than the cations.[69] For this reason, in borate melts, addition of alkali or alkali-earth oxide gradually increases in the electrical conductivity along with the increasing of the concentration of cation. According to previous studies concerning about the electrical conductivity in the alkali borate melts,[70, 71] anomaly behavior could not be observed indicating the independent of electrical conductivity from borate structure.

The electrical conductivity can be expressed by a function of ion-oxygen attraction parameter (I) which is atomic fraction of total basic oxide cation over total acidic oxide cation.[60] In addition, electrical conductivity shows positive relationship between temperature and ionic radius of alkali oxide.

1.3. Thermal Conductivity of the Molten Oxide

Thermal conductivity of molten oxide system has been paid attention due to its practical and academic importance. The observed thermal conductivity, called effective thermal conductivity (λ_{eff}), can be expressed by the summation of each different thermal conductivity; lattice thermal conductivity (λ_L), radiation thermal conductivity (λ_R) and electronic thermal conductivity (λ_{el}).[72]

$$\lambda_{eff} = \lambda_L + \lambda_R + \lambda_{el} \tag{1-12}$$

The lattice thermal conductivity (λ_L) is based on the heat transfer by phonon. Because scattering of phonon results in the decrease in thermal conductivity, thermal conductivity by phonon is significantly influenced by the change of disordering of network structure in the glass and molten oxide system.[73] Over the 800 K, radiative heat transfer in the clear glass becomes dominant factor.[74] At higher temperature of the transparent molten oxide glass system, more than 90 % of heat is transferred by the radiation conduction. Assuming the steady state along with grey-body conditions, radiative thermal conductivity of an optically thick sample can be calculated by a function of absorption coefficient and refractive index.[72] On the other hand, thermal conductivity by electron is insignificant in the molten oxide system as long as the composition of transition metallic oxide does not exceed 70%.[72, 75]

1.3.1. Thermal Conductivity Measurement Techniques

Although understanding of thermal conductivity by phonon is significant for the process control in the glass and steelmaking field, precise measurement of thermal conductivity by phonon is challenging due to the notorious radiation and convection effect at high temperature.[76] The measurement method for thermal conductivity by phonon can be classified into two large groups; one is steady-state and another one is non-steady-state method. In steady-state method, thermal conductivity is determined by the temperature profile across a sample contacting directly with a heat source.[72] However, steady-state method requires a relatively long measurement time in order to obtain the steady state of thermal profile across the sample.[75] In addition, during the measurement, contribution of radiation and convection is significant due to the long measurement time. For these reasons, at high temperature, thermal conductivity by phonon transfer cannot be precisely measured using steady-state method.

In order to investigate the thermal conductivity of molten oxide system, non-steady state measurement method has been modified for the last few decades. For the measurement of molten oxide system, two measurement techniques have been widely adopted; one is laser-flash method and another one is hot-wire method. Two techniques have in common that both two method apply a constant energy and monitor the temperature change with time. Because the thermal conductivity can be measured within approximately 10 s by non-steady-state method, effect of radiation and convection is insignificant, compared to the steady-state method.

Since the first introduction of laser flash method in 1961, this technique has been widely adopted for the purpose of measurement of thermal diffusivity and heat capacity in the various materials.[77] During the measurement, the front surface is heated by a single pulse laser resulting in an increasing temperature of the opposite surface. Then, thermal diffusivity is calculated from the increasing temperature. However, due to the leakage of heat from measurement sample, the sufficient accuracy cannot be achieved at high temperature. Several improvement of laser-flash method has been introduced in order to overcome various problem occurred during the measurement. In 1990s, Ogura et al.,[78] developed three-layered laser flash method. Although it has the merit of relatively small heat leakage, calculation of thermal conductivity by phonon transfer requires various physical properties related with radiation such as absorption coefficient.[79] For this reason, recently, Ohta et al. [79, 80], revised the three-layered laser flash method and introduced new method, called front heating-front detection laser flash method. Distinct from previous laser-flash methods, the laser pulse is irradiated on the bottom of platinum crucible during the front-heating front-detection technique. Assuming the one-dimensional heat flow along with semi-infinite thickness of liquid sample,[80] thermal conductivity is calculated by measurement of the temperature decay at the bottom of surface. Since the thermal conductivity is measured within only 12 ms, front-heating front detection technique does not consider the additional process for distinguishing radiation effect from observed thermal conductivity data. However, although the front heating-front detection laser-flash method has the merit of simple processing and easy data processing,[81] the effect of radiation on thermal conductivity measurement is still controversial, especially at high temperature.[75] Figure 1-10 shows the three different laser flash method; conventional, three-layered and front heating-front detection laser flash method.[75]

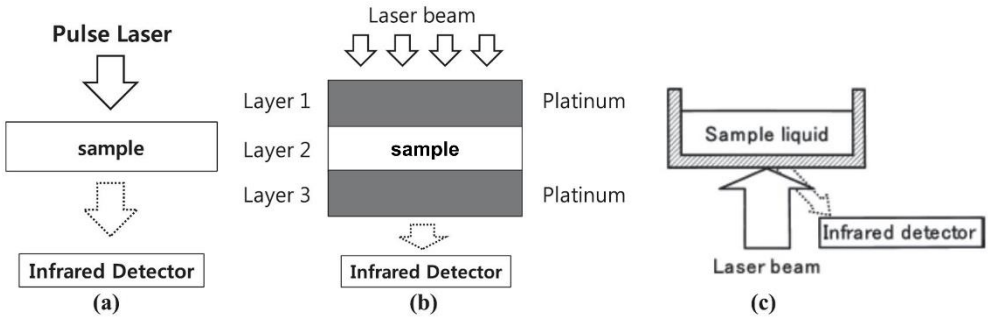

Fig.1-10. Three different laser flash method; **(a)** conventional, **(b)** three-layered and **(c)** front heating-front detection laser flash method.[75] [Reprinted with permission from *ISIJ Int.* Vol. 54 No. 9, pp.2008–2016 (2014). Copyright (2014) The Iron and Steel Institute of Japan.]

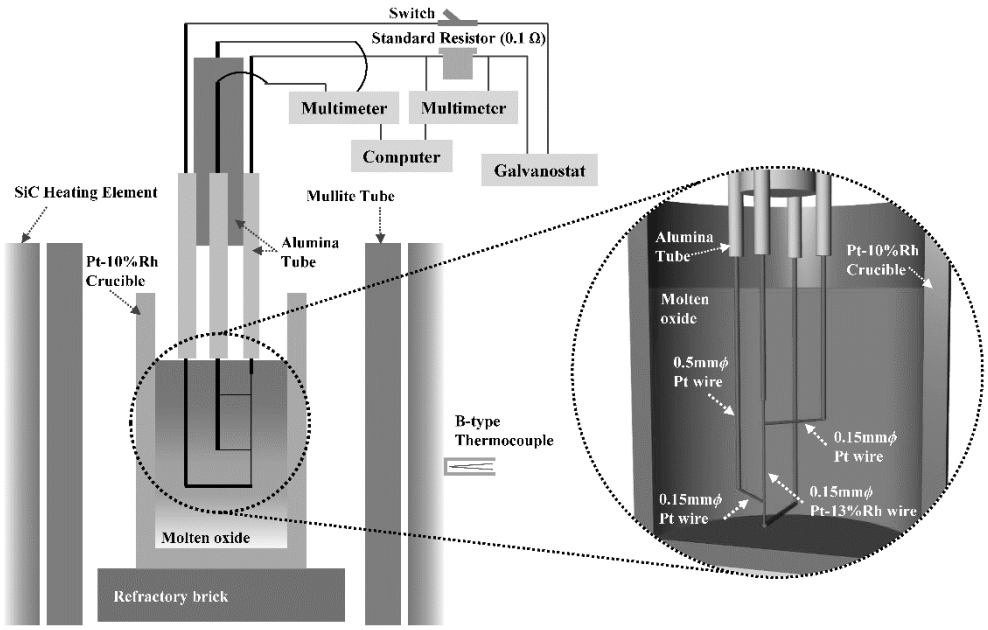

Fig.1-11. Schematic diagram of the transient hot-wire method for molten oxide system.

Figure 1-11 shows the schematic diagram of the hot-wire method for molten oxide system. The hot-wire method, also known as line-source method, is the one of the non-steady-state method. Because the hot-wire method uses a very thin metal wire, the effect of radiation is relatively insignificant even at high temperature.[82] Since transient hot-wire technique firstly introduced in 1780's, this method has been widely used for the measurement of precise thermal conductivity measurement of solid, liquid and even gas phase material.[83]

During the thermal conductivity measurement of molten oxide system, a thin Pt-13%Rh wire is placed in the middle of molten oxide sample and heated up by the applied constant

current. The generated heat is transferred from hot-wire into molten oxide system resulting in increasing temperature. If the hot-wire is long enough, the temperature change of molten oxide system resulting from constant heat flux Q can be expressed by a continuous line heat source solution.[84]

$$\Delta T = \frac{Q}{4\pi\lambda}\left(\ln\frac{4\kappa t}{r^2} - \gamma\right) = \frac{Q}{4\pi\lambda}\left(\ln t + \ln\frac{4\kappa}{r^2 e^{\gamma}}\right) \qquad (1\text{-}13)$$

Here, ΔT is the temperature change of hot-wire, Q is the heat generation per unit length of hot-wire, λ is the thermal conductivity, κ is the thermal diffusivity, r is the radius of hot-wire, t is the time, and γ is the Euler's constant; 0.5772. The continuous line heat source solution can be adopted when the length and diameter ratio of hot-wire is larger than 30.[85] Following the differentiation of equation (1-13), thermal conductivity can be expressed by the equation (1-14).

$$\lambda = \left(\frac{Q}{4\pi}\right) \Big/ \left(\frac{dT}{d\ln t}\right) \qquad (1\text{-}14)$$

Because a constant current is applied by galvanostat, heat generation per unit length of hot-wire (Q) can be calculated by the following equation.

$$Q = \frac{VI}{m} = I^2\frac{R_T}{m} \qquad (1\text{-}15)$$

$$R_T = R_0(1 + AT + BT^2) \qquad (1\text{-}16)$$

Above equation, V, I, m, R_T, and R_0 represent the voltage, current, length of hot-wire, resistance per unit length at T °C, and resistance per unit length at 0 °C, respectively. Equation (1-16) shows the empirical linear relationship between R_T and R_0. According to Kang and Morita[86], constant of A and B for Pt-13%Rh wire is 1.557×10^{-3} and -1.441×10^{-7}, respectively. During the measurement, R_T is obtained by applying infinitely small current which could not heat up the experimental sample.

From the Ohm's law, the following equation can be obtained at the given temperature T.

$$\frac{dV}{dT} = I\frac{dR_T}{dT} = IR_0(A + 2BT) \qquad (1\text{-}17)$$

From the equation (1-14), (1-15) and (1-17), the thermal conductivity can be expressed as the function of voltage and time.

$$\lambda = \left(\frac{I^3 R_T R_0 (A + 2BT)}{4m\pi} \right) \Big/ \left(\frac{dV}{d \ln t} \right) \qquad (1\text{-}18)$$

Using the four-terminal sensing,[87] the voltage change of hot-wire is recorded in real-time. Therefore, thermal conductivity of the molten oxide system can be easily calculated by the slope of V versus ln t.

According to Kwon et al.[88] and Healy et al.[89] who studied about the errores occurred during the thermal conductivity measurement, appropreately designed hot-wire method can measure thermal conductivity of liquid with the error of less than 0.31 % . Although they considered low temperature; below 100 ^{o}C, effect of other variables; such as convection and current leakage seems insignificant during the thermal conductivity measurement even at high temperature. In order to reduce the radiative heat transfer, a thin Pt-13%Rh wire of 0.15mm ϕ is used during the thermal conductivity measurement. The effect of free convection can be reduced by placing the upper level of the sample in the highest temperature zone.[90] In addition, if there is convection effect, the linearity between voltage and time could not be observed. As a result, the thermal conductivity by phonon transfer can be obtained within the region where the linear relationship between voltage and time exists. Recently, several studies have evaluated the experimental conditions which affect the precision of the measurement.[91, 92] A computational fluid dynamics (CFD) calculation[91] revealed that it was critical to determine the resistivity and the temperature coefficient of resistance of the hot-wire in order to obtain an accurate thermal conductivity. In addition, Kang et al.[92] calculated the current leakage by semi-qauntitative evaluation, and reported that the current leakage is 2 % (at most) in the various silicate melts which contain less than 20 wt% FeO_x.

Recently, Mills[93] found that thermal conductivity of molten slag system measured by laser-flash method is approximately 10 times than by hot-wire method implying possibility of the effect of radiation in laser-flash method. Therefore, it can be inferred that thermal conductivity of molten oxide system is more precisely measured by using the hot-wire method at high temperature.

1.3.2. Thermal Conductivity of the Ironmaking and Steelmaking Slag

In the ironmaking and steelmaking field, understanding of thermal conductivity of the molten oxide system is significant because it is closely related with the operation conditions, quality of final products and recycling of iron-making/steelmaking slag.

For the recycle of blast furnace slag, the slag is slowly cooled down in the atmosphere or rapidly quenched by using rotary cup atomizer or air blast method. Highly crystallized slag can be recycled as cement concrete for road construction or fertilizer. On the other hand, non-crystalline blast furnace slag can be used as Portland cement for construction owing to its properties of cement when it is ground.[94] Therefore, in order to recycle the blast furnace slag as Portland cement, proper fineness and glass state should be achieved. Since the characteristic fine-granular shape and glass state are mainly determined by a cooling rate, understanding of thermal conductivity of blast furnace slag is important. For this reason, the thermal conductivity measurement in the molten $CaO\text{-}SiO_2\text{-}Al_2O_3$ system; which is the typical blast furnace slag system, has been carried out by both hot-wire method[86, 90, 95] and laser-flash method[96]. According to Kang and Morita[86], thermal conductivity is affected by both composition and temperature. Depolymerization of silicate network structure and increasing temperature result in lowering thermal conductivity. In addition, amphoteric behavior of aluminum oxide leads to both increasing and decreasing of thermal conductivity. However, thermal conductivity results obtained by laser-flash method [96], did not show any relationship between molten oxide structure and thermal conductivity. In addition, thermal conductivity keeps constant with change of temperature.

During the steelmaking process, understanding of thermal conductivity of the molten slag system is significant, because it is closely related to the quality of final products and refractory life-time. Recently, many works have been focused on the development of heat flow of the whole steelmaking chain. However, due to the short of information concerning about thermal conductivity of ladle slag, ladle slag is hardly considered during the simulation.[93] For the purpose of better understand of heat flow, understanding of thermal conductivity of ladle slag is important. Glaser and Sichen[93] measured thermal conductivity of the conventional ladle slag system; $CaO\text{-}SiO_2\text{-}Al_2O_3\text{-}MgO$ system, using the hot-wire method. Their results show the negative temperature dependence of thermal conductivity within the experimental region between 1773 K and 1923 K. They reported that formation of solid state in the slag results in the significant increasing of thermal conductivity. On the other hands, Kang et al.[97], who measured thermal conductivity in the steelmaking slag system of $CaO\text{-}SiO_2\text{-}FeO_x$ system, reported that addition of FeO_x results in the decreasing of thermal conductivity due to the basic oxide behavior of FeO_x. Considering the structural information of FeO_x obtained by

Mössbauer, they found the linear relationship between thermal conductivity and the NBO/T; which is the relative fraction of the number of non-bridging oxygen over total tetrahedral cation, implying the effect of molten oxide structure on thermal conductivity.

In addition, during the continuous casting process, irregular horizontal heat transfer through mold flux results in the "longitudinal cracking" and "star cracking" on the final product. Therefore, understanding of thermal conductivity of mold flux system is practically important in terms of quality control. Many studies[87, 98–100] have been carried out in order to find out the relationship between structure of mold flux system and thermal conductivity at high temperature of molten state. These works[87, 98–100] commonly observed the structure dependence of thermal conductivity. Addition of basic oxide, such as sodium oxide or calcium oxide, decreases thermal conductivity as a result of depolymerization of silicate network structure.[87, 98] Susa et al.[100], found that fluorides play a role of network modifier resulting in the lowering thermal conductivity. According to Mills[101], phonon transfer along silicate network chain or ring has much lower thermal resistivity($1/\lambda$) than from chain to chain. Similarly, Susa et al.[100] observed that more ionic bonding has the greater thermal resistivity. Therefore, it can be concluded that the positive relationship between thermal conductivity and network structure is closely related to the formation of covalent bond which has low thermal resistivity.

Not only the steelmaking process, but also the ferroalloy making process, understanding of thermal conductivity is significant. During the operation of submerged arc furnace (SAF) which is widely used in manganese ferroalloy producing, "freeze" lining is applied in order to insulate the refractory and prevent direct contact with molten metal and slag.[102] "Freeze" lining can enhance the refractory lifetime because it prevents the wear mechanism; such as alkali attack, thermal stress and dissolution of refractory. According to Steenkamp et al.[103], who measured thermal conductivity in the CaO-SiO_2-Al_2O_3-MgO-MnO system, "freeze" lining becomes thicker with higher thermal conductivity indicating that thermal conductivity is the major factor determining the thickness of "freeze" lining

1.3.3. Thermal Conductivity of the Oxide Glass.

Compared to other crystalline materials, the glass system has relatively low thermal conductivity; approximately 0.5 – 5.5 $Wm^{-1}K^{-1}$.[104] Despite of such low value, thermal conductivity of glass system significantly effects on the processing of thin layer glass and quenching rate.[105] Therefore, understanding of thermal conductivity is prerequisite for the furnace construction and energy balance in the glassmaking process of melting, annealing and forming glass.[74, 106]

The thermal conductivity of solid state glass material has been studied with varying temperature. Zaitlin and Anderson[107], who measured thermal conductivity of borosilicate glass below 30 K, reported that thermal conductivity can be well predicted by the Debye model. Tohmori et al.[108], found that thermal conductivity of the sodium borate glass system is mainly determined by the change of phonon mean free path of collision. Between 150 K and room temperature, formation of 4-coordinated boron increases in thermal conductivity along with longer phonon mean free path. Similarly, Ghoneim and Halawa[109] found that the formation of both BO_4 and SiO_4 structure groups increases in the thermal conductivity along with an extension of the phonon mean free path in the sodium borosilicate glass at room temperature. Other studies[110–112] also reported dominant effect of network structure on thermal conductivity in the various glass systems; $CaO\text{-}SiO_2\text{-}Al_2O_3$, $SiO_2\text{-}Al_2O_3\text{-}Y_2O_3$, $SiO_2\text{-}Na_2O\text{-}RO$ ($R=Mg^{2+}$, Ca^{2+}, Sr^{2+}, Ba^{2+}), and $SiO_2\text{-}Li_2O\text{-}ZnO$ system.

Besides network structure of glass, other variables; sound velocity and heat capacity, also affect the thermal conductivity at low temperature.[73, 110] In addition, in the case of boron oxide, the structure change cannot be simply expected based on the compositional change. As a result, adopting the empirical equation of thermal conductivity[113, 114] into varying glass composition systems has limitation showing tremendous discrepancy depending on the compositions and temperature.

1.4. Research objective

As previously reviewed, understanding of physical properties of oxide system is significant in terms of scientific and industrial viewpoint. Especially, boron oxide (B_2O_3); used in the various industrial field playing characteristic roles in the oxide system, shows complicated change of both short- and intermediate-range order structure at the molten state. For this reason, the relationship between physical property and borate structure has not been fully understood.

Compared to other physical properties, thermal conductivity measurement of molten oxide system is challenging due to tremendous convection and radiation effect at high temperature. Owing to the recent modification and improvement of thermal conductivity measurement techniques, several studies have been carried out in the molten oxide system. However, the previous works mainly focused on the silicate or aluminate bearing system. Although, few researchers reported the relationship between borate structure and thermal conductivity, their works were performed in the glass state at relatively low temperature. Considering that borate structure is affected by the temperature, studying of thermal conductivity in the molten state is significant in the aspect of optimization and control of the industrial process during the steelmaking and glassmaking process.

The aim of present work is finding the relationship between thermal conductivity and the borate structure in the various molten oxide system. Using the hot-wire technique which can provide higher accuracy than laser-flash method at high temperature, thermal conductivity of the molten borate system was measured. In addition, the structural information was obtained with an aid of structural investigation methods; MAS-NMR, 3Q-MAS and Raman spectroscopy.

In chapter II, thermal conductivity of molten B_2O_3 was measured with varying temperature in the molten state. In order to elucidate the effect of both silicate and borate structure on thermal conductivity, thermal conductivity of B_2O_3-SiO_2 system was measured along with structural investigation by MAS NMR, 3Q MAS and Raman spectroscopy. In chapter III, thermal conductivity of various alkali-borate system was measured. Both temperature dependence and compositional dependence of thermal conductivity were observed along with effect of cations on thermal conductivity. From the thermal conductivity of molten Na_2O-SiO_2 binary system, different effect between silicate and borate structure on thermal conductivity was found; understanding of not only short-range order but also intermediate-range order structure is important in the borate system. In chapter IV, thermal conductivity of the Na_2O-B_2O_3-SiO_2 system was measured in order to evaluate the effect of both borate and silicate structure on thermal conductivity, simultaneously. In chapter V, thermal conductivity was

measured in the $CaO\text{-}SiO_2\text{-}B_2O_3$ mold flux system and the effect of intermediate-range order structure on thermal conductivity was considered. In chapter VI, thermal conductivity of alkali borate glass system was investigated. The conflicting temperature dependence of thermal conductivity in the glass and liquid state was discussed. Also, the temperature where thermal conductivity shows maximum was considered. Finally, in chapter VII, thermal conductivity prediction model was discussed for mold flux design. Based on the phonon-like vibration in the glass and liquid oxide system, the thermal conductivity prediction model was established.

References

[1] P. Enghag, *Encyclopedia of the Elements: Encyclopedia of the elements : technical data, history, processing, applications*. Wiley-VCH, Weinheim, 2008.

[2] K.J. Rao, *Structural chemistry of glasses*. Elsevier, 2002.

[3] E. Brandaleze, G. Di Gresia, L. Santini, A. Martín, and E. Benavidez, "Mould Fluxes in the Steel Continuous Casting Process;" pp. 1–30 in *Sci. Technol. Cast. Process.* Edited by M. Srinivasan. InTech, 2012.

[4] D. Schubert, "Boron Oxides, Boric Acid, and Borates;" pp. 1–68 in *Kirk-Othmer Encycl. Chem. Technol.* John Wiley & Sons, 2011.

[5] S. Louhenkilpi, "Continuous Casting of Steel;" pp. 373–434 in *Treatise Process Metall.* Edited by S. Seetharaman. Elsevier, Oxford, UK, 2014.

[6] J. Youn and J. Shim, *Ferrous Metallurgy for Specialists (Vol.2)*. Deayoong, 2004.

[7] T. Emi, "Steelmaking Technology for the Last 100 Years: Toward Highly Efficient Mass Production Systems for High Quality Steels," *ISIJ Int.*, **55** [1] 36–66 (2015).

[8] K.C. Mills, P.E. Ramirez-Lopez, and P.D. Lee, "Insights into the continuous casting process provided by mathematical modelling;" pp. 158–167 in *SANO Symp.* The University of Tokyo, Tokyo, 2008.

[9] K.C. Mills and A.B. Fox, "The Role of Mould Fluxes in Continuous Casting-So Simple Yet So Complex," *ISIJ Int.*, **43** [10] 1479–1486 (2003).

[10] K.C. Mills, "How Mold Fluxes Work;" pp. 435–475 in *Treatise Process Metall.* Edited by S. Seetharaman. Elsevier, Oxford, UK, 2014.

[11] J.E. Jin and Y.K. Lee, "Effects of Al on microstructure and tensile properties of C-bearing high Mn TWIP steel," *Acta Mater.*, **60** [4] 1680–1688 (2012).

[12] J. Mahieu, B.C. Cooman, and J. Maki, "Phase transformation and mechanical properties of si-free CMnAl transformation-induced plasticity-aided steel," *Metall. Mater. Trans. A*, **33A** 2573–2580 (2002).

[13] X. Yu, G.H. Wen, P. Tang, and H. Wang, "Investigation on viscosity of mould fluxes during continuous casting of aluminium containing TRIP steels," *Ironmak. Steelmak.*, **36** [8] 623–630 (2009).

[14] J.L. Li, Q.F. Shu, and K. Chou, "Effect of Al2O3/SiO2 mass ratio on viscosity of $CaO–Al_2O_3–SiO_2–CaF_2$ slag," *Ironmak. Steelmak.*, **42** [2] 154–160 (2015).

[15] X.H. Huang, J.L. Liao, K. Zheng, H.H. Hu, F.M. Wang, and Z.T. Zhang, "Effect of B2O3 addition on viscosity of mould slag containing low silica content," *Ironmak. Steelmak.*, **41** [1] 67–74 (2014).

[16] A.B. Fox, K.C. Mills, D. Lever, C. Bezerra, C. Valadares, I. Unamuno, J.J. Laraudogoitia, and J. Gisby, "Development of Fluoride-Free Fluxes for Billet Casting," *ISIJ Int.*, **45** [7] 1051–1058 (2005).

[17] K.C. Mills, A.B. Fox, Z. Li, and R.P. Thackray, "Performance and properties of mould fluxes," *Ironmak. Steelmak.*, **32** [1] 26–34 (2005).

[18] S. Sridhar, K.C. Mills, O.D.C. Afrange, H.P. Lörz, and R. Carli, "Break temperatures of mould fluxes and their relevance to continuous casting," *Ironmak. Steelmak.*, **27** [3] 238–242 (2000).

[19] J.L. Klug, "Crystallisation Control for Fluorine-free Slags Using the Single Hot Thermocouple Technique;" Universidade Federal do Rio Grande do Sul, 2012.

[20] G.H. Kim and I. Sohn, "Role of B_2O_3 on the Viscosity and Structure in the CaO-Al_2O_3-Na_2O-Based System," *Metall. Mater. Trans. B*, **45** 86–95 (2013).

[21] L.Y. Chen, G.H. Wen, C.L. Yang, F. Mei, C.Y. Shi, and P. Tang, "Development of low-fluoride and titanium-bearing mould fluxes for medium carbon peritectic steel slab casting," *Ironmak. Steelmak.*, **42** [2] 105–111 (2015).

[22] S.Y. Choi, D.H. Lee, D.W. Shin, S.Y. Choi, J.W. Cho, and J.M. Park, "Properties of F-free glass system as a mold flux: Viscosity, thermal conductivity and crystallization behavior," *J. Non-Cryst. Solids*, **345-346** 157–160 (2004).

[23] M. Sakamoto, "溶融酸化物の構造および熱力学的性質・物性への影響;" The University of Tokyo, 2012.

[24] R.L. Naro, J.F. Wallace, and Y. Zhu, *Elimination and Neutralization of Boron in Ductile Irons*. Strongsville, Ohio, 2004.

[25] R.A. Smith., "Boric Oxide, Boric Acid, and Borates;" in *Ullmann's Encycl. Ind. Chem.* 2012.

[26] M. Hubert and A.J. Faber, "On the structural role of boron in borosilicate glasses," *Phys. Chem. Glasses B*, **55** [3] 136–158 (2014).

[27] T. Kloss, G. Lautenschläger, and K. Schneider, "Advances in the process of floating borosilicate glasses and some recent applications for specialty borosilicate float glasses," *Glass Technol-Part A*, **41** [6] 177–181 (2000).

[28] L.P. Pavlova and D. Lepkova, "Low melting borate containing glasses for capacitor ceramics.pdf," *Glass Technol-Part A*, **41** [6] 204–205 (2000).

[29] D. Ehrt, "Structure , properties and applications of borate glasses," *Glass Technol-Part A*, **41** [6] 182–185 (2000).

[30] M.J. Plodinec, "Borosilicate glasses for nuclear waste imobilisation," *Glass Technol-Part A*, **41** [6] 186–192 (2000).

[31] J.C. Lapp, P.L. Bocko, and J.W. Nelson, "Advanced glass substrates for flat panel displays;" pp. 129–138 in *Adv. Flat Panel Disp. Technol.* Edited by P.S. Friedman. San Jose, CA, 1994.

[32] K. Bange, H. Jain, and C.G. Pantano, *Functional Glasses : Properties and Applications for Energy and Information*. Syracuse, Sicily, Italy, 2013.

[33] M.K. Mahapatra and K. Lu, "Glass-based seals for solid oxide fuel and electrolyzer cells - A review," *Mater. Sci. Eng. R Reports*, **67** 65–85 (2010).

[34] J.W. Fergus, "Sealants for solid oxide fuel cells," *J. Power Sources*, **147** 46–57 (2005).

[35] B.H.W.S. De Jong, R.G.C. Beerkens, P.A. van Nijnatten, and E. Le Bourhis, "Glass, 4. Uses and Economic Aspects;" pp. 1–7 in *Ullmann's Encycl. Ind. Chem.* Wiley-VCH, 2000.

[36] K.L. Ley, M. Krumpelt, R. Kumar, J.H. Meiser, and I. Bloom, "Glass-ceramic sealants for solid oxide fuel cells: Part I. Physical properties," *J. Mater. Res.*, **11** [6] 1489–1493 (1996).

[37] F. Tietz, "Thermal expansion of SOFC materials," *Ionics*, **5** 129–139 (1999).

[38] A.C. Wright, G. Dalba, F. Rocca, and N.M. Vedishcheva, "Review Borate versus silicate glasses : why are they so different ?," *Phys. Chem. Glasses B*, **51** [5] 233–265 (2010).

[39] G.N. Greaves and S. Sen, *Inorganic glasses, glass-forming liquids and amorphizing solids*, *Adv. Phys.*, **56** 1–166 (2007).

[40] P. Umari and A. Pasquarello, "Fraction of Boroxol Rings in Vitreous Boron Oxide from a First-Principles Analysis of Raman and NMR Spectra," *Phys. Rev. Lett.*, **95** [September] 6–9 (2005).

[41] P.J. Bray and J.G. O'Keefe, "Nuclear magnetic resonance investigation of the structure of alkali borate glasses," *Phys. Chem. Glasses*, **4** [2] 37–46 (1963).

[42] J. Zhong and P.J. Bray, "Change in boron coordination in alkali borate glasses, and mixed alkali effects, as elucidated by NMR," *J. Non-Cryst. Solids*, **111** 67–76 (1989).

[43] T. Yano, N. Kunimine, S. Shibata, and M. Yamane, "Structural investigation of sodium borate glasses and melts by Raman spectroscopy. II. Conversion between BO_4 and BO_2O^- units at high temperature," *J. Non-Cryst. Solids*, **321** [3] 147–156 (2003).

[44] W.J.J. Dell, P.J.J. Bray, and S.Z.Z. Xiao, "^{11}B NMR studies and structural modeling of Na_2O-B_2O_3-SiO_2 glasses of high soda content," *J. Non-Cryst. Solids*, **58** [1] 1–16 (1983).

[45] L.-S. Du and J.F. Stebbins, "Nature of Silicon−Boron Mixing in Sodium Borosilicate Glasses: A High-Resolution ^{11}B and ^{17}O NMR Study," *J. Phys. Chem. B*, **107** [37] 10063–10076 (2003).

[46] H. Inoue, A. Masuno, and Y. Watanabe, "Modeling of the structure of sodium borosilicate glasses using pair potentials.," *J. Phys. Chem. B*, **116** [40] 12325–31 (2012).

[47] B. MYSEN, *Relationships between silicate melt structure and petrologic processes*, *Earth-Science Rev.*, **27** 281–365 (1990).

[48] R.E. Youngman, S.T. Haubrich, J.W. Zwanziger, M.T. Janicke, and B.F. Chmelka, "Short-and Intermediate-Range Structural Ordering in Glassy Boron Oxide.," *Science*, **269** 1416–1420 (1995).

[49] F. Galeener, "The structure and vibrational excitations of simple glasses," *J. Non-Cryst. Solids*, **123** 182–196 (1990).

[50] S.R. Elliott, "Medium-range structural order in covalent amorphous solids," *Nature*, **354** [6353] 445–452 (1991).

[51] A.C. Wright, "Borate structures: crystalline and vitreous," *Phys. Chem. Glasses B*, **51** [1] 1–39 (2010).

[52] R.E. Youngman and J.W. Zwanziger, "Network Modification in Potassium Borate Glasses: Structural Studies with NMR and Raman Spectroscopies," *J. Phys. Chem.*, **100** [41] 16720–16728 (1996).

[53] P.E. Stallworth and P.J. Bray, "Nuclear Magnetic Resonance in Glass;" pp. 77–149 in *Glas. Sci. Technol. Vol. 4B - Adv. Struct. Anal.* Edited by D.R. Uhlmann and N.J. Kreidl. Academic Press, San Diego, CA, 1990.

[54] K.J.D. MacKenzie and M.E. Smith, *Multinuclear solid-state NMR of inorganic materials*. Pergamon, Oxford, 2002.

[55] L. Frydman, "Fundamentals of Multiple-Quantum Magic-Angle Spinning NMR on Half-Integer Quadrupolar Nuclei;" pp. 262–274 in *Encycl. Nucl. Magn. Reson. Adv. NMR*, 1st ed. Edited by D.M. Grant and R.K. Harris. Wiley, 2002.

[56] J.-P. Amoureux, C. Fernandez, and S. Steuernagel, "Z Filtering in MQMAS NMR," *J. Magn. Reson. Ser. A*, **123** [1] 116–118 (1996).

[57] J.W. Robinson, E.M.S. Frame, and G.M. Frame II, *Undergraduate Instrumental Analysis*, 6th ed. MARCEL DEKKER, New York, 2005.

[58] Y. Fujioka, "Principle of Infrared Absorption Spectroscopy and Its Application," *Bull. Iron Steel Inst. Japan*, **19** [3] 173–179 (2014).

[59] T. Takahashi, "Principles and Applications of Raman Spectroscopy," *Bull. Iron Steel Inst. Japan*, **19** [5] 318–324 (2014).

[60] Y. Waseda and J.M. Toguri, *The Structure and Properties of Oxide Melts*. World Scientific, Singarpore, 1998.

[61] M. KUNUGI, A. KONISHI, S. TAKEUCHI, and T. YAMATE, "Density of Alkali Borate Glasses," *J. Soc. Mater. Sci. Japan*, **21** [230] 978–980 (1972).

[62] D.R. Uhlmann and R.R. Shaw, "The thermal expansion of alkali borate glasses and the boric oxide anomaly," *J. Non-Cryst. Solids*, **1** [5] 347–359 (1969).

[63] N.M.N. Bobkova, "Thermal Expansion of Binary Borate Glasses and Their Structure," *Glass Phys. Chem.*, **29** [5] 501–507 (2003).

[64] Y. Tanaka, Y. Benino, T. Nanba, S. Sakida, and Y. Miura, "Correlation between basicity and coordination structure in borosilicate glasses," *Phys. Chem. Glasses B*, **50** [5] 289–293 (2009).

[65] P.-C. LI, A.C. GHOSE, and G.-J. SU, "Viscosity Determination of Boron Oxide and Binary Borates," *J. Am. Ceram. Soc.*, **45** [2] 83–88 (1962).

[66] W. Kim, "Modeling Viscosity of Molten Slags and Glasses;" École Polytechnique de Montréal, 2011.

[67] S. Ren, J. Zhang, L. Wu, W. Liu, Y. Bai, X. Xing, B. Su, and D. Kong, "Influence of B_2O_3 on Viscosity of High Ti-bearing Blast Furnace Slag," *ISIJ Int.*, **52** [6] 984–991 (2012).

[68] Z. Zhang and R.G. Reddy, "Experimental Determination and Modeling of Na_2O-SiO_2-B_2O_3 Melts Viscosities," *High Temp. Mater. Proc.*, **23** [4] 247–260 (2004).

[69] F.D. Richardson, *Physical chemistry of melts in metallurgy*. Academic Press, London, 1974.

[70] H. Doweidar, Y.M. Moustafa, G.M. El-Damrawi, and R.M. Ramadan, "Electrical conduction in alkali borate glasses; a unique dependence on the concentration of modifier ions," *J. Phys.: Condens. Matter*, **20** [3] 035107 (2008).

[71] L. Shartsis, W. Capps, and S. Spinner, "Viscosity and electrical resistivity of molten alkali borates," *J. Am. Ceram. Soc.*, **36** [10] 319–326 (1953).

[72] K.C. Mills, *Slag atlas*, 2nd ed. Verlag Stahleisen GmbH, Dusseldorf, 1995.

[73] C. Kittel, "Interpretation of the thermal conductivity of glasses," *Phys. Rev.*, **75** [6] 972–974 (1949).

[74] B.H.W.S. De Jong, R.G.C. Beerkens, P.A. van Nijnatten, and E. Le Bourhis, "Glass, 1. Fundamentals;" in *Ullmann's Encycl. Ind. Chem.* Wiley-VCH, 2000.

[75] Y. Kang, J. Lee, and K. Morita, "Thermal Conductivity of Molten Slags: A Review of Measurement Techniques and Discussion Based on Microstructural Analysis," *ISIJ Int.*, **54** [9] 2008–2016 (2014).

[76] A. Nagashima, "Viscosity, thermal conductivity, and surface tension of high-temperature melts," *Int. J. Thermophys.*, **11** [2] 417–432 (1990).

[77] Y. Waseda and H. Ohta, "Current views on thermal conductivity and diffusivity measurements of oxide melts at high temperature," *Solid State Ionics*, **22** 263–284 (1987).

[78] G. Ogura, I.-K. Suh, H. Ohta, and Y. Waseda, "Thermal diffusivity measurement of boron oxide melts by laser flash method," *J. Ceram. Soc. Jpn.*, **98** [3] 305–307 (1990).

[79] H. Ohta, H. Shibata, and Y. Waseda, "Recent Progress In Thermal Diffusivity Measurement of Molten Oxides by The Laser Flash Method;" pp. 453–462 in *Yazawa Int. Symp.* Edited by F. Kongoli, K. Itagaki, C. Yamauchi and H.Y. Sohn. TMS (The Minerals, Metals & Materials Society), San Diego, CA, 2003.

[80] H. Ohta, H. Shibata, H. Hasegawa, T. Kowatari, Y. Shiroki, S.-Y. Kitamura, and Y. Waseda, "Thermal Conductivity of R-Na_2O-SiO_2 (R = Al_2O_3, CaO) Melts," *J. Manuf. Sci. Prod.*, **13** [1-2] 115–119 (2013).

[81] H. Hasegawa, H. Ohta, H. Shibata, and Y. Waseda, "Recent Development in the Investigation on Thermal Conductivity of Silicate Melts," *High Temp. Mater. Proc.*, **31** [4-5] 491–499 (2012).

[82] K.C. Mills, L. Yuan, Z. Li, and G. Zhang, "Estimating viscosities, electrical & thermal conductivities of slags," *High Temp. - High Press.*, **42** 237–256 (2013).

[83] M.J. Assael, K.D. Antoniadis, and W. a. Wakeham, "Historical Evolution of the Transient Hot-Wire Technique," *Int. J. Thermophys.*, **31** [6] 1051–1072 (2010).

[84] H.S. Carslaw and J.C. Jaeger, *Conduction of heat in solids*, 2nd Ed. Oxford University Press, London, 1959.

[85] J. Blackwell, "The axial-flow error in the thermal-conductivity probe," *Can. J. Phys.*, **34** [4] 412–417 (1956).

[86] Y. Kang and K. Morita, "Thermal conductivity of the $CaO-Al_2O_3-SiO_2$ system," *ISIJ Int.*, **46** [3] 420–426 (2006).

[87] S. Ozawa, R. Endo, and M. Susa, "Thermal Conductivity Measurements and Prediction for $R_2O-CaO-SiO_2$ (R= Li, Na, K) Slags," *Tetsu-to-Hagane*, **93** [6] 416–423 (2007).

[88] S.Y. Kwon and S. Lee, "Precise measurement of thermal conductivity of liquid over a wide temperature range using a transient hot-wire technique by uncertainty analysis," *Thermochim. Acta*, **542** 18–23 (2012).

[89] J.J. Healy, J.J. de Groot, and J. Kestin, "The theory of the transient hot-wire method for measuring thermal conductivity," *Phys. B+C*, **82** [2] 392–408 (1976).

[90] K. Nagata, M. Susa, and K.S. Goto, "Thermal conductivities of slags for ironmaking and steelmaking," *Tetsu-to-Hagane*, **11** [11] 1417–1424 (1983).

[91] B. Glaser, L. Ma, and D. Sichen, "Determination of Experimental Conditions for Applying Hot Wire Method to Thermal Conductivity of Slag," *Steel Res. Int.*, **84** [7] 649–663 (2013).

[92] Y. Kang, J. Lee, and K. Morita, "Comment on 'Thermal Conductivity Measurements of Some Synthetic $Al_2O_3-CaO-SiO_2$ Slags by Means of a Front-Heating and Front-Detection Laser-Flash Method,'" *Metall. Mater. Trans. B*, **44** [6] 1321–1323 (2013).

[93] B. Glaser and D. Sichen, "Thermal Conductivity Measurements of Ladle Slag Using Transient Hot Wire Method," *Metall. Mater. Trans. B*, **44B** [1] 1–4 (2012).

[94] Y. Kang, "Thermal Conductivity of Na_2O-SiO_2 and $CaO-Al_2O_3-SiO_2$ melt;" The University of Tokyo, 2004.

[95] K. Nagata and K.S. Goto, "Heat Conductivity and Mean Free Path of Phonons in Metallurgical Slags;" pp. 875–889 in *Second Int. Symp. Metall. Slags Fluxes*. Edited by H.A. Fine and D.R. Gaskell. The Metallurgical Society of AIME, Warrendale, Pa., 1984.

[96] H. Hasegawa, Y. Hoshino, T. Kasamoto, Y. Akaida, T. Kowatari, Y. Shiroki, H. Shibata, H. Ohta, *et al.*, "Thermal Conductivity Measurements of Some Synthetic $Al_2O_3-CaO-SiO_2$ Slags by Means of a Front-Heating and Front-Detection Laser-Flash Method," *Metall. Mater. Trans. B*, **43** [6] 1405–1412 (2012).

[97] Y. Kang, K. Nomura, K. Tokumitsu, H. Tobo, and K. Morita, "Thermal Conductivity of the Molten $CaO-SiO_2-FeO_x$ System," *Metall. Mater. Trans. B*, **43** [6] 1420–1426 (2012).

[98] S. Ozawa and M. Susa, "Effect of Na_2O additions on thermal conductivities of $CaO–SiO_2$ slags," *Ironmak. Steelmak.*, **32** [6] 487–493 (2005).

[99] X. Qiu, B. Xie, X. Qing, J. Diao, Q. Huang, and S. Wang, "Effects of Transition Metal Oxides on Thermal Conductivity of Mould Fluxes," *J. Iron Steel Res. Int.*, **20** [11] 27–32 (2013).

[100] M. Susa, S. Kubota, M. Hayashi, and K.C. Mills, "Thermal conductivity and structure of alkali silicate melts containing fluorides," *Ironmak. Steelmak.*, **28** [5] 390–395 (2001).

[101] K.C. Mills, "The Influence of Structure on the Physico-chemical Properties of Slags.," *ISIJ Int.*, **33** [1] 148–155 (1993).

[102] P.L. Duncanson and J.D. Toth, "The truths and myths of freeze lining technology for submerged arc furnaces;" pp. 488–499 in *INFACON X Transform. through Technol.* The South African Institute of Mining and Metallurgy, Cape Town, South Africa, 2004.

[103] J.D. Steenkamp, M. Tangstad, and P.C. Pistorius, "Thermal conductivity of solidified manganese-bearing slags — A preliminary investigation;" pp. 327–344 in *South. African Pyrometallurgy 2011 Int. Conf.* Edited by R.T. Jones and P. den Hoed. The Southern African Institute of Mining and Metallurgy, Johannesburg, South Africa, 2011.

[104] L.R. Pinckney, "Glass Ceramics;" in *Ullmann's Encycl. Ind. Chem.* Wiley-VCH, 2000.

[105] R. Gardon, "A Review of Radiant Heat Transfer in Glass," *J. Am. Ceram. Soc.*, **44** [7] 305–312 (1961).

[106] L. Van Der Tempel, G. Melis, and T. Brandsma, "Thermal conductivity of a glass: I. Measurement by the glass–metal contact," *Glass Phys. Chem.*, **26** [6] 606–611 (2000).

[107] M. Zaitlin and A. Anderson, "Thermal Conductivity of Borosilicate Glass," *Phys. Rev. Lett.*, **33** [19] 1158–1161 (1974).

[108] M. Tohmori, T. Sugawara, S. Yoshida, and J. Matsuoka, "Thermal conductivity of sodium borate glasses at low temperature," *Phys. Chem. Glas. Eur. J. Glas. Sci. Technol. Part B*, **50** [6] 358–360 (2009).

[109] N.A. Ghoneim and M.M. Halawa, "Effect of boron oxide on the thermal conductivity of some sodium silicate glasses," *Thermochim. Acta*, **83** [2] 341–345 (1985).

[110] M. Susa, M. Watanabe, S. Ozawa, and R. Endo, "Thermal conductivity of $CaO–SiO_2–Al_2O_3$ glassy slags: Its dependence on molar ratios of Al_2O_3/CaO and SiO2/Al2O3," *Ironmak. Steelmak.*, **34** [2] 124–130 (2007).

[111] S. Samal, J. Lee, D.-Y. Jeong, and H. Kim, "Characterization of thermal conductivity of $SiO_2–Al_2O_3–Y_2O_3$ glasses," *Thermochim. Acta*, **604** 1–6 (2015).

[112] M.M. Ammar, S. Gharib, M.M. Halawa, K. El Badry, N.A. Ghoneim, and H.A. El Batal, "Thermal conductivity of some silicate glasses in relation to composition and structure," *J. Non-Cryst. Solids*, **53** [1-2] 165–172 (1982).

[113] M.M. Ammar, M.M. Halawa, N.A. Ghoneim, A.F. Abbas, and H.A. El Batal, "Thermal Conductivity of Lead Borate Glasses," *J. Am. Ceram. Soc.*, **65** [10] c174–c175 (1982).

[114] M.K. Choudhary and R.M. Potter, "Heat Transfer in Glass-Forming Melts;" pp. 249–293 in *Prop. Glas. Melts*, 1st ed. Edited by L.. D. Pye, A. Montenero and I. Joseph. CRC Press, Boca Raton, 2005.

Chapter II

Thermal Conductivity of the molten B_2O_3, B_2O_3-SiO_2 system

2.1 Background

Although understanding of the relationship between thermal conductivity and the borate structure is significant, due to its complicated structure change of B_2O_3 and experimental difficulty of thermal conductivity measurement, even thermal conductivity of pure B_2O_3 melt has not been fully investigated especially in the molten state. Until 1970's, the molten borate structure was controversial. Several models; random network model, quasi-crystalline model and molecular model were proposed in order to explain the borate structure.[1] Owing to the development of structural investigation techniques; such as NMR, Raman spectroscopy or molecular dynamic calculation, the borate structure in the molten state was revealed and widely accepted as random network structure consisting of boroxol ring.

However, recent structural investigation studies performed at high temperature of molten state show that the borate structure of pure B_2O_3 is changed with increasing temperature. Along with a structural change, several anomalous physical properties change of molten B_2O_3 can be observed. For instance, density change with temperature shows that borate structure has intermediate structure between dense and open structure within the temperature region from glass transition temperature to approximately 1273 K. In addition, activation energy which is the frictional resistance for viscous flow shows non-Arrhenius behavior between 573 and 1273 K. As previously mentioned, physical properties of molten oxide is closely related to the change of network structure. Therefore, considering the temperature dependence of other physical properties of the molten B_2O_3, it can be inferred that thermal conductivity will be also affected by varying temperature.

In this chapter, thermal conductivity of molten B_2O_3 was investigated. In addition, in order to evaluate the effect of borate and silicate network structure on thermal conductivity, thermal conductivity of the B_2O_3-SiO_2 binary system was studied along with structural investigation.

2.2 Experiment

2.2.1. Sample Preparation

For the measurement of the thermal conductivity of the B_2O_3, a powder mixture of reagent grade was pre-melted in a platinum crucible and kept at 1273, in order to dehydrate, and homogenize the mixture. After 2 hours, the melt was quenched on a copper plate. The resultant glass was finely crushed and placed in a Pt-10%Rh crucible (I.D: 32 mm, O.D: 38 mm, height: 70 mm).

In the case of B_2O_3-SiO_2 system, the sample was prepared in a different way, due to the high viscosity of the material. The finely ground powder mixture of B_2O_3, SiO_2 and Fe_2O_3 was brought to 200 MPa in order to obtain pellet with a diameter of 12 mm. Fe_2O_3 was added in order to reduce the spin-lattice relaxation time for the MAS-NMR measurements of the ^{29}Si isotope. Addition of paramagnetic ions results in the short relaxation time by an aid of fluctuating magnetic fields. However, higher concentration of paramagnetic ions (as rule of thumb, 5 % of Fe_2O_3) leads to the shift of signal intensity along with broadening of spectra.[2] For this reason, 0.1 mol % of Fe_2O_3 was added.

The sample pellet equipped with a hot-wire consisting of a 0.15 mmϕ Pt-13%Rh wire and a Pt wire, was placed on a platinum mesh plate and pre-melted at 1773 K for 24 hours.

2.2.2. Thermal Conductivity Measurement

Using the hot-wire method, the thermal conductivity of the B_2O_3 was measured. Using a PID (proportional integral differential) controller and calibrated B-type thermocouple, sample temperature was controlled. The upper part of sample is intentionally placed at the highest temperature zone, in order to avoid natural convection during measurement. Approximately 90 g of pre-melted sample is heated in an electric resistance furnace equipped with SiC at 1673 K, and then held for 1 hour to obtain a homogeneous molten oxide. Thermal conductivity was measured at 100 K intervals from 1673 K to the liquidus temperature of 873 K. Using a galvanostat, a constant current of 0.8–1.5 A was supplied to a 0.15mmϕ Pt-13%Rh hot-wire, and any voltage change between the two terminals of the wire was monitored by a digital multimeter. A linear relationship between ΔV and lnt was obtained within 0.8–2.0 seconds, and the thermal conductivity, λ ($Wm^{-1}K^{-1}$), was calculated by the equation (1-18).

For the B_2O_3-SiO_2 system, the conventional approach, with a hot-wire driven into the molten oxide at high temperature, was inapplicable, due to its extremely high viscosity. Figure

2-1 shows the schematic diagram of the modified thermal conductivity measurement apparatus used for the B_2O_3-SiO_2 system. Before the sample was pre-melted, a 0.15 mmϕ Pt-13%Rh wire was welded with a 0.15 mmϕ Pt wire and placed inside the sample pellet. After the pre-melting stage, the full circuit of the apparatus was established, and the sample hung on the alumina lance. Then, the measurement device was placed in the zone at the highest temperature of a vertical furnace equipped with a SiC heating element. After an hour at 1773 K, the thermal conductivity of the sample was measured from 1773 K to 1623 K at intervals of 50 K intervals.

During the measurement, to ensure the thermal equilibrium of the system, the furnace temperature was decreased at a rate of 3 K/min and held for 15 minutes at the target temperature. To confirm the reproducibility of the results, the measurement was repeated three times at the same temperature, with a 5-minutes interval between one measurement and the following one.

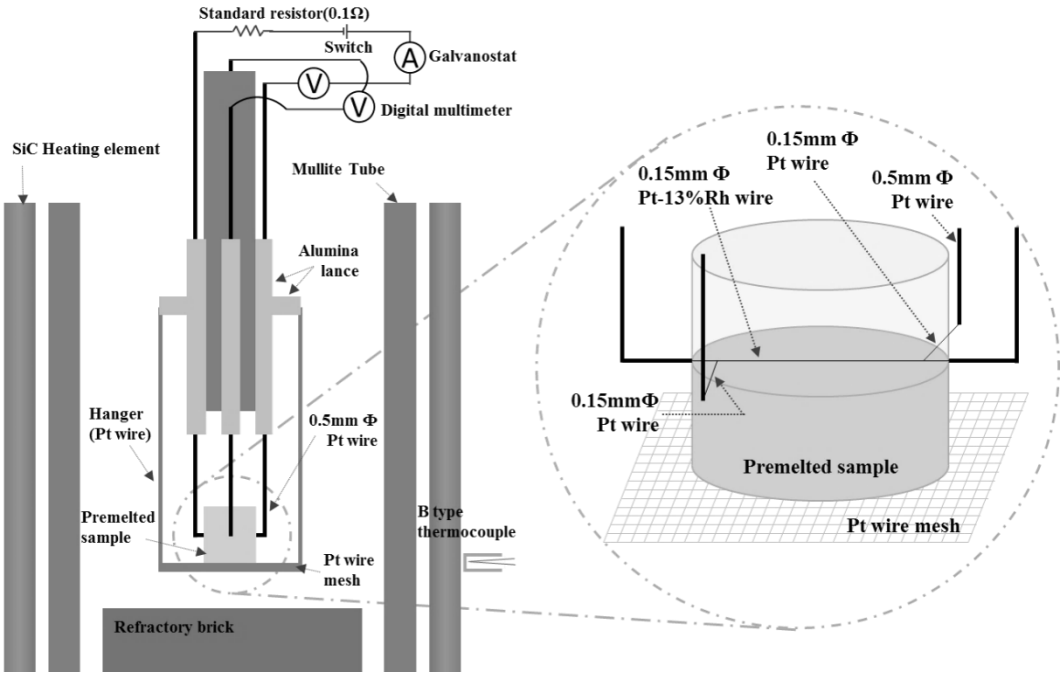

Fig. 2-1. Schematic diagram of the thermal conductivity measurement apparatus for the molten B_2O_3-SiO_2 binary system.

2.2.3. Analytical Procedures

2.2.3.1. Determination of the boron concentration in the sample

Following the measurement of thermal conductivity by the hot-wire method, the solidified samples were re-melted. The melts were poured onto a water-cooled copper plate and quickly covered with a copper block. The obtained glass was ground and sieved using a 100 μmϕ mesh. In order to evaluate the boron oxide concentration in the B_2O_3-SiO_2 system, approximately 0.01 g of the ground sample was transferred into 100 ml of beaker. Following the addition of acid-solution (10 ml of distilled water + 15 ml of HCl + 5 ml of HNO_3), the beaker was placed on the hot-plate covered with watch glass, and then heated at 493 K for several hours. When the almost of the acid solution was evaporated, approximately 5 ml of $HClO_4$ was added, and kept on heating until white smoke appeared.

The heated beaker was cooled down at room temperature. The solution was filtered using a filter paper (ash contents 0.1 mg/circle) attached on glass funnel, and transferred into 100 ml of volumetric flask. After rinsing the beaker and filter paper several times by distilled water, the final volume was made to given 100 ml. In order to obtain the homogeneous concentration across the solution, the volumetric flask was kept for 24 hours.

Using the inductively coupled plasma atomic emission spectroscopy (ICP-AES; SPS7700, SII NanoTechnology, Japan), final concentration of boron was determined. Diluting the 1000 ppm of boron standard solution (Kanto chemical, Tokyo, Japan), 1, 2, 5 and 10 ppm of boron standard solution was prepared. Using the four standard solutions, calibration line of boron was drawn from 0 to 10 ppm showing larger than 0.999 of correlation coefficient. During the analysis, 249.773 nm of wavelength was chosen for boron as analytical wavelength.

Table 2-1 shows the final composition of boron oxide in theB_2O_3-SiO_2 system.

2.2.3.2. Determination of the silicon concentration in the sample

The SiO_2 content was determined by silica gravimetric method. The analyzed final compositions are listed in Table 2-1.

The detailed procedures are described as follows.

① The 0.1 g of ground sample (*w*) is transferred into 100 ml beaker, and then dissolved in 50 ml of diluted HCl (1:1) solution at 423 K on the hot-plate.

② 5 ml of HNO_3 and 10 ml of $HClO_4$ are added, and then the solution is heated at 493 K until white smoke is observed.

③ The residual of transparent gel is rinsed by 30 ml of diluted HCl (1:4). Using rubber policeman, the remained gel is transferred onto filter paper attached on the glass funnel. In order to eliminate the acid-soluble elements, the filter and residual are washed several times using diluted HCl (1:10) followed by hot distilled water.

④ After drying, the filter paper along with residuals is transferred into Pt-crucible. In the muffle furnace, the filter paper is burnt and removed at 1373 K.

⑤ After 1 hour, Pt-crucible is transferred into the desiccator and cooled down. The remained white particle is observed on the bottom of Pt-crucible.

⑥ Using digital weighing scale, the weight of residual along with Pt-crucible is determined. (w_i)

⑦ In order to remove Si from residual particle, 5 ml of HF and 3 – 4 drops of diluted H_2SO_4 (1:1) is added into the Pt-crucible. Then, the Pt-crucible is heated at 330 °C on hot-plate. During the heating process, SiO_2 in the residual particle is removed by the following reaction.

$$SiO_2(s) + 4HF(l) = 2H_2O(l) + SiF_4(g) \qquad (2\text{-}1)$$

⑧ Following the confirmation of no residual in the Pt-crucible, the Pt-crucible is transferred into muffle furnace and heated at 1373 K for 30 min.

⑨ After cooling down in a desiccator, the final weight of Pt-crucible is weighed. (w_f).

⑩ The weight fraction of SiO_2 (w_{SiO2}) in the initial sample can be calculated by the following equation (2-2).

$$w_{SiO_2} = \frac{w_i - w_f}{w} \qquad (2\text{-}2)$$

Table 2-1. Initial and final composition of the present experiment.

Initial (mol %)				**Final (mol %)**			**Remarks**
B_2O_3	**SiO_2**	**Fe_2O_3**		**B_2O_3**	**SiO_2**	**Fe_2O_3**	**$BO_{1.5}/SiO_2$**
100	-	-		100	-	-	-
9.1	90.8	0.1		9.7	90.2	0.1	0.2
16.6	83.2	0.1		17.0	82.9	0.1	0.4
23.0	76.8	0.1		22.9	77.0	0.1	0.6

2.2.4. Structural Investigation

2.2.4.1. X-ray diffraction (XRD) analysis

After the thermal conductivity measurement, structure of quenched glass sample was investigated. Using X-ray diffraction (XRD; RINT 2500, Rigaku, Tokyo, Japan), non-crystalline state was determined. The powder sample was placed on the glass plate grooved with 2.1 cm x 1.5 cm and 0.01 cm depth. The evenly flatten powder was fixed using the solution mixture of cellulose adhesive (Cemendine C; Cemendine cooperative, Tokyo, Japan) and a volatile organic solvent; acetone. The diffraction pattern was continuously collected within 2θ = 10 – 90 degree at a scanning rate 2 degree/min and sampling rate 0.02 degree. During the analysis, X-ray was generated using copper tube operated at 50 kV and 300 mA. Divergence slit (DS) and scattering slit (SS) were 1 degree, and receiving slit (RS) was 10 mm. Figure 2-2 shows the XRD spectra of B_2O_3-SiO_2 glass sample.

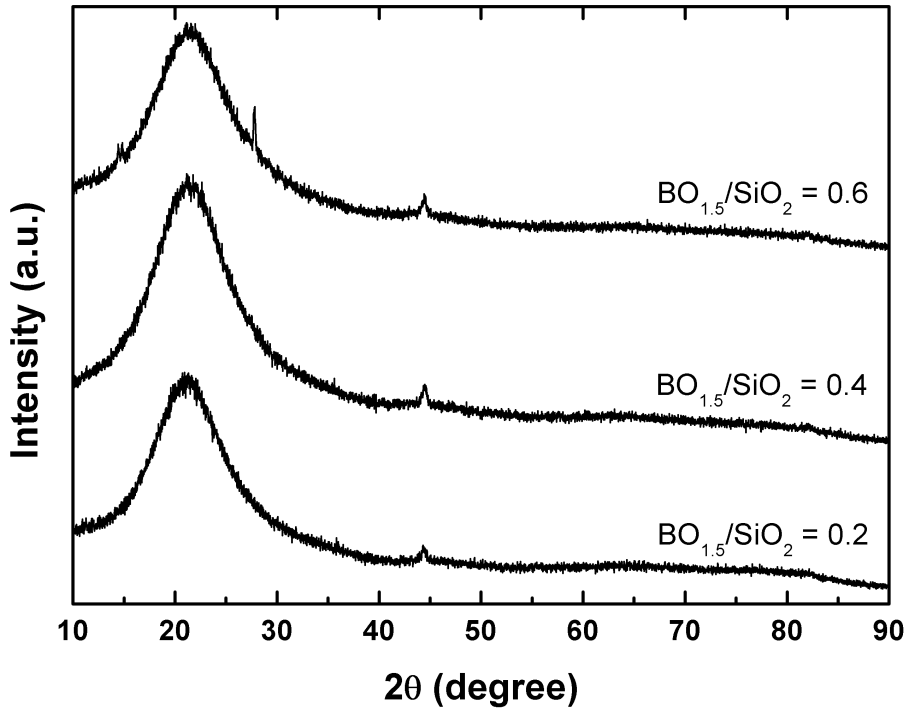

Fig. 2-2. X-ray diffraction pattern of B_2O_3-SiO_2 system.

2.2.4.2. MAS NMR and 3Q MAS analysis

Solid state ^{29}Si, ^{11}B magic angle spinning (MAS) and ^{11}B triple quantum magic angle spinning (3Q-MAS) NMR spectra were recorded at 11.74 T using a FT-NMR spectrometer

(ECA-500, JEOL, Japan). The Larmor frequency was 99.4 MHz for ^{29}Si MAS NMR and 160.4 MHz for ^{11}B MAS and 3Q-MAS NMR. Each sample was placed in a ZrO_2 holder (Inner diameter 4 mm) and spun at 16 kHz. Before the analysis, standards of ^{11}B and ^{29}Si MAS NMR were calibrated using a saturated H_3BO_3 solution (19.49 ppm) and 3-(Trimethylsilyl) propionic-2,2,3,3-d_4 acid sodium salt (98 atom % D) (1.445 ppm).

The spin-lattice relaxation time (T_1); the recovery time of magnetization along z-axis right after pulse excitation,[3] and 90 degree pulse were determined by saturation-recovery method. Figure 2-3 shows the saturation-recovery of ^{29}Si MAS NMR spectra for determination of the spin-lattice relaxation time. It can be observed that addition of Fe_2O_3; which has unpaired electron, drastically decreases in spin-lattice relaxation time. The detailed conditions for the MAS NMR measurements are summarized in Table 2-2. For the ^{11}B 3Q-MAS NMR measurement, a three-pulse z-filter sequence[4] was adopted. The first and second pulses of duration were set to 4.9 μs and 1.7 μs, respectively, and the third pulse of duration was set to 14 μs with a relaxation delay of 5 s.

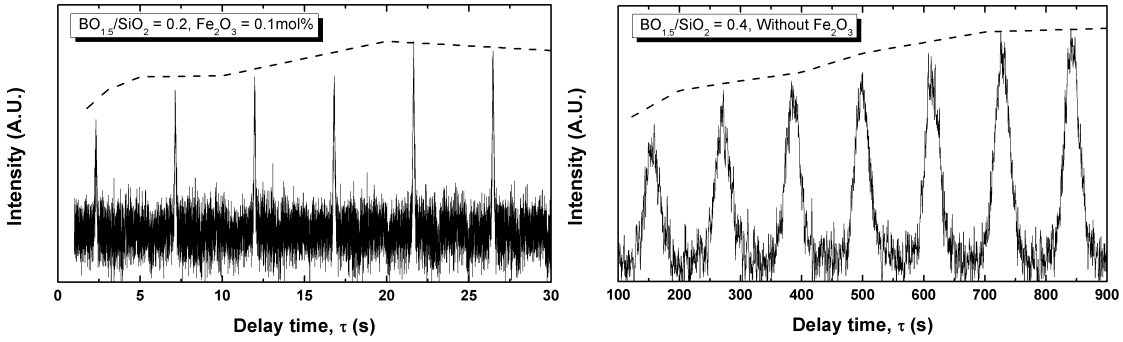

Fig. 2-3. The saturation-recovery of ^{29}Si MAS NMR spectra for spin-lattice relaxation time. **(a)** $BO_{1.5}/SiO_2$ = 0.2, with 0.1 mol% of Fe_2O_3, **(b)** $BO_{1.5}/SiO_2$ = 0.4, without Fe_2O_3

Table 2-2. Experimental conditions for the MAS-NMR measurements.

Nuclear Property	**^{11}B**	**^{29}Si**
Nuclear Spin	3/2	1/2
Larmor frequency [MHz]	160.4	99.4
RF pulse intensity [kHz]	61	45
Repetition times	64	1000
Flip angle [rad]	π/6	π/2
Delay time [s]	5	20
Spinning rate [kHz]	16	16

In order to confirm the effect of Fe_2O_3 addition on the structure of B_2O_3-SiO_2 system and broadening of NMR spectrum, ^{29}Si MAS NMR spectra was carried out in the system with/without Fe_2O_3. As shown in Figure 2-4, any significant difference cannot be observed in the presence of Fe_2O_3 indicating the negligible effect of 0.1 mol% Fe_2O_3 on the present B_2O_3-SiO_2 binary system.

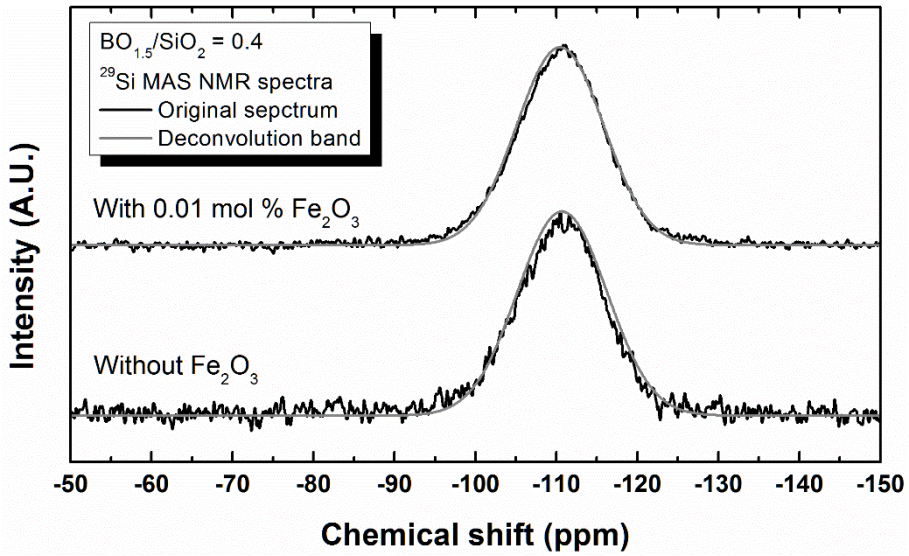

Fig. 2-4. ^{29}Si MAS NMR spectra of the B_2O_3-SiO_2 system with/without Fe_2O_3.

2.2.4.3. Raman spectroscopy

Structural investigation was carried out using Raman spectroscopy (T-64000, Horiba Jobin-Yvon, France), with excitation provided by an argon ion laser with the wavelength of 514 nm operated at 100 mW.

The powder sample was placed on the glass plate. Ar ion laser was irradiated through microscope lens of x50 magnification. The backscattered Raman signal was collected by liquid nitrogen cooled charge-coupled device (CCD) in the wavenumber range of 400 to 1600cm^{-1}. Although Raman spectroscopy provides information on molecular vibrations, the structural information cannot be obtained directly from the Raman spectra. Thus, in order to obtain the structural information, the spectra separating procedure was preceded by Gaussian deconvolution using PeakFit (Ver.4.06) software.

2.3 Results and Discussion

2.3.1. Evaluation of the Experimental Errors During thermal conductivity measurement

As previously mentioned, due to the radiation and convection effect, measurement of thermal conductivity in the molten oxide system is challenging at high temperature. In addition, it results in the significant experimental errors overestimating the thermal conductivity. Although a hot-wire method has a merit on measuring thermal conductivity at high temperature, qualitative evaluation of experimental error is required. Therefore, the experimental errors occurred during the thermal conductivity measurement will be discussed in this section.

2.3.1.1. Convection effect during the thermal conductivity measurement

At high temperature, thermal gradient in the molten oxide system can result in the tremendous convection along with drastic increasing of thermal conductivity. In order to reduce the natural convection, top of the liquid oxide melt was deliberately placed at the hottest temperature zone. However, during the measurement, the heating-up of hot-wire results in the increase in temperature of molten oxide system along with partial temperature difference. Such temperature gradient would lead to the convection.

In order to determine the effect of convection, the change of Rayleigh number with varying time was considered. Figure 2-5 shows the schematic diagram of heat penetration during a hot-wire measurement.

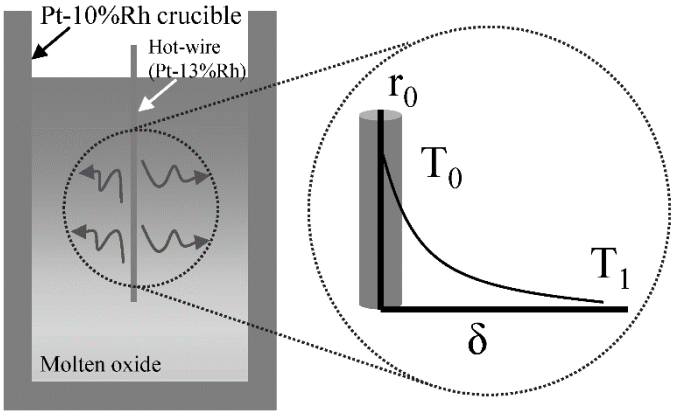

Fig. 2-5. Schematic diagram of heat penetration during a hot-wire measurement.

When a current is applied, heat is generated in a thin hot-wire; radius of r_0. Since it is a non-steady state method, the heat penetration distance will be varying with time. δ is the the penetration distance. T_0 and T_1 is the temperature at the surface of hot-wire and δ, respectively. The heat penetration distance (δ) is the function of time (t). Tokura et al.,[5] reported that heat penetration distance from the hot-wire can be expressed by the following equation.

$$\delta \approx \left(24\alpha r_0 t\right)^{1/3} + r_0 \tag{2-3}$$

Above equation (2-3) is valid when ($\delta - r_0$) >> $4r_0$. α represents the thermal diffusivity.

It has been reported that free convection is occurred when Rayleigh number (Ra) is larger than 1000. Therefore, calculation of Rayleigh number in the present molten oxide system is significant in order to evaluate the effect of free convection during the experiment. Rayleigh number can be expressed by the following equation, which is the product of Grashof number and Prandtl number.

$$Ra = \frac{\beta \Delta T g L^3}{\nu \alpha} \tag{2-4}$$

Where β is thermal expansion coefficient of slag, ΔT is temperature difference, g is gravitational acceleration, L is characteristic length, v is kinetic viscosity. L can be substituted with heat penetration distance (δ). Combine the equation (1-13), (2-3) and (2-4), Rayleigh number can be deduced by following equation.

$$Ra = \frac{\beta g Q}{4\pi\lambda\nu\alpha}\left[(24\alpha r_0 t)^{1/3} + r_0\right]^3 \ln\left(\frac{4\alpha t}{r_0^2 C}\right) \tag{2-5}$$

Where C is the exponential of Euler's constant; 1.78. Using the equation (2-5) along with following physical properties of molten B_2O_3 system at 1273 K, Rayleigh number was calculated. Thermal expansion coefficient of molten B_2O_3 (β) is 100 ppm / K at the temperature range between 1273 and 1473 K.[6] Thermal diffusivity (α) is 4.325 cm^2s^{-1} at 1273 K.[7] Kinematic viscosity; the ratio of dynamic viscosity to density is 0.0065 $m^2\ s^{-1}$.[8] Considering the present thermal conductivity value, Rayleigh number is calculated and it is shown in Fig. 2-6. Compared to Rayleigh number of pure water at 298 K, present molten B_2O_3 shows much lower Rayleigh number. Due to the much higher kinematic viscosity and thermal diffusivity, B_2O_3 shows much lower Rayleigh number even at high temperature of

1273 K. Therefore, it can be conclude that there is no free convection effect during the thermal conductivity measurement of molten oxide system within 10 s; which is the typical measuring time.

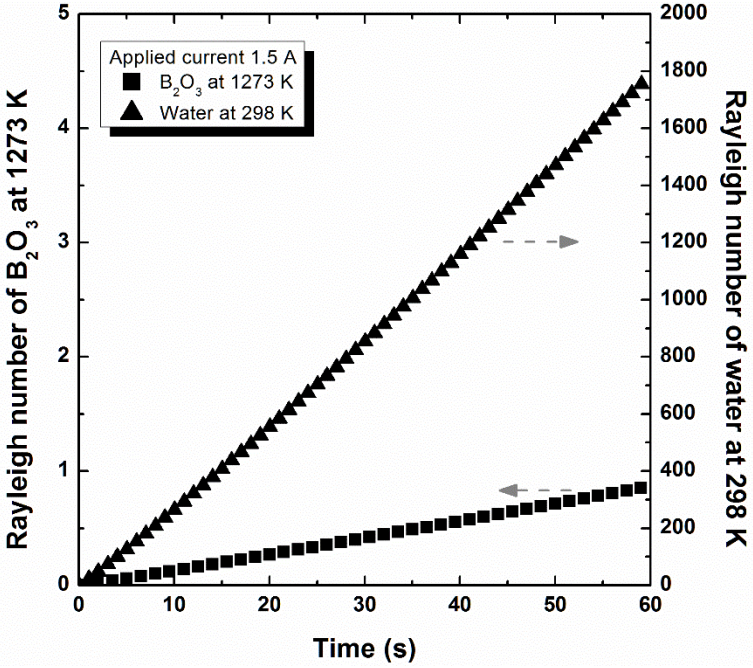

Fig. 2-6. Calculated Rayleigh number of molten B_2O_3 at 1273 K (left) and water at 298 K (right) with varying time.

2.3.1.2. Radiation effect during the thermal conductivity measurement

Although a hot-wire method uses extremely thin wire, the heat can be transferred from the surface of hot-wire by radiation and it becomes significant with higher temperature during the thermal conductivity measurement.

Using the Stefan–Boltzmann law for grey-body radiation, the radiation heat at the surface of hot wire was estimated.

$$q = \varepsilon E_b = \varepsilon \sigma T_s^4 \qquad (2\text{-}6)$$

where q is the radiated heat energy, ε is the emissivity, σ is the Stefan-Boltzmann constant, T_s is the surface temperature (K). During the calculation, emissivity of Pt-13%Rh wire was extrapolated on the basis of empirical equation of emissivity of Pt- 10%Rh wire.[9]

$$\varepsilon = 0.751(T\rho)^{0.5} - 0.632(T\rho) + 0.670(T\rho)^{1.5} - 0.607(T\rho)^2 \qquad (2\text{-}7)$$

where, ρ is the resistivity, and T is the temperature of hot-wire (^oC). The temperature change of hot-wire along with heat generation was evaluated by the voltage change. Considering the resistivity of hot-wire, the radiation heat during the measurement was evaluated. In Fig. 2-7, change of radiation heat along with applied power at 1273 K is displayed. After 5 s of experiment, the ratio of radiation heat to the applied power; which is the net heat flow, becomes approximately 0.69 % at 1273 K. This value is accordance with the previously calculated value of 1 % in the transparent slag at 1273 K after 5 s of experiment.[10] Especially, within the thermal conductivity measurement region; which is 0.8 to 2 s, radiation heat takes less than 0.51 % over total heat flow. Therefore, it can be concluded that radiation effect is not significant during the thermal conductivity measurement using a hot-wire method.

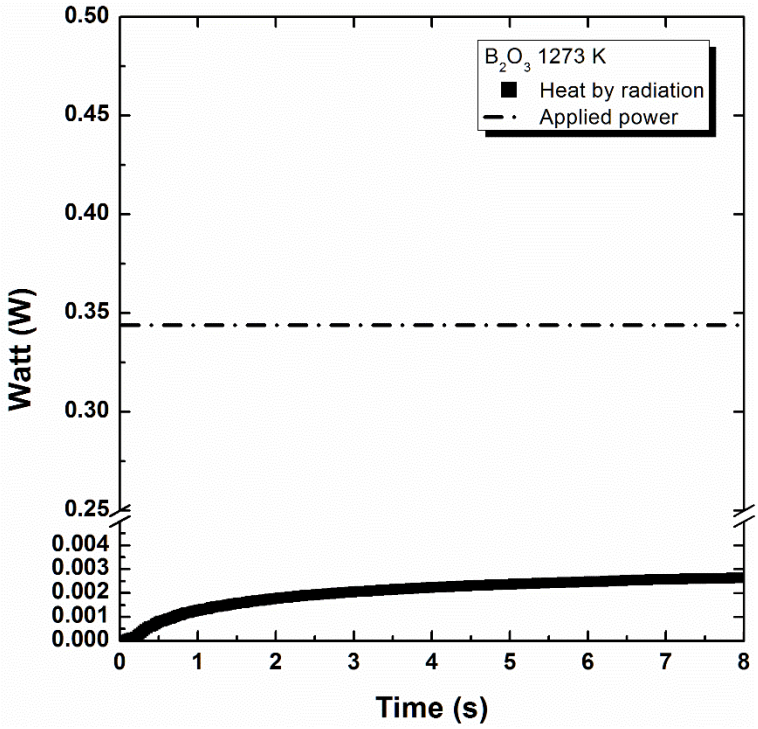

Fig. 2-7. Change of radiation heat (black rectangular) with varying time at a fixed temperature of 1273 K. Dashed line indicates the applied power.

2.3.1.3. Another errors during the thermal conductivity measurement

Due to the high temperature experimental condition along with usage of various measurement apparatuses, several systematic errors are evolved during the thermal

conductivity measurement. During the experiments, the temperature of sample was controlled by the PID (proportional integral differential) controller and calibrated B-type thermocouple (Pt-30%Rh/Pt-6%Rh) within±3 K. In order to heat the hot wire, constant current was applied by galvanostat, and the current was determined between the standard resistor of 0.1 Ω (Yokogawa 2792, Yokogawa, Tokyo, Japan); accuracy of 0.01%. Any voltage change between the potential leads at a four-terminal hot-wire sensor was recorded using digital multimeter (Keithley 2000, Keithley instruments, Cleveland,OH,USA); accuracy of 0.002%. The systematic errors are listed in Table 2-3.

At each temperature, the thermal conductivity was measured three times at intervals of 5 min to examine the reproducibility. The random error was determined by the standard deviation of the repetitive measurements[11], and it is displayed in the figures as error bar.

Table 2-3. Estimation of the systematic errors on the thermal conductivity measurement.

Uncertainty component	Relative uncertainty
Temperature calibration	0.2 %
Accuracy of standard resistor	0.01 %
Resolution of digital multimeter	0.002 %
Heat by radiation	< 0.7 %

2.3.2. Thermal Conductivity of the Molten B_2O_3

Thermal conductivity of molten B_2O_3 was measured. Although several previous studies reported the thermal conductivity of B_2O_3 melt, hot-wire method has not been adopted. From the measurement of thermal conductivity using hot-wire method, the validity of hot-wire technique can be confirmed. In addition, measurement temperature of previous study has been carried out below 1273 K. Considering that melting process of glass and steelmaking process requires relatively high temperature, thermal conductivity data of higher temperature is in demand.

In order to confirm the temperature dependence, thermal conductivity of B_2O_3 melt was measured from 1673 K to 873 K and it is shown in Fig. 2-8. From the results reported by Nilsson et al.[12] on the thermal conductivity of vitreous boron oxide measured at room temperature, it seems that the thermal conductivity of B_2O_3 gradually increases with an increase in temperature up to 1400 K, and then decreases. Compared to previously reported thermal conductivity data; which was measured by coaxial cylinders technique[13], present works shows relatively low thermal conductivity.

Ogura et al.[7] measured thermal diffusivity using three-layered laser-flash method from 1000 to 1400 K. According to their result, thermal diffusivity also gradually increases with higher temperature. Referring to thermal diffusivity along with heat capacity and density,[7, 8, 14] thermal conductivity of molten B_2O_3 was calculated by following equation on the basis of the equation with appropriate references.

$$\lambda = C\rho\kappa \tag{2-8}$$

where λ is the thermal conductivity ($Wm^{-1}K^{-1}$), C is the specific heat capacity ($Jkg^{-1}K^{-1}$), ρ is the density (kg/m^3) and κ is the thermal diffusivity (m^2/s). The calculated thermal conductivity of B_2O_3 is plotted in Fig. 2-8, and it is in excellent accordance with the measured thermal conductivity, supporting the validity of the measurements carried out in the present work.

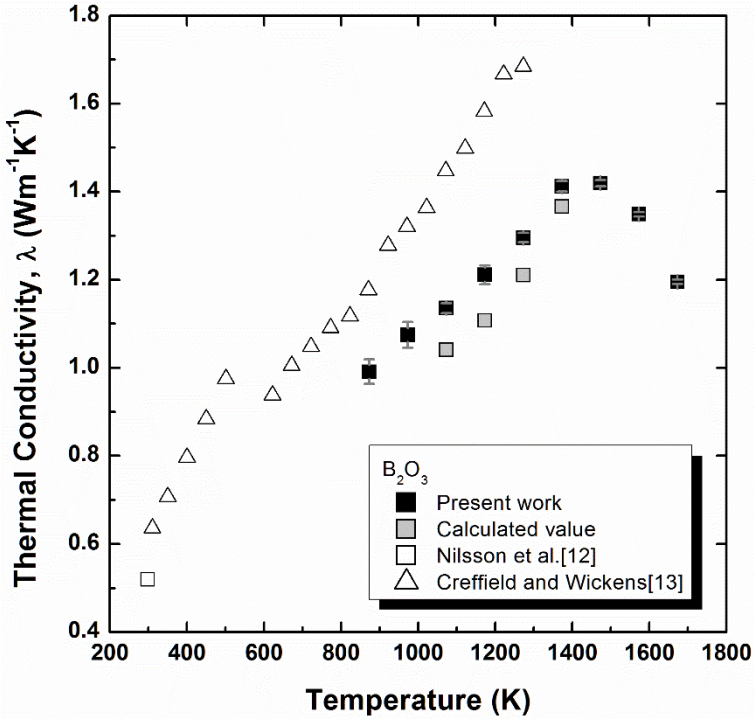

Fig. 2-8. Change of thermal conductivity with varying temperature.

In a dielectric material, the thermal energy is mainly transferred not by electrons, but by phonons,[15] through the quantized normal modes of lattice vibration. Analogous to the kinetic theory, Kittel[16] expressed the thermal conductivity (λ) caused by phonons as the transport of energy by particles. Considering the particle diffusion, the flux density J_n can be expressed by the function of particle diffusion constant (D) and gradient of the particle concentration (grad n) along the system which is also known as Fick's law.

$$J_n = -D \,\text{grad}\, n \tag{2-9}$$

Assuming the particle diffusion in the z direction of hemisphere, the new equation can be obtained.

$$J_n^z = \frac{1}{2}[n(z-l_z) - n(z+l_z)]\bar{v}_z = -\frac{dn}{dz}\bar{v}_z l_z \tag{2-10}$$

The $\bar{v}_z$ is the particle speed on the z axis, l_z is the z component of the mean free path and dn/dz is the particle flux density in the z axis. In order to expressed $\bar{v}_z l_z$ in terms of $\bar{v}l$, a projection with the angle of θ was considered along with the surface area of hemisphere.

$$< \bar{v}_z l_z >= \bar{v} l \frac{2\pi r^2 \int_0^{\frac{1}{2}\pi} \cos^2\theta \sin\theta d\theta}{2\pi r^2} = \frac{1}{3}\bar{v} l \tag{2-11}$$

In the equation (2-10), according to the substitution of $\bar{v}_z l_z$ with calculated average value of $< \bar{v}_z l_z >$, it can be obtained that equation (2-11) represents particle diffusion coefficient of *D*.

Analogy to Fick's law, thermal conductivity is expressed by the Fourier's law.

$$J_u = -\lambda \text{ grad } \tau \tag{2-12}$$

The J_u represents the energy flux density, the λ is thermal conductivity and the grad τ means temperature gradient. Because Kittel[16] assumed thermal conductivity as the transport of energy by particle, the energy flux density(J_u) can be expressed by the function of particle diffusivity (*D*) and the gradient of energy density;

$$J_u = -D\frac{d\rho_u}{dx} = -D\frac{d\rho_u}{d\tau}\frac{d\tau}{dx} = -DC\frac{d\tau}{dx} \tag{2-13}$$

$$\lambda = DC \tag{2-14}$$

On comparison with (2-12), it can be inferred that the thermal conductivity (λ) is expressed by in terms of particle diffusivity (*D*) and heat capacity per unit volume ($d\rho_u/d\tau$). Therefore, thermal conductivity can be finally expressed by the following equation;

$$\lambda = \frac{1}{3}C\bar{v} l \tag{2-15}$$

According to Ziman,[17] the mean particle velocity can be approximated as the average velocity of sound (*s*); thus, the thermal conductivity is mainly determined by both the specific heat capacity and the phonon mean free path of collision. At the high temperature of a molten oxide system, where the specific heat capacity becomes constant, the thermal conductivity is mainly determined by a change in the phonon mean free path, which gradually decreases with the increasing temperature due to both the structural changes and an increase in the phonon-phonon interaction. A decrease in the phonon mean free path results in a decrease of the

thermal conductivity at higher temperatures; such a negative temperature dependence of thermal conductivity has been reported for several molten oxide and fluoride systems.[10, 18–26]

However, in the present study, a positive temperature dependence of thermal conductivity was observed below 1400 K implying that the phonon mean free path of the molten B_2O_3 system does not decrease at higher temperatures, in contrast with other systems.

Various structural investigations[27–32] of molten B_2O_3 have commonly found that boroxol ring structure breaks up with higher temperature by formation of BO_3 triangles in random network. Grimsditch et al.[30] studied the temperature dependence of a hypersonic sound wave and found the existence of transverse modes between glass transition temperature and 1300 K of B_2O_3 system, indicating the presence of a coordinated network in the intermediate-range order. Similarly, Misawa[31], who measured molten B_2O_3 structure using pulsed neutron total scattering, found that structural units gradually change into chain-like segments in the three-dimensional networks as a result of opening of boroxol ring above glass transition temperature. Therefore, it can be inferred that the structure of boron oxide changes with higher temperatures forming an incorporated random network structure. Wright et al.[33] also reported such a breaking of borate structure along with formation of BO_3 triangles in random network and called it *Double bond-switching mechanism*; which is shown in Fig. 2-9.

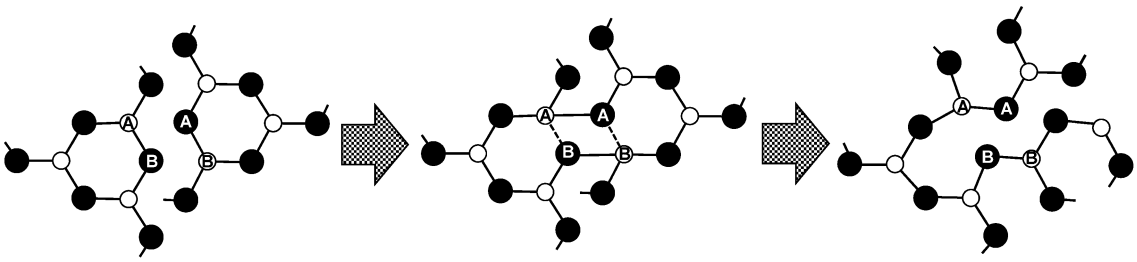

Fig. 2-9. *Double bond-switching mechanism.* (Black and grey circles represent oxygen and boron, respectively.)

Such structural change would result in the higher thermal conductivity with increasing temperature below 1400 K. Using the equation (2-15) with data from selected references[8, 14, 30], the phonon mean free path of the B_2O_3 system for a range of temperatures was calculated, and it is summarized on Table 2-4.

Table 2-4. Calculated phonon mean free path of the B_2O_3 melts with varying temperature.

Temp.	**Thermal conductivity**	**Heat capacity**[14]	**Sound velocity**[30]	**Density**[8]	**Mean free path**
(K)	($Wm^{-1}K^{-1}$)	($Jkg^{-1}K^{-1}$)	(km/s)	(g/cm^3)	(Å)
873	0.99	1829.14	1.16	1.61	8.7
973	1.08	1829.14	1.16	1.58	9.6
1073	1.14	1829.14	1.16	1.56	10.3
1173	1.21	1829.14	1.16	1.54	11.1
1273	1.3	1829.14	1.16	1.53	12.0

The phonon mean free path increased gradually from 0.87 nm to 1.20 nm with increasing the temperature within the range of 873 K - 1273 K. It could be inferred that such an increase the phonon mean free path along with the higher thermal conductivity results from the change of the borate structure into an incorporated random network structure.

On the other hand, above 1400 K; approximately the temperature at which the structure change terminates[1], negative temperature dependence of thermal conductivity can be observed. As previously mentioned that several physical properties shows distinguishing characteristic temperature region approximately between 600 K and 1300 K. In this temperature region, the change of volume and apparent activation energy of viscous flow shows intermediate structure characteristic which is the mixing of dense-open structure. However, above 1300 K, the physical properties of B_2O_3 melt shows only open structure characteristic. Therefore, it can be inferred that the structural change of borate structure would terminate at approximately 1400 K resulting in the change of temperature dependence of thermal conductivity.

It can be concluded that thermal conductivity of B_2O_3 gradually increases with higher temperature as a result of structural change; which is known as *Double bond-switching mechanism*. However, approximately above 1400 K, negative temperature dependence of thermal conductivity is observed due to the termination of characteristic structural change of B_2O_3 along with increase in the thermally broken bonds of borate structure. In addition, due to the increasing of phonon-phonon interaction at higher temperatures, phonon mean free path becomes shorten resulting in lowering thermal conductivity.

2.3.3. Thermal Conductivity of the Molten B_2O_3-SiO_2 System

Both B_2O_3 and SiO_2 have been known that it plays network forming oxide in the oxide melt system. As a result, borosilicate has a great viscosity even at high temperature of liquid state.[34] However, thermal conductivity of the molten B_2O_3-SiO_2 has not been reported yet. Considering that both oxide forms network forming characteristic, it could be inferred that thermal conductivity of the borosilicate melts can be simply obtained by its weighted average of the thermal conductivity for the pure SiO_2 and B_2O_3.

In Figure 2-10, the thermal conductivity of the B_2O_3-SiO_2 binary system, that is $BO_{1.5}$/SiO_2 with a mole ratio of 0.2, is displayed along with the reported thermal conductivity of pure SiO_2.[35] It can be observed that thermal conductivity of B_2O_3-SiO_2 binary melt remains constant with changing the temperature. The weighted average; which is approximately 1.88 $W{\cdot}m^{-1}{\cdot}K^{-1}$ at 1623 K, shows much higher thermal conductivity than the present measured thermal conductivity of the B_2O_3-SiO_2 system.

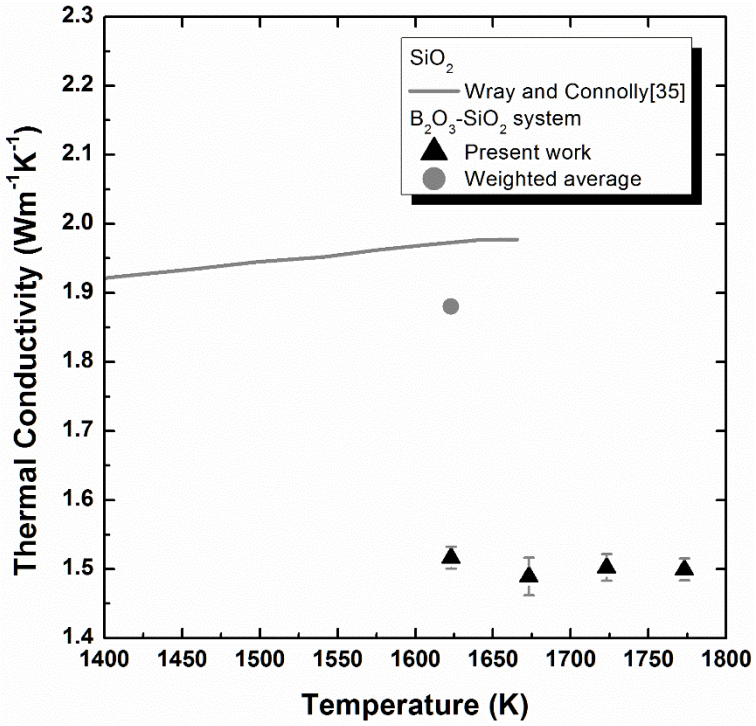

Fig. 2-10. Temperature dependence of thermal conductivity in the B_2O_3-SiO_2 binary system.

Considering that thermal conductivity is closely related to the molten oxide structure, it can be inferred that large difference between measured thermal conductivity and weighted

average is related to the molten borosilicate structure.

In order to confirm the structure of borosilicate system, structural investigation was carried out using the MAS NMR, 3Q MAS, and Raman spectroscopy. In addition, structural investigation was carried out not only the borosilicate structure which $BO_{1.5}/SiO_2$ ratio is 0.2, but also other compositions; $BO_{1.5}/SiO_2$ = 0.4 and 0.6, in order to confirm the borate structure in the B_2O_3-SiO_2 system.

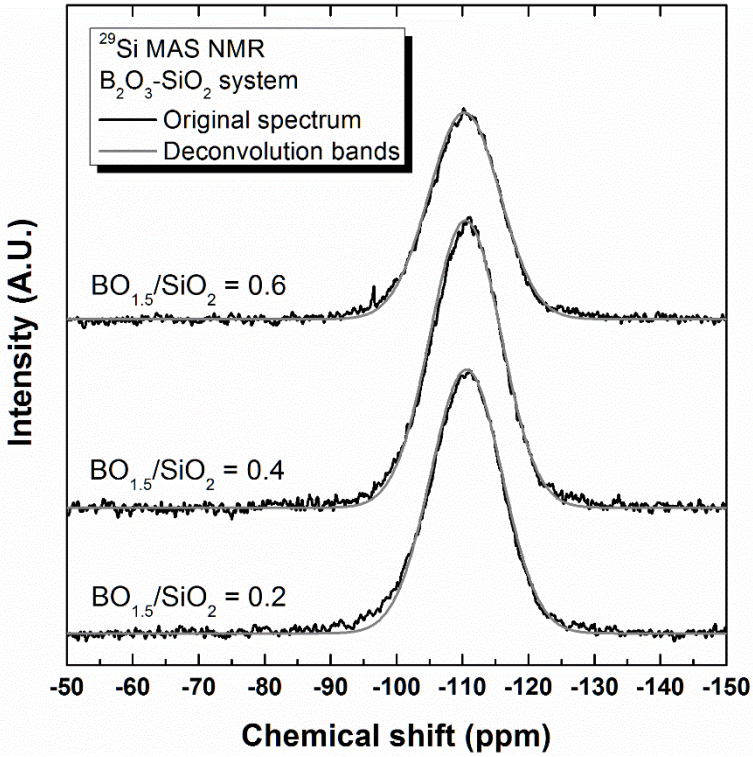

Fig. 2-11. ^{29}Si MAS NMR spectra of the quenched B_2O_3-SiO_2 glass.

Figure 2-11 shows the MAS-NMR analysis result of ^{29}Si in the B_2O_3-SiO_2 system, which used in the present work, with only one peak observed at -110.7 ppm of chemical shift. Namba et al.[36] analyzed the structure of alkali borosilicate glasses using the MAS-NMR and attributed the peak around -110 ppm to the Q^4 species of the silicate network, which is SiO_4 tetrahedron with 4 bridging oxygens and 0 non-bridging oxygen. This is consistent with the ^{29}Si MAS-NMR peak observed around -110.7 ppm in the present work, indicating that in our B_2O_3-SiO_2 system, only the SiO_4 tetrahedron with 4 bridging oxygens exists. Therefore, it can be inferred that only Q^4 unit exists in the B_2O_3-SiO_2 system.

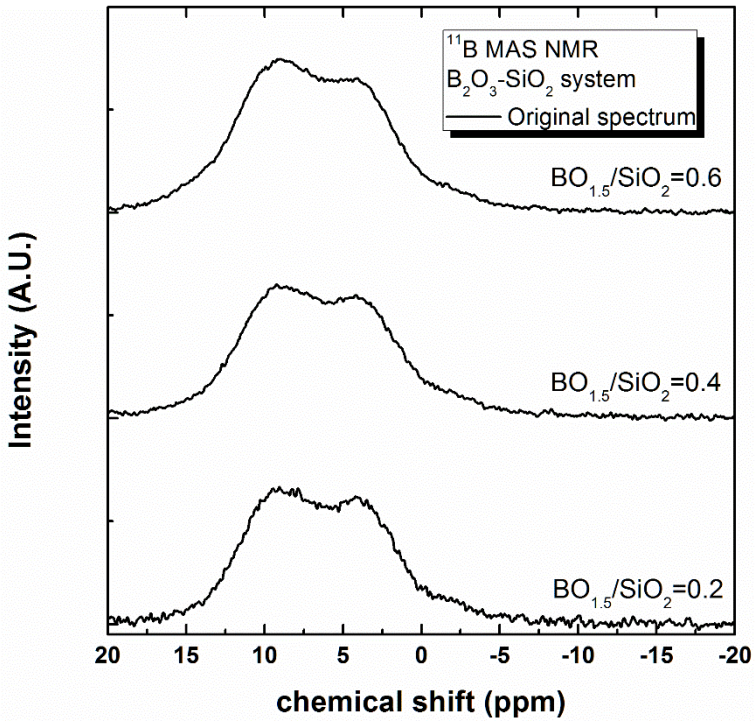

Fig. 2-12. ^{11}B MAS NMR spectra of the quenched B_2O_3-SiO_2 glass.

Figure 2-12 shows the MAS-NMR analysis results of ^{11}B in the B_2O_3-SiO_2 system. According to Namba et al.,[36] the asymmetric broad peak of ^{11}B observed between 20 and -20 ppm of chemical shift is attributed to the 3-coordinated boron in the BO_3 unit indicating that only the 3-coordinated boron exists in the present B_2O_3-SiO_2 system. Significant difference was not observed along with increasing of the $BO_{1.5}/SiO_2$ ratio.

As previously mentioned, due to the large nuclear spin quantum number of ^{11}B (I = 3/2), electric distribution does not show spherical shape and it results in the nuclear quadrupole moment. For this reason, MAS NMR spectrum of each non-ring and ring structure has second order quadrupolar lineshape. Therefore, simple Gaussian deconvolution of ^{11}B MAS spectra does not give any meaningful information.

In order to find out the relative fraction of ring and non-ring structure, 3Q MAS analysis was carried out. The 3Q-MAS spectrum of ^{11}B in the B_2O_3-SiO_2 system is shown in Fig. 2-13. Two peaks centered at approximately 12 and 15 ppm were deconvoluted using a Gaussian fit. Angeli et al.[37] found that, in the Na_2O-B_2O_3-SiO_2 system bearing 2 mol % of ZrO_2, a BO_3-non-ring structure is observed at around 11.5 ppm and a BO_3-ring structure is observed at a lower field region; around 15.3 ppm, on account of the narrow distribution of the B-O-B angles. Therefore, in the present 3Q-MAS spectrum, the two peaks at 12 and 15 ppm are attributed to a BO_3-non-ring and to a BO_3-ring, respectively. In Table 2-5, position of the center of each spectrum and its relative fraction are summarized.

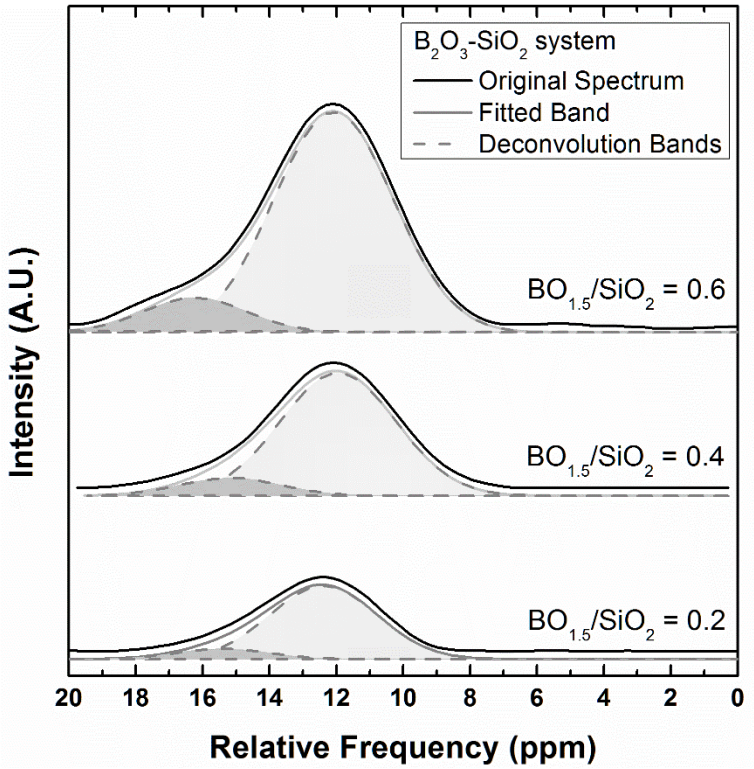

Fig. 2-13. ^{11}B 3Q MAS spectra of the quenched B_2O_3-SiO_2 glass.

Table 2-5. The centered position and its relative fraction of BO_3-non-ring and BO_3-ring structure in the ^{11}B 3Q MAS with varying $BO_{1.5}/SiO_2$ ratio.

$BO_{1.5}/SiO_2$	BO_3-Non-ring		BO_3-Ring	
	Center of the peak (ppm)	**Relative fraction (%)**	**Center of the peak (ppm)**	**Relative fraction (%)**
0.2	12.4	89.13	15.4	10.87
0.4	12.0	88.7	15.2	11.3
0.6	12.1	88.0	16.2	12.0

The relative fraction of each structure was estimated on the basis of the area calculation. It found to be approximately 89 % of BO_3-non-ring and 11 % of BO_3-ring. In addition, the relative fraction of BO_3-ring increases with higher B_2O_3 concentration. It can be inferred that and certain amount of B_2O_3 does not mix with SiO_4 network structure forming separate BO_3 ring structure. However, the environment of BO_3 non-ring structure is not clearly understood from the spectra of MAS NMR and 3Q MAS.

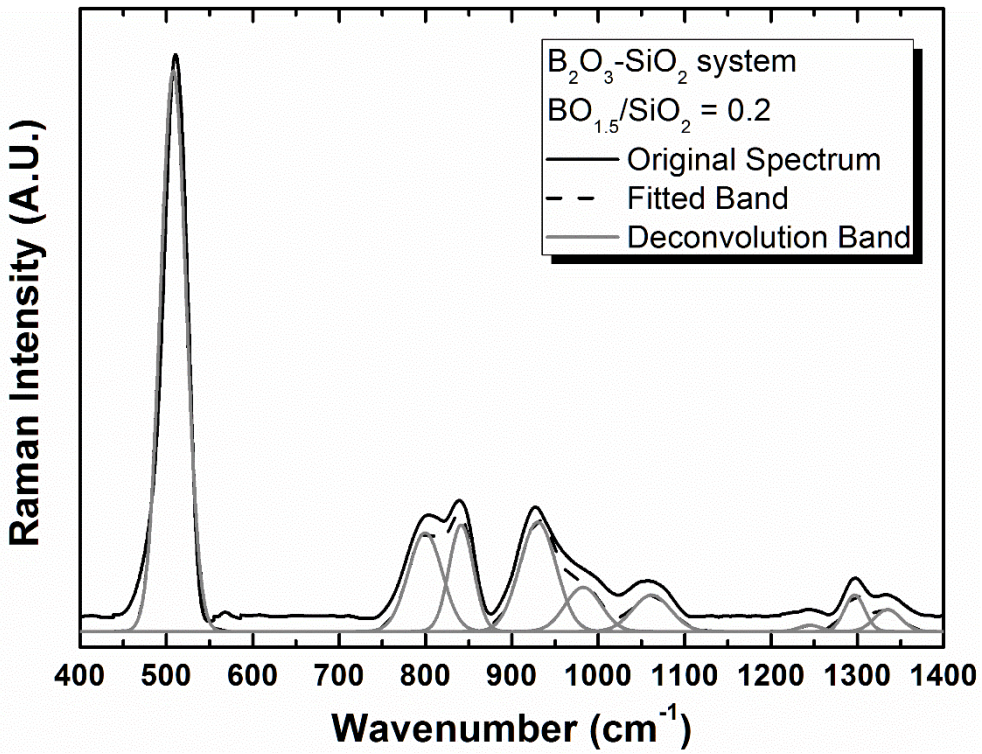

Fig. 2-14. Raman spectroscopy of the quenched B_2O_3-SiO_2 glass where $BO_{1.5}/SiO_2 = 0.2$.

Table 2-6. Raman band data as reported in the literature[38, 39] and as observed in the present study for the B_2O_3-SiO_2 system.

Reported position (cm^{-1})	**Assignments**	**Observed position (cm^{-1})**
475	Bending or rocking of B-O-B, B-O-Si and Si-O-Si bridging bonds	508
810	Symmetric breathing vibration of the boroxol ring	800, 841
935	B-O-Si bridging bond	930, 982
1000 - 1200	Stretching region of Si-O bond	1061
1250 - 1500	Stretching region of B-O bond	1245, 1296, 1335

Because Raman spectroscopy is more sensitive to the presence of intermediate range order structure[40], structural investigation of B_2O_3-SiO_2 system was carried out using the Raman spectroscopy in order to investigate the intermediate range order structure. Figure 2-14 shows the Raman spectrum and the related Gaussian deconvolution bands of the B_2O_3-SiO_2 system considered in the present work. It should be noted that in the solid state, various molecules have statistical distribution of environment showing Gaussian profile.[41] For this reason, in the

present study, the structure of present system was identified using Gaussian deconvlution band referring to the appropriate references.[38, 39] These are shown in Table 2-6. The presence of both the boroxol ring and the B-O-Si network was observed.

Considering the NMR and Raman spectra results, it was possible to verify that the structure of the B_2O_3-SiO_2 system used in the present work consisted of a mixture of boroxol rings (BO_3-rings) and borosilicate network, comprising planar 3-coordinated boron (BO_3-non-rings) along with fully polymerized tetrahedral silicate network (Q^4). This result is in accordance with previous structure studies for B_2O_3-SiO_2 binary system.[42–45] According to Lee and Stebbins[43], in the B_2O_3-SiO_2 system, the extent of intermixing increases with higher temperature leading to an increasing of [4]Si-O-[3]B bond. Considering the better degree of Si/B mixing for BO_3-non-rings[42] along with its stability at higher temperature, the structure change of the molten B_2O_3-SiO_2 system would result from increasing of relative fraction of BO_3-non-ring structure with higher temperature. However, according to other structure studies[27, 28, 46], it can be postulated that BO_3-ring structure can exist at even high temperature[27, 28] and the relative fraction of Q^4 silicate unit in the B_2O_3-SiO_2 system would not be affected by temperature change[46]. Therefore, it can be inferred that present structure unit obtained at room temperature would be similar to the structure unit in the molten B_2O_3-SiO_2 system indicating that present work is qualitatively valid to predict the structure of molten B_2O_3-SiO_2 system.

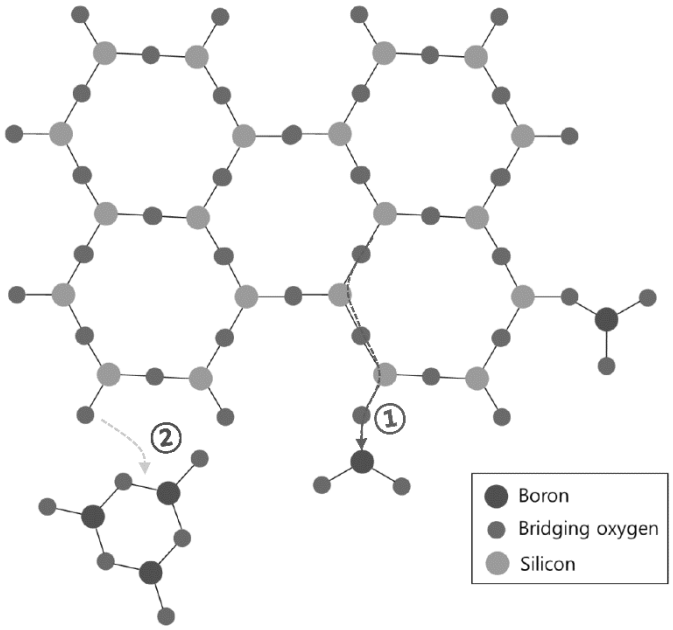

Fig. 2-15. Schematic diagram of structure of the B_2O_3-SiO_2 glass melt. Two types of B_2O_3 exist; one is associated with silicate network and another is boroxol ring.

Figure 2-15 shows the schematic diagram of structure of the present B_2O_3-SiO_2 system. Boron oxide exists in two type; one is non-ring type 3-coordinated boron which is associated with silicate network and another is ring type 3-cooridnated boron which is clustered as boroxol ring.

The phonon transfer is closely related to the structure of molten oxide. According to Mills[18], the thermal resistance ($1/\lambda$) associated with the phonon transfer along a network chain or ring is lower than the phonon transfer from chain to chain or from ring to ring or from chain to ring in the liquid melts. Therefore, it can be inferred that phonon transfer from borosilicate network to the clustered boroxol ring (second path in Fig.2-15) has much lower thermal conductivity than the phonon transfer along the borosilicate network (first path in Fig.2-15). As a result, despite of the network forming characteristic of B_2O_3 and SiO_2, the great difference between measured thermal conductivity and weighted average is observed due to the formation of boroxol ring structure resulting in an increase in the amount of phonon transfer from chain to ring.

2.4 Short Summary

In this chapter, thermal conductivity of pure B_2O_3 melt and molten B_2O_3-SiO_2 system was measured using a transient hot-wire method along with structural investigation. In addition, several errors affecting on the thermal conductivity measurement was considered.

The calculated of Rayleigh number indicates that in the present molten oxide system, natural convection does not occur within the measurement time period which is less than 10 s. In the case of radiation effect from the surface of heated hot-wire, it was less than 1 % of total generated heat at 1273 K. The systematic errors resulting from the precision of the various experiment apparatus were considered.

The thermal conductivity of pure B_2O_3 melt linearly increases with higher temperature, and reaches maximum approximately at 1400 K. Considering the temperature dependence of borate structure, it was inferred that structure change from boroxol ring to random network structure results in the increasing of thermal conductivity along with longer phonon mean free path. Calculated phonon mean free path also supported the effect of structure change on thermal conductivity. On the other hands, above 1400 K, due to the termination of the structural change, thermal conductivity decreases with higher temperature along with increase in thermally broken bonds.

The molten B_2O_3-SiO_2 system shows lower thermal conductivity than expected due to the existence of clustered boroxol ring. According to the structural investigation by MAS NMR, 3Q MAS and Raman spectroscopy, it was confirmed that boron exists as two type of 3-coordinated boron; ring and non-ring type. While non-ring 3-coordinated boron associates with silicate network, ring type 3-coordinated boron exists as clustered form. Formation of boroxol ring results in an increasing of phonon transfer from chain to ring which has higher thermal resistivity. For this reason, in spite of network forming behavior of B_2O_3 and SiO_2, thermal conductivity of the B_2O_3-SiO_2 melt shows much lower value than weighted average.

References

[1] J. Krogh-Moe, "The structure of vitreous and liquid boron oxide," *J. Non-Cryst. Solids*, **1** [4] 269–284 (1969).

[2] K.J.D. MacKenzie and M.E. Smith, *Multinuclear solid-state NMR of inorganic materials*. Pergamon, Oxford, 2002.

[3] T.D.W. Claridge, *High-Resolution NMR Techniques in Organic Chemistry*, 1st ed. Elsevier Science, Oxford, 1999.

[4] J.-P. Amoureux, C. Fernandez, and S. Steuernagel, "Z Filtering in MQMAS NMR," *J. Magn. Reson. Ser. A*, **123** [1] 116–118 (1996).

[5] I. Tokura, H. Saito, K. Kishinami, and Y. Takekawa, "Application of the Transient Hot-Wire Method on Thermal Conduductivity Measurement of Solid-Liquid Mixtures," *Mem. Muroran Inst. Technol. Sci. Eng.*, **40** 63–73 (1990).

[6] L. Shartsis, W. Capps, and S. Spinner, "Density and Expansivity of Alkali Borates and Density Characteristics of Some Other Binary Glasses," *J. Am. Ceram. Soc.*, **36** [2] 35–43 (1953).

[7] G. Ogura, I.-K. Suh, H. Ohta, and Y. Waseda, "Thermal diffusivity measurement of boron oxide melts by laser flash method," *J. Ceram. Soc. Jpn.*, **98** [3] 305–307 (1990).

[8] A. Napolitano, P.B. Macedo, and E.G. Hawkins, "Viscosity and Density of Boron Trioxide," *J. Am. Ceram. Soc.*, **48** [12] 613–616 (1965).

[9] D. Bradley and A.G. Entwistle, "Determination of the emissivity, for total radiation, of small diameter platinum-10% rhodium wires in the temperature range 600-1450 C," *Br. J. Appl. Phys.*, **12** [12] 708–711 (1961).

[10] K. Nagata and K.S. Goto, "Heat Conductivity and Mean Free Path of Phonons in Metallurgical Slags;" pp. 875–889 in *Second Int. Symp. Metall. Slags Fluxes*. Edited by H.A. Fine and D.R. Gaskell. The Metallurgical Society of AIME, Warrendale, Pa., 1984.

[11] J.S. Bendat and A.G. Piersol, *Random Data: Analysis and Measurement Procedures*, 4th ed. Wiley, Hoboken, NJ, 2010.

[12] O. Nilsson, O. Sandberg, and G. Bäckström, "Thermal conductivity of B_2O_3 glass under pressure," *Int. J. Thermophys.*, **6** [3] 267–273 (1985).

[13] G. K. Creffield and A. J. Wickens, "Thermal conductivity of anhydrous borax, boric oxide, and sodium sulfate," *J. Chem. Eng. Data*, **20** [3] 223–225 (1975).

[14] J.C. Southard, "The Thermal Properties of Crystalline and Glassy Boron Trioxide," *J. Am. Chem. Soc.*, **63** [11] 3147–3150 (1941).

[15] W.D. Kingery, "Thermal Conductivity: XII, Temperature Dependence of Conductivity for Single-Phase Ceramics," *J. Am. Ceram. Soc.*, **38** [7] 251–255 (1955).

[16] C. Kittel and H. Kroemer, "Kinetic Theory;" pp. 389–421 in *Therm. Phys.*, 2nd ed. W. H. Freeman, New York, NY, 1980.

[17] J.M. Ziman, *Electrons and Phonons : The theory of transport phenomena in solids*. Oxford University Press, London, 1960.

[18] K.C. Mills, "The Influence of Structure on the Physico-chemical Properties of Slags.," *ISIJ Int.*, **33** [1] 148–155 (1993).

[19] M. Hayashi, H. Ishii, M. Susa, H. Fukuyama, and K. Nagata, "Effect of ionicity of nonbridging oxygen ions on thermal conductivity of molten alkali silicates," *Phys. Chem. Glasses*, **42** [1] 6–11 (2001).

[20] Y. Kang and K. Morita, "Thermal conductivity of the CaO-Al_2O_3-SiO_2 system," *ISIJ Int.*, **46** [3] 420–426 (2006).

[21] Y. Kang, K. Nomura, K. Tokumitsu, H. Tobo, and K. Morita, "Thermal Conductivity of the Molten CaO-SiO_2-FeO_x System," *Metall. Mater. Trans. B*, **43** [6] 1420–1426 (2012).

[22] M. Susa, M. Watanabe, S. Ozawa, and R. Endo, "Thermal conductivity of CaO–SiO_2–Al_2O_3 glassy slags: Its dependence on molar ratios of Al_2O_3/CaO and SiO_2/Al_2O_3," *Ironmak. Steelmak.*, **34** [2] 124–130 (2007).

[23] S. Ozawa and M. Susa, "Effect of Na2O additions on thermal conductivities of CaO–SiO_2 slags," *Ironmak. Steelmak.*, **32** [6] 487–493 (2005).

[24] S. Ozawa, R. Endo, and M. Susa, "Thermal Conductivity Measurements and Prediction for R_2O-CaO-SiO_2(R= Li, Na, K) Slags," *Tetsu-to-Hagane*, **93** [6] 416–423 (2007).

[25] M. Kishimoto, M. Maeda, K. Mori, and Y. Kawai, "Thermal conductivity and specific heat of metallurgical slags;" pp. 891–905 in *Second Int. Symp. Metall. Slags Fluxes*. Edited by H.A. Fine and D.R. Gaskell. The Metallurgical Society of AIME, Warrendale, Pa., 1984.

[26] Y. Ishii, K. Sato, M. Salanne, P. a Madden, and N. Ohtori, "Thermal conductivity of molten alkali metal fluorides (LiF, NaF, KF) and their mixtures.," *J. Phys. Chem. B*, **118** [12] 3385–91 (2014).

[27] G. Ferlat, T. Charpentier, A. Seitsonen, A. Takada, M. Lazzeri, L. Cormier, G. Calas, and F. Mauri, "Boroxol Rings in Liquid and Vitreous B_2O_3 from First Principles," *Phys. Rev. Lett.*, **101** [6] 065504 (2008).

[28] G.E. Walrafen, S.R. Samanta, and P.N. Krishnan, "Raman investigation of vitreous and molten boric oxide," *J. Chem. Phys.*, **72** [1] 113–120 (1980).

[29] G.E. Walrafen, M.S. Hokmabadi, P.N. Krishnan, S. Guha, and R.G. Munro, "Low-frequency Raman scattering from vitreous and molten B_2O_3," *J. Chem. Phys.*, **79** [8] 3609–3620 (1983).

[30] M. Grimsditch, R. Bhadra, and L. Torell, "Shear waves through the glass-liquid transformation," *Phys. Rev. Lett.*, **62** [22] 2616–2619 (1989).

[31] M. Misawa, "Structure of vitreous and molten B_2O_3 measured by pulsed neutron total scattering," *J. Non-Cryst. Solids*, **122** [1] 33–40 (1990).

[32] A. Hassan, L. Torell, L. Börjesson, and H. Doweidar, "Structural changes of B_2O_3 through the liquid-glass transition range: A Raman-scattering study," *Phys. Rev. B*, **45** [22] 12797–12805 (1992).

[33] A.C. Wright, G. Dalba, F. Rocca, and N.M. Vedishcheva, "Review Borate versus silicate glasses : why are they so different ?," *Phys. Chem. Glasses B*, **51** [5] 233–265 (2010).

[34] K.C. Mills, *Slag atlas*, 2nd ed. Verlag Stahleisen GmbH, Dusseldorf, 1995.

[35] K.L. Wray and T.J. Connolly, "Thermal Conductivity of Clear Fused Silica at High Temperatures," *J. Appl. Phys.*, **30** [11] 1702–1705 (1959).

[36] T. Nanba, M. Nishimura, and Y. Miura, "A theoretical interpretation of the chemical shift of ^{29}Si NMR peaks in alkali borosilicate glasses," *Geochim. Cosmochim. Acta*, **68** [24] 5103–5111 (2004).

[37] F. Angeli, T. Charpentier, D. De Ligny, and C. Cailleteau, "Boron Speciation in Soda-Lime Borosilicate Glasses Containing Zirconium," *J. Am. Ceram. Soc.*, **93** [9] 2693–2704 (2010).

[38] R.J. Bell, A. Carnevale, C.R. Kurkjian, and G.E. Peterson, "Structure and phonon spectra of SiO_2, B_2O_3 and mixed SiO_2-B_2O_3 glasses," *J. Non-Cryst. Solids*, **35-36** 1185–1190 (1980).

[39] T. Furukawa and W.B. White, "Raman Spectroscopy of Heat-Treated B_2O_3-SiO_2 Glasses," *J. Am. Ceram. Soc.*, **64** [8] 443–447 (1981).

[40] S.R. Elliott, "Medium-range structural order in covalent amorphous solids," *Nature*, **354** [6353] 445–452 (1991).

[41] M. Bradley, *Curve Fitting in Raman and IR Spectroscopy : Basic Theory of Line Shapes and Applications*. 2007.

[42] L.-S. Du and J.F. Stebbins, "Nature of Silicon−Boron Mixing in Sodium Borosilicate Glasses: A High-Resolution ^{11}B and ^{17}O NMR Study," *J. Phys. Chem. B*, **107** [37] 10063–10076 (2003).

[43] S.K. Lee and J.F. Stebbins, "Extent of intermixing among framework units in silicate glasses and melts," *Geochim. Cosmochim. Acta*, **66** [2] 303–309 (2002).

[44] S.K. Lee, C.B. Musgrave, P. Zhao, and J.F. Stebbins, "Topological Disorder and Reactivity of Borosilicate Glasses: Quantum Chemical Calculations and ^{17}O and ^{11}B NMR Study," *J. Phys. Chem. B*, **105** [50] 12583–12595 (2001).

[45] A. Soleilhavoup, J.-M. Delaye, F. Angeli, D. Caurant, and T. Charpentier, "Contribution of first-principles calculations to multinuclear NMR analysis of borosilicate glasses.," *Magn. Reson. Chem. MRC*, **48 Suppl 1** [July] S159–70 (2010).

[46] T. Yano, S. Shibata, and T. Maehara, "Structural Equilibria in Silicate Glass Melts Investigated by Raman Spectroscopy," *J. Am. Ceram. Soc.*, **89** [1] 89–95 (2006).

Chapter III

Thermal Conductivity of the Molten Alkali Borate and Sodium Silicate System

3.1 Background

In the previous chapter, the relationship between thermal conductivity and borate structure in the pure B_2O_3 and B_2O_3-SiO_2 melt was studied along with structure investigation. In practice, glass and mold flux system consist of not only B_2O_3 but also various alkali oxide. According to previous studies[1–4], physical properties of borate glass and melt are significantly changed by addition of alkali and alkali-earth oxide. Hayashi et al.[5], who measured thermal conductivity in the alkali-silicate melt, observed different thermal conductivity depending on the type of alkali oxide at the same alkali oxide concentration. In addition, recently Ohta et al.[6] found the effect of alkali oxide on thermal conductivity in the molten CaO-SiO_2-M_2O (M = Li, Na, and K) system when the NBO/T ratio was approximately same. It can be inferred that not only the network structure change but also the cation effect should be considered during the thermal conductivity measurement.

However, effect of alkali oxide on thermal conductivity in the molten B_2O_3 system has not reported despite of its practical importance. Considering that various type of alkali oxide is added into the glass and mold flux system, understanding of the effect of different type of alkali oxide on thermal conductivity is important in order to control and optimize the operation process. Therefore, in the present chapter, thermal conductivity was measured in the molten R_2O-B_2O_3 system (R = Li, Na and K) with varying concentration and the effect of both borate structure and cation type was evaluated. In addition, thermal conductivity of the sodium silicate system was studied in order to compare the effect of borate and silicate network structure on thermal conductivity.

3.2 Experiment

3.2.1. Sample Preparation

The powder mixtures of the weighed reagent grades of B_2O_3, SiO_2, Li_2CO_3, Na_2CO_3 and K_2CO_3 were placed in a platinum crucible and maintained at a temperature between 1473 K and 1723 K, depending on the oxide melting temperature. The powder mixture was pre-melted for 2 h in order to decarbonate, dehydrate and homogenize the mixture. The melted sample was quenched on a water-cooled copper plate. The obtained vitreous sample was crushed and placed into a Pt-10%Rh crucible (I.D: 32 mm, O.D: 38 mm, height: 70 mm). The Pt-10%Rh crucible was placed into a SiC equipped vertical furnace in order to measure the thermal conductivity using the transient hot-wire method.

3.2.2. Thermal Conductivity Measurement

Using the hot-wire method, the thermal conductivities of the alkali borate and sodium silicate were measured. Using a PID (proportional integral differential) controller and calibrated B-type thermocouple, sample temperature was controlled. The upper part of sample is intentionally placed at the highest temperature zone, in order to avoid natural convection during measurement. Approximately 90 g of pre-melted sample is heated in an electric resistance furnace equipped with SiC at 1273 K or 1573 K, depending on the melting temperature. After held for 1 hour to obtain a homogeneous molten oxide. Thermal conductivity was measured at 50 K intervals to the liquidus temperature. Using a galvanostat, a constant current of 0.8–1.5 A was supplied to a 0.15mmϕ Pt-13%Rh hot-wire, and any voltage change between the two terminals of the wire was monitored by a digital multimeter. A linear relationship between ΔV and lnt was obtained within 0.8–2.0 seconds, and the thermal conductivity, λ ($Wm^{-1}K^{-1}$), was calculated by the equation (1-18).

During the measurement, to ensure the thermal equilibrium of the system, the furnace temperature was decreased at a rate of 3 K/min and held for 15 minutes at the target temperature. To confirm the reproducibility of the results, the measurement was repeated three times at the same temperature, with a 5-minutes interval between one measurement and the following one.

3.2.3. Analytical Procedures

3.2.3.1. Determination of the boron and alkali oxide concentration in the sample

Following the measurement of thermal conductivity, the solidified sample was placed in a muffle furnace and re-melted at 1373 K or 1673 K, depending on the oxide melting temperature. After 1 h, the sample was quenched on a water-cooled copper plate and quickly covered with another copper block. The obtained non-crystalline solid was ground and sieved using a 100 μmϕ mesh. Approximately 0.01 g or 0.1 g of the ground powder sample was transferred into 100 ml of beaker. Following the addition of acid-solution (10 ml of distilled water + 15 ml of HCl + 5 ml of HNO_3), the beaker was placed on the hot-plate covered with watch glass, and then heated at 493 K for several hours. When the almost of the acid solution was evaporated, approximately 5 ml of $HClO_4$ was added, and kept on heating until white smoke appeared.

The heated beaker was cooled down at room temperature. The solution was filtered using a filter paper (ash contents 0.1 mg/circle) attached on glass funnel, and transferred into 100 ml, 250 ml or 500 ml of volumetric flask, depending on the concentrations. After rinsing the beaker and filter paper several times by distilled water, the final volume was made to given volume of the volumetric flask. In order to obtain the homogeneous concentration across the solution, the volumetric flask was kept for 24 hours.

Using the inductively coupled plasma atomic emission spectroscopy (ICP-AES; SPS7700, SII NanoTechnology, Japan), final concentration of boron, lithium, sodium and potassium was determined. Diluting the 1000 ppm of B, Li, Na and K standard solution (Kanto chemical, Tokyo, Japan), four different standard solutions (10, 20, 40, 100 ppm) were prepared for each elements. Calibration line shows larger than 0.999 of correlation coefficient. During the analysis, 249.773 nm, 670.784 nm, 588.995 nm and 766.490 nm of wavelength were chosen for boron, lithium, sodium and potassium as analytical wavelength. Table 3-1 shows the final composition of alkali borate system.

3.2.3.2. Determination of the silicon concentration in the sample

The SiO_2 content in the Na_2O-SiO_2 system was determined by silica gravimetric method. The analyzed final compositions of sodium silicate system are listed in Table 3-1. The detailed procedures were described in the previous chapter.

Table 3-1. Initial and final composition of the present experiment.

	Initial Compositions (mol %)					**Final Compositions (mol %)**				
	B_2O_3	**SiO_2**	**Li_2O**	**Na_2O**	**K_2O**	**B_2O_3**	**SiO_2**	**Li_2O**	**Na_2O**	**K_2O**
1	90	-	10	-	-	90.9	-	9.1	-	-
2	80	-	20	-	-	81	-	19	-	-
3	70	-	30	-	-	70.7	-	29.3	-	-
4	90	-	-	10	-	90.3	-	-	9.7	-
5	80	-	-	20	-	79.7	-	-	20.3	-
6	70	-	-	30	-	68.9	-	-	31.1	-
7	90	-	-	-	10	90.4	-	-	-	9.6
8	80	-	-	-	20	80.5	-	-	-	19.5
9	70	-	-	-	30	69.7	-	-	-	30.3
10	-	80	-	20	-	-	80.5	-	19.5	-
11	-	70	-	30	-	-	71.4	-	28.6	-
12	-	60	-	40	-	-	61.3	-	38.7	-

3.3 Results and Discussion

3.3.1. Evaluation of the Experimental Errors Due to the Current Leakage

Due to the dissolution of Al_2O_3 in the borate melt, in the present thermal conductivity measurement, aluminum oxide insulation tube could not be adopted. Instead of that, we used bare Pt and Pt-13%Rh wire without any sheath. However, several researchers[7] pointed out the possibility of current leakage during the thermal conductivity measurement. Considering that electric conductivity significantly increases with higher concentration of cation; such as alkali ion, evaluation of the current leakage.

Using the semi-quantitative evaluation, recently, Kang et al.[8] reported that no significant current leakage is occurred during the hot-wire measurement in the molten oxide system. According to their study, insignificant difference between measured and reference resistance was observed indicating low current leakage.

Likewise, in the present study, current leakage was investigated by the semi-quantitative evaluation. The reference resistance of Pt-13%Rh hot wire was obtained by equation (1-16). Figure 3-1 shows the relationship between measured resistance and reference resistance of Pt-13%Rh hot wire in the various alkali borate and sodium silicate melts. As shown in Fig. 3-1, all measured resistance have lower value than reference resistance. The average of resistance difference is approximately 8 %.

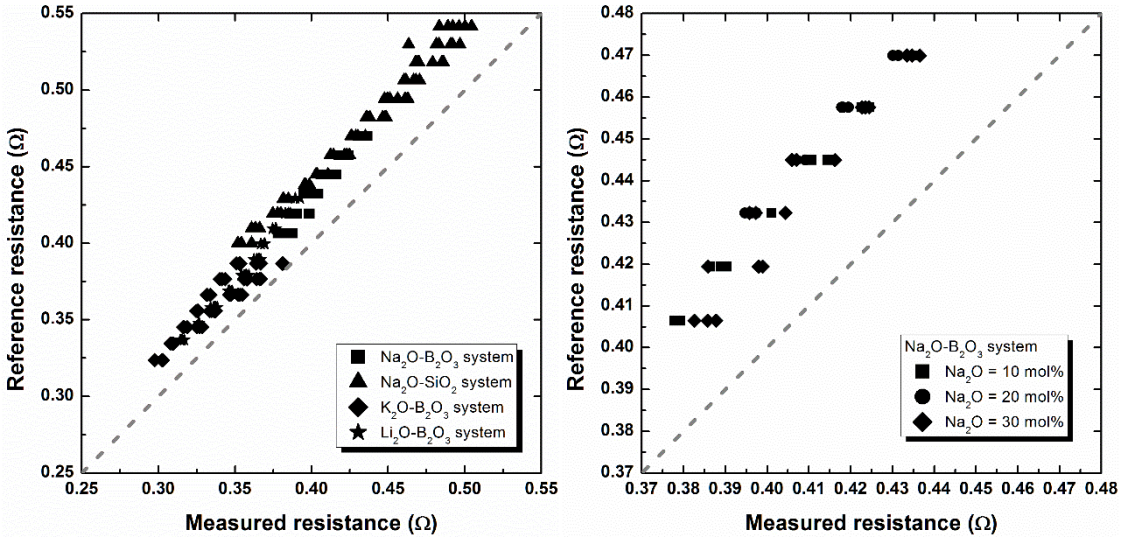

Fig. 3-1. The measured and reference resistance of Pt-13%Rh hot wire **(a)** in the R_2O-B_2O_3 (R = Li, Na, and K), Na_2O-SiO_2 melts **(b)** in the molten Na_2O-B_2O_3 system.

However, although electrical resistivity decreases with higher concentration of alkali ion, the difference between measured and reference resistance was not affected by the alkali oxide concentration in the molten Na_2O-B_2O_3 system (as shown in Fig. 3-1(b)). Therefore, it can be inferred that lower measured resistance does not mainly result from the current leakage.

As previously mentioned, thermal conductivity consists of three different mechanisms; lattice thermal conductivity, radiation thermal conductivity and electronic thermal conductivity. In the alkali borate system, there would be certain amount of current leakage, thus, the effect of electronic thermal conductivity should be considered. According to the Wiedemann-Franz law, thermal conductivity by electron (λ_e) can be obtained by the simple relationship between theoretical Lorenz number (L_0) and electrical resistivity (ρ_e) at the given temperature (T). In the present study, theoretical Lorenz number was approximated using the equation proposed by Sommerfeld; where the mean free path for thermal transport and electrical transport are same.[9]

$$\lambda_e = \frac{TL_0}{\rho_e} \tag{3-1}$$

$$L_0 = \frac{\pi^2 k_B^2}{3e^2} = 2.44 \times 10^{-8}\ \mathrm{W\Omega K^{-2}} \tag{3-2}$$

k_B and e indicate Boltzmann constant and charge of an electron, respectively. It should be noted that equation (3-2) is designed for the metal where the electrical thermal conductivity plays major role. Considering that low electrical conductivity of dielectric molten oxide system, mean free path of electrical transport should be shorter than mean free path for thermal transport. Therefore, it can be inferred that present calculated thermal conductivity by electron would be somewhat overestimated than the real value.

Referring to the appropriate reference of electrical conductivity of the molten alkali-borate system,[3] thermal conductivity by electron was calculated and it is shown in Fig. 3-2. The calculated thermal conductivity by electron is much lower than measured thermal conductivity; which is approximately 1.0 $Wm^{-1}K^{-1}$, indicating negligible effect of electron thermal conductivity during thermal conductivity measurement.

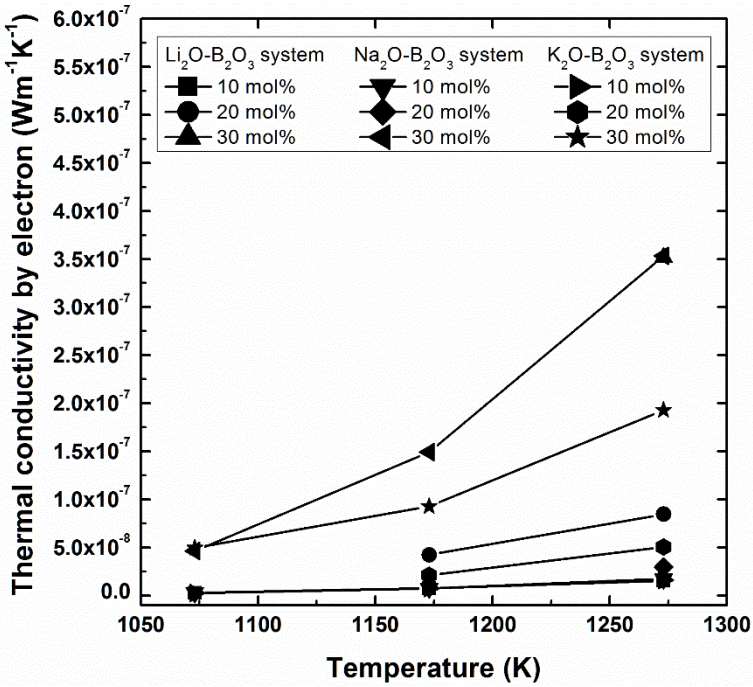

Fig. 3-2. Electronic thermal conductivity in the molten alkali-borate system.

3.3.2. Thermal Conductivity in the Molten Na_2O-SiO_2 system

Figure 3-3 shows the temperature dependence of thermal conductivity in the molten Na_2O-SiO_2 system. It was observed that the thermal conductivity initially increased at the lower temperatures, and then stabilized just below a specific temperature, approximately 100 – 150 K above its liquidus temperature.

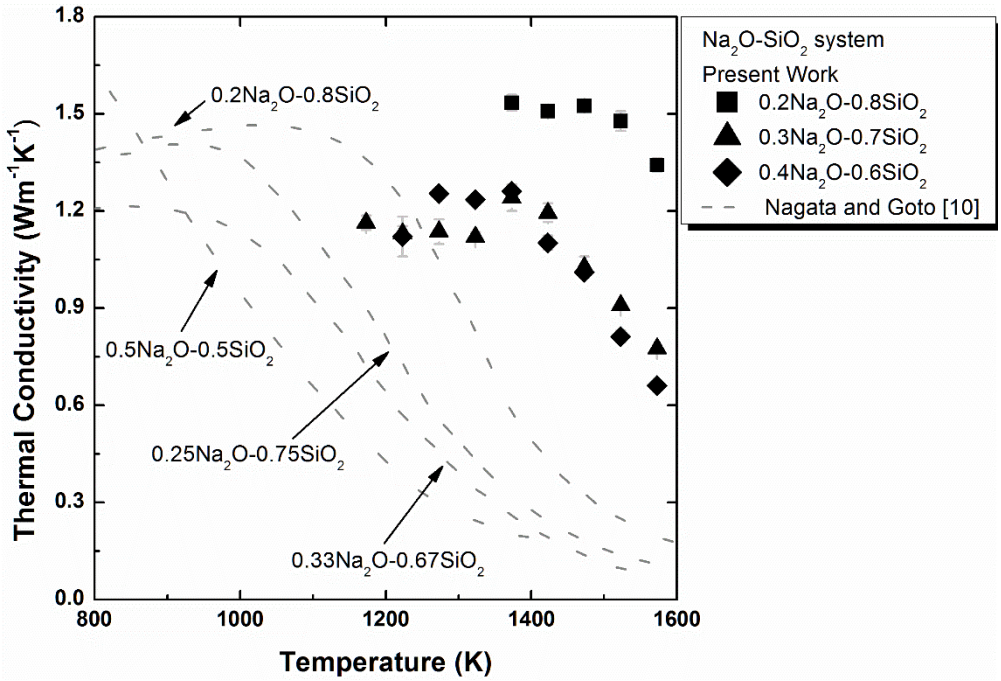

Fig. 3-3. Temperature dependence of thermal conductivity in the Na_2O-SiO_2 system.

Compared to Nagata and Goto's work[10], who measured the thermal conductivity using the same hot-wire method employed in the present work, our results show higher thermal conductivity; approximately 0.3 ~ 1.2 $W \cdot m^{-1} \cdot K^{-1}$. During the measurement, Nagata and Goto used alumina tube to cover the Pt-wire resulting in the dissolution of Al_2O_3 in the sodium silicate system. They observed approximately 2 wt% of Al_2O_3 after experiment. It seems the aluminum oxide concentration over total molten oxide sample seems very low. However, we have to consider that there is no natural convection during the experiment. It means that the dissolved Al_2O_3 will be concentrated around the Pt hot-wire due to slow diffusion of aluminum oxide in the molten oxide system; where driving force is only chemical potential difference. Therefore, the concentrated Al_2O_3 causes significant thermal conductivity difference along with structural change.

Using equation (2-15), the phonon mean free path of the $Na_2O/4SiO_2$ system was calculated

on the basis of its thermal conductivity, sound velocity[10], density[11] and calculated specific heat capacity. The specific heat of the molten oxide system used in the present work was estimated by following an empirical equation: [12, 13]

$$C_{P,T} = \frac{0.00146T^2 \sum a_i p_i + 2T \sum a_i p_i + \sum c_i p_i}{(0.00146T + 1)^2} \qquad (3\text{-}3)$$

where p_i is the weight fraction of the oxides, a_i is a temperature constant, 0.000829 for Na_2O and 0.000468 for SiO_2, c_i is the specific heat at 273 K, 0.223 for Na_2O and 0.166 for SiO_2, T is the temperature (^{o} C), and $C_{p,T}$ is the specific heat capacity (cal/(g·K)) at the temperature T. The calculated phonon mean free path are summarized in Table 3-1.

Table 3-2. Calculated mean free path in the molten Na_2O-$4SiO_2$ system along with thermal conductivity, heat capacity, sound velocity[10] and density[11].

Temperature (K)	**Thermal conductivity ($Wm^{-1}K^{-1}$)**	**Heat capacity ($JKg^{-1}K^{-1}$)**	**Sound velocity[10] (km/s)**	**Density[11] (kg/m^3)**	**Mean free path (nm)**
1573	1.342	1434.9	5.0	2203.9	0.25
1523	1.477	1441.3	5.1	2213.1	0.27
1473	1.524	1447.2	5.1	2221.2	0.28
1423	1.508	1452.7	5.1	2229.8	0.28
1373	1.534	1457.8	5.1	2238.4	0.28

Results of the calculation shows that the phonon mean free path initially increased at lower temperatures, from 0.25 nm at 1573 K to 0.28 nm at 1473 K, and then remained constant. This is in excellent accordance with previously reported phonon mean free path, which was approximately 0.22 nm at 1400 K in the 28.3 mol % Na_2O/71.7 mol % SiO_2 binary system.[14] Compared to the 0.7 nm of phonon mean free path found in the quartz glass at 373 K,[15] the present value is even lower, indicating a decrease in the mean free path of collision (l) at higher temperatures. Therefore, the negative temperature dependence of thermal conductivity in the Na_2O-SiO_2 system should be attributed to a change in the phonon mean free path.

In Fig. 3-3, at a constant temperature of 1573 K, the thermal conductivity decreased with any addition of Na_2O. Interestingly, a drastic decrease in the thermal conductivity can be observed when the Na_2O concentration increases from 20 to 30 mol %. According to Maekawa et al.[16] who studied the relative fraction of Q^n species in the Na_2O-SiO_2 glass by

MAS-NMR, the silicate network structure is depolymerized at a higher Na_2O concentration, causing a decrease in Q^4 units. Referring to their results[16], the number of non-bridging oxygen atoms bonded to the 4-coordinated silicon atom (NBO/T_{Si}) was estimated using the following equation. The calculated NBO/T_{si} are listed in Table 3-3.

$$NBO/T_{Si} = 4 - \left([Q^0]\times 0 + [Q^1]\times 1 + [Q^2]\times 2 + [Q^3]\times 3 + [Q^4]\times 4\right) \qquad (3\text{-}4)$$

Table 3-3. Relative fraction of Q^n species[16] and calculated NBO/T_{si} of the Na_2O-SiO_2 system.

mol% Na_2O	***Q^4***	***Q^3***	***Q^2***	***Q^1***	***NBO/T_{Si}***
20	0.50	0.49	0.01	0.00	0.51
30	0.19	0.75	0.05	0.00	0.86
40	0.02	0.62	0.35	0.01	1.35

Although there was a considerable decrease in thermal conductivity between 20 and 30 mol % of Na_2O, no sudden change in the NBO/T_{si} was observed.

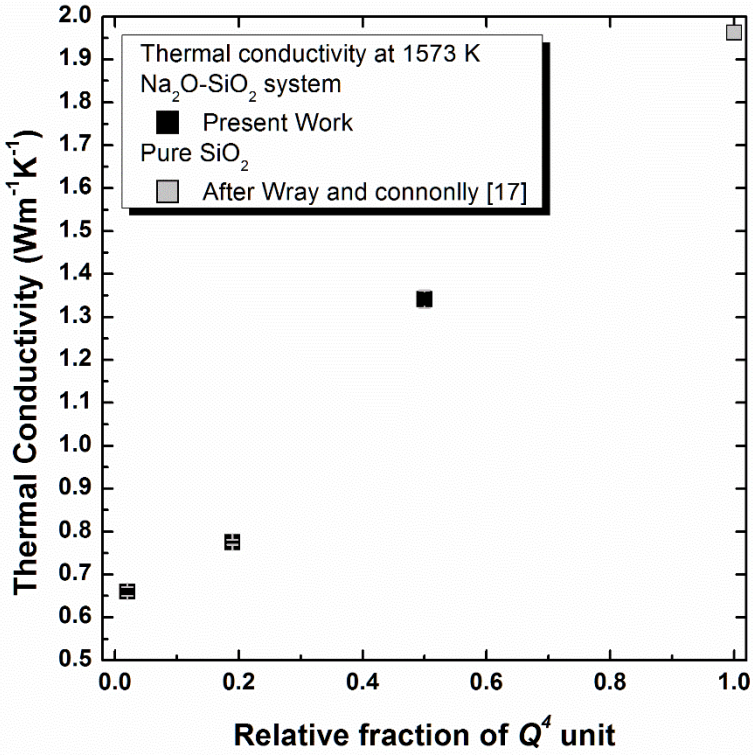

Fig. 3-4. The relationship between thermal conductivity and the Q^4 unit in the molten Na_2O-SiO_2 system at 1573 K.

On the other hands, the extent of the change of Q^4; gradually decreased from 0.50 into 0.19 and from 0.19 into 0.02 with the addition of Na_2O, was similar to that observed for the thermal conductivity, indicating the existence of a linear relation. As shown in Fig.3-4, the linear relationship between thermal conductivity and Q^4 unit in the molten sodium silicate system at 1573 K can be observed. It can be inferred that addition of sodium oxide into pure SiO_2 system[17] results in the gradual decreasing of thermal conductivity along with depolymerization of Q^4 units.

Mysen[18] suggested that the viscosity could be simply expressed as a function of Q^4, which is a criterion to evaluate the amount of fully polymerized structure, and found a positive linearity in the alkali silicate melts. Park[19] observed a linear relations between the Q^4 structural unit and the viscosity in the CaO-SiO_2-MgO and in the CaO-SiO_2-MnO systems. In addition, he suggested that both density and electrical conductivity should be expressed as a linear function of the Q^4 structural unit. Recently, Hasegawa et al.[7] reported that the thermal conductivity decreases exponentially with increasing NBO/T within the range 0 to 1, whereas it becomes almost constant for NBO/T above 1. It seems that, similar to other physical properties of molten oxide systems, the thermal conductivity is mainly affected by the fully polymerized network structure in the silicate system.

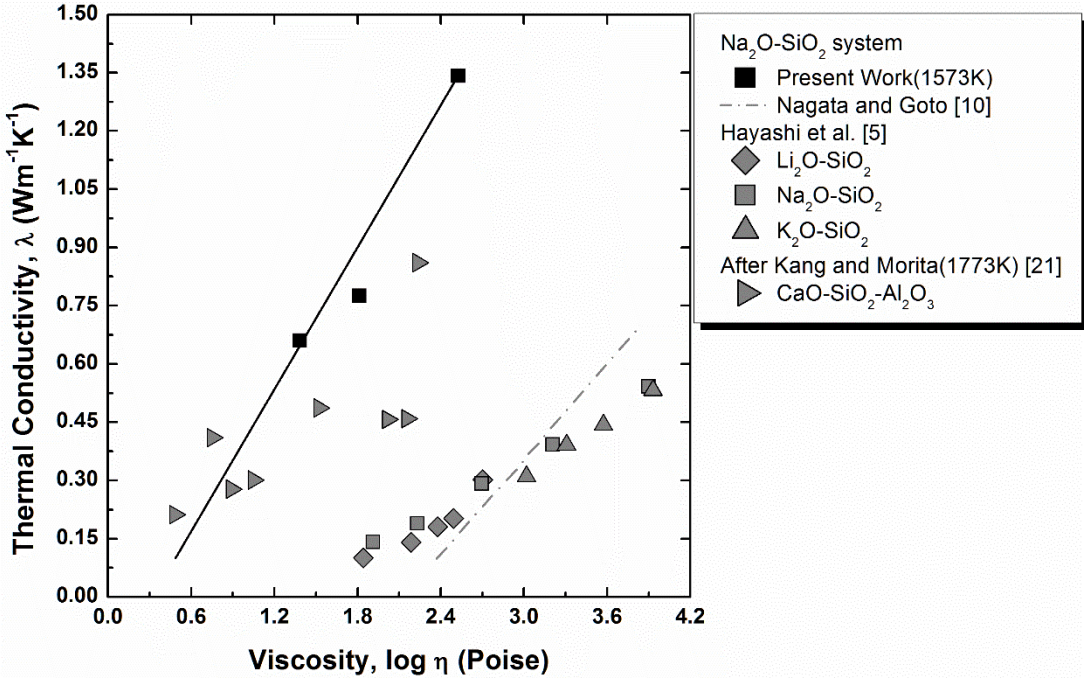

Fig. 3-5. Relationship between viscosity and thermal conductivity of the alkali silicate systems and of the CaO–SiO_2–Al_2O_3 system.

In Fig. 3-5, the relation between the thermal conductivity and the viscosity of molten oxide is displayed. The viscosity data for the Na_2O-SiO_2 system at 1573 K were obtained from a previous work[20]. In the case of the CaO-SiO_2-Al_2O_3 ternary system, thermal conductivity was obtained by Kang and Morita's work[21] and the viscosity was calculated using a thermochemical calculation program, FactSage™ 6.4. The linear relation derived for Na_2O-SiO_2 system shows a steeper slope and a higher intercept with respect to the results found in the literature[5]; however, it is valid in a different silicate system, namely the CaO-SiO_2-Al_2O_3 system. Similar to viscosity, which is mainly determined by the silicate network structure, it can be inferred that the thermal conductivity is also mainly affected by the structural change in the silicate network.

3.3.3. Thermal Conductivity in the Molten Na_2O-B_2O_3 system

Figure 3-6 shows the thermal conductivity change as a function of temperature in the Na_2O-B_2O_3 system. The thermal conductivity initially increases at the lower temperatures and becomes almost constant just below 1073 K. Similar to the negative temperature dependence of thermal conductivity observed for the Na_2O-SiO_2 system, this behavior should be attributed to a change in the phonon mean free path of collision (*l*) along with a change in the borate structure.

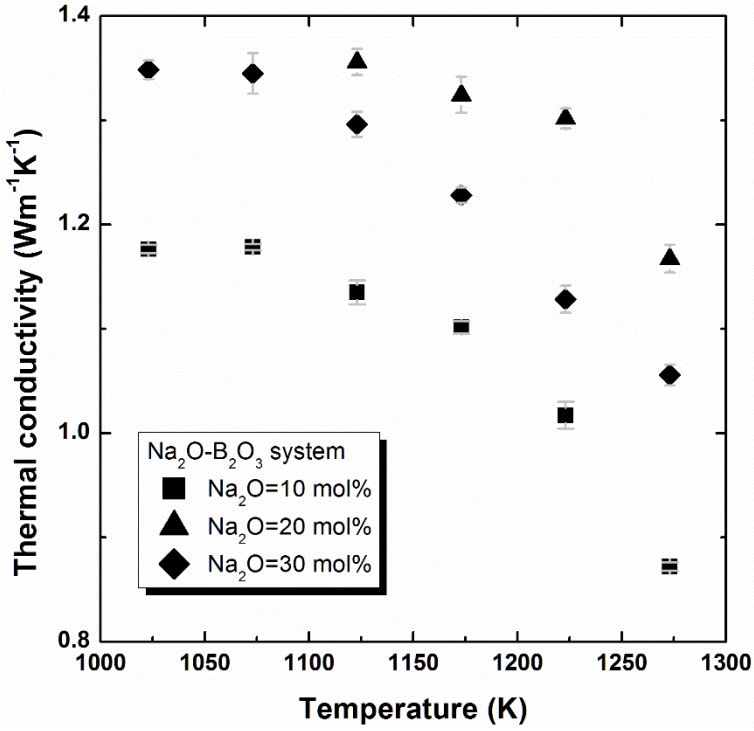

Fig. 3-6. Relationship between thermal conductivity and temperature in the Na_2O-B_2O_3 system.

Yano et al.[22] studied the borate structure in the Na_2O-B_2O_3 binary system using a high temperature Raman spectroscopy. In their study[23], they deconvoluted Raman spectra with Gaussian fitting at the region between 1000 and 1600 cm^{-1}. Within the high frequency region, they distinguished 6 different bands; indicating boroxol ring and loose BO_3 (denoted as SB1, SB2 and SB3), BO_3 triangle (denoted as SB5), and BO_2O^- units (denoted as SB4 and SB6). Based on the area of each SB units, they calculated the ratio (*S*) between asymmetric 3-coordinated boron and symmetric 3-coordinated boron.

$$S = \frac{I_{SB4} + I_{SB6}}{I_{SB1} + I_{SB2} + I_{SB3} + I_{SB5}} = k\frac{N_{3a}}{N_{3s}} \quad (3\text{-}5)$$

I_{SB} represents the intensity of each SB units, N_{3a} is the mole fraction of asymmetric 3-coordinated boron, N_{3s} is the mole fraction of symmetric 3-cooridinated boron and k is the correlation constant. In their study, they assumed that original symmetric 3-coordinated boron changes into both asymmetric 3-coordinateed boron and 4-coordinated boron by addition of alkali oxide, and it is proportional to mole fraction of alkali oxide.

$$N_{3a} + N_4 = \frac{x}{1-x} \quad (3\text{-}6)$$

As a result, following relation can be derived; N_4 and x are the mole fraction of 4-coorindated boron and alkali oxide, respectively.

$$N_{3s} + N_{3a} + N_4 = 1 \quad (3\text{-}7)$$

$$N_{3s} = \frac{1-2x}{1-x} \quad (3\text{-}8)$$

Combined equation (3-5), (3-6) and (3-8), the following equation can obtained.

$$N_4 = 1 - \left(1 + \frac{S}{k}\right)\left(\frac{1-2x}{1-x}\right) \quad (3\text{-}9)$$

It should be noted that they obtained k using ^{11}B NMR. They assumed that k is constant and independent from the temperature change. Although their two assumptions need more detailed investigation, in the present study, their high temperature borate structure was adopted in order to find the relationship between thermal conductivity and the borate structure.

According to Yano et al.[22], the amount of 4-coordinated boron decreases as the temperature increases, due to the formation of 3-coordinated boron with a NBO. Therefore, it can be inferred that a structural change from 4-coordinated boron to 3-coordinated boron with a NBO at the higher temperatures results in a decrease in thermal conductivity along with a shortening of the mean free path.

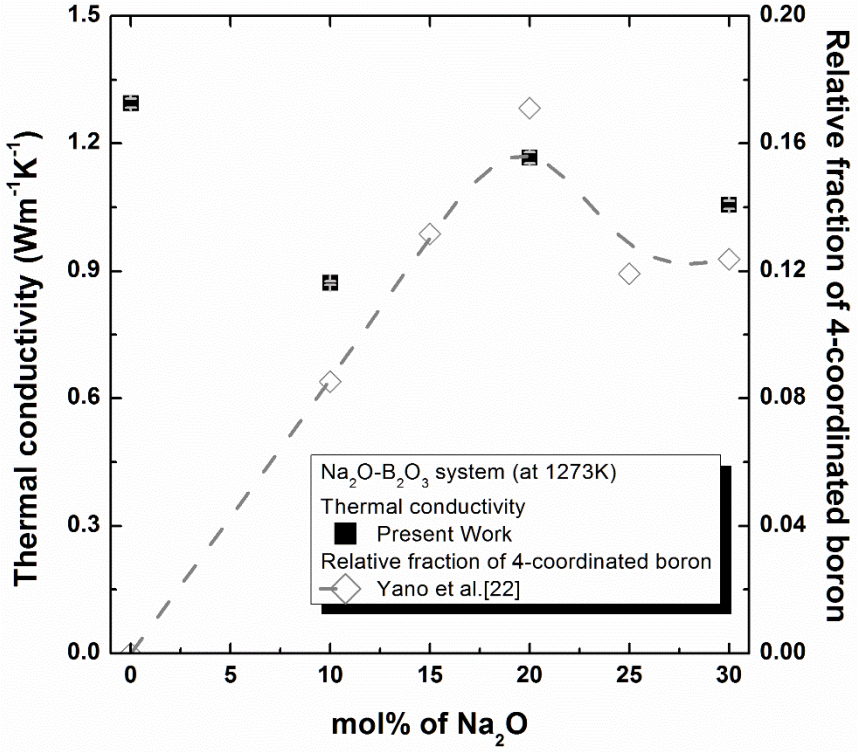

Fig. 3-7. Change of thermal conductivity and relative fraction of 4-coordinated boron[22] as a function of mol % of Na_2O at 1273 K

The thermal conductivity of 1273 K and the relative fraction of 4-coordinated boron[22] obtained at 1273 K by high temperature Raman spectroscopy were shown in Fig. 3-7 with varying mole percentage of Na_2O in the Na_2O-B_2O_3 system. In the region of $Na_2O \geq 10$ mol %, the change of thermal conductivity with varying Na_2O concentration shows a positive linear relation with the change of relative fraction of 4-coordinated boron. Both thermal conductivity and 4-coordinated boron initially increase for a higher Na_2O concentration, but decrease with a Na_2O concentration higher than 20 mol %. Similar relations between the 4-coordinated boron and other physical properties could be observed for the thermal expansion coefficient of the Na_2O-B_2O_3 system. According to Uhlmann and Shaw[24], the thermal expansion coefficient decreases when the Na_2O concentration increases to about 20 mol %, then it begins to increase. Richardson[25] explained that the formation of 4-coordinated boron tightens the structure and results in the decrease of the thermal expansion coefficient. However, at higher concentrations of Na_2O, the structure is weakened and it easily expands resulting in an increase of the coefficient of thermal expansion, due to the break-down of B-O-B bonds by formation of 3-coordinated boron with a non-bridging oxygen (NBO). Analogously, it seems that the thermal conductivity is also affected by both 4-coordinated boron and 3-coordinated boron with a NBO. At 1273 K, an addition of Na_2O in the B_2O_3

system results in the formation of a network structure based on 4-coordinated boron along with the increase of thermal conductivity due to a longer phonon mean free path. On the other hand, for a Na_2O concentration higher than 20 mol %, the thermal conductivity decreases due to a shortening of the mean free path, which results from the depolymerization of 4-coordinated boron due to the formation of 3-coordinated boron with a NBO. The formation of 4-coordinated boron is accompanied by the formation of a tetraborate unit, which is a three-dimensional network structure, thus explaining the observed increase or decrease in the thermal conductivity according to the change in the relative fraction of 4-coordinated boron.

Finally, in the region of $Na_2O < 10$ mol %, any change in thermal conductivity does not show a positive relationship with the change of 4-coordinated boron. According to Li et al.,[26] Na_2O plays two opposite roles in the borate melts: one is the breakdown of the coordinated structure with the formation of single bonded oxygens, the other one is the formation of 4-coordinated boron. The authors[26] suggested that in the region of $Na_2O < 10$ mol %, the first role is dominant, resulting in a decrease of viscosity for higher Na_2O concentrations. Considering these two phenomena, in the region of $Na_2O < 10$ mol %, any structural change from boroxol ring to tetraborate unit for higher Na_2O concentrations[23] should be accompanied by a rupture of the borate structure and by an increase of disorder. For this reason, the thermal conductivity would decrease for higher Na_2O concentrations due to a shorter phonon mean free path.

In Fig.3-8, the relationship between thermal conductivity and the relative fraction of 4-coorindated boron is displayed. While the thermal conductivity of the Na_2O-SiO_2 system is linearly correlated with the Q^4 unit, a linear relationship between thermal conductivity and 4-coordinated boron in the Na_2O-B_2O_3 system can be only observed within the region where the structure is mainly composed of tetraborate unit (10 mol % $\leq Na_2O \leq$ 30 mol %). In the region of low Na_2O concentration ($Na_2O < 10$ mol %), the thermal conductivity of the Na_2O-B_2O_3 system cannot be simply predicted on the basis of the relative fraction of 4-coordinated boron, due to the change of borate structure from boroxol ring to tetraborate unit along with increase of disorder. Therefore, it can be inferred that in the Na_2O-B_2O_3 system, not only the change of short-range order, such as the relative fraction of 3- or 4-coordinated boron, but also the change of the super-structure in the intermediate-range order, such as the boroxol ring and the tetraborate unit, affects the thermal conductivity.

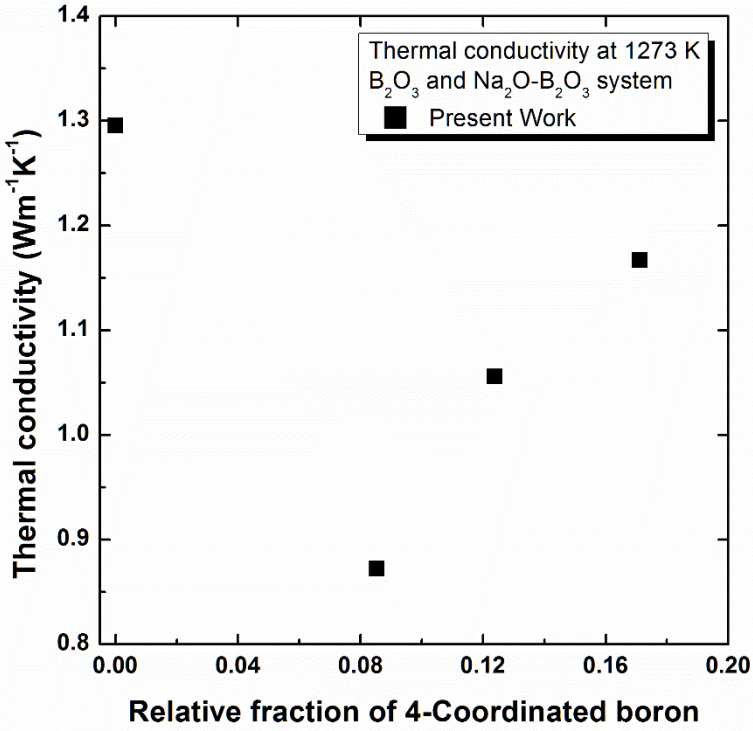

Fig. 3-8. Relationship between thermal conductivity and the relative fraction of 4-cooridnated boron.

3.3.4. Thermal Conductivity in the Molten R_2O-B_2O_3 (R= Li and K) system

3.3.4.1. Effect of temperature on thermal conductivity

Figure 3-9 shows the temperature dependence of the thermal conductivity in the Li_2O-B_2O_3 system. In the Li_2O = 30mol% system, the thermal conductivity steadily increases as the temperature decreases. Furthermore, in the case of the lithium borate system which has 10 and 20 mol% Li_2O, the thermal conductivity initially increases as the temperature decreases, and it then reaches a plateau or suddenly decreases at a temperature of approximately 1050 K.

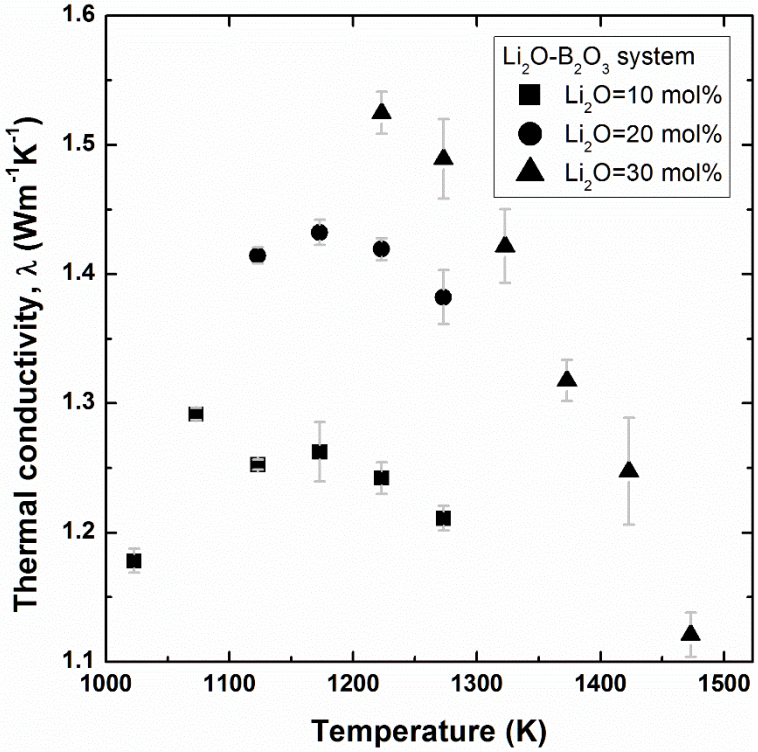

Fig. 3-9. The temperature dependence of thermal conductivity in the molten Li_2O-B_2O_3 system.

Figure 3-10 shows the relationship between the thermal conductivity and temperature in the molten K_2O-B_2O_3 system. In the K_2O = 10 mol% system, the thermal conductivity initially increases, but it reaches a plateau as the temperature decreases. Following the sudden decrease in the thermal conductivity at approximately 1100 K, constant thermal conductivity is maintained again. In the K_2O = 20 mol% system, the thermal conductivity gradually increases as the temperature decreases, but it drastically decreases at a temperature of 1150

K. Finally, within the potassium borate system with 30 mol% K_2O, the thermal conductivity initially increases, and then reaches a plateau as the temperature decreases.

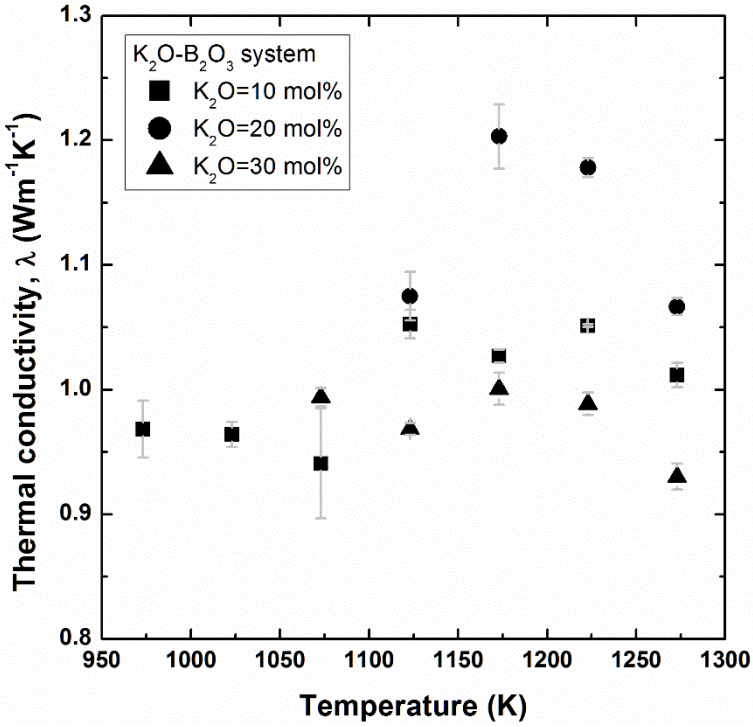

Fig. 3-10. The temperature dependence of thermal conductivity in the molten K_2O-B_2O_3 system.

According to equation (2-15), thermal conductivity is a function of specific heat capacity, mean particle velocity, and phonon mean free path of collision. Kingery[27] reported that the mean particle velocity and the heat capacity become constant above the Debye temperature (100 – 1000 K). Therefore, it can be inferred that a negative temperature dependence of thermal conductivity results from the negative temperature dependence of the mean free path of collision.

In order to confirm the variables affecting the present thermal conductivity, the Debye temperature of the K_2O-B_2O_3 and Li_2O-B_2O_3 systems should be evaluated.

Recently, Inaba et al.[28] successfully calculated the heat capacity and Young's modulus of oxide glass using a one-dimensional Debye-model, indicating that the lattice vibrational spectrum displays the characteristics of a one-dimensional continuum in the oxide glass system. They[28] reported that assumption of one-dimensional continuum for the polymerized glass materials; consisting of chain or layer structure, is more suitable than three-dimensional continuum.

Equation (3-10) shows the equation for the calculation of one-dimensional Debye

temperature.[28]

$$\Theta_{D1} = \left(\frac{3}{2}\right)\left(\frac{h}{k}\right)\left(\frac{N_A}{V_a}\right)^{1/3}\sqrt{\frac{2V_P G_t}{\rho}} \qquad (3\text{-}10)$$

Where, Θ_{D1} is the one-dimensional Debye temperature (K), h is Planck's constant (6.63×10^{-34} m^2 kg s^{-1}), k is the Boltzmann constant (1.38×10^{-23} m^2 kg s^{-2} K^{-1}), N_A is Avogadro's number (6.02×10^{23} mol^{-1}), V_p is the ionic packing ratio, G_t is the dissociation energy (J m^{-3}) and ρ is the density (kg m^{-3}). Figure 3-11 shows the calculated one-dimensional Debye temperatures of the present Li_2O-B_2O_3 and K_2O-B_2O_3 along with Na_2O-B_2O_3 systems. During the calculation, the density for the present borate system and the ionic radius of the metal and oxygen ions were obtained from appropriate references.[29–31] In addition, the relative fractions of 3- and 4-coordinate boron were also considered.

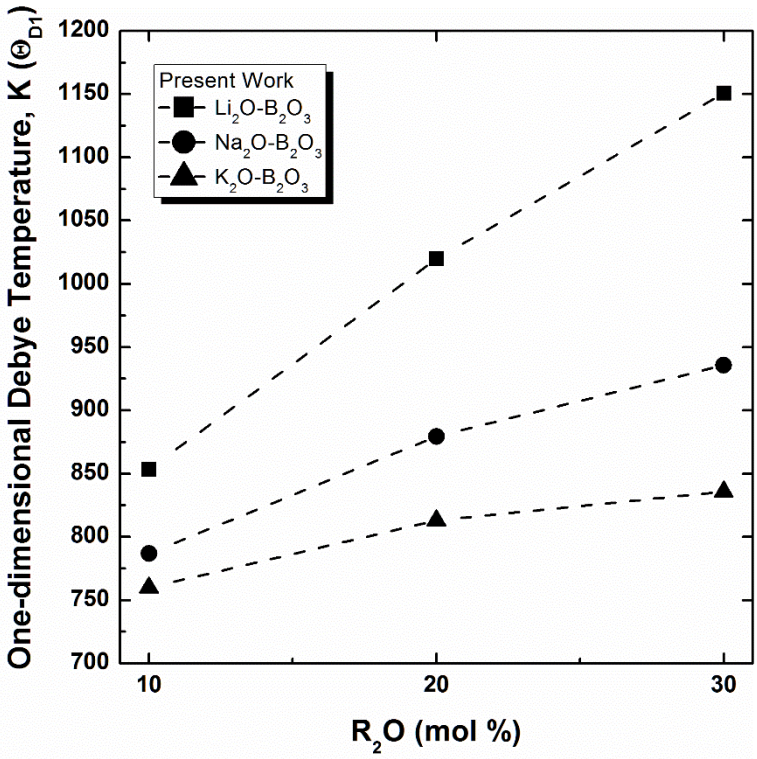

Fig. 3-11. The relationship between the calculated one-dimensional Debye temperature (Θ_{D1}) and the concentration of R_2O in the Li_2O-B_2O_3, Na_2O-B_2O_3 and K_2O-B_2O_3 systems.

According to Saddeek[32], the Debye temperature of the K_2O-B_2O_3 system is 342.9, 354.5 and 386.6 K for K_2O = 10, 20, and 30 mol%, respectively. Therefore, it can be found that

calculated one-dimensional Debye temperature shows much a higher value than the conventional Debye temperature (which considers the three-dimensional continuum). However, it is still lower than the present experimental temperature range; indicating that the present measurements were conducted above the Debye temperature. Therefore, it can be inferred that the change in the phonon mean free path of collision (*l*) mainly affects the thermal conductivity.

From equation (2-15), the phonon mean free path of collision (*l*) was calculated with varying temperature in the present Li_2O-B_2O_3, K_2O-B_2O_3 and Na_2O-B_2O_3 systems. During the calculation, the specific heat was obtained by following a modified empirical equation:[28]

$$C_P / n = 3R\left[1 - \exp\left(-5\frac{T}{\Theta_{D1}}\right)\right] \qquad (3\text{-}11)$$

Where C_P is the specific heat capacity (J mol^{-1} K^{-1}) , n is the number of atoms in the compound, R is a gas constant; 8.314 J mol^{-1} K^{-1}, T is the temperature (K), and Θ_{D1} is the calculated one-dimensional Debye-Temperature (K). The density was directly obtained[1] or extrapolated by varying the R_2O-B_2O_3 binary (R = Li, Na, K) system of the K_2O = 11.6, 19.5 mol% and the Na_2O = 28.7 mol% systems.[33] The mean particle velocity (v) was obtained from the measured longitudinal sound velocity.[2, 34, 35] During the calculation, the sound velocity of the Na_2O = 30 mol% and the Li_2O = 10 mol% systems was indirectly obtained from the Na_2O = 33.3 mol% and the Li_2O = 9.1 mol% systems. The calculated phonon mean free path is summarized in Table 3-4, 3-5 and 3-6, in addition to the measured thermal conductivity.

Table 3-4. The thermal conductivity and the calculated phonon mean free path of the Li_2O-B_2O_3 system with varying temperature.

	Li_2O = 10 mol%		**Li_2O = 20 mol%**	
Temperature (K)	**Thermal conductivity ($Wm^{-1}K^{-1}$)**	**Phonon mean free path (Å)**	**Thermal conductivity ($Wm^{-1}K^{-1}$)**	**Phonon mean free path (Å)**
1273	1.21	5.33	1.38	4.02
1223	1.24	5.40	1.42	4.03
1173	1.26	5.42	1.43	3.97
1123	1.25	5.31	1.41	3.83
1073	1.29	5.40		
1023	1.18	4.87		

Table 3-5. The thermal conductivity and the calculated phonon mean free path of the Na_2O-B_2O_3 system with varying temperature.

	Na_2O = 30 mol%	
Temperature (K)	**Thermal conductivity ($Wm^{-1}K^{-1}$)**	**Phonon mean free path (Å)**
1273	1.056	4.8
1223	1.128	5.0
1173	1.228	5.3
1123	1.296	5.4
1073	1.345	5.3

Table 3-6. The thermal conductivity and the calculated phonon mean free path of the K_2O-B_2O_3 system with varying temperature.

	K_2O = 10 mol%		**K_2O = 20 mol%**	
Temperature (K)	**Thermal conductivity ($Wm^{-1}K^{-1}$)**	**Phonon mean free path (Å)**	**Thermal conductivity ($Wm^{-1}K^{-1}$)**	**Phonon mean free path (Å)**
1273	1.01	2.35	1.07	2.26
1223	1.05	2.38	1.18	2.38
1173	1.03	2.27	1.20	2.30
1123	1.05	2.26	1.08	1.95
1073	0.94	1.96		
1023	0.96	1.94		

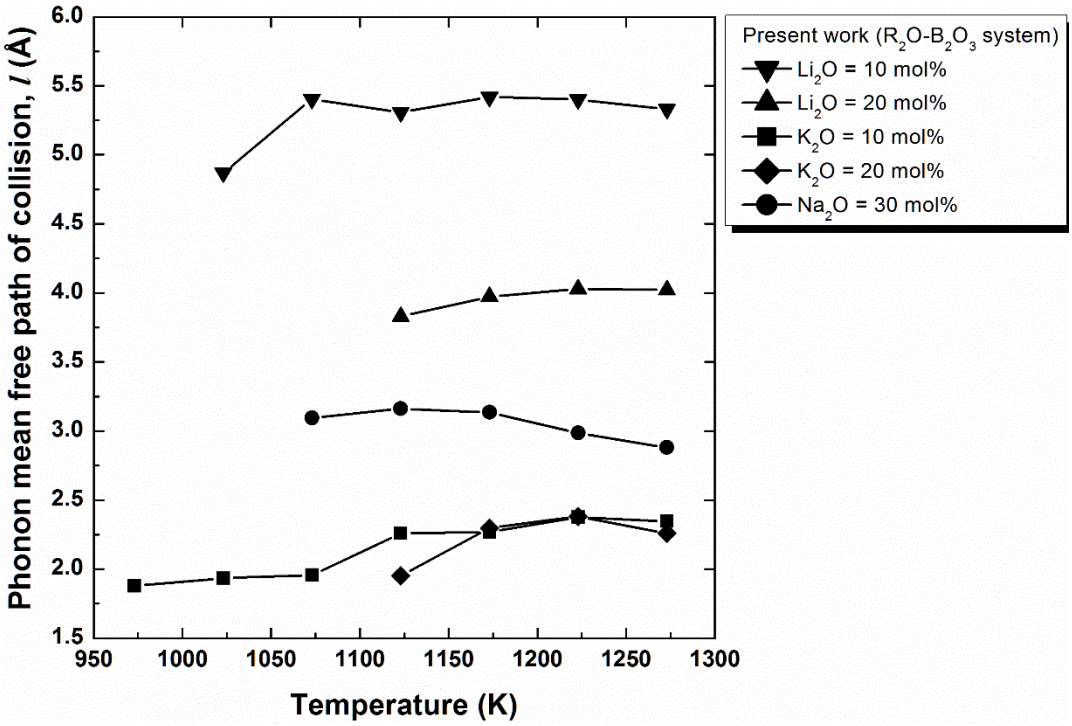

Fig. 3-12. The relationship between the calculated one-dimensional Debye temperature (Θ_{D1}) and the concentration of R_2O in the Li_2O-B_2O_3, Na_2O-B_2O_3 and K_2O-B_2O_3 systems.

In Fig. 3-12, the change in the phonon mean free path (l) with varying temperature for the Li_2O-B_2O_3, K_2O-B_2O_3, and Na_2O-B_2O_3 systems are shown. The increase in the phonon mean free path as the temperature decreases can be observed in the high temperature region; which is between 1173 K and 1273 K. However, below a temperature of approximately 1173 K, the phonon mean free path decreases or remains constant as the temperature decrease. The overall tendency in the change of the phonon mean free path correlates with the changes in the thermal conductivity. Therefore, it can be concluded that at temperatures above the Debye temperature, the change in the phonon mean free path mainly affects the thermal conductivity of the molten alkali borate system.

For the alkali borates and alkali borosilicate melts, there is an equilibrium between the 3-coordinate boron with the NBO and 4-coordinate boron:[22, 36]

$$BO_3 + NBO \leftrightarrow BO_4 \qquad (3\text{-}12)$$

Both the temperature and the concentration of the alkali oxide affect the equilibrium of equation (5); a decrease in the temperature or an addition of low alkali contents results in a

shift in the equilibrium (to the right).[36] Using high temperature Raman spectroscopy, Osipov and Osipova[37] recently confirmed the temperature dependence of the relative fraction of 4-coordinate boron in the Li_2O-B_2O_3, Na_2O-B_2O_3, and K_2O-B_2O_3 systems, reporting an increase in the 4-coordinate boron as the temperature decreased. Therefore, in the present study, the increase in the phonon mean free path results from the formation of 4-coordinate boron in addition to the formation of a three-dimensional network structure.

However, at temperatures between 1073 and 1173 K, a sudden decrease in the phonon mean free path and the thermal conductivity can be observed as the temperature decreases. The relative fraction of 4-coordinate boron steadily increases as the temperature decreases, and the intermediate-range order of the borate structure also changes depending on the temperature.[37] Therefore, this drastic decrease in both the phonon mean free path and the thermal conductivity with the decrease in the temperature could be related to a change in the intermediate-range order. However, a thorough structural investigation is required.

3.3.4.2. Effect of alkali oxide composition on thermal conductivity

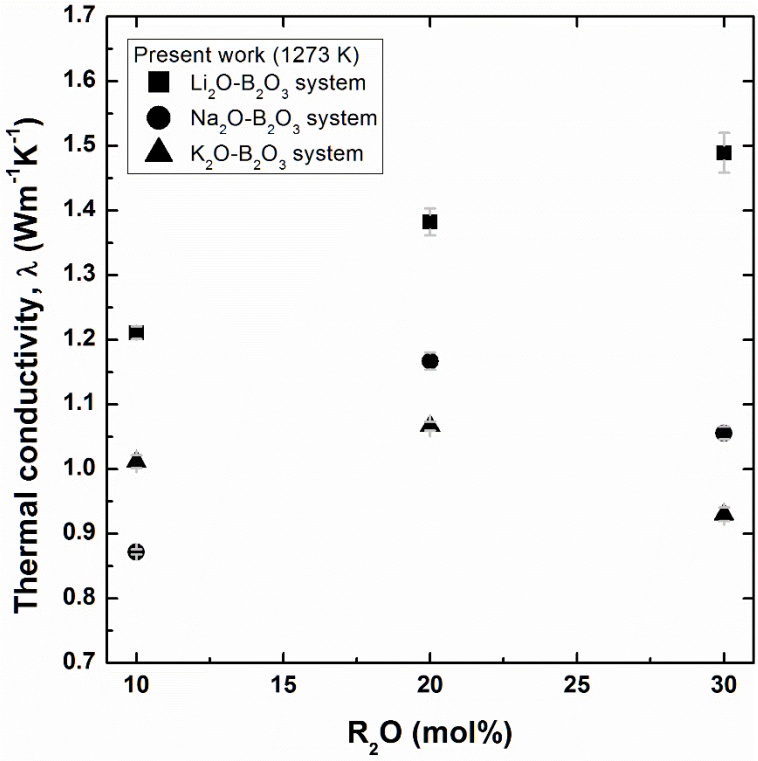

Fig. 3-13. The relationship between the thermal conductivity and the concentration of alkali oxide in the R_2O-B_2O_3 system at 1273 K.

Figure 3-13 shows the relationship between the thermal conductivity and the alkali oxide

concentration at 1273 K. In the Li_2O-B_2O_3 system, the thermal conductivity gradually increases with the addition of Li_2O. Furthermore, a conflicting effect of K_2O on the thermal conductivity can be observed in the K_2O-B_2O_3 system; the thermal conductivity initially increases as the K_2O concentration increases. However, the thermal conductivity decreases above K_2O = 20 mol%. This conflicting effect of alkali oxide on the thermal conductivity has also been observed in the Na_2O-B_2O_3 system. In the sodium borate system, it was determined that this conflicting effect (which was particularly observed between 10 and 30 mol% Na_2O) results from a change in the relative fraction of 4-coordinate boron. Likewise, it could be postulated that the present composition dependence of thermal conductivity is closely related to the change in the borate structure as the alkali oxide concentration varies.

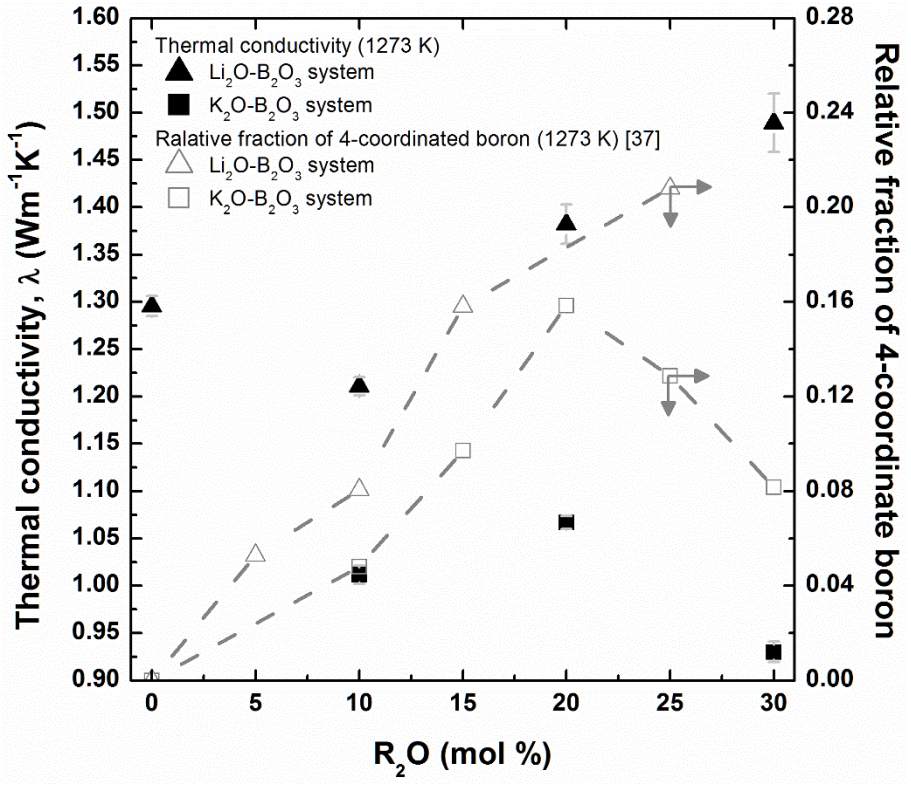

Fig. 3-14. The change in the thermal conductivity (black solid; left) and the relative fraction of 4-coordinate boron[37] (grey line; right) as a function of the mol % of R_2O at 1273 K. (R = Li, K)

The change in the thermal conductivity and the relative fraction of 4-coordinate boron[37] with varying concentration of Li_2O and K_2O at 1273 K are shown in Fig. 3-14. In the region of Li_2O (or K_2O)>10 mol%, a positive relationship can be observed between the thermal conductivity and the relative fraction of 4-coordinate boron. This was obtained with the aid of high temperature Raman spectroscopy at 1273 K.[37] The change in the boron coordination

number from 3 to 4 is accompanied by a structural change from the planar network of the boroxol ring to the three dimensional structure of tetraborate and diborate units. Owing to the formation of a three dimensional network structure, the thermal conductivity increases, along with a longer phonon mean free path. Furthermore, in the K_2O-B_2O_3 system, an addition of more than 20 mol% K_2O leads to the formation of NBO. This is as a result of the change from a BO_4 tetrahedron to an asymmetric BO_3 triangle within the diborate group.[37] As a result, both the phonon mean free path and the thermal conductivity decrease.

Below 10 mol% Li_2O and K_2O, while the relative fraction of 4-coordinate boron increases, the thermal conductivity decreases with the addition of alkali oxide. A similar negative dependence has been observed between the viscosity[3, 26] and 4-coordinate boron. In the Na_2O-B_2O_3 system, it was inferred that speculated that because the structure changes from a boroxol ring to a tetraborate or diborate unit, an increase in disorder accompanied by the rupture of the super-structural groups results in a decrease in the thermal conductivity as the Na_2O concentration increases. Likewise, in the Li_2O-B_2O_3 and K_2O-B_2O_3 systems, a change in the intermediate-range order structure more dominantly affects the thermal conductivity in the region below 10 mol% Li_2O and K_2O. In addition, the change in the intermediate-range order structure is different, depending on the type of modifier cation.[37] As a result, within the range of 0 to 10 mol% R_2O, the extent of the decrease in the thermal conductivity would be different, depending on the type of cation.

3.3.4.3. Effect of cation on thermal conductivity

As shown in Fig. 3-13, at a fixed R_2O = 20 and 30 mol%, the thermal conductivity is in the hierarchy order of Li_2O-B_2O_3 > Na_2O-B_2O_3 > K_2O-B_2O_3, for the relative systems.

To clarify the effect of the cations on the thermal conductivity, the thermal conductivity was plotted as a function of 4-coordinate boron, as shown in Fig. 3-15. It should be noted that the relative fraction of 4-coordinate boron for the Li_2O = 30 mol% system was extrapolated from the linear relationship between the concentration of Li_2O and the relative fraction of 4-coordinate boron[37], as shown in Fig. 3-14. In addition, the relationship between the thermal conductivity and 4-coordinate boron was only considered for the R_2O = 20 and 30 mol% systems, because the effect of the intermediate-range order on the thermal conductivity is dominant below 10 mol% R_2O. For a relative fraction of 4-coordinate boron of approximately 0.17, a variation in the thermal conductivity can be observed depending on the type of cation, indicating the effect of cations on the thermal conductivity.

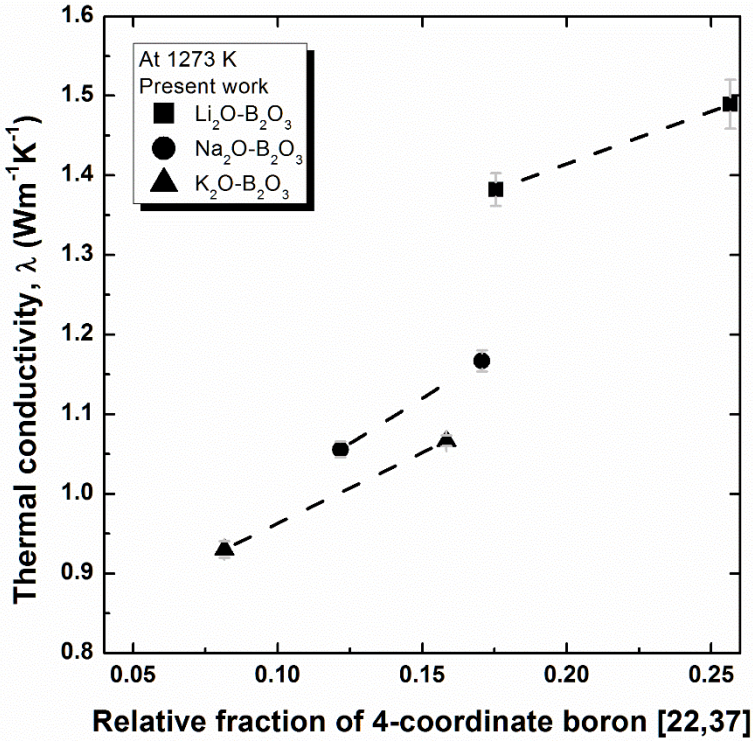

Fig. 3-15. The relationship between the thermal conductivity and the relative fraction of 4-coordinate boron[22, 37] in the R_2O-B_2O_3 system at 1273 K.

This effect of cations on the physical properties has been reported for the alkali borate system.[3, 24, 26, 33, 38] The viscosity[3, 26] and electrical conductivity[38] are in the hierarchy order of Li_2O-B_2O_3 > Na_2O-B_2O_3 > K_2O-B_2O_3 for the relative systems, and the opposite order can be observed for the apparent specific volume[33] and the coefficient of thermal expansion[24]. It was commonly inferred that the physical properties of the alkali borate system are affected by the type of cation because of the different cation field strengths (in the hierarchy order of Li>Na>K).

The effect of cations on the oxide structure can be evaluated by the use of the ionization potential (Z/r^2), which is the ratio of the charge of the cation (Z) to the square of the cation radius (r).[39] The calculated ionization potential, which represents the bond strength between the NBO and the cation, was determined as 1.73, 0.96 and 0.53 for Li_2O, Na_2O, and K_2O, respectively.[40] Therefore, it can be inferred that the rigidity of the structure is in the hierarchy order of Li_2O-B_2O_3 > Na_2O-B_2O_3 > K_2O-B_2O_3. In Fig. 3-12, a similar hierarchy can be observed for the phonon mean free path of collision. The longer phonon mean free path for the Li_2O-B_2O_3 system can be attributed to the greater rigidity of the network structure.

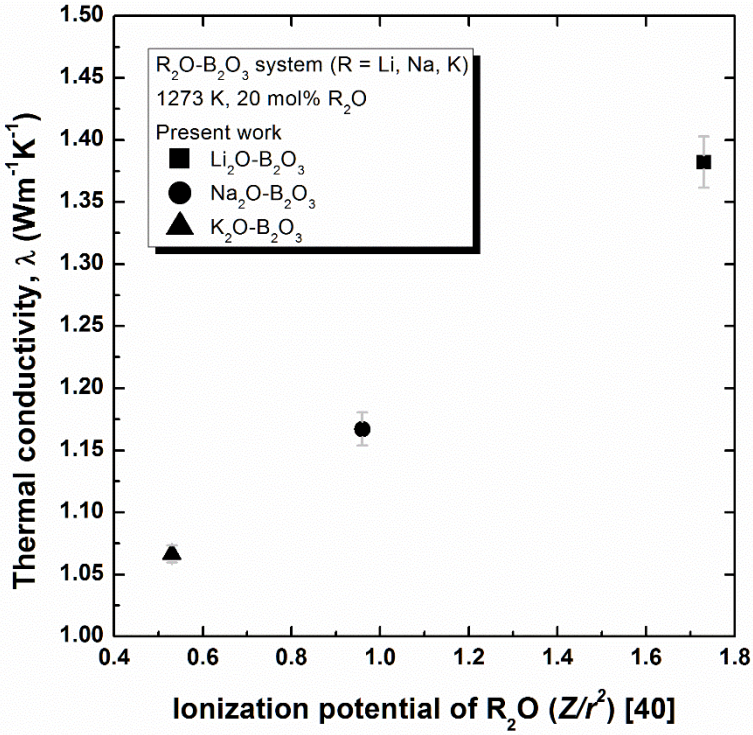

Fig. 3-16. The relationship between the thermal conductivity and the ionization potential[40] of R_2O in the R_2O-$4B_2O_3$ system at 1273 K.

As shown in Fig. 3-16, the linear relationship between the thermal conductivity and the ionization potential of the alkali oxide can be observed in the 20 mol% R_2O–B_2O_3 system at a temperature of 1273 K. Considering that these systems have almost the same relative fraction of 4-coordinate boron (approximately 0.17), the linear relationship between the thermal conductivity and the ionization potential implies that the thermal conductivity is affected by the bond strength between the NBO and the cation.

According to Mills et al.,[41] the thermal conductivity of the molten oxide system is determined by the rigidity of the network structure (which is related to the M-O bond strength). In addition, as mentioned above, Hayashi et al.[5] measured the thermal conductivity in the molten alkali silicate system and reported that the ionic character of the chemical bond between the cation and the NBO affects the thermal resistance ($1/\lambda$); in the hierarchy order of Li_2O-SiO_2 < Na_2O-SiO_2 < K_2O-SiO_2. Likewise, it can be concluded that the thermal conductivity of the molten alkali borate system is affected by the type of cation because of the change in both the rigidity of the structure and the thermal resistance.

3.4 Short Summary

In this chapter, thermal conductivity of the various molten alkali-borate system was measured by an aid of transient hot-wire method. In addition, thermal conductivity of sodium silicate system was also investigated in order to compare the effect of silicate and borate structure on thermal conductivity.

In the molten oxide system, negative temperature dependence of thermal conductivity was commonly observed at the higher temperature region. From the calculation of mean free path of collision, it was confirmed that negative temperature dependence results from the change of phonon mean free path; which is inversely proportional to absolute temperature. In addition, calculated one-dimensional Debye temperature supports that during the thermal conductivity measurement, other variables; mean particle velocity and heat capacity, keep constant. However, below certain temperature, thermal conductivity does not change with temperature change.

In the Na_2O-SiO_2 melt, positive linear relationship between thermal conductivity and Q^4 unit was observed. In addition, it was observed that viscosity and thermal conductivity of Na_2O-SiO_2 and CaO-SiO_2-Al_2O_3 shows linear relationship supporting the major effect of Q^4 unit on thermal conductivity in the molten Na_2O-SiO_2 system. However, in the molten Na_2O-B_2O_3 system, positive linear relationship between thermal conductivity and the relative fraction of 4-cooridnated boron can be only observed within the region where tetraborate and diborate is dominant. It was inferred that at the low alkali oxide concentration region; where boroxol ring structure is dominant, the change of intermediate range order structure significantly effects on the physical properties of alkali borate melts.

Finally, cation effect on thermal conductivity was investigated in the various alkali borate system. It was observed that calculated phonon mean free path shows hierarchy of Li_2O-B_2O_3 > Na_2O-B_2O_3 > K_2O-B_2O_3. Likewise, thermal conductivity also decreases with change of alkali oxide from lithium to sodium and from sodium to potassium. In order to evaluate the cation effect, ionization potential was considered. The linear relationship between ionization potential and thermal conductivity was observed among the three different alkali borate systems which have similar relative fraction of 4-coordinated boron. It can be concluded that thermal conductivity of molten borate system is affected by not only the borate network structure, but also the type of cation.

References

[1] X.M. Shi, Q. Wang, C.X. Li, X.J. Niu, F.P. Wang, and K.Q. Lu, "Densities of Li_2O–B_2O_3 melts," *J. Cryst. Growth*, **290** [2] 637–641 (2006).

[2] M. Kawashima, Y. Matsuda, S. Aramomi, and S. Kojima, "High Temperature Brillouin Scattering of Potassium Borate Glasses," *Japanese J. Appl. Phys.*, **49** [7] 07HB02 (2010).

[3] L. Shartsis, W. Capps, and S. Spinner, "Viscosity and electrical resistivity of molten alkali borates," *J. Am. Ceram. Soc.*, **36** [10] 319–326 (1953).

[4] L. SHARTSIS and H.F. SHERMER, "Surface Tension, Density, Viscosity, and Electrical Resistivity of Molten Binary Alkaline-Earth Borates," *J. Am. Ceram. Soc.*, **37** [11] 544–551 (1954).

[5] M. Hayashi, H. Ishii, M. Susa, H. Fukuyama, and K. Nagata, "Effect of ionicity of nonbridging oxygen ions on thermal conductivity of molten alkali silicates," *Phys. Chem. Glasses*, **42** [1] 6–11 (2001).

[6] H. Ohta, J. Kojima, G. Maejono, H. Shibata, and S. Sukenaga, "Thermal Conductivity of CaO-SiO_2-M_2O(M=Li,Na,K) Silicate Melts;" p. 109 in *169th ISIJ Meet.* The Iron and Steel Institute of Japan (ISIJ), Tokyo, 2015.

[7] H. Hasegawa, H. Ohta, H. Shibata, and Y. Waseda, "Recent Development in the Investigation on Thermal Conductivity of Silicate Melts," *High Temp. Mater. Proc.*, **31** [4-5] 491–499 (2012).

[8] Y. Kang, J. Lee, and K. Morita, "Comment on 'Thermal Conductivity Measurements of Some Synthetic Al_2O_3-CaO-SiO_2 Slags by Means of a Front-Heating and Front-Detection Laser-Flash Method,'" *Metall. Mater. Trans. B*, **44** [6] 1321–1323 (2013).

[9] G.J.K. Harrington, G.E. Hilmas, and W.G. Fahrenholtz, "Effect of carbon on the thermal and electrical transport properties of zirconium diboride," *J. Eur. Ceram. Soc.*, **35** [3] 887–896 (2015).

[10] K. Nagata and K.S. Goto, "Heat Conductivity and Mean Free Path of Phonons in Metallurgical Slags;" pp. 875–889 in *Second Int. Symp. Metall. Slags Fluxes*. Edited by H.A. Fine and D.R. Gaskell. The Metallurgical Society of AIME, Warrendale, Pa., 1984.

[11] L.W. Tilton, "Density formula for alkali silicate glasses from annealing to glass-processing temperatures," *J. Res. Natl. Bur. Stand.*, **61** [6] 463–467 (1958).

[12] D.E. Sharp and L.B. Ginther, "Effect of Composition and Temperature on the Specific Heat of Glass," *J. Am. Ceram. Soc.*, **34** [9] 260–271 (1951).

[13] H. Scholze, *Glass*. Springer New York, New York, NY, 1991.

[14] M. Kishimoto, M. Maeda, K. Mori, and Y. Kawai, "Thermal conductivity and specific heat of metallurgical slags;" pp. 891–905 in *Second Int. Symp. Metall. Slags Fluxes*. Edited by H.A. Fine and D.R. Gaskell. The Metallurgical Society of AIME, Warrendale, Pa., 1984.

[15] C. Kittel, "Interpretation of the thermal conductivity of glasses," *Phys. Rev.*, **75** [6] 972–974 (1949).

[16] H. Maekawa, T. Maekawa, K. Kawamura, and T. Yokokawa, "The structural groups of alkali silicate glasses determined from ^{29}Si MAS-NMR," *J. Non-Cryst. Solids*, **127** [1] 53–64 (1991).

[17] K.L. Wray and T.J. Connolly, "Thermal Conductivity of Clear Fused Silica at High Temperatures," *J. Appl. Phys.*, **30** [11] 1702–1705 (1959).

[18] B.O. Mysen, "Transport and configurational properties of silicate melts: Relationship to melt structure at magmatic temperatures," *Phys. Earth Planet. Inter.*, **107** [1-3] 23–32 (1998).

[19] J.H. Park, "Composition–structure–property relationships of CaO–MO–SiO_2 (M=Mg^{2+}, Mn^{2+}) systems derived from micro-Raman spectroscopy," *J. Non-Cryst. Solids*, **358** [23] 3096–3102 (2012).

[20] K.C. Mills, *Slag atlas*, 2nd ed. Verlag Stahleisen GmbH, Dusseldorf, 1995.

[21] Y. Kang and K. Morita, "Thermal conductivity of the CaO-Al_2O_3-SiO_2 system," *ISIJ Int.*, **46** [3] 420–426 (2006).

[22] T. Yano, N. Kunimine, S. Shibata, and M. Yamane, "Structural investigation of sodium borate glasses and melts by Raman spectroscopy. II. Conversion between BO_4 and BO_2O^- units at high temperature," *J. Non-Cryst. Solids*, **321** [3] 147–156 (2003).

[23] T. Yano, N. Kunimine, S. Shibata, and M. Yamane, "Structural investigation of sodium borate glasses and melts by Raman spectroscopy. I. Quantitative evaluation of structural units," *J. Non-Cryst. Solids*, **321** [3] 137–146 (2003).

[24] D.R. Uhlmann and R.R. Shaw, "The thermal expansion of alkali borate glasses and the boric oxide anomaly," *J. Non-Cryst. Solids*, **1** [5] 347–359 (1969).

[25] F.D. Richardson, *Physical chemistry of melts in metallurgy*. Academic Press, London, 1974.

[26] P.-C. LI, A.C. GHOSE, and G.-J. SU, "Viscosity Determination of Boron Oxide and Binary Borates," *J. Am. Ceram. Soc.*, **45** [2] 83–88 (1962).

[27] W.D. Kingery, *Introduction to ceramics*. John Wiley & Sons, New York, 1967.

[28] S. Inaba, S. Oda, and K. Morinaga, "Heat capacity of oxide glasses at high temperature region," *J. Non-Cryst. Solids*, **325** [1-3] 258–266 (2003).

[29] H. Doweidar, G.M. El-Damrawi, Y.M. Moustafa, and R.M. Ramadan, "Density of mixed alkali borate glasses: A structural analysis," *Phys. B Condens. Matter*, **362** [1-4] 123–132 (2005).

[30] N.A. Sharaf, A.A. Ahmed, and A.F. Abbas, "Mixed alkali effect on density , refractive index and related properties of alkali borate glasses," *Phys. Chem. Glasses*, **39** [2] 76–82 (1998).

[31] R.D. Shannon and C.T. Prewitt, "Effective ionic radii in oxides and fluorides," *Acta Crystallogr. Sect. B Struct. Crystallogr. Cryst. Chem.*, **25** [5] 925–946 (1969).

[32] Y.B. Saddeek, "Structural analysis of alkali borate glasses," *Phys. B Condens. Matter*, **344** [1-4] 163–175 (2004).

[33] L. SHARTSIS, W. CAPPS, and S. SPINNER, "Density and Expansivity of Alkali Borates and Density Characteristics of Some Other Binary Glasses," *J. Am. Ceram. Soc.*, **36** [2] 35–43 (1953).

[34] J.O. Bockris and E. Kojonen, "The Compressibilities of Certain Molten Alkali Silicates and Borates," *J. Am. Chem. Soc.*, **82** [17] 4493–4497 (1960).

[35] K. Nagata, K. Ohira, H. Yamada, and K.S. Goto, "Velocity and absorption coefficient of ultrasonic waves in molten and glassy silicates and borates," *Metall. Trans. B*, **18** [3] 549–555 (1987).

[36] M. Hubert and A.J. Faber, "On the structural role of boron in borosilicate glasses," *Phys. Chem. Glasses B*, **55** [3] 136–158 (2014).

[37] A.A. Osipov and L.M. Osipova, "Raman study of binary alkali borate glasses and melts in wide temperature range;" pp. 121–142 in *Prop. Struct. Oxide Glas.* Edited by V.P. Klyuev and B.Z. Pevzner. Research Signpost, Kerala, 2010.

[38] H. Doweidar, Y.M. Moustafa, G.M. El-Damrawi, and R.M. Ramadan, "Electrical conduction in alkali borate glasses; a unique dependence on the concentration of modifier ions," *J. Phys.: Condens. Matter*, **20** [3] 035107 (2008).

[39] B.O. Mysen and P. Richet, *Silicate Glasses and Melts*, 1st ed. Elsevier, Amsterdam, 2005.

[40] K.C. Mills, L. Yuan, Z. Li, K. Chou, and G. Zhang, "The factors affecting the thermophysical properties of slags and glasses;" in *Ninth Int. Conf. Molten Slags, Fluxes Salts*. Edited by K.-C. Chou. The Chinese Society for Metals, Beijing, China, 2012.

[41] K.C. Mills, L. Yuan, Z. Li, and G. Zhang, "Estimating viscosities, electrical & thermal conductivities of slags," *High Temp. - High Press.*, **42** 237–256 (2013).

Chapter IV

Thermal Conductivity of the molten Na_2O-B_2O_3-SiO_2 system

4.1 Background

In the previous chapters, we have measured thermal conductivity in the simple borate systems; pure B_2O_3, alkali borate system, along with some silicate based systems. The different effect of silicate and borate structure was observed; while alkali silicate system showed simple linear relationship between thermal conductivity and silicate structure, conflicting effect of B_2O_3 was observed depending on the intermediate range order borate structure.

Due to the network forming characteristic, the most of glass and mold flux system contains both B_2O_3 and SiO_2. According to Dell and Bray model,[1] in the Na_2O-B_2O_3-SiO_2 system, the addition of sodium oxide initially associates with 3-coordinated boron resulting in the coordination change from 3 to 4 coordinated boron. Further addition of alkali oxide leads to the coordination change from 4 to 3 coordinated boron with the formation of non-bridging oxygen (NBO) and depolymerization of the silicate network structure. As a result of the complicated structural change, the physical properties of the sodium borosilicate system cannot be simply estimated by a simple linear approximation based on chemical compositions.[2]

Several studies have been conducted in order to elucidate the relationship between structure and its physical properties in the Na_2O-B_2O_3-SiO_2 system.[3–8] Depending on Na_2O/B_2O_3 ratio[3] or SiO_2/Na_2O ratio[4], the conflicting effect of B_2O_3 on the viscosity in the molten sodium borosilicate system was observed. Although understanding the thermal conductivity of the molten oxide system is practically important for the thermal processing of the glass[9] and continuous casting process of steelmaking, the effect of both silicate and borate structure on the thermal conductivity has not been simultaneously considered in the molten state.

Therefore, in this chapter, in order to evaluate the effect of both borate and silicate structure, thermal conductivity was measured in the molten Na_2O-B_2O_3-SiO_2 system along with structural investigation using ^{11}B and ^{29}Si MAS NMR, Raman spectroscopy.

4.2 Experiment

4.2.1. Sample Preparation

The experimental compositions of present work are shown in Fig. 4-1. The samples were prepared with fixed K ratios (SiO_2/B_2O_3) of 0.5, 1.0, and 2.0, and various R ratios (Na_2O/B_2O_3). To investigate the glass structure of the present system, the experiments were performed outside the "No glass" region[10].

Reagent grade SiO_2, B_2O_3, and Na_2CO_3 were weighed and subsequently ground in an agate mortar for 20 min to obtain a homogeneously distributed mixture. The powder mixture was then transferred to a platinum crucible and kept in the temperature range of 1423–1573 K, depending on its melting temperature, to enable it to decarbonate, dehydrate, and homogenize. After 2 h, the melt was quenched on a water-cooled copper plate, and then it was finely crushed. The product was transferred to a Pt-10%Rh crucible (inner diameter (ID): 32 mm; outer diameter (OD): 38 mm; height: 70 mm), and the thermal conductivity was measured by the hot-wire method in the molten state.

After the measurement, the solidified sample was re-melted at 1373 K, quenched by pouring it onto a water-cooled copper plate, and then quickly covered with a copper block. The obtained glass was ground and sieved under 100 μm ϕ mesh.

For the ^{29}Si MAS NMR measurement, additional samples containing 0.1 mol % Fe_2O_3 to reduce the spin-lattice relaxation time were prepared.[11] The procedure followed to prepare the samples was the same as that described above.

4.2.2. Thermal Conductivity Measurement

The Pt-10%Rh crucible, filled with approximately 90 g of the pre-melted sample, was placed in a vertical furnace equipped with a SiC heating element. The sample was held for 1 h at 1273 K to obtain a homogeneous phase, and then the thermal conductivity of the Na_2O-B_2O_3-SiO_2 system was measured from 1273 K to the liquidus temperature at intervals of 50 K. The temperature of sample was controlled by the PID (proportional integral differential) controller and calibrated B-type thermocouple (Pt-30%Rh/Pt-6%Rh) within ± 3 K. To ensure the thermal equilibrium of the system, the furnace temperature was reduced at a rate of 3 K/min and held for 15 min at the target temperature. At each temperature, the thermal conductivity was measured three times at intervals of 5 min to examine the reproducibility.

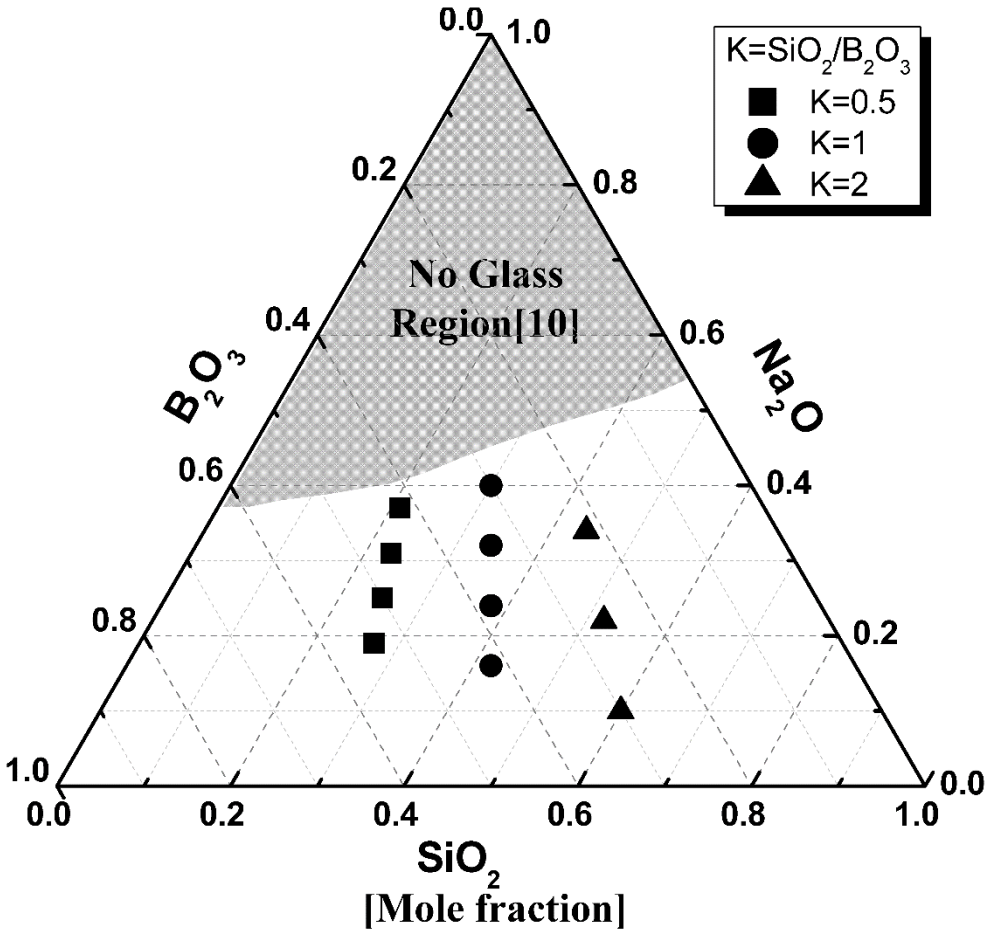

Fig. 4-1. Experimental compositions of the Na_2O-B_2O_3-SiO_2 system.

4.2.3. Analytical Procedures

4.2.3.1. Determination of the boron and sodium concentration in the sample

Approximately 0.01 g of the ground powder sample was transferred into 100 ml of beaker. Following the addition of acid-solution (10 ml of distilled water + 15 ml of HCl + 5 ml of HNO_3), the beaker was placed on the hot-plate covered with watch glass, and then heated at 493 K for several hours. When the almost of the acid solution was evaporated, approximately 5 ml of $HClO_4$ was added, and kept on heating until white smoke appeared.

The heated beaker was cooled down at room temperature. The solution was filtered using a filter paper (ash contents 0.1 mg/circle) attached on glass funnel, and transferred into 250 ml or 500 ml of volumetric flask, depending on the concentrations. After rinsing the beaker and filter paper several times by distilled water, the final volume was made to given volume of the volumetric flask. In order to obtain the homogeneous concentration across the solution,

the volumetric flask was kept for 24 hours.

Using the inductively coupled plasma atomic emission spectroscopy (ICP-AES; SPS7700, SII NanoTechnology, Japan), final concentration of boron and sodium was determined. Diluting the 1000 ppm of B and Na standard solution (Kanto chemical, Tokyo, Japan), four different standard solutions (1, 2, 4, 10 ppm) were prepared for each elements. Calibration line showed larger than 0.999 of correlation coefficient. During the analysis, 249.773 nm, and 588.995 nm of wavelength were chosen for boron and sodium as analytical wavelength, respectively. Table 4-1 shows the final composition of alkali borate system.

4.2.3.2. Determination of the silicon concentration in the sample

The SiO_2 content in the Na_2O-B_2O_3-SiO_2 system was determined by silica gravimetric method. The analyzed final compositions are listed in Table 4-1. The detailed procedures were described in the previous chapter.

Table 4-1. Initial and final composition of the present experiment.

	Initial compositions mol % (Weighed)			**R (Na_2O/B_2O_3)**	**K (SiO_2/B_2O_3)**	**Final compositions mol % (Analyzed)**		
	Na_2O	SiO_2	B_2O_3			Na_2O	SiO_2	B_2O_3
1	37.0	21.0	42.0	0.88	0.5	35.2	19.8	45.0
2	31.0	23.0	46.0	0.67	0.5	30.6	23.0	46.4
3	25.0	25.0	50.0	0.50	0.5	24.3	23.2	52.5
4	19.0	27.0	54.0	0.35	0.5	18.1	25.4	56.5
5	40.0	30.0	30.0	1.33	1.0	37.4	30.6	32.0
6	32.0	34.0	34.0	0.94	1.0	29.6	34.9	35.5
7	24.0	38.0	38.0	0.63	1.0	23.4	37.9	38.7
8	16.0	42.0	42.0	0.38	1.0	15.2	42.3	42.5
9	34.0	44.0	22.0	1.55	2.0	32.8	44.5	22.7
10	22.0	52.0	26.0	0.85	2.0	21.1	52.2	26.7
11	10.0	60.0	30.0	0.33	2.0	9.4	59.8	30.8

4.2.4. Structural Investigation

After obtaining confirmation of the non-crystalline state by X-ray Diffraction (XRD; RINT 2500, Rigaku, Japan), a structural investigation of the samples was conducted by using MAS

NMR. Figure 4-2 shows the x-ray diffraction pattern of glass Na_2O-B_2O_3-SiO_2 system.

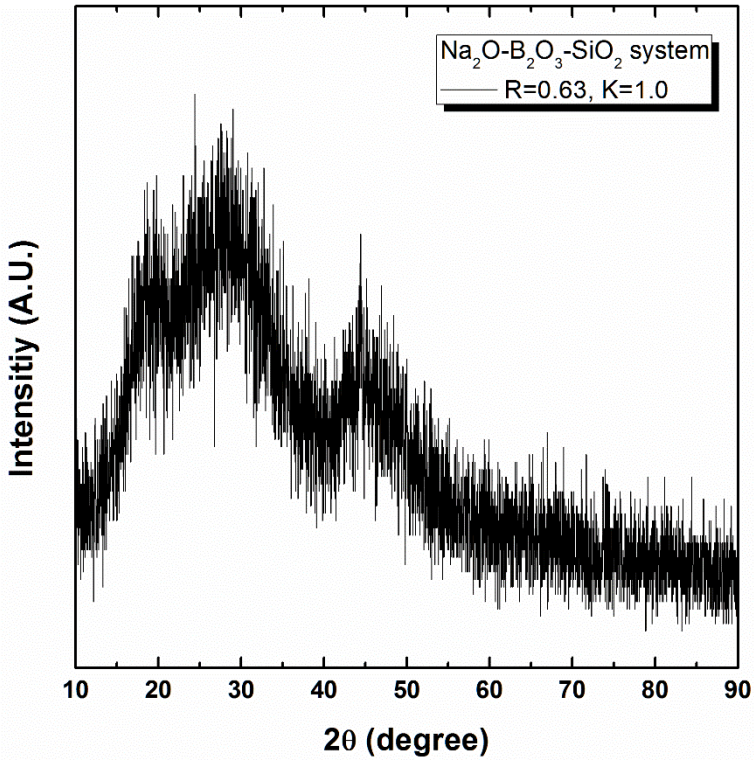

Fig. 4-2. X-ray diffraction pattern of non-crystalline Na_2O-B_2O_3-SiO_2 system.

Solid state ^{11}B and ^{29}Si MAS NMR spectra were recorded at 11.74 T using a Fourier transform (FT) NMR spectrometer (ECA-500, JEOL, Japan). The Larmor frequency was 160.4 MHz for ^{11}B MAS NMR and 99.4 MHz for ^{29}Si MAS NMR. Each sample was placed in a 4 mm ZrO_2 holder and spun at 16 kHz. Using a saturated H_3BO_3 solution (19.49 ppm) and 3-(Trimethylsilyl) propionic-2,2,3,3-d_4 acid sodium salt (98 atom % D) (1.445 ppm), the standards of ^{11}B and ^{29}Si MAS NMR were calibrated. The detailed conditions adopted for the MAS NMR measurements are reported in Table 4-2. After the measurements, the ^{29}Si MAS NMR data were fitted by a Gaussian function with the 'OriginPro (Ver.8.5)' software to obtain structural information.

In addition, intermediate range order structure of sodium borosilicate system was investigated by back-scattering Raman spectroscopy (T-64000, Horiba Jobin-Yvon, France). The powder sample was irradiated by an argon ion laser with the wavelength of 514 nm operated at 100 mW. The detailed measurement conditions were explained in the previous chapter.

Table 4-2. Experimental conditions for the ^{11}B and ^{29}Si MAS NMR measurements.

Nuclear Property	**^{11}B**	**^{29}Si**
Nuclear Spin	3/2	1/2
Larmor frequency [MHz]	160.4	99.4
RF pulse intensity [kHz]	66	50
Repetition times	64	1000
Flip angle [rad]	π/6	π/2
Delay time [s]	5	20
Spinning rate [kHz]	16	16

4.2.5. Determination of the Glass Transition Temperature

In order to find the glass transition temperature of quenched sample, differential thermal analysis (DTA) was carried out using TG-DTA (Thermo plus TG 8120, Rigaku, Tokyo, Japan). Approximately 0.02 g of powdered sample was filled in the platinum pan (ID: 5 mm; OD: 5.05 mm; height: 2.5 mm) and placed on the platinum plate at the end of ceramic rod. A similar quantity of reference sample (Al_2O_3) was filled in the same size of platinum pan and placed on the platinum plate at the end of another ceramic rod. Under the argon atmosphere, the samples were heated up from room temperature to 1123 K at a rate of 5 K/min. The differential thermocouple temperature was recorded as function of time. After it reaches target temperature, the sample was cooled down at a rate of 20 K/min. The glass transition temperature was determined from the heating curve by standard test method (E1356-08) proposed by American Society for Testing Materials (ASTM).[12]

4.3 Results and Discussion

4.3.1. Effect of Temperature on Thermal Conductivity

Figure 4-3 shows the temperature dependence of the thermal conductivity with varying R and K ratios. As explained in previous section, due to the negative temperature dependence of phonon mean free path, thermal conductivity also decreases with higher temperature.

In the low-temperature region, the thermal conductivity of the oxide system initially increases with increasing temperature as a result of the increase in both the specific heat capacity (C) and the mean particle velocity (v), as described by equation (1).[13, 14] However, above the Debye temperature, owing to the approximately constant specific heat capacity (C) and mean particle velocity (v), the thermal conductivity of the oxide system decreases with increasing temperature as a result of the decrease in the phonon mean free path of collision (l), which is proportional to the inverse of the temperature ($1/T$). [15–18] Hence, it can be inferred that thermal conductivity reaches the maximum value around the Debye temperature, and then it decreases with higher temperatures. Therefore, identifying the Debye temperature in the oxide system is essential to evaluate the temperature at which thermal conductivity shows the maximum and to determine which variables mainly affect the thermal conductivity at the given temperature.

Using the equation (3-10), the one-dimensional Debye temperature of the present sodium borosilicate system was calculated. During the calculation, the density was estimated from reference[6]. In addition, the relative fraction of both 3- and 4-coordinated boron was also considered. Figure 4-4 shows the one-dimensional Debye temperature of the current Na_2O-B_2O_3-SiO_2 system with varying R and K ratios. The one-dimensional Debye temperature of the present system can be found between 920 K and 1060 K. In this work, all the measurements were carried out above the one-dimensional Debye temperature, indicating that specific heat capacity and mean particle velocity could be characterized as constant. Therefore, the thermal conductivity of the present system is mainly affected by the change of the mean free path of collision (l), which is inversely proportional to the temperature, resulting in the decrease in thermal conductivity with increasing temperature.

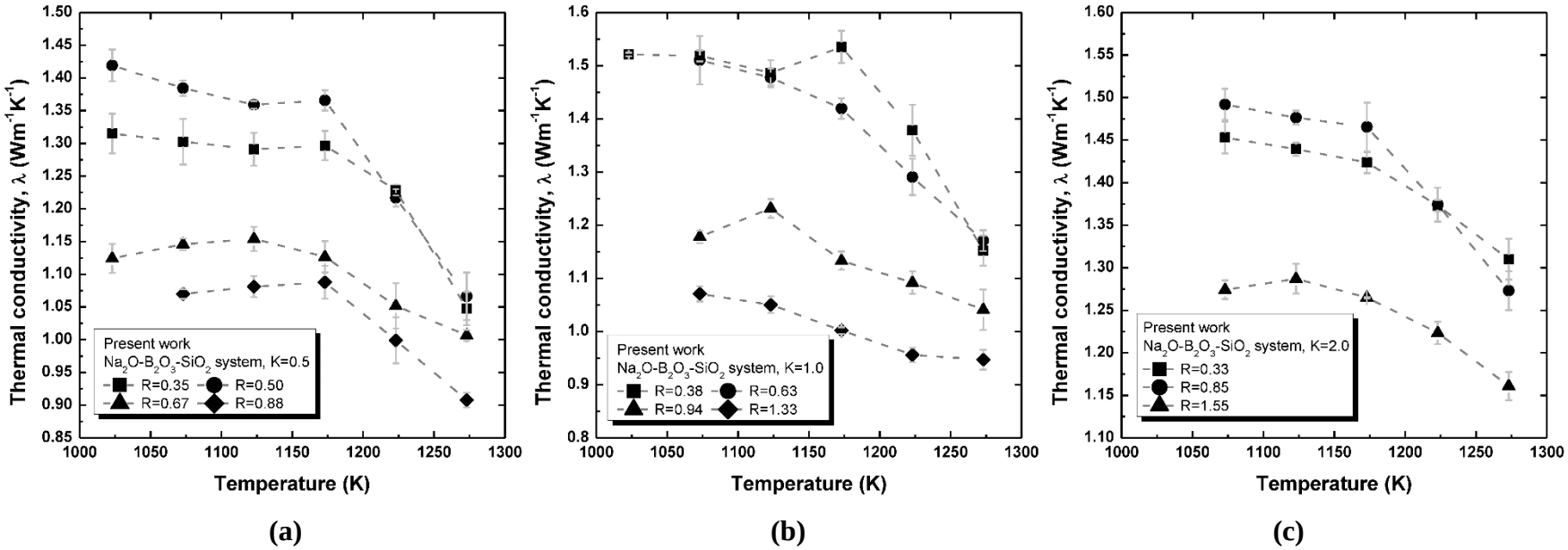

Fig. 4-3. Temperature dependence of the thermal conductivity in the Na_2O-B_2O_3-SiO_2 system for (a) K = 0.5, (b) K = 1.0, and (c) K = 2.0.

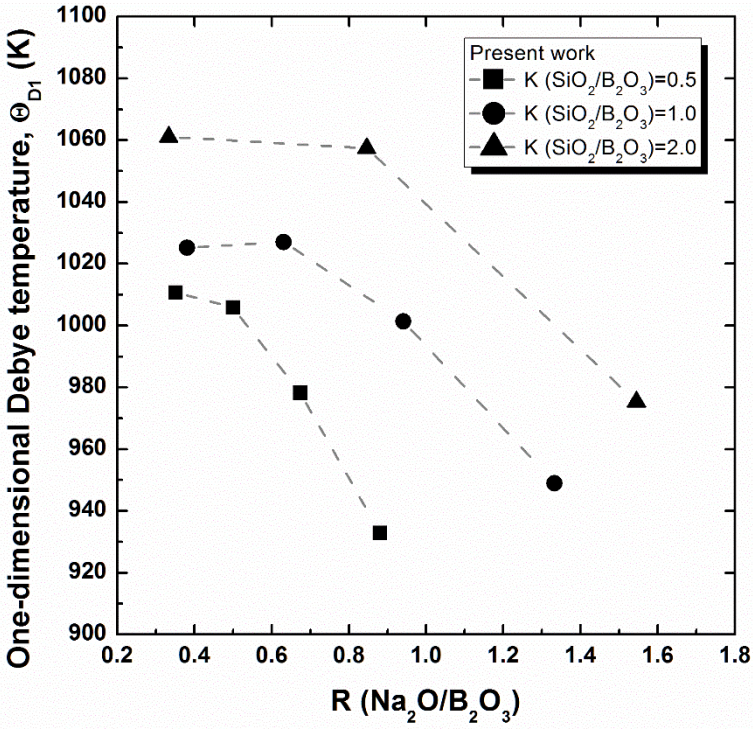

Fig. 4-4. Relationship between the R ratio and the calculated one-dimensional Debye temperature of the present system at a fixed K ratio

In Fig. 4-4, the one-dimensional Debye temperature decreases with higher R or lower K ratio. According to Inaba et al.[19], the one-dimensional Debye temperature is related to the interatomic bonding between network forming cations and anions. Therefore, the decrease in the one-dimensional Debye temperature with higher R or lower K ratios reflects the weakening of the bonding strength. Because of the formation of 4-coordinated boron, which has a weaker bonding strength than 3-coordinated boron[20], and the depolymerization of the silicate network, the bonding strength decreases at higher R ratios reducing the one-dimensional Debye temperature.

4.3.2. Effect of borate and silicate structures on thermal conductivity

The change of thermal conductivity with varying Na_2O/B_2O_3 ratio at 1273 K is shown in Fig. 4-5. The conflicting effect of the R ratio on thermal conductivity can be observed at the fixed values of K = 0.5 and 1.0. Thermal conductivity initially increases with increasing R ratio, but after reaching a maximum at approximately R = 0.5, it decreases. On the other hand, at K = 2.0, only a monotonous decrease in thermal conductivity can be observed in the current work. Such a change of thermal conductivity with varying R ratio is in good agreement with the change of 4-coordinated boron. In addition, a higher thermal conductivity can be observed at higher K ratios across the entire range of R ratios, indicating a significant effect of SiO_2 on thermal conductivity.

In order to find out the relationship between the relative fraction of 4-coordinated boron and thermal conductivity, borate structure was investigated using ^{11}B MAS NMR. Compared to other infrared spectroscopy, ^{11}B MAS NMR has the virtue of readily distinguishing between 3- and 4-coordinated boron. In addition, the silicate network structure was evaluated using ^{29}Si MAS NMR. Due to the weak Raman intensity of Q^4 unit in the high frequency region[21], Raman spectroscopy is not suitable for the silicate structure investigation, especially consisting of a large proportion of Q^4 unit. Therefore, in the present study, the relative fraction of silicate structure unit was determined by the relative area ratio of ^{29}Si MAS NMR spectra.

Figure 4-6 shows the ^{11}B MAS NMR spectra of the current Na_2O-B_2O_3-SiO_2 system. Du and Stebbins[22] studied the structure of the sodium borosilicate system reporting that each 3-coordinated boron and 4-coordinated boron is centered on 12 and 0 ppm, respectively. Nanba et al.[23] found that the asymmetric broad peak observed between 20 and −20 ppm can be attributed to 3-coordinated boron in the BO_3 unit. On the basis of the references[22, 23], the present MAS NMR spectra were identified and the relative fractions of 3- and 4-coordinated boron were calculated based on the area ratio.

Figure 4-7 shows the change of 4-coordinated boron with varying R ratio at a fixed K ratio. Although the relative fraction of 4-coordinated boron obtained in the present work is about 5 pct point higher than that in the previous work[23], the overall tendency shows an excellent accordance between the values. The relative fraction of 4-coordinated boron initially increases with increasing R ratio, reaches a maximum around R = 0.6 – 0.8, and then decreases.

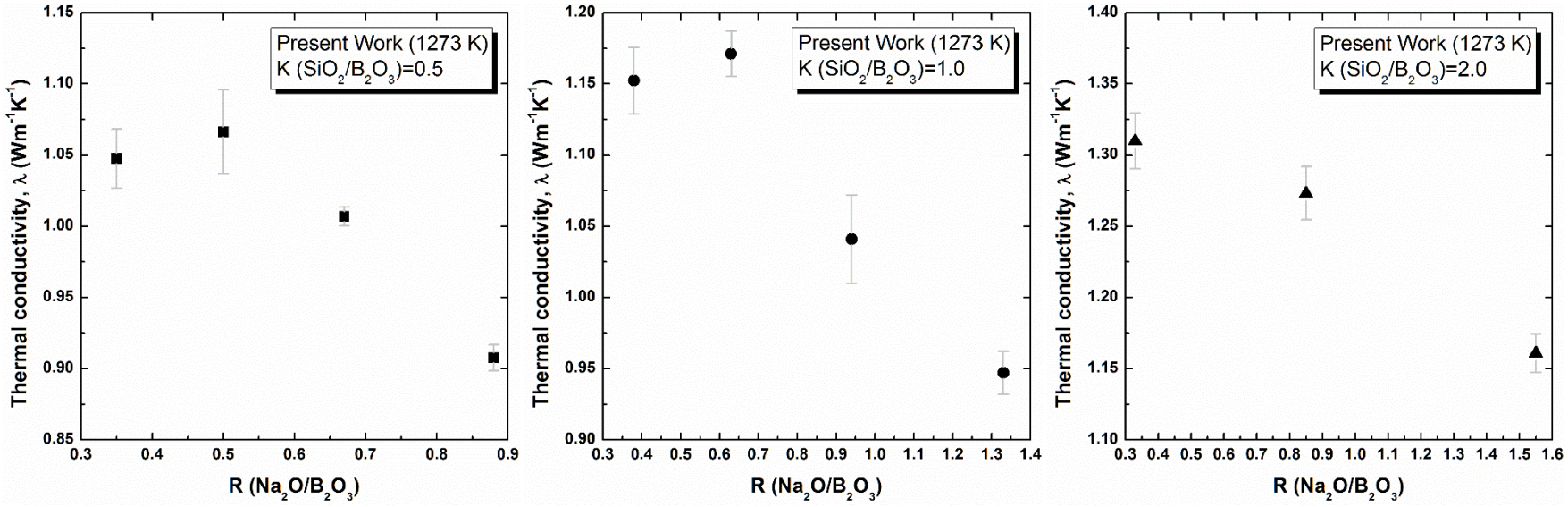

(a) **(b)** **(c)**

Fig. 4-5. Relationship between the R ratio and the thermal conductivity of the Na_2O-B_2O_3-SiO_2 system at 1273 K for different K ratios: (a) K = 0.5, (b) K = 1.0, and (c) K = 2.0.

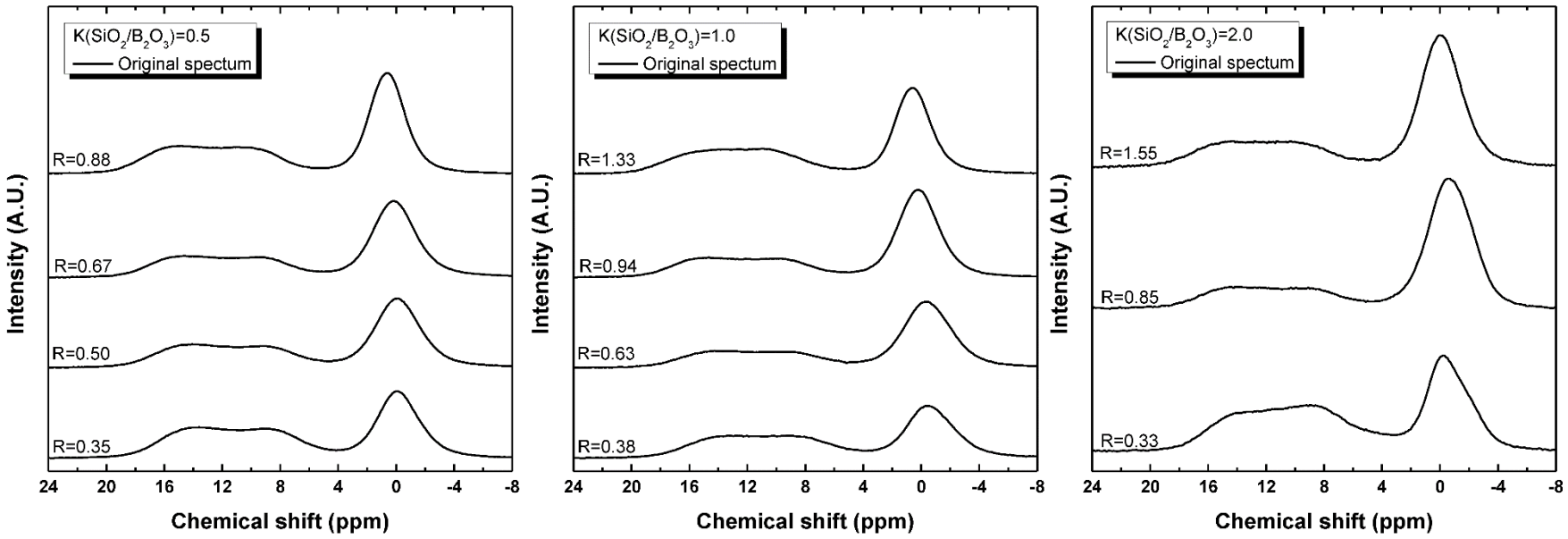

Fig. 4-6. ^{11}B MAS NMR spectra with varying R ratio for (a) K = 0.5, (b) K = 1.0, and (c) K = 2.0.

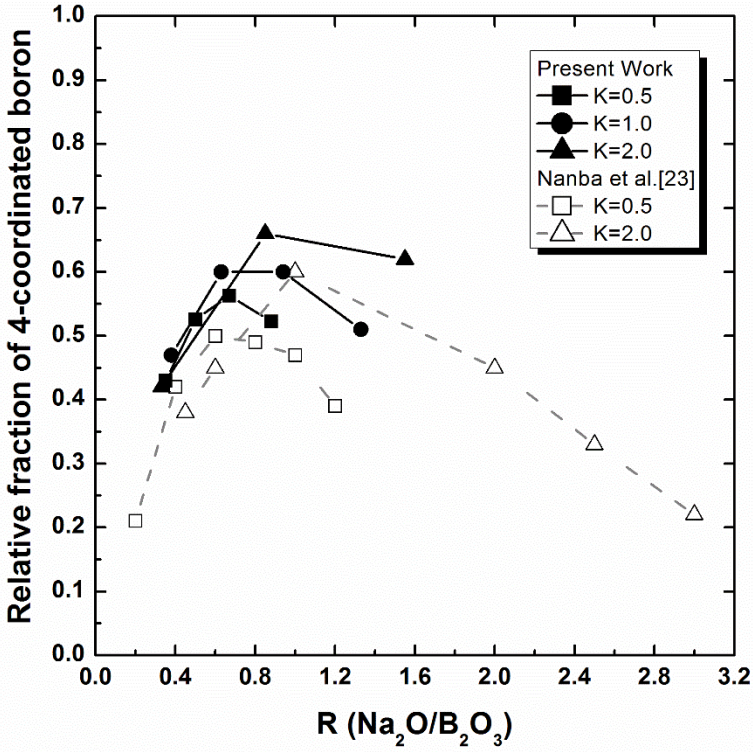

Fig. 4-7. Relationship between the R ratio and the relative fraction of 4-coordinated boron at a fixed K ratio.

Figure 4-8 and 4-9 show the Raman spectra of the present Na_2O-B_2O_3-SiO_2 system. Using Gaussian deconvolution, the obtained Raman spectra were identified from appropriate references.[24–32]

Several studies[27, 33] reported that isolated diborate units are observed within 490 – 570 cm^{-1} of Raman wavelength. However, as shown in Fig 4-8(a) and Fig. 4-9, the present Raman spectrum at the region of 300 – 600 cm^{-1} increases with higher SiO_2 concentration. Therefore, in the present study, the Raman band observed within 300 – 600 cm^{-1} was considered as silicate related band. In addition, although Bunker et al.[24] assigned 630 cm^{-1} band as danburite-like ring structure; which is the mineral composed of $CaB_2Si_2O_8$, this Raman band was considered as metaborate ring structure in the present study. They assigned 630 cm^{-1} peak as danburite-like ring structure due to no metaborate spectrum in their study.[24] However, in the present study, metaborate peaks can be observed at the higher frequency region. Therefore, it is more reasonable that 630 cm^{-1} band is assigned as the metaborate ring structure. The detailed reference and observed peak position of Raman spectroscopy along with related structural units are summarized in Table 4-3.

Table 4-3. Reference and observed peak positions of Raman and its related structures in the Na_2O-B_2O_3-SiO_2 system

Reference position (cm^{-1})	**Assignments**	**Observed position (cm^{-1})**
300 – 600	Mixed stretching & bending modes of Si-O-Si bridging bonds[24]	400 – 510
630	Metaborate ring structure[28–30]	630 – 640
670	Tetraborate structure[26]	680 – 710
700 – 850	Symmetric stretching vibrations of borate rings of various types[24–27]	710 – 850
850 – 1150	Stretching region of Si-O bond[31]	900 – 1150
1250 – 1400	Vibration of BO_3 triangle units in boroxol ring or loose BO_3 units[32]	1250 – 1400
1480 – 1550	Stretching of $B\text{-}O^-$ bonds in metaborate structures[32]	1440 – 1550

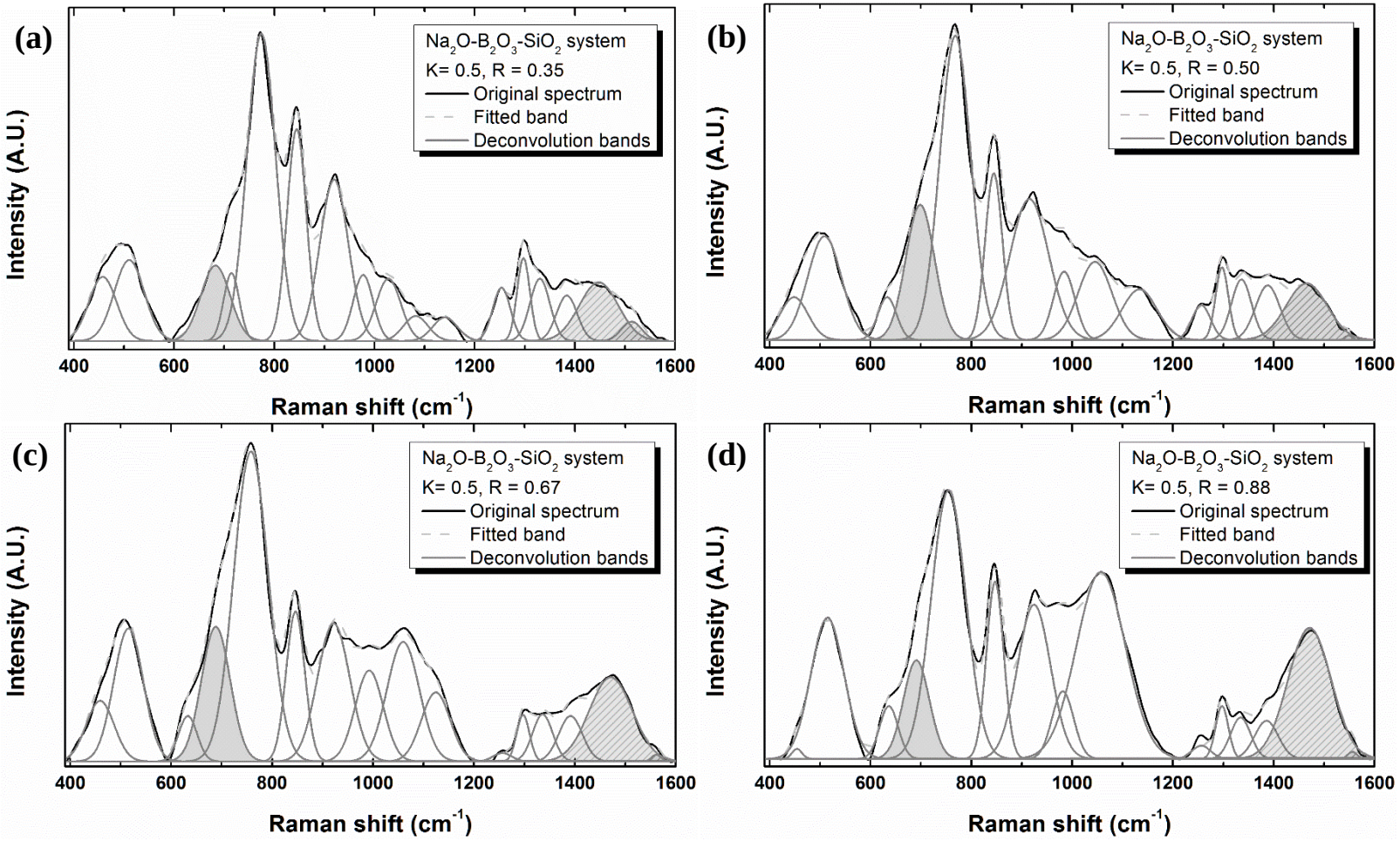

Fig. 4-8. Raman spectra and its Gaussian decovolution bands of the non-crystalline Na_2O-B_2O_3-SiO_2 samples with R ratio of (a) 0.35, (b) 0.50, (c) 0.67, and (d) 0.88 at a fixed K ratio of 0.5.

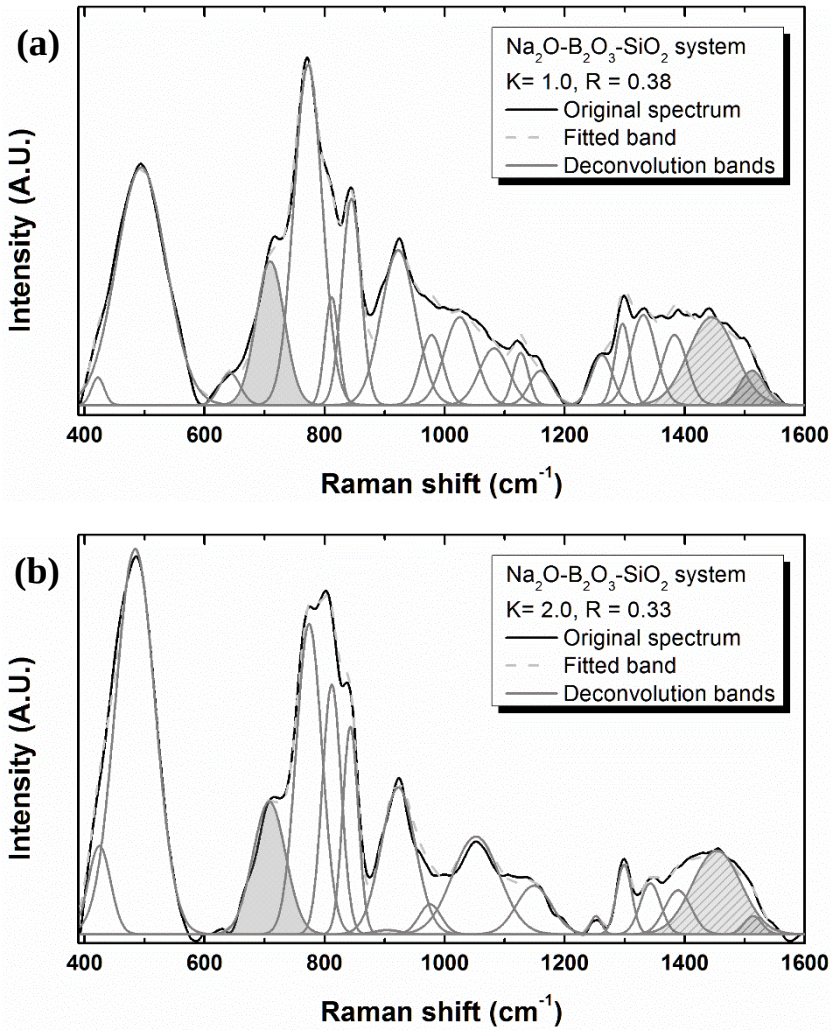

Fig. 4-9. Raman spectra and its Gaussian decovolution bands of the glass Na_2O-B_2O_3-SiO_2 samples with (a) K ratio of 1.0 at a R ratio of 0.38 and (b) K ratio of 2.0 at a R ratio of 0.33.

In Figure 4-8 and 4-9, the Raman bands related to tetraborate structure and metaborate structure are shaded without pattern and with dense-pattern, respectively. The relative fraction of tetraborate and metaborate structure was calculated based on the area fraction; each band area over total area of borate structure related bands.

Figure 4-10 shows the change of tetraborate and metaborate units with varying R ratio at a fixed K ratio of 0.5. It should be noted that the relative fraction of tetraborate units does not give quantitative information, and only can give qualitative information. Although 670 cm^{-1} peak of Raman spectrum is the characteristic band for tetraborate unit,[26] the spectrum related to tetraborate is also observed within 700 – 850 cm^{-1} region. However, within this region, other borate structures; such as boroxol rings, diborate and tetraborate groups, also contributes to the overall Raman bands. And it is hard to distinguish only tetraborate structure from other

borate structure. Therefore, the real relative fraction of tetraborate structure should be larger than the relative fraction obtained from 670 cm^{-1} peak. For this reason, in Fig. 4-10 and 4-16, the relative fraction of tetraborate unit was plotted as amount of tetraborate structure in arbitrary unit (A.U.).

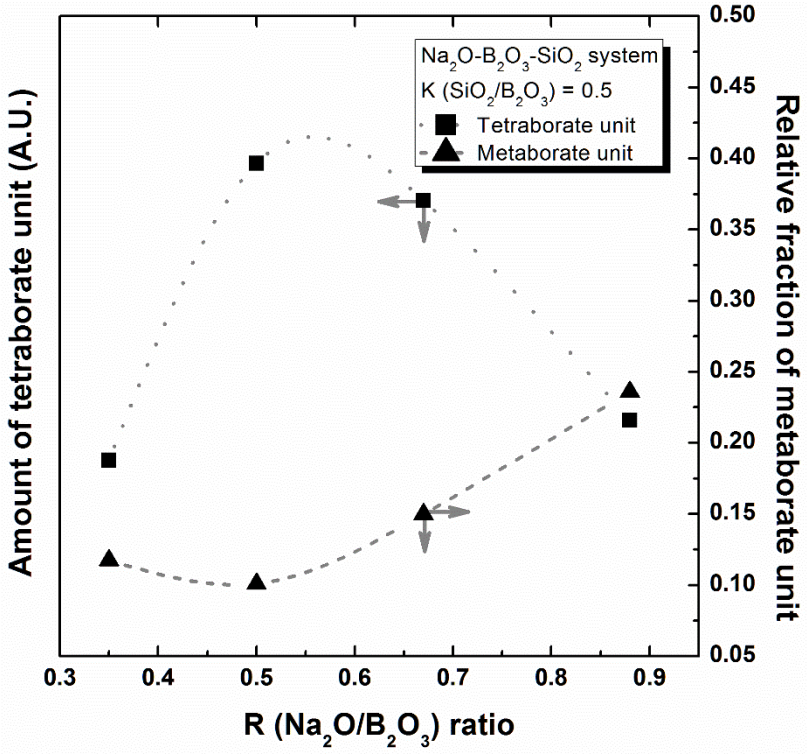

Fig. 4-10. The relationship between R ratio and the relative fraction of tetraborate and metaborate units at a fixed K ratio of 0.5. (The grey dashed lines have been drawn as a guide)

Figure 4-11 shows the ^{29}Si MAS NMR spectra of the present Na_2O-B_2O_3-SiO_2 system with varying R and K ratios. According to Maekawa et al.[34], who studied the alkali-silicate glass structure using ^{29}Si MAS NMR, the Q^4, Q^3, and Q^2 units of the silicate network are observed within the ranges −110 through −95 ppm, −92 through −85 ppm, and −80 through −75 ppm, respectively. Similar chemical shifts of the Q^n species for ^{29}Si MAS NMR were reported by Nanba et al.[23], who measured and calculated the sodium borosilicate glasses structure using MAS NMR and first-principle MO calculation. Based on the references[23, 34], the present ^{29}Si MAS NMR spectra were identified and the Gaussian deconvolution was carried out.

The change in the relative fraction of each Q^n species for the silicate structure with varying R and K ratios is shown in Fig. 4-12. Compared to the previous work[23], a similar structure change of the silicate network can be observed. The increase in the Na_2O/B_2O_3 ratio results in the depolymerization of the silicate network.

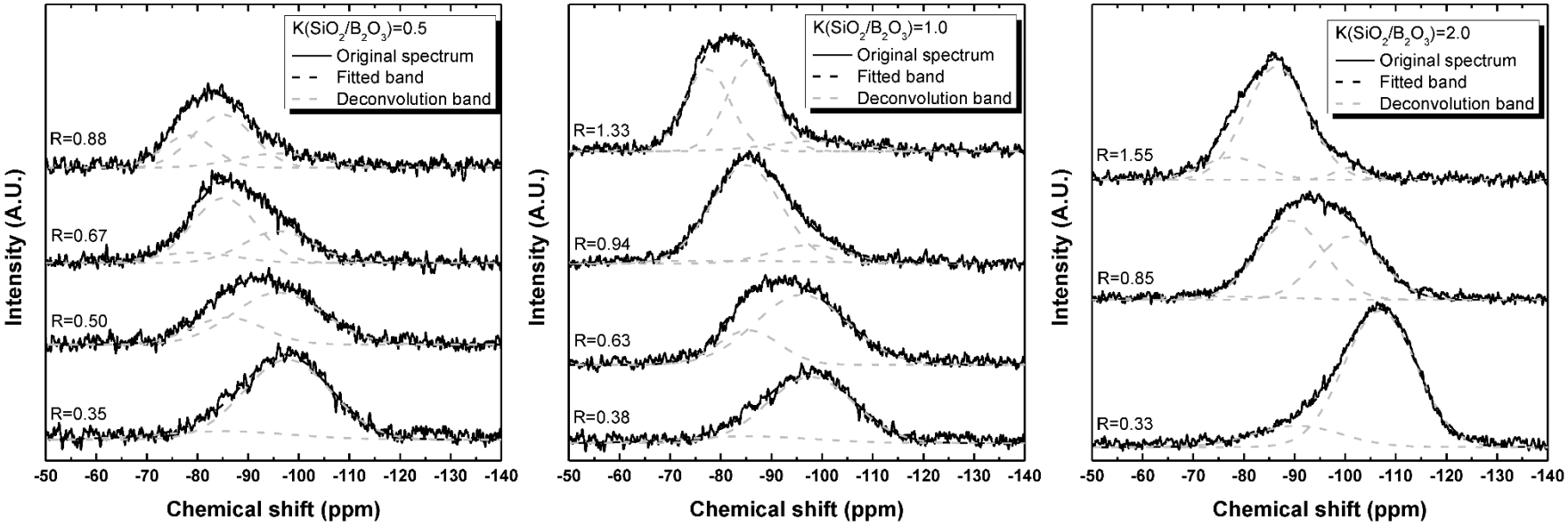

Fig. 4-11. ^{29}Si MAS NMR spectra with varying the R ratio for (a) K = 0.5, (b) K = 1.0, and (c) K = 2.0.

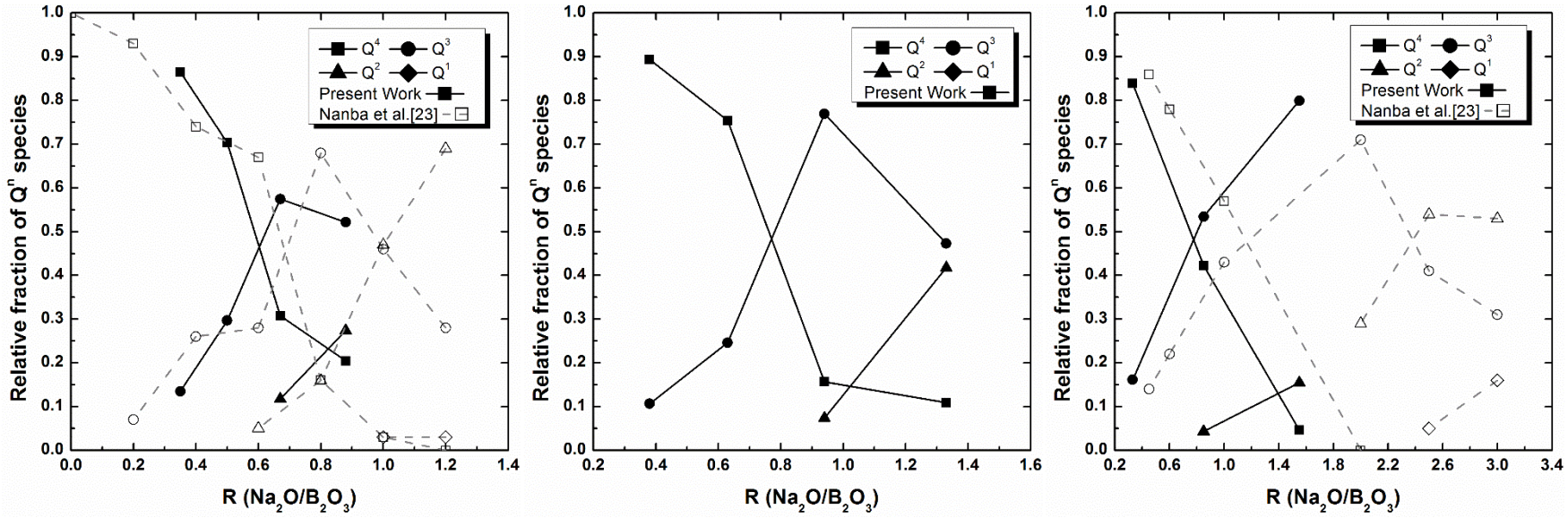

Fig. 4-12. Relationship between the R ratio and the relative fraction of the Q^n species for (a) K = 0.5, (b) K = 1.0, and (c) K = 2.0.

Owing to the considerable change of the boron coordination number at different temperatures in the molten state, many researchers have focused on the relationship between the borate structure change and the quenching rate along with the fictive temperature (T_f), where the glass structure is in equilibrium.[35–38] In addition, Yano et al.[39] reported the change of the silicate structure at different temperatures in the molten alkali silicate system using high-temperature Raman spectroscopy. It should be noted that the present structural investigations carried out in the quenched glass system could not provide exact structural information at 1273 K.

The fictive temperature can be calculated by the relationship between cooling rate and glass transition temperature.[40–42]

$$\frac{\log q_1 - \log q_2}{\frac{1}{T_{f1}} - \frac{1}{T_{f2}}} = -\frac{\Delta H_A}{2.3R} \tag{4-1}$$

The q_1 is the cooling rate during differential thermal analysis, q_2 is the cooling rate of molten oxide quenching, T_{f1} is the glass transition temperature, T_{f2} is the fictive temperature, ΔH_A is the activation enthalpy for relaxation around glass transition temperature and R is gas constant.

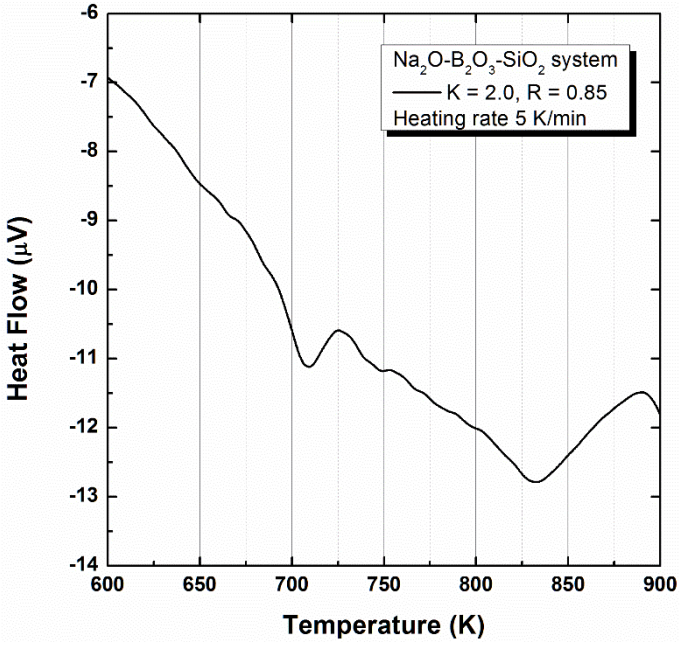

Fig. 4-13. The DTA thermal curve for the Na_2O-B_2O_3-SiO_2 glass sample at a fixed K ratio of 2.0 and R ratio of 0.85.

Figure 4-13 shows the DTA thermal curve for the present Na_2O-B_2O_3-SiO_2 system where K ratio is 2.0 and R ratio is 0.85. Using the *Standard test method*,[12] the midpoint temperature; 692 K, was determined as glass transition temperature.

It should be noted that, in the present study, both q_1 and T_{f1} were obtained from the heating curve of DTA. It has been reported that the glass transition temperatures determined from cooling and heating curve are not exactly same due to the thermal history remained in the glass powder sample.[43] However, in the present study, it was assumed that glass transition temperature would be almost same regardless of heating or cooling process.

According to Wu and Stebbins,[41] the activation enthalpy for relaxation around glass transition temperature can be obtained from viscosity data. Using the thermochemical calculation program (FactSage™ 6.4), viscosity of molten and glass sodium borosilicate system was calculated at different temperature. Figure 4-14 shows the viscosity change as function of inverse temperature.

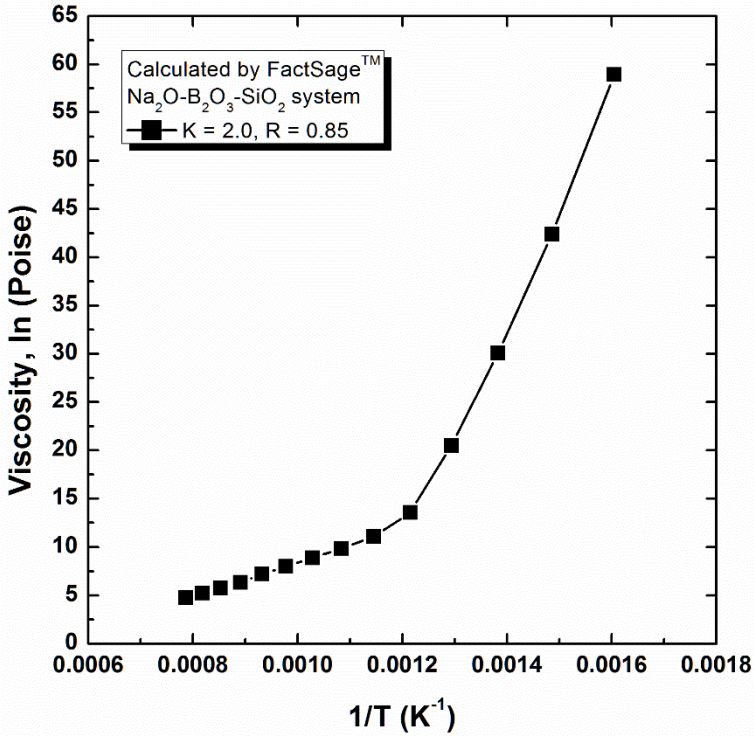

Fig. 4-14. The relationship between inverse temperature and calculated viscosity of the Na_2O-B_2O_3-SiO_2 system where K is 2.0 and R is 0.85.

From the slope around glass transition temperature, the activation enthalpy was obtained; 1025.927 kJ/mol. Although cooling rate is different from the thermal diffusivity and thickness of sample,[36] it was assumed that cooling rate was same among present experiment samples.

The cooling rate of copper plate quenching was considered as 1.9 K/s.[35] Using equation (4-1), the fictive temperature of the Na_2O-B_2O_3-SiO_2 system (K = 2.0, R = 0.85) was calculated; 704 K.

It should be noted that the fictive temperature is much lower than present experimental temperature. However, assuming that the fictive temperature (T_f) and the structural change rate are similar across the experiment composition, it is worth considering the present ^{11}B and ^{29}Si MAS NMR results to qualitatively evaluate the effect of the structure on thermal conductivity.

As shown in Fig. 4-7, 4-coordinated boron increases until it reaches an R ratio of 0.6 –0.8. In addition, according to Raman spectroscopy results; shown in Fig. 4-10, it can be inferred that such an increasing of 4-coordinated boron results from the increasing of tetraborate structure. In the same glass system, Konijnendijk and Stevels[29] also reported that the increase in 4-coordinated boron is related to the formation of diborate and tetraborate units, which have a 3-dimensional network structure. Although the silicate network structure is gradually depolymerized at higher R ratios, it seems that the extent of the Q^n species change is relatively small; less than 15 pct point, in the region where R is lower than 0.5 for K = 0.5, and than 0.6 for K = 1.0. Recently, Inoue et al.[44] calculated the structure of the glass Na_2O-B_2O_3-SiO_2 system using pair potentials by means of the MD technique. Within the R ratio range of 0 – 0.5 at the fixed values of K = 0.5 and 2.0, they found that the relative fraction of NBO in the Si–O and B–O bonds is kept almost constant, being less than 0.05. Therefore, below R = 0.5, the depolymerization of the silicate network structure is relatively insignificant, but the change of the borate structure from 3- to 4-coordinated boron is dominant. Considering the formation of the 3-dimensional network structure along with the increase in 4-coordinated boron, the structure of the molten Na_2O-B_2O_3-SiO_2 system becomes more polymerized at higher R ratios, resulting in an increase in the phonon mean free path of collision (l). For this reason, the thermal conductivity of the present system initially increases with increasing R ratio (Figure. 4-5).

On the other hand, as shown in Fig. 4-5, the thermal conductivity of the system gradually decreases above the R ratio of 0.5 – 0.6. Although the relative fraction of 4-coordinated boron increases within the R ratio range of 0.6 – 0.8, it seems that thermal conductivity is not significantly affected by the change of 4-coordinated boron. As shown in Fig. 4-12, a drastic decrease in the Q^4 species along with the increase in the Q^3 species can be observed above the R ratio of 0.5 – 0.6, indicating the significant depolymerization of the silicate network. According to Inoue et al.[44], a drastic increasing of the fraction of the NBOs in the B–O and Si–O networks can be observed above R = 0.5 at the fixed K = 0.5 and 2.0. Therefore, owing to the formation of NBO and the depolymerization of the silicate structure, thermal

conductivity gradually decreases when the R ratio increases above 0.5 – 0.6. In addition, borate structure change from tetraborate into metaborate structure; 3-coordinated boron associated with NBO, accelerates the decreasing of thermal conductivity above R ratio of 0.5 – 0.6. (Figure 4-10)

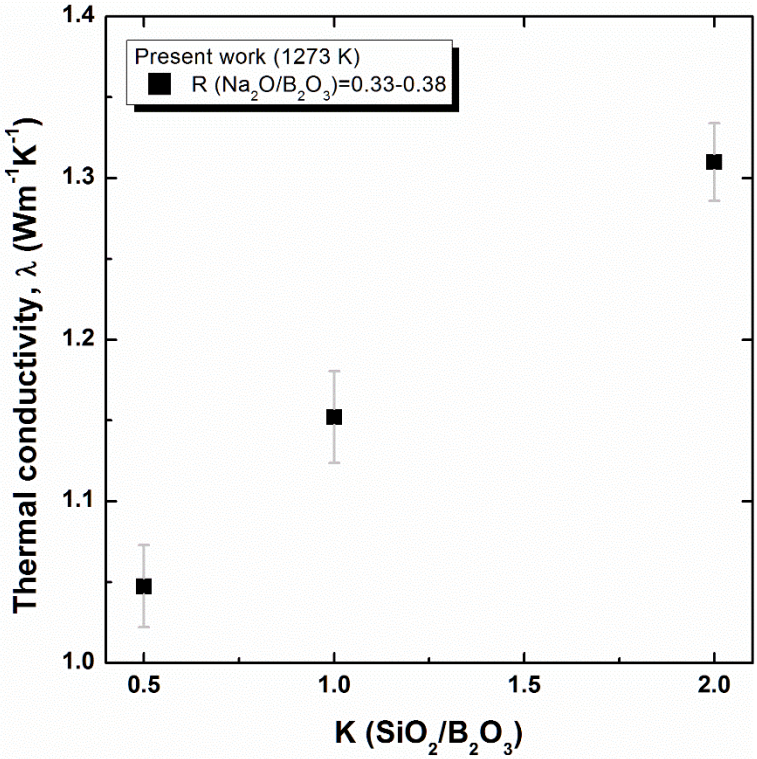

Fig. 4-15. Relationship between the K ratio and the thermal conductivity of the present system at 1273 K.

Figure 4-15 shows the relationship between the change of the K ratio and thermal conductivity obtained for the R ratio in the range of 0.33–0.38 at 1273 K. Thermal conductivity gradually increases with increasing the K ratio. Considering the similar relative fraction of 4-coordinated boron and the similar relative fraction of Q^n species; 0.84 – 0.89 for the Q^4 unit and 0.11 – 0.16 for the Q^3 unit, it seems that the change in thermal conductivity with varying the K ratio results from the substitution of SiO_2 for B_2O_3. A similar result, namely, an increase in thermal conductivity at higher SiO_2 content, has been reported by Ghoneim and Halawa[5], who measured thermal conductivity in the glass Na_2O-B_2O_3-SiO_2 system. They inferred that the formation of a rigid and compact structure by increasing the SiO_2 content results in a longer phonon mean free path of collision (l) along with an increase in thermal conductivity.

According to Du and Stebbins[22], who studied the glass Na_2O-B_2O_3-SiO_2 structure using ^{11}B

and ^{17}O NMR, the average mean number of Si coordinated to 4-coordinated boron increases for higher Si/(Si + B) ratios. In Fig.4-16, the change of tetraborate unit obtained by Raman spectroscopy was plotted as function of K ratio. It can be found that the amount of tetraborate unit increases with higher K ratio. Such an increasing of tetraborate structure would indirectly support increasing of the average mean network of Si associated with 4-coordinated boron with higher K ratio.

Recently, Koroleva and Shabunina[45] investigated glass structure in the Na_2O-B_2O_3-SiO_2 system using Raman spectroscopy. According to their simulation of high-frequency Raman spectrum, Q^{34} silicate structure; Q^3 unit associated with Q^4 unit, increases with higher K ratio at a fixed R ratio. In addition, both ^{17}O triple quantum (3Q) MAS[22] and MD calculation[44] observed the increase in the Si–O–Si bond at higher K ratios in the Na_2O-B_2O_3-SiO_2 system.

Therefore, I canbe concluded that thermal conductivity increases for higher K ratios because of the increase in the total amount of the silicate network structure and the more effective mixing of Si and 4-coordinated boron.

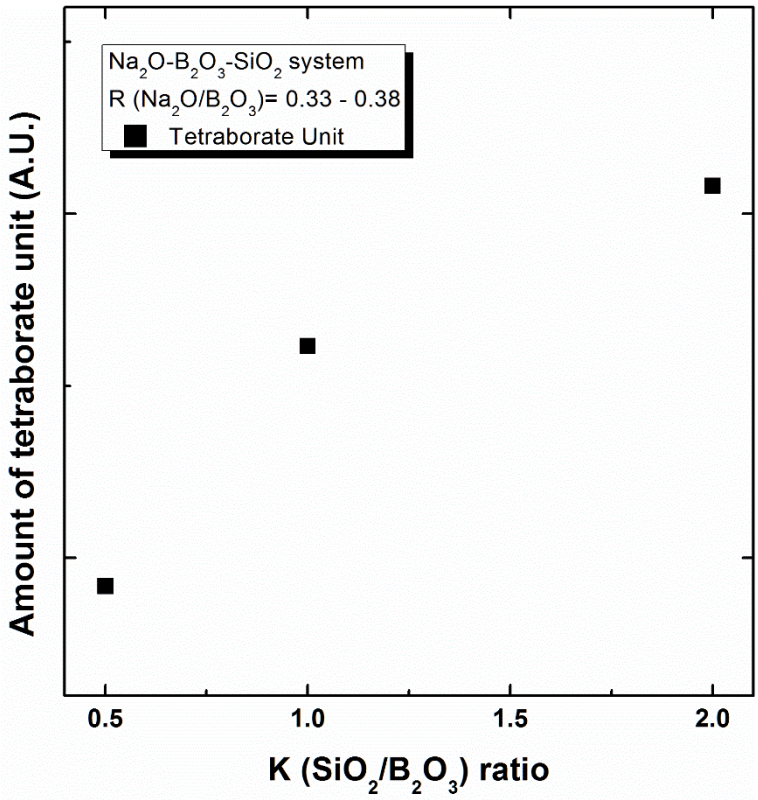

Fig. 4-16. The relationship between K ratio and the relative fraction of tetraborate units at R ratio of 0.33 – 0.38.

4.4 Short Summary

In this chapter, thermal conductivity of the molten Na_2O-B_2O_3-SiO_2 system was measured across a temperature range from 1273 K to its liquidus temperature with varying R ratio (Na_2O/B_2O_3) at a fixed K ratio (SiO_2/B_2O_3). Thermal conductivity decreased at higher temperature because of the shortening of phonon mean free path of collision (l). The one-dimensional Debye temperature (Θ_{D1}) of the present sodium borosilicate system was calculated. The one-dimensional Debye temperature decreases at higher R or lower K ratio, reflecting the change in the bonding strength along with the composition change.

Using the ^{11}B and ^{29}Si MAS NMR, the structure of the glass Na_2O-B_2O_3-SiO_2 system was investigated. It was observed that the relative fraction of 4-coordinated boron initially increases with increasing R ratio, and then subsequently decreases. On the other hand, the silicate network structure was gradually depolymerized with increasing R ratio. Raman spectra revealed that increasing of 4-cooridnated boron is closely related to the formation of tetraborate unit; which is the three-dimensional network structure.

At 1273 K, the conflicting effect of the R ratio on thermal conductivity was observed for the fixed K ratios of 0.5 and 1.0. Thermal conductivity initially increased with increasing R ratio, but gradually decreased above R = 0.5. Thus, owing to the increase in 4-coordinated boron along with formation of tetraborate units, thermal conductivity increases. However, for an R ratio above 0.5, owing to the drastic increase in NBO along with depolymerization of silicate network, thermal conductivity decreases with increasing R ratio.

Finally, the effect of the K ratio on thermal conductivity was evaluated. Owing to the increase in the total amount of the silicate network structure and the better mixing between 4-coordinated boron and silicon, thermal conductivity increases at higher K ratios.

References

1 W.J.J. Dell, P.J.J. Bray, and S.Z.Z. Xiao, "11B NMR studies and structural modeling of Na_2O-B_2O_3-SiO_2 glasses of high soda content," *J. Non-Cryst. Solids*, **58** [1] 1–16 (1983).

2 Y. Tanaka, Y. Benino, T. Nanba, S. Sakida, and Y. Miura, "Correlation between basicity and coordination structure in borosilicate glasses," *Phys. Chem. Glasses B*, **50** [5] 289–293 (2009).

3 Y. Shiraishi, L. Gra'na'sy, Y. Waseda, and E. Matsubara, "Viscosity of glassy Na_2O-B_2O_3-SiO_2 system," *J. Non-Cryst. Solids*, **95-96** 1031–1038 (1987).

4 Z. Zhang and R.G. Reddy, "Experimental Determination and Modeling of Na_2O-SiO_2-B_2O_3 Melts Viscosities," *High Temp. Mater. Proc.*, **23** [4] 247–260 (2004).

5 N.A. Ghoneim and M.M. Halawa, "Effect of boron oxide on the thermal conductivity of some sodium silicate glasses," *Thermochim. Acta*, **83** [2] 341–345 (1985).

6 M. Barlet, A. Kerrache, J.-M. Delaye, and C.L. Rountree, "SiO_2–Na_2O–B_2O_3 density: A comparison of experiments, simulations, and theory," *J. Non-Cryst. Solids*, **382** [15] 32–44 (2013).

7 D. Ehrt and R. Keding, "Electrical conductivity and viscosity of borosilicate glasses and melts," *Phys. Chem. Glasses*, **50** [3] 165–171 (2009).

8 A. Grandjean, M. Malki, V. Montouillout, F. Debruycker, and D. Massiot, "Electrical conductivity and 11B NMR studies of sodium borosilicate glasses," *J. Non-Cryst. Solids*, **354** [15-16] 1664–1670 (2008).

9 L. Van Der Tempel, G. Melis, and T. Brandsma, "Thermal conductivity of a glass: I. Measurement by the glass–metal contact," *Glass Phys. Chem.*, **26** [6] 606–611 (2000).

10 M. IMAOKA, "Studies on the Glass Formation Range of Borate Systems," *J. Ceram. Assoc. Japan*, **69** [789] 282–306 (1961).

11 M. Sakamoto, Y. Yanaba, H. Yamamura, and K. Morita, "Relationship between Structure and Thermodynamic Properties in the CaO–SiO_2–$BO_{1.5}$ Slag System," *ISIJ Int.*, **53** [7] 1143–1151 (2013).

12 ASTM E1356-08, *Standard Test Method for Assignment of the Glass Transition Temperatures by Differential Scanning Calorimetry*. West Conshohocken, PA, 2014.

13 M. Susa, M. Watanabe, S. Ozawa, and R. Endo, "Thermal conductivity of CaO–SiO_2–Al_2O_3 glassy slags: Its dependence on molar ratios of Al_2O_3/CaO and SiO_2/Al_2O_3," *Ironmak. Steelmak.*, **34** [2] 124–130 (2007).

14 K. Nagata and K.S. Goto, "Heat Conductivity and Mean Free Path of Phonons in Metallurgical Slags;" pp. 875–889 in *Second Int. Symp. Metall. Slags Fluxes*. Edited by H.A. Fine and D.R. Gaskell. The Metallurgical Society of AIME, Warrendale, Pa., 1984.

15 Y. Kang and K. Morita, "Thermal conductivity of the CaO-Al_2O_3-SiO_2 system," *ISIJ Int.*, **46** [3] 420–426 (2006).

[16] Y. Kang, K. Nomura, K. Tokumitsu, H. Tobo, and K. Morita, "Thermal Conductivity of the Molten CaO-SiO_2-FeO_x System," *Metall. Mater. Trans. B*, **43** [6] 1420–1426 (2012).

[17] K. Nagata, M. Susa, and K.S. Goto, "Thermal conductivities of slags for ironmaking and steelmaking," *Tetsu-to-Hagane*, **11** [11] 1417–1424 (1983).

[18] S. Ozawa and M. Susa, "Effect of Na2O additions on thermal conductivities of CaO–SiO_2 slags," *Ironmak. Steelmak.*, **32** [6] 487–493 (2005).

[19] S. Inaba, S. Oda, and K. Morinaga, "Heat capacity of oxide glasses at high temperature region," *J. Non-Cryst. Solids*, **325** [1-3] 258–266 (2003).

[20] W.-F. Du, K. Kuraoka, T. Akai, and T. Yazawa, "Study of Al_2O_3 effect on structural change and phase separation in Na2O-B2O3-SiO2 glass by NMR," *J. Mater. Sci.*, **35** [19] 4865–4871 (2000).

[21] Y.Q. Wu, G.C. Jiang, J.L. You, H.Y. Hou, H. Chen, and K. Di Xu, "Theoretical study of the local structure and Raman spectra of CaO-SiO_2 binary melts," *J. Chem. Phys.*, **121** [2004] 7883–7895 (2004).

[22] L.-S. Du and J.F. Stebbins, "Nature of Silicon−Boron Mixing in Sodium Borosilicate Glasses: A High-Resolution ^{11}B and ^{17}O NMR Study," *J. Phys. Chem. B*, **107** [37] 10063–10076 (2003).

[23] T. Nanba, M. Nishimura, and Y. Miura, "A theoretical interpretation of the chemical shift of ^{29}Si NMR peaks in alkali borosilicate glasses," *Geochim. Cosmochim. Acta*, **68** [24] 5103–5111 (2004).

[24] B.C. Bunker, D.R. Tallant, R.J. Kirkpatrick, and G.L. Turner, "Multinuclear nuclear magnetic resonance and Raman investigation of sodium borosilicate glass structures," *Phys. Chem. Glasses*, **31** [1] 30–41 (1990).

[25] A.A. Osipov and L.M. Osipova, "Structure of glasses and melts in the Na_2O-B_2O_3 system from high-temperature Raman spectroscopic data: I. Influence of temperature on the local structure of glasses and melts," *Glass Phys. Chem.*, **35** [2] 121–131 (2009).

[26] D. Manara, a. Grandjean, and D.R.R. Neuville, "Advances in understanding the structure of borosilicate glasses: A Raman spectroscopy study," *Am. Mineral.*, **94** [5-6] 777–784 (2009).

[27] E.I. Kamitsos, M.A. Karakassides, and G.D. Chryssikos, "Vibrational spectra of magnesium-sodium-borate glasses. 2. Raman and mid-infrared investigation of the network structure," *J. Phys. Chem.*, **91** [5] 1073–1079 (1987).

[28] W.L.W.L. Konijnendijk and J.M.J. Stevels, "The structure of borate glasses studied by Raman scattering," *J. Non-Cryst. Solids*, **18** [3] 307–331 (1975).

[29] W.L. Konijnendijk and J.M. Stevels, "The structure of borosilicate glasses studied by Raman scattering," *J. Non-Cryst. Solids*, **20** [2] 193–224 (1976).

[30] T. Furukawa and W.B. White, "Raman Spectroscopy of Heat-Treated B_2O_3-SiO_2 Glasses," *J. Am. Ceram. Soc.*, **64** [8] 443–447 (1981).

[31] B.O. Mysen and P. Richet, *Silicate Glasses and Melts*, 1st ed. Elsevier, Amsterdam, 2005.

[32] T. Yano, N. Kunimine, S. Shibata, and M. Yamane, "Structural investigation of sodium borate glasses and melts by Raman spectroscopy. I. Quantitative evaluation of structural units," *J. Non-Cryst. Solids*, **321** [3] 137–146 (2003).

[33] G. Padmaja and P. Kistaiah, "Infrared and raman spectroscopic studies on alkali borate glasses: Evidence of mixed alkali effect," *J. Phys. Chem. A*, **113** [11] 2397–2404 (2009).

[34] H. Maekawa, T. Maekawa, K. Kawamura, and T. Yokokawa, "The structural groups of alkali silicate glasses determined from 29Si MAS-NMR," *J. Non-Cryst. Solids*, **127** [1] 53–64 (1991).

[35] F. Angeli, O. Villain, S. Schuller, T. Charpentier, D. de Ligny, L. Bressel, and L. Wondraczek, "Effect of temperature and thermal history on borosilicate glass structure," *Phys. Rev. B*, **85** [5] 054110 (2012).

[36] T.J. Kiczenski and J.F. Stebbins, "The development of a rapid quenching device for the study of the dependence of glass structure on fictive temperature," *Rev. Sci. Instrum.*, **77** [1] 013901 (2006).

[37] S. Peuget, E.A. Maugeri, T. Charpentier, C. Mendoza, M. Moskura, T. Fares, O. Bouty, and C. Jégou, "Comparison of radiation and quenching rate effects on the structure of a sodium borosilicate glass," *J. Non-Cryst. Solids*, **378** 201–212 (2013).

[38] J. Wu, M. Potuzak, and J.F. Stebbins, "High-temperature in situ ^{11}B NMR study of network dynamics in boron-containing glass-forming liquids," *J. Non-Cryst. Solids*, **357** [24] 3944–3951 (2011).

[39] T. Yano, S. Shibata, and T. Maehara, "Structural Equilibria in Silicate Glass Melts Investigated by Raman Spectroscopy," *J. Am. Ceram. Soc.*, **89** [1] 89–95 (2006).

[40] C.T. Moynihan, A.J. Easteal, D.C. Tran, J.A. Wilber, and E.P. Donovan, "Heat Capacity and Structural Relaxation of Mixed-Alkali Glasses," *J. Am. Ceram. Soc.*, **59** [3-4] 137–140 (1976).

[41] J. Wu and J.F. Stebbins, "Quench rate and temperature effects on boron coordination in aluminoborosilicate melts," *J. Non-Cryst. Solids*, **356** [41-42] 2097–2108 (2010).

[42] T.J. Kiczenski and J.F. Stebbins, "The Effect of Fictive Temperature on the Structural Environment of Fluorine in Silicate and Aluminosilicate Glasses," *J. Am. Ceram. Soc.*, **89** [1] 57–64 (2006).

[43] C.T. Moynihan and P.B. Macedo, "Dependence of the glass transition temperature on heating rate and thermal history," *J. Phys. Chem.*, **75** [21] 3379–3381 (1971).

[44] H. Inoue, A. Masuno, and Y. Watanabe, "Modeling of the structure of sodium borosilicate glasses using pair potentials.," *J. Phys. Chem. B*, **116** [40] 12325–31 (2012).

[45] O.N. Koroleva and L.A. Shabunina, "Effect of the ratio R = $[Na_2O]/[B_2O_3]$ on the structure of glass in the Na_2O-B_2O_3-SiO_2 system," *Russ. J. Gen. Chem.*, **83** [2] 238–244 (2013).

Chapter V

Thermal Conductivity of the molten $CaO-B_2O_3$ and $CaO-SiO_2-B_2O_3$ system

5.1 Background

In the previous chapters, thermal conductivity in the various alkali-borate and alkali borosilicate melts was investigated along with structural investigation. It was observed that not only the borate and silicate network structure but also ionization potential of alkali ions are closely related to the thermal conductivity of molten oxide system. However, the previous thermal conductivity measurement has been mainly carried out at the relatively low alkali oxide concentration region; where 4-coordinated boron plays significant role.

The typical glass and mold flux system consist of considerable amount of alkali-earth oxide; such as calcium oxide. For this reason, a large portion of asymmetric 3-coordinated boron is commonly observed along with the symmetric 3-cooridnated boron and 4-coordinated boron. The effect of alkali-earth oxide on the physical properties of borate melts have been studied by several researchers.[1, 2] Recently, Wang et al.[1] measured viscosity in the molten $CaO-SiO_2-B_2O_3-TiO_2$ mold flux system reporting the effect of both borate and silicate network structure on thermal conductivity. Sakamoto[2] observed the conflicting effect of B_2O_3 on the viscosity in the molten $CaO-SiO_2-B_2O_3$ system; where CaO/SiO_2 ratio is approximately unity. Compared to viscosity, effect of alkali-earth oxide on the thermal conductivity of borate or borosilicate melt has not been reported, in spite of its practical importance.

Therefore, in the present chapter, thermal conductivity of the calcium borate and calcium borosilicate system was measured along with structural investigation. The composition which is similar to the commercial mold flux system was chosen. In order to evaluate the effect of asymmetric 3-coordinated boron structure on thermal conductivity, structure investigation of ^{11}B MAS NMR, 3Q MAS and Raman spectroscopy was carried out finding thermal conductivity is closely related with the change of both silicate and borate structure.

5.2 Experiment

5.2.1. Sample Preparation

For the $CaO-B_2O_3$ system, due to the high crystallization tendency and two-liquid region, thermal conductivity was measured within the glass formation region where mole fraction of CaO is between 0.33 and 0.5. For the $CaO-SiO_2-B_2O_3$ system, experiment composition was chosen similar to the typical mold flux compositions; where CaO/SiO_2 ratio is approximately unity with relatively low B_2O_3 concentration.

Samples were prepared using reagent grade SiO_2 and B_2O_3, and CaO calcined from $CaCO_3$. The powder mixtures were pre-melted in a Pt crucible at 1773 K for 30 minutes. After quenching on a water-cooled copper plate, the resultant glass was finely crushed and placed in a Pt-10%Rh crucible (I.D: 32mm, O.D: 38mm, height: 70mm).

5.2.2. Thermal Conductivity Measurement

The transient hot-wire method was adopted in this study for measuring the thermal conductivity of the molten slags. Using a PID (proportional integral differential) controller and calibrated B-type thermocouple, sample temperature was controlled. The upper part of sample is intentionally placed at the highest temperature zone, in order to avoid natural convection during measurement. Approximately 90 g of pre-melted sample is heated in an electric resistance furnace equipped with SiC at 1573 or 1773 K, and then held for 1 hour to obtain a homogeneous molten slag. Thermal conductivity was measured at 50 K intervals to the liquidus temperature. Using a galvanostat, a constant current of 0.8–1.5 A was supplied to a 0.15mmϕ Pt-13%Rh hot-wire, and any voltage change between the two terminals of the wire was monitored by a digital multimeter. A linear relationship between ΔV and ln$t$ was obtained within 0.8–2.0 seconds, and the thermal conductivity, λ ($Wm^{-1}K^{-1}$), was calculated by the equation (1-18).

During the measurement, to ensure the thermal equilibrium of the system, the furnace temperature was decreased at a rate of 3 K/min and held for 15 minutes at the target temperature. To confirm the reproducibility of the results, the measurement was repeated three times at the same temperature, with a 5-minutes interval between one measurement and the following one.

5.2.3. Analytical Procedures

5.2.3.1. Determination of the boron and calcium concentration in the sample

Following the measurement of thermal conductivity by the hot-wire method, the solidified samples were re-melted at 1773 K and 1873 K for $CaO-SiO_2-B_2O_3$ and $CaO-B_2O_3$ system, respectively. The melts were poured onto a water-cooled copper plate and quickly covered with a copper block. The obtained vitreous glass was ground and sieved using a 100 μmϕ mesh. In order to evaluate the chemical composition, approximately 0.01 g of the ground sample was transferred into 100 ml of beaker. Following the addition of acid-solution (10 ml of distilled water + 15 ml of HCl + 5 ml of HNO_3), the beaker was placed on the hot-plate covered with watch glass, and then heated at 493 K for several hours. When the almost of the acid solution was evaporated, approximately 5 ml of $HClO_4$ was added, and kept on heating until white smoke appeared.

The heated beaker was cooled down at room temperature. The solution was filtered using a filter paper (ash contents 0.1 mg/circle) attached on glass funnel, and transferred into 100 or 500 ml of volumetric flask. After rinsing the beaker and filter paper several times by distilled water, the final volume was made. In order to obtain the homogeneous concentration across the solution, the volumetric flask was kept for 24 hours.

Using the inductively coupled plasma atomic emission spectroscopy (ICP-AES; SPS7700, SII NanoTechnology, Japan), final concentration of boron was determined. Diluting the 1000 ppm of boron standard solution (Kanto chemical, Tokyo, Japan), 10, 20, 50 and 100 ppm of boron standard solution was prepared. Using the four standard solutions, calibration line was drawn from 0 to 100 ppm showing larger than 0.999 of correlation coefficient. During the analysis, 249.773 nm and 393.336 nm of wavelength were chosen for boron and calcium as analytical wavelength, respectively.

Table 5-1 shows the final composition the present work.

5.2.3.2. Determination of the silicon concentration in the sample

The SiO_2 content was determined by silica gravimetric method. The analyzed final compositions are listed in Table 5-1.

The detailed procedures were described in the previous chapter.

Table 5-1. Initial and final composition of the present experiment.

Initial composition (mol%)			Final composition (mol%)			Note
CaO	SiO_2	$BO_{1.5}$	CaO	SiO_2	$BO_{1.5}$	
31.25	-	68.75	28.25	-	71.75	$BO_{1.5}$/CaO = 2.2
25	-	75	22.33	-	77.67	$BO_{1.5}$/CaO = 3.0
20.83	-	79.17	18.75	-	81.25	$BO_{1.5}$/CaO = 3.8
45.5	49.5	5.0	46.2	48.4	5.4	CaO/SiO_2 = 0.92
40.7	44.3	15.0	41.0	43.0	16.1	CaO/SiO_2 = 0.92
35.9	39.1	25.0	34.7	38.1	27.3	CaO/SiO_2 = 0.92
50.8	44.2	5.0	51.5	43.1	5.4	CaO/SiO_2 = 1.15
45.5	39.5	15.0	45.0	37.8	17.2	CaO/SiO_2 = 1.15
40.1	34.9	25.0	39.0	35.9	25.1	CaO/SiO_2 = 1.15
55.1	39.9	5.0	55.6	39.0	5.4	CaO/SiO_2 = 1.38
49.3	35.7	15.0	48.1	36.3	15.6	CaO/SiO_2 = 1.38
43.5	31.5	25.0	42.7	32.1	25.2	CaO/SiO_2 = 1.38

5.2.4. Structural Investigation

After obtaining confirmation of the non-crystalline state by X-ray Diffraction (XRD; RINT 2500, Rigaku, Japan), a structural investigation of the samples was conducted by using ^{11}B MAS NMR, 3Q MAS and Raman spectroscopy. Figure 5-1(a) and 5-1(b) show the x-ray diffraction pattern of glass CaO-B_2O_3 and CaO-SiO_2-B_2O_3 system, respectively.

Solid state ^{11}B MAS NMR spectra were recorded at 11.74 T using a Fourier transform (FT) NMR spectrometer (ECA-500, JEOL, Japan). The Larmor frequency was 160.4 MHz for ^{11}B MAS NMR. Each sample was placed in a 4 mm ZrO_2 holder and spun at 16 kHz. Using a saturated H_3BO_3 solution (19.49 ppm), the standards of ^{11}B MAS NMR were calibrated. The detailed conditions adopted for the MAS NMR measurements are reported in Table 5-2. For the ^{11}B 3Q-MAS NMR measurement, a three-pulse z-filter sequence[3] was adopted. The first and second pulses of duration were set to 4.7 μs and 1.9 μs, respectively, and the third pulse of duration was set to 12 μs with a relaxation delay of 5 s. After the measurements, the ^{11}B 3Q MAS data were fitted by a Gaussian function with the 'Peakfit (Ver. 4.06)' software to obtain structural information.

The intermediate range order structure of the CaO-SiO_2-B_2O_3 system was investigated by back-scattering Raman spectroscopy (T-64000, Horiba Jobin-Yvon, France). The powder sample was irradiated by an argon ion laser with the wavelength of 514 nm operated at 100 mW. The detailed measurement conditions were explained in the previous chapter.

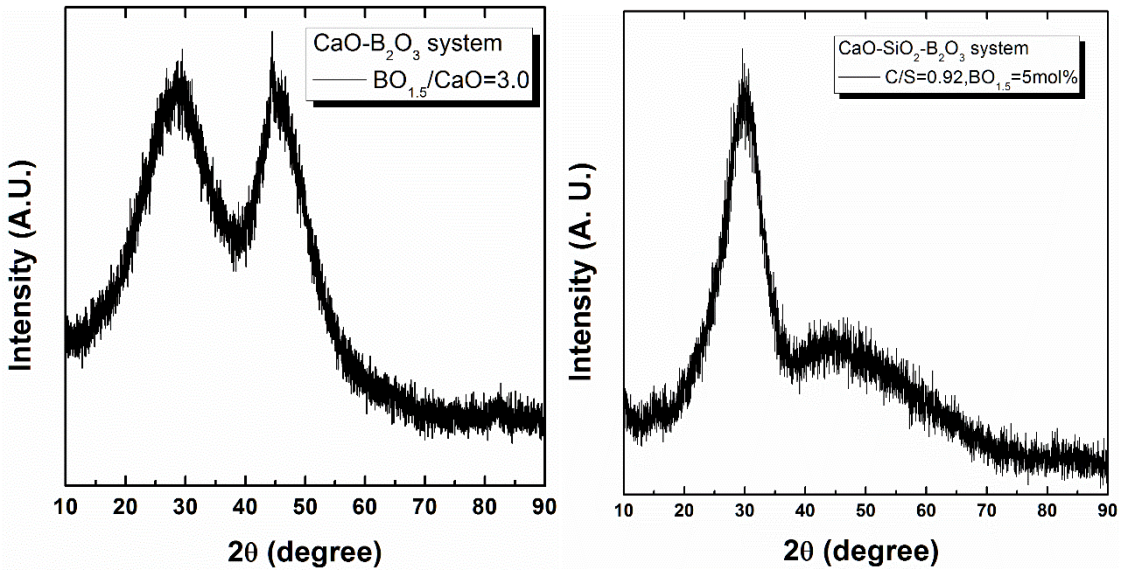

(a) **(b)**

Fig. 5-1. X-ray diffraction pattern of non-crystalline **(a)** CaO-B_2O_3 and **(b)** CaO-SiO_2-B_2O_3 system.

Table 5-2. Experimental conditions for the ^{11}B MAS NMR for CaO-B_2O_3 system.

Nuclear Property	**^{11}B**
Nuclear Spin	3/2
Larmor frequency [MHz]	160.4
RF pulse intensity [kHz]	60.976
Repetition times	64
Flip angle [rad]	π/6
Delay time [s]	5
Spinning rate [kHz]	16

5.3 Results and Discussion

5.3.1. Thermal Conductivity of the CaO-B_2O_3 System

Figure 5-2 shows the temperature dependence of the calcium borate melt with varying $BO_{1.5}$/CaO ratio. It was commonly observed that thermal conductivity decreases with increasing temperature. Similar to previous molten borate system, negative temperature dependence would result from the change of phonon mean free path.

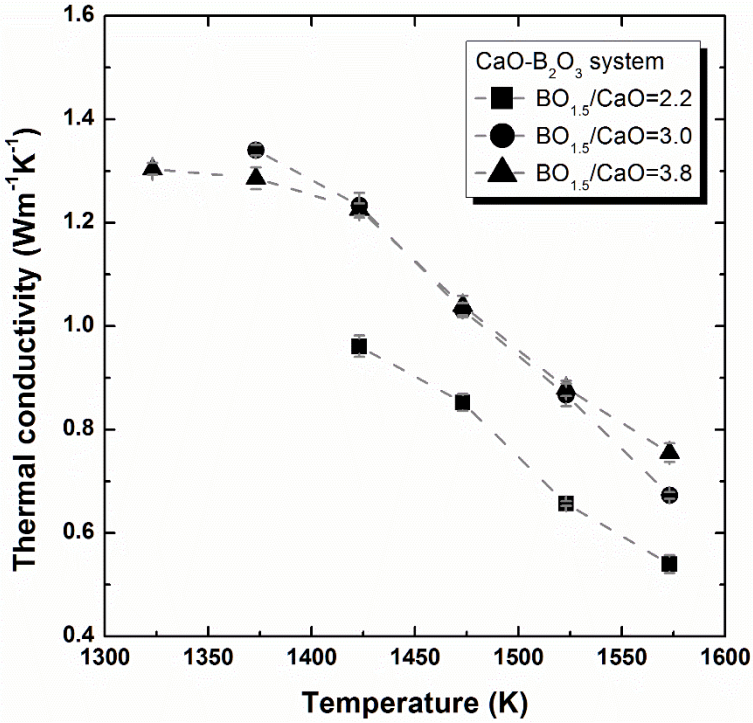

Fig. 5-2. The relationship between thermal conductivity and temperature in the CaO-B_2O_3 system with varying $BO_{1.5}$/CaO ratio.

In order to find the relationship between thermal conductivity and the chemical compositions, the thermal conductivity at 1573 K was plotted as a function of $BO_{1.5}$/CaO ratio. As shown in Fig. 5-3, it can be observed that thermal conductivity increases with B_2O_3 addition.

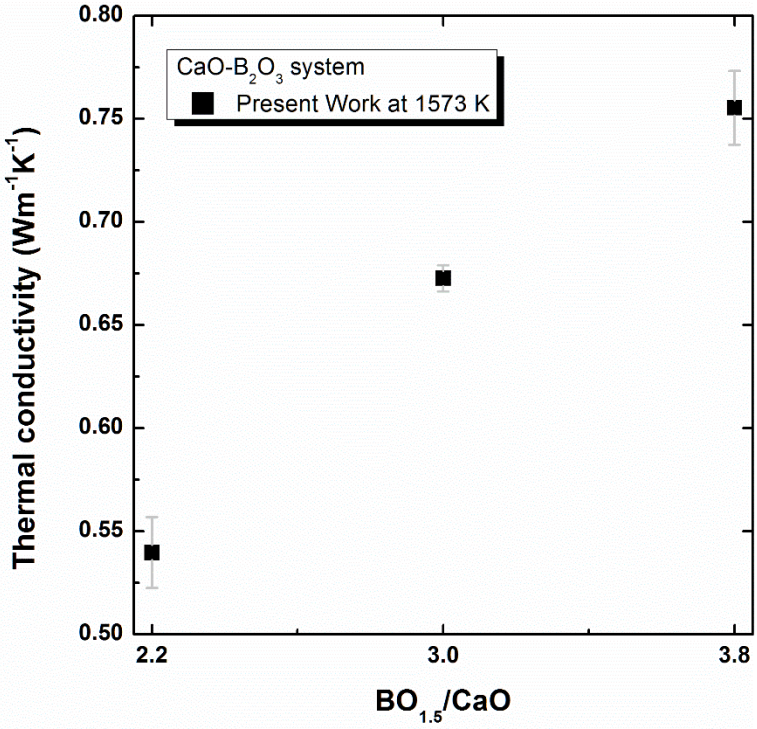

Fig. 5-3. The relationship between thermal conductivity and $BO_{1.5}$/CaO ratio in the CaO-B_2O_3 system at 1573 K.

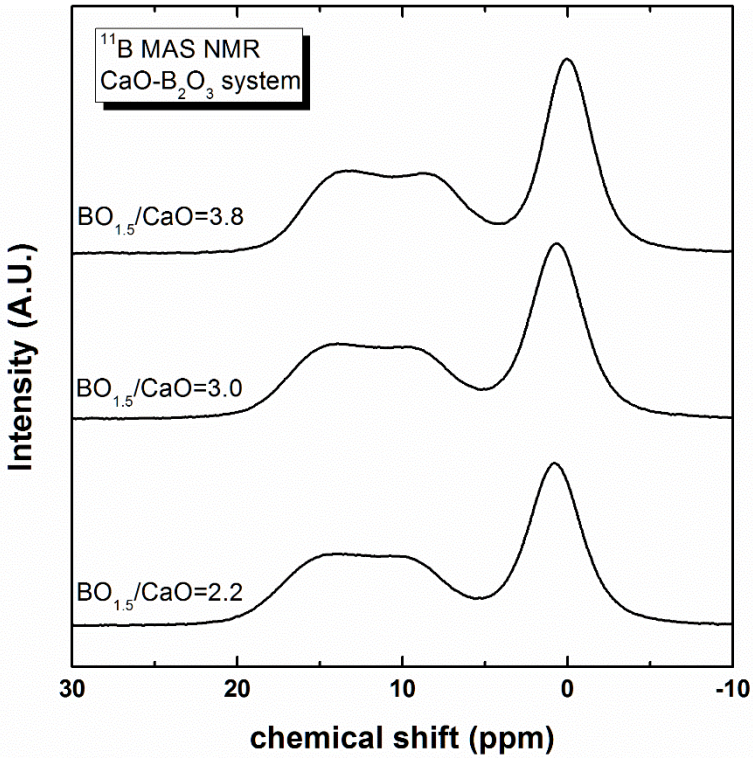

Fig. 5-4. ^{11}B MAS NMR spectra with varying $BO_{1.5}$/CaO ratio in the CaO-B_2O_3 system.

Using the ^{11}B MAS NMR and 3Q MAS, the structural investigation of the $CaO-B_2O_3$ system was carried out. Figure 5-4 shows the ^{11}B MAS NMR spectra of the $CaO-B_2O_3$ glass system with varying $BO_{1.5}$/CaO ratio. Du and Stebbins[4] studied the structure of the sodium borosilicate system reporting that each 3-coordinated boron and 4-coordinated boron is centered at 12 and 0 ppm, respectively. Nanba et al.[5] found that the asymmetric broad peak observed between 20 and −20 ppm can be attributed to 3-coordinated boron in the BO_3 unit. On the basis of the references,[4, 5] the present ^{11}B MAS NMR spectra were identified. It should be noted that the chemical shift of ^{11}B shifts to the right side of x-axis with higher B_2O_3 concentration indicating the more electric shielded boron nuclei. According to area ratio, the relative fraction of 4-coordinated boron and 3-coordinated boron was obtained. The relative fraction of both 4- and 3-coordinated boron was kept constant which are 0.46 and 0.54, respectively. Using IR spectroscopy and MD simulation, Ohtori et al.[6] also observed similar result that the relative fraction of 4-coordinated boron of the $CaO-B_2O_3$ system is almost kept constant with higher CaO concentration within CaO = 35 – 50 mole %. It is quite interesting that although the relative fraction of 4-coordinated boron keeps almost constant, thermal conductivity increases with higher B_2O_3 concentration. In order to evaluate the borate structure thoroughly, the more detailed structure of 3 and 4 coordinated boron was investigated using ^{11}B 3Q MAS.

Figure 5-5 shows the ^{11}B 3Q MAS spectra of the $CaO-B_2O_3$ system. Du and Stebbins,[4] who studied borate structure in the $Na_2O-B_2O_3-SiO_2$ system using ^{11}B 3Q MAS, assigned 42, 33 and -2 ppm as 3-coordinated boron in ring sites, 3-coordinated boron in non-ring sites and 4-coordinated boron, respectively. Considering higher magnetic field of 14.1 T and higher spinning rate of 20 kHz in the Du and Stebbins works,[4] it can be inferred that different peak position was observed in their study. According to Sakamoto,[2] in the ^{11}B 3Q MAS, the ring type and non-ring type 3-coordinated boron peak are observed at lower and higher magnetic field region, respectively. Therefore, in the present study, the 4-coordinated boron, 3-coordinated boron in non-ring sites and 3-coordinated boron in ring sites were determined to -3, 15 and 18 ppm, respectively. Using the Gaussian deconvolution, each spectrum was identified. In Table 5-3, peak position and area ratio of each structural bands are summarized.

It should be noted that in Fig. 5.5, the peak observed below 20 ppm is attributed to the formation of spinning sidebands. In the present work, this band was ignored during Gaussian deconvolution.

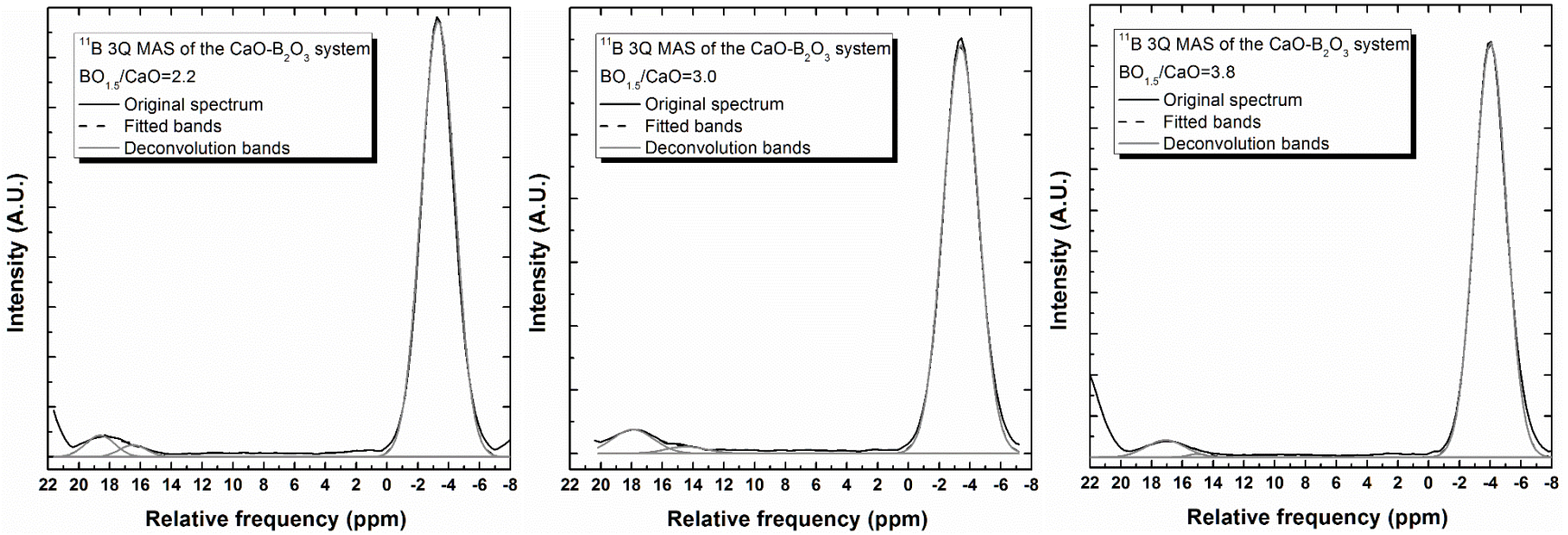

(a) **(b)** **(c)**

Fig. 5-5. ^{11}B 3Q MAS spectra with varying $BO_{1.5}$/CaO ratio of **(a)** 2.2, **(b)** 3.0 and **(c)** 3.8.

Table 5-3. The peak position and area ratio of the 4-coordinated boron, ring type and non-ring type 3-coordinated boron obtained from ^{11}B 3Q MAS spectra of the CaO-B_2O_3 system.

	Peak Position (ppm)			Area (%)		
	[4]B	[3]B-non-ring	[3]B-ring	[4]B	[3]B-non-ring	[3]B-ring
BC2.2	-3.31	16.49	18.62	93.86	2.08	4.05
BC3.0	-3.40	14.48	17.92	91.86	1.77	6.37
BC3.8	-4.02	15.02	17.10	94.84	0.42	4.75

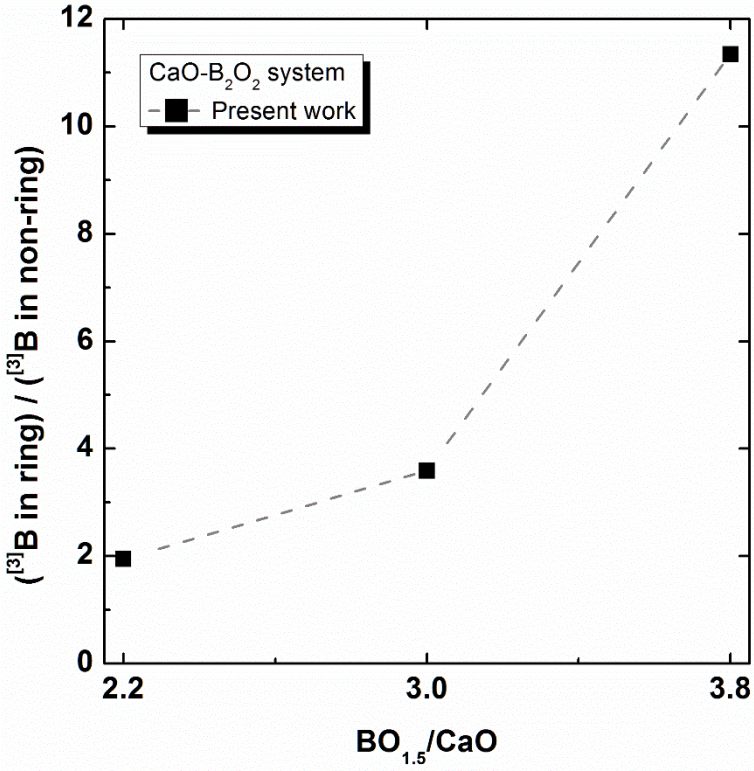

Fig. 5-6. The relationship between $BO_{1.5}$/CaO ratio and (3-coordinated boron in boroxol ring)/ (3-coordinated boron in non-ring site) ratio in the CaO-B_2O_3 system.

In Table 5-3, it can be found that the relative fraction of 4-coordinated boron obtained by ^{11}B 3Q MAS is much larger than the relative fraction of 4-coordinated boron observed by ^{11}B MAS NMR spectra. During the 3Q MAS NMR analysis, the sensitivity of 3Q MAS spectra is closely related to the excitation efficiency of multiple quantum transition and the transition efficiency from multiple quantum to single quantum. Due to the nuclear quadrupole coupling constant (C_Q) dependence of 3Q MAS efficiency, 3Q MAS spectra cannot give quantitative structural information.[7] However, both two types of 3-coordinated boron have similar C_Q

value and thus, the relative fraction of two different 3-cooridnated boron (ring and non-ring) can be compared, directly.

From the ^{11}B MAS NMR spectra, it was observed that the relative fraction of 4- and 3-cooridnated born was kept constant with varying $BO_{1.5}$/CaO ratio. According to the ^{11}B 3Q MAS spectra, it can be found that ring-type 3-coorindated boron increases with higher $BO_{1.5}$/CaO ratio. Considering the high concentration of B_2O_3 in the present CaO-B_2O_3 system, it can be inferred that the borate structure exists both 4-coorindated and 3-coorindinated boron forming network structure. Therefore, the ring-type 3-coordinated boron indicates the network forming boroxol ring structure not the boroxol ring cluster observed in the B_2O_3-SiO_2 system.

In Fig 5-6, change of the ratio; ring to non-ring type 3-coorindated boron, was plotted as function of $BO_{1.5}$/CaO ratio. The present ^{11}B 3Q MAS results are excellent accordance with the previous CaO-B_2O_3 structure investigation by Raman spectroscopy.[8] According to Maniu et al.,[8] addition of CaO results in the formation of chain type metaborate groups and orthoborate groups (BO_3^{3-}) along with the depolymerization of boroxol ring and ring-based unit, which is pentaborate.

Therefore, it can be concluded that the decreasing of thermal conductivity with lower $BO_{1.5}$/CaO ratio results from the structural change from network forming 3-coorindated boron (ring-type 3-coordinated boron) into depolymerized 3-coordinated boron (non-ring-type 3-coordinated boron).

5.3.2. Thermal Conductivity of the CaO-SiO_2-B_2O_3 System

5.3.2.1. Effect of temperature and composition on thermal conductivity

The thermal conductivities obtained from the CaO-SiO_2-B_2O_3 slag system at various temperatures are shown in Fig. 5-7. From this, it can be seen that the thermal conductivity is gradually increased with lower temperature.

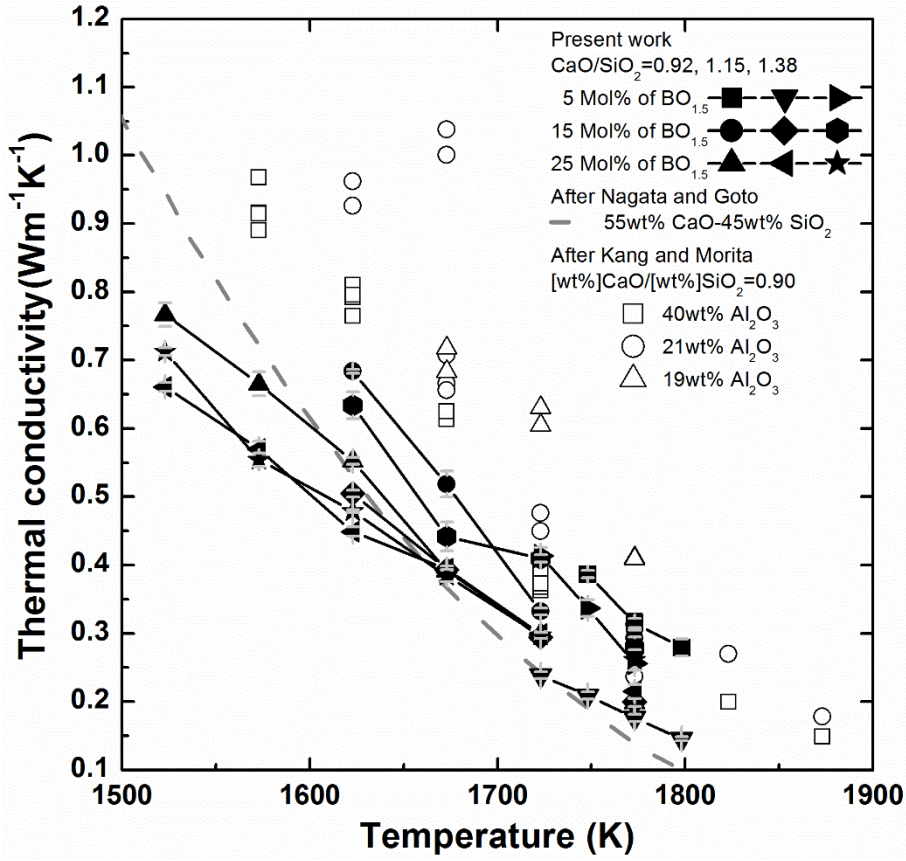

Fig. 5-7. Temperature dependence of thermal conductivity in the CaO-SiO_2-B_2O_3 oxide system.

As discussed in the previous chapters, in most ceramics systems, heat is mainly transmitted through quantized lattice vibration, known as phonon vibration.[9] According to equation (2-15), the thermal conductivity transferred by phonon can be expressed in terms of the total specific heat (C), the mean particle velocity (v), and the phonon mean free path of collision (l). Since the total heat capacity (C) and mean particle velocity (v) become approximately constant for most ceramics near and above the Debye temperature (100–1000 K), [9] the thermal conductivity would therefore be mainly affected by its mean free path (l) at higher temperature.[9, 10]

It can therefore be considered that the observed temperature dependence of the thermal conductivity results from a decrement of the mean free path (l) with higher temperature. Compared to the thermal conductivity of a CaO-SiO_2 binary system, as reported by Nagata and Goto[11], the 1.38 CaO/SiO_2 ratio of the present study produces a relatively higher thermal conductivity above 1700 K, which is approximately equivalent to the liquidus temperature of the CaO-SiO_2 slag system. According to Ammar et al.,[12] an increase in the disorder of a network structure in silicate glass results in a shortening of the phonon free path. Mills[13] also suggested that the phonons transfer along the silicate chain, or ring, is relatively easier than from chain to chain. Therefore, the addition of boron to a CaO-SiO_2 based slag system is believed to increase the mean free path of the phonons by changing the network structure of molten oxides.

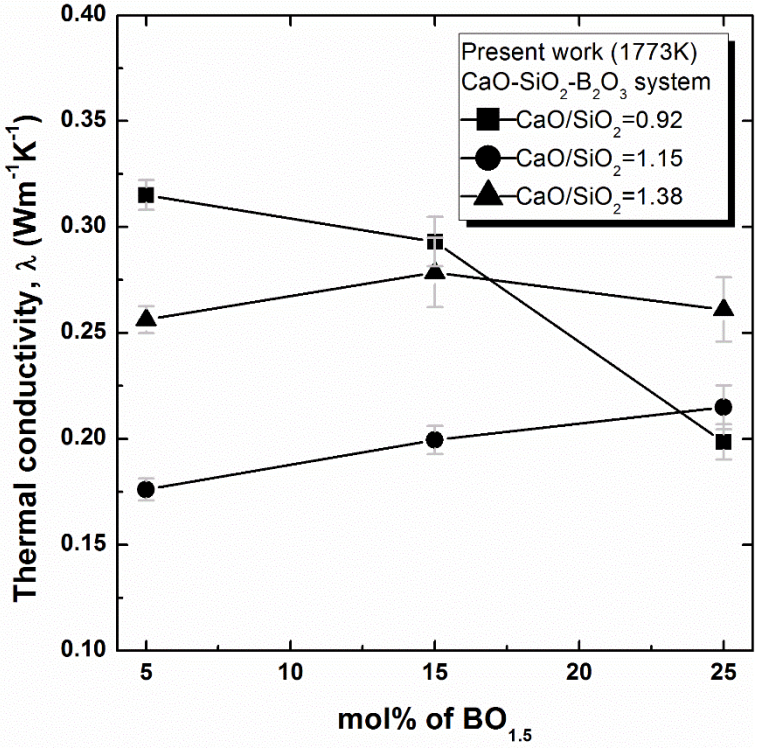

Fig. 5-8. Relationship between thermal conductivity and $BO_{1.5}$ concentration at a fixed CaO/SiO_2 ratio.

The effect of boron oxide concentration on thermal conductivity is shown in Fig. 5-8. From this, it can be seen that the addition of boron oxide has opposite effects on thermal conductivity depending on the CaO/SiO_2 ratio. When this ratio is 0.92, the thermal conductivity is reduced at higher boron oxide concentrations. However, at higher ratios of 1.15 and 1.38, the thermal conductivity either remains unchanged or increases slightly with

increasing boron oxide concentration. Fox et al.[14] reported that such a conflicting effect of boron oxide on the physical properties is due to the nature of boron coordination, and that similar behavior should be observed in the case of the viscosity. Figure 5-9 shows the change in thermal conductivity as a function of CaO/SiO_2 ratio at a fixed concentration ($BO_{1.5}$). In all cases, the thermal conductivity decreases or remains constant with an increase in basicity when the CaO/SiO_2 ratio is smaller than 1.15, whereas it increases with increasing basicity when the CaO/SiO_2 ratio is greater than 1.15.

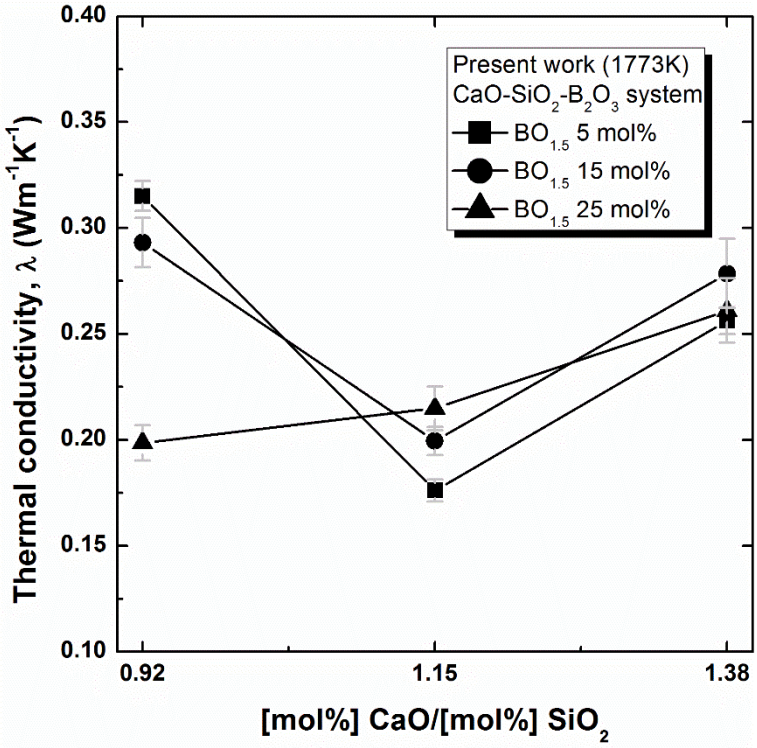

Fig. 5-9. Relationship between thermal conductivity and CaO/SiO_2 ratio at a fixed $BO_{1.5}$ concentration.

Teixeira et al.[15] reported that the activity coefficient of $BO_{1.5}$ in a CaO-SiO_2 binary slag system increases with basicity in acidic slag compositions, while decreasing under basic conditions. They explained that at a molar ratio of CaO/SiO_2 less than 0.86, boron oxide is incorporated into the silicate network. On the other hand, B_2O_3 behaves as an acidic oxide under conditions of higher basicity, thus resulting in a decrease in the activity coefficient of boron oxide with increasing CaO/SiO_2 ratio. Although Teixeira's works were carried out at relatively low boron oxide concentrations, their results are nonetheless worthy of qualitative consideration. From a thermodynamic point of view, it can be inferred that owing to the acidic behavior of boron oxide, the addition of boron oxide should lead to polymerization of the

silicate resulting in an increase in thermal conductivity with higher $BO_{1.5}$ concentrations at CaO/SiO_2 ratios of 1.15, 1.38. With a ratio of 0.92 the boron oxide is incorporated into the silicate structure, thus B_2O_3 addition would change the nature of this network structure and disrupt the movement of phonon, thereby reducing its thermal conductivity. Such variation in the boron oxide state with slag basicity would therefore explain the vastly different effects of B_2O_3 addition on thermal conductivity.

Similarly, the basicity dependency of thermal conductivity is related to the change of state of boron oxide. Since boron oxide is incorporated into silicate networks at low basicity, thermal conductivity is mainly affected by the resulting change of silicate structure. Consequently, at a CaO/SiO_2 ratio of 0.92, the addition of basic oxide leads to a depolymerization of the silicate structure and a resulting decrease in thermal conductivity. On the other hand, under more basic conditions, it is likely that the change in borate structure also effects the change in thermal conductivity. More detailed structural investigation will be discussed in the following sections.

5.3.2.2. Investigation of structure by Raman spectroscopy and its effect on thermal conductivity

Figure 5-10 shows the Raman spectra and related Gaussian deconvoluted bands of non-crystalline $CaO-SiO_2-B_2O_3$ within a 400 to 1600 cm^{-1} range of Raman shift. These Raman spectra have been identified from appropriate references[16–23] and are listed in Table 5-4. Owing to the complicated structure of boron oxide, the possibility of a borate structure existing within the $CaO-SiO_2$ system was investigated; and an annular metaborate group, chain-type metaborate group, pyroborate group and six-membered borate ring were all considered in the present study. It should be noted that a danburite structure of $CaO•B_2O_3•2SiO_2$ (one BO_4^- unit is surrounded by three SiO_4 and one BO_4^-) was not considered which is observed around 630cm^{-1} of Raman shift.[20] According to Osipov et al[24], a danburite spectrum is observed at 614 cm^{-1} with a complete absence of peaks within the 1400-1500cm^{-1} range, however, spectra within the range were found almost the entire compositions in the current study. In addition, a fully-polymerized tetrahedral silicate (SiO_4) unit, which is an essential component for danburite, was rarely observed. Consequently, the Raman spectra around 600–650 cm^{-1} were assigned to ring-breathing vibrations of ring-type metaborate units instead of danburite.

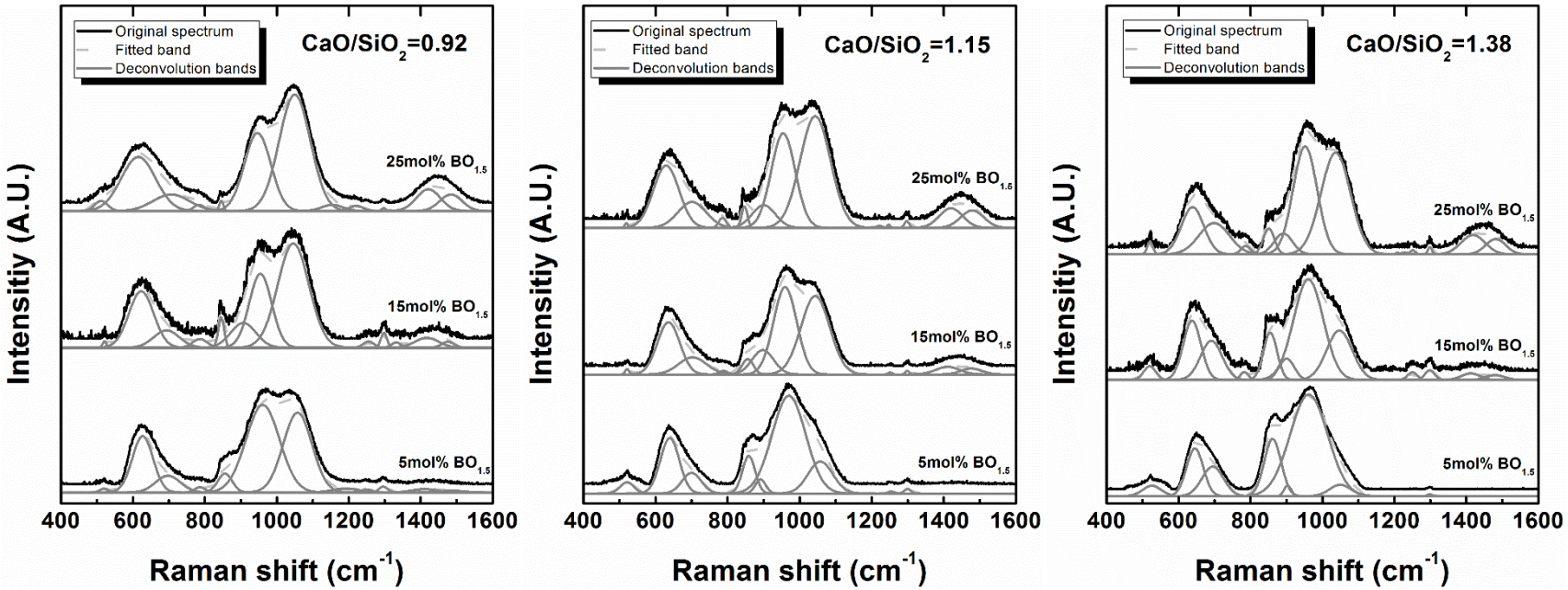

Fig. 5-10. Raman spectra and its Gaussian decovolution bands of the non-crystalline $CaO-SiO_2-B_2O_3$ samples with 5, 15, 25 mol% of $BO_{1.5}$ at a fixed CaO/SiO_2 ratio of (a) 0.92, (b) 1.15, (c) 1.38.

Table 5-4. Reference peak positions of Raman and its structures in the CaO-SiO_2-B_2O_3 system.

Reference position (cm^{-1})	**Assignments**
490-570	"Isolated" diborate units[18, 22]
600-650	Ring-breathing vibration of ring-type metaborate[16, 18, 19, 22]
700-730	B-O-B stretching in chain metaborates[16, 19]
750-780	Breathing vibration of a six membered ring containing both BO_3 triangles and BO_4 tetrahedra[17, 18, 22]
850	Symmetric stretching vibrations of tetrahedral silicate units with 4 non-bridging oxygens[21]
900	Symmetric stretching vibrations of tetrahedral silicate units with 3 non-bridging oxygens[21]
950-1000	Symmetric stretching vibrations of tetrahedral silicate units with 2 non-bridging oxygens[21]
1050-1100	Symmetric stretching vibrations of tetrahedral silicate units with 1 non-bridging oxygens[21]
1150	Asymmetric silicon-oxygen stretching vibrations within a fully-polymerized tetrahedral silicate network[21]
1200-1300	Symmetric stretching vibration of terminal B-O^- bonds in pyroborate unit[16, 19, 17]
1410	Stretching of B-O^- bonds attached to BO_4 unit[20, 23]
1480	Stretching of B-O^- bonds attached to BO_3 unit[20, 23]

The integration of Gaussian deconvoluted spectra of silicate structural units, and their relative fractions, are summarized in Fig. 5-11. Q^n species indicate the SiO_4 tetrahedron with n of bridging oxygen and (4-n) of non-bridging oxygen. It is worth noting that the silicate structure is more polymerized with a higher boron oxide concentration, or a lower CaO/SiO_2 ratio. This polymerization tendency was observed in every composition of this study, and the results are therefore in accordance with a previous structural study by MAS-NMR spectroscopy.[25] However, compared to these MAS-NMR results, the absolute value of the relative fraction of each silicate structure does show some discrepancy. In the MAS-NMR analysis of Angeli et al.[26], the effect of Ca ions on ^{29}Si chemical shift is more significant than silicate polymerization; and for this reason, they considered Raman spectroscopy as a complementary structural data tool. The discrepancy in the relative fractions of the silicate structure obtained by Raman spectroscopy and MAS-NMR would therefore likely be caused by the effect of the second neighbor's nature on ^{29}Si chemical shift in MAS-NMR.

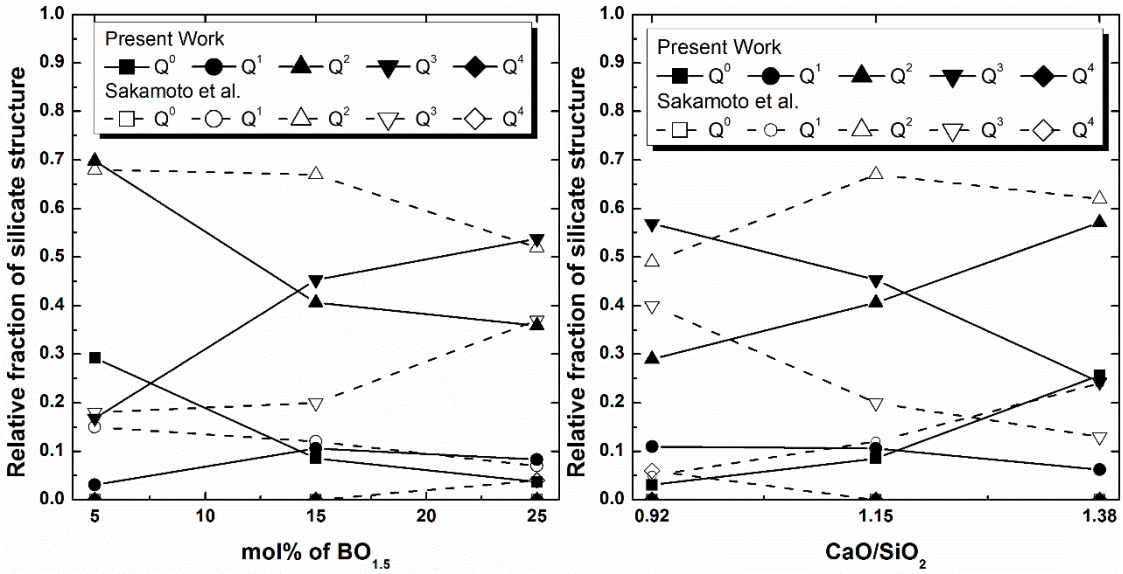

Fig. 5-11. . Relationship between the relative fraction of silicate structure and (a) mol% of $BO_{1.5}$ at fixed CaO/SiO_2 ratio of 1.15, and (b) CaO/SiO_2 ratio at a fixed 15mol% of $BO_{1.5}$

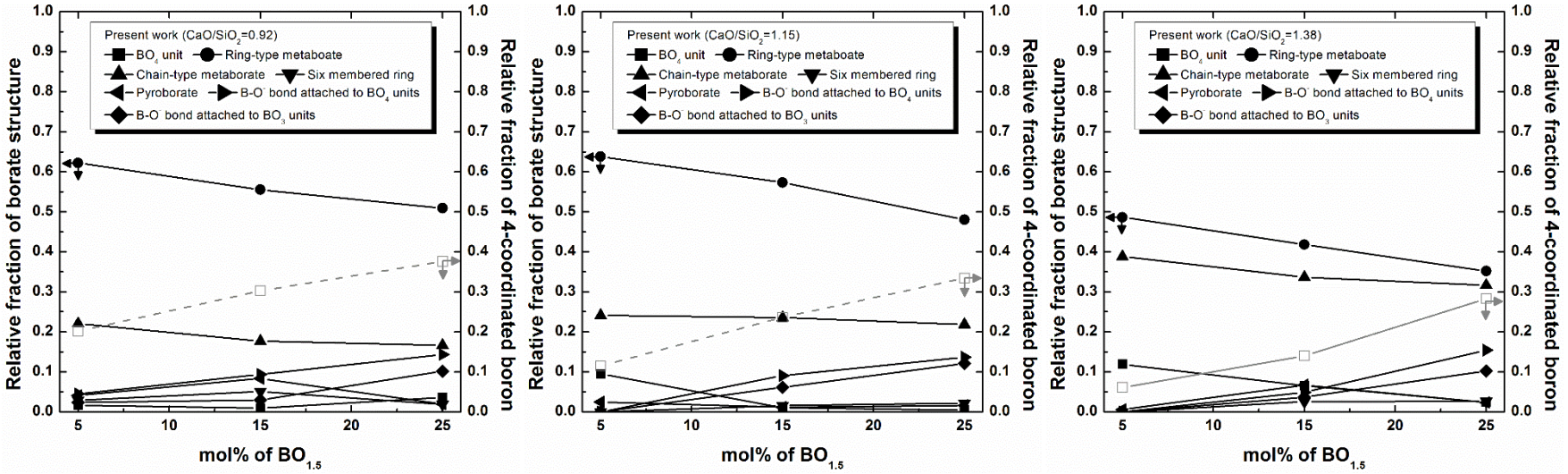

(a) **(b)** **(c)**

Fig. 5-12. Relationship between the relative fraction of borate structure and mol% of $BO_{1.5}$ at fixed CaO/SiO_2 ratio of (a) 0.92, (b) 1.15, and (c) 1.38.

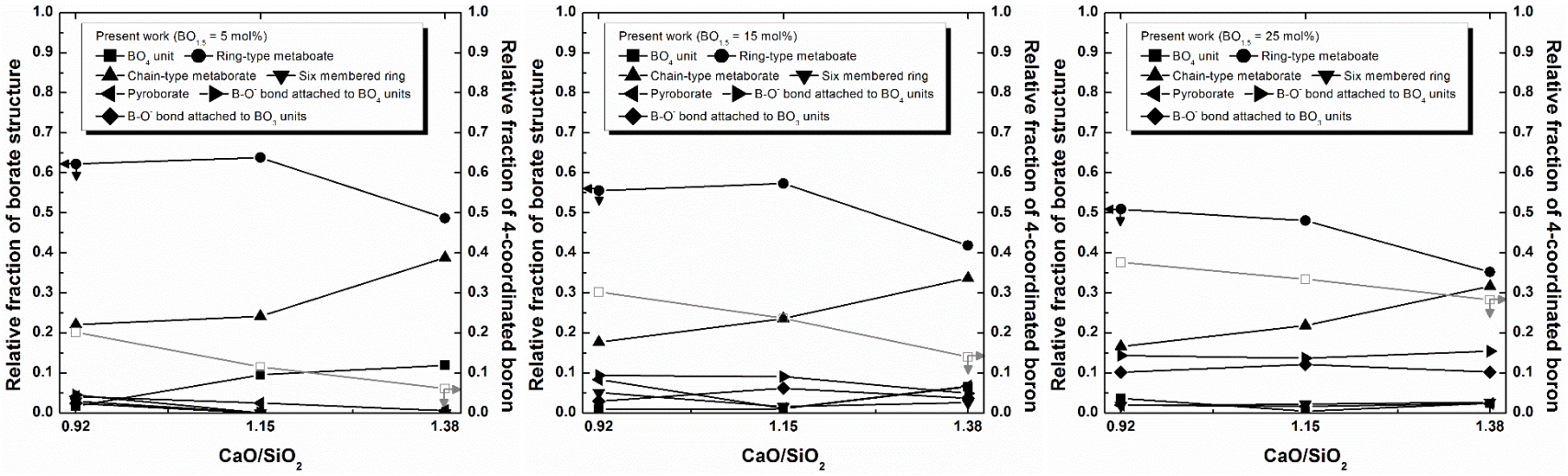

Fig. 5-13. Relationship between the relative fraction of borate structure and CaO/SiO_2 ratio mol% at fixed mol% of $BO_{1.5}$ (a) 5mol%, (b) 15mol%, and (c) 25mol%.

In Fig. 5-12, the addition of $BO_{1.5}$ leads to both increase in the stretching vibration of $B\text{-}O^-$ attached to BO_4 and BO_3 units and decrease in ring-type metaborate units, regardless of the basicity. It can be inferred that the structure of molten slag becomes polymerized with increasing boron oxide concentration. Sakamoto et al.[25] also reported a similar increment of 4-coordinated boron with higher B_2O_3 concentration, using MAS-NMR analysis. It can therefore be considered that the increment of thermal conductivity with a higher $BO_{1.5}$ concentration, at CaO/SiO_2 ratios of 1.15 and 1.38, results from the polymerization of a network structure supporting the acidic behavior of boron oxide. However, in the case of a CaO/SiO_2 ratio of 0.92, the thermal conductivity is reduced in spite of this polymerization due to the increase in boron oxide concentration. As explained in section 3.1, this may be related to the incorporated state of boron oxide in silicate network structures. It seems likely that an increase of $BO_{1.5}$ concentration results in a larger polymerized borate structure incorporated in the silicate structure, thus contributing to a decrease in thermal conductivity by disrupting the movement of phonons.

The relative borate structural fraction with varying CaO/SiO_2 ratio at a fixed $BO_{1.5}$ concentration is shown in Fig. 5-13. This demonstrates the decrease in ring-type metaborate, and related increase in chain-type metaborate, at CaO/SiO_2 ratios of more than 1.15. Since boron oxide is incorporated into the silicate network structure at low basicity, the dependency of thermal conductivity on CaO/SiO_2 ratio is mainly affected by this change in the silicate network structure. An initial decrease or lack of change in the thermal conductivity with higher CaO/SiO_2 ratios therefore results from depolymerization of silicate structure, as-supported by the results of Raman spectroscopy. On the other hand, at CaO/SiO_2 ratios of greater than 1.15, the thermal conductivity increases with higher basicity as a result of an increment of chain-type metaborate, which enhances the movement of phonons by lengthening the network structure. However, it is still unclear as to why this increment of chain-type metaborate has a greater influence over the thermal conductivity than the depolymerization of the silicate structure. More thorough investigation incorporating both thermodynamic and structural aspects is therefore needed to elucidate these conflicting effects of borate and silicate structure on thermal conductivity.

5.3.2.3. Relations between activation energy and its molten structure

In silicate melts, the energy required to break oxygen bonds can be determined by measuring the activation energy of transport.[27] In the case of viscosity, the temperature dependency is simply described by the Arrhenius equation; from which the apparent activation energy can be derived. As an analogy to viscosity, Kang and Morita[28] expressed

thermal conductivity as an Arrhenius-type equation, based on the relationship between the mean free path and the number of thermally broken bonds. Using this equation, values for the apparent activation energy of thermal conductivity were obtained, and are plotted in Fig. 5-14. The activation energy of the present slag system was between 91 kJ/mol to 243 kJ/mol, which is similar values compared to other B_2O_3 bearing slag systems.[1, 29]

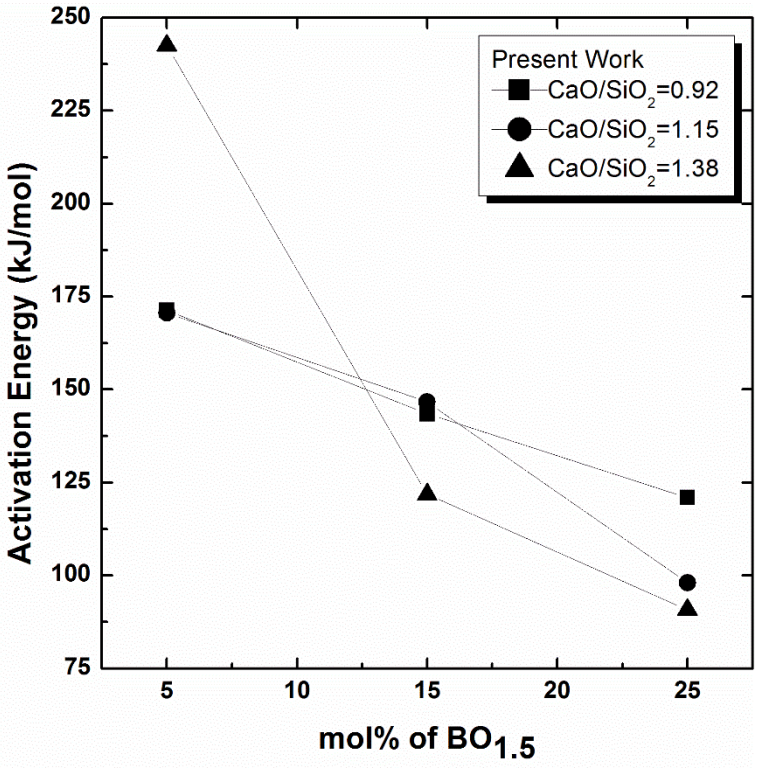

Fig. 5-14. Change of activation energy with varying mol% of $BO_{1.5}$ at different CaO/SiO_2 ratio.

The results of the present study show that the activation energy of thermal conductivity decreases with a higher $BO_{1.5}$ concentration, indicating an increment in the number of thermally broken bonds or a decrement in the required energy to break oxygen bonds. This result seems to be contradictory to the network formation with higher boron oxide concentration explained in section 5.3.2.2. However, Wang et al.[1] measured the viscosity in the B_2O_3 and TiO_2 bearing mold flux system, reporting the decreasing of activation energy with polymerization due to the increase in boron oxide concentration. They explained that the formation of weaker B-O bonds in the network structure leads to a lowering of the activation energy. It is therefore concluded that the increase of B-O bonds in the network structure caused by the addition of $BO_{1.5}$ to a CaO/SiO_2 system results in a weakening of the network bond energy, and thus a decrease in the activation energy.

5.4 Short Summary

Thermal conductivity of the CaO-B_2O_3 was measured, and the effect of borate structure change was evaluated using ^{11}B MAS NMR and 3Q MAS spectroscopy. It was found that thermal conductivity was mainly affected by the change of ratio between symmetric and asymmetric 3-coordinated boron. The addition of CaO results in the depolymerization of borate network structure, especially the 3-coordinated planar ring borate network structure. The formation of metaborate units along with the increasing of the non-ring 3-cooridnated boron leads to decrease in thermal conductivity by decreasing phonon mean free path.

In order to see the effect of borate structure related to asymmetric 3-coordinated boron, thermal conductivity was measured in the molten CaO-SiO_2-B_2O_3 system at the high CaO concentration region; which is the typical composition of mold flux system. It was found that the thermal conductivity was reduced with higher temperatures for every compositional range tested, and is the result of a decrease in the mean free path (l). However, the addition of boron oxide was found to result in both an increment and decrement of thermal conductivity, depending on the CaO/SiO_2 ratio. At a relatively low CaO/SiO_2 ratio of 0.92, B_2O_3 is incorporated into silicate networks and higher concentrations therefore lead to reduced thermal conductivity by disrupting the movement of phonons. However, at higher basicities of 1.15 and 1.38, the thermal conductivity is increased at higher $BO_{1.5}$ concentrations through the polymerization of both borate and silicate networks. It was also found that the thermal conductivity was initially decreased or remained constant with an increase in basicity, but was increased with CaO/SiO_2 ratios of greater than 1.15. It was thought that at a relatively low basicity, boron oxide incorporated in the silicate structure and depolymerization of silicate structure at higher CaO/SiO_2 ratios would mostly have an effect on thermal conductivity. Contrarily, it was found that with a higher basicity the thermal conductivity is in fact increased by an increment of a chain-type metaborate structure. A decrement of activation energy with increasing $BO_{1.5}$ concentration was also observed, indicating a weakening of the bond energy by increasing of B-O bonds in the network structure of BO_4 and BO_3 units.

References

[1] Z. Wang, Q. Shu, and K. Chou, "Viscosity of Fluoride-Free Mold Fluxes Containing B_2O_3 and TiO2," *Steel Res. Int.*, **84** [8] 766–776 (2013).

[2] M. Sakamoto, "溶融酸化物の構造および熱力学的性質・物性への影響;" The University of Tokyo, 2012.

[3] J.-P. Amoureux, C. Fernandez, and S. Steuernagel, "Z Filtering in MQMAS NMR," *J. Magn. Reson. Ser. A*, **123** [1] 116–118 (1996).

[4] L.-S. Du and J.F. Stebbins, "Nature of Silicon−Boron Mixing in Sodium Borosilicate Glasses: A High-Resolution ^{11}B and ^{17}O NMR Study," *J. Phys. Chem. B*, **107** [37] 10063–10076 (2003).

[5] T. Nanba, M. Nishimura, and Y. Miura, "A theoretical interpretation of the chemical shift of ^{29}Si NMR peaks in alkali borosilicate glasses," *Geochim. Cosmochim. Acta*, **68** [24] 5103–5111 (2004).

[6] N. Ohtori, K. Takase, I. Akiyama, Y. Suzuki, K. Handa, I. Sakai, Y. Iwadate, T. Fukunaga, *et al.*, "Short-range structure of alkaline-earth borate glasses by pulsed neutron diffraction and molecular dynamics simulation," *J. Non-Cryst. Solids*, **293-295** [1] 136–145 (2001).

[7] S.K. Lee and J.F. Stebbins, "Nature of Cation Mixing and Ordering in Na-Ca Silicate Glasses and Melts," *J. Phys. Chem. B*, **107** [14] 3141–3148 (2003).

[8] D. Maniu, T. Iliescu, I. Ardelean, S. Cinta-Pinzaru, N. Tarcea, and W. Kiefer, "Raman study on B_2O_3–CaO glasses," *J. Mol. Struct.*, **651-653** 485–488 (2003).

[9] W.D. Kingery, *Introduction to ceramics*. John Wiley & Sons, New York, 1967.

[10] J.M. Ziman, *Electrons and Phonons : The theory of transport phenomena in solids*. Oxford University Press, London, 1960.

[11] K.C. Mills, *Slag atlas*, 2nd ed. Verlag Stahleisen GmbH, Dusseldorf, 1995.

[12] M.M. Ammar, S. Gharib, M.M. Halawa, K. El Badry, N.A. Ghoneim, and H.A. El Batal, "Thermal conductivity of some silicate glasses in relation to composition and structure," *J. Non-Cryst. Solids*, **53** [1-2] 165–172 (1982).

[13] K.C. Mills, "The Influence of Structure on the Physico-chemical Properties of Slags.," *ISIJ Int.*, **33** [1] 148–155 (1993).

[14] A.B. Fox, K.C. Mills, D. Lever, C. Bezerra, C. Valadares, I. Unamuno, J.J. Laraudogoitia, and J. Gisby, "Development of Fluoride-Free Fluxes for Billet Casting," *ISIJ Int.*, **45** [7] 1051–1058 (2005).

[15] L.A.V. Teixeira, Y. Tokuda, T. Yoko, and K. Morita, "Behavior and State of Boron in CaO–SiO_2 Slags during Refining of Solar Grade Silicon," *ISIJ Int.*, **49** [6] 777–782 (2009).

[16] R.K. Brow, D.R. Tallant, and G.L. Turner, "Raman and 11B nuclear magnetic resonance spectroscopic studies of alkaline-earth lanthanoborate glasses," *J. Am. Ceram. Soc.*, **79** [9] 2410–2416 (1996).

[17] B.P. Dwivedi and B.N. Khanna, "Cation dependence of raman scattering in alkali borate glasses," *J. Phys. Chem. Solids*, **56** [1] 39–49 (1995).

[18] E.I. Kamitsos, M.A. Karakassides, and G.D. Chryssikos, "Vibrational spectra of magnesium-sodium-borate glasses. 2. Raman and mid-infrared investigation of the network structure," *J. Phys. Chem.*, **91** [5] 1073–1079 (1987).

[19] H. Li, Y. Su, L. Li, and D.M. Strachan, "Raman spectroscopic study of gadolinium(III) in sodium-aluminoborosilicate glasses," *J. Non-Cryst. Solids*, **292** [1-3] 167–176 (2001).

[20] D. Manara, a. Grandjean, and D.R.R. Neuville, "Advances in understanding the structure of borosilicate glasses: A Raman spectroscopy study," *Am. Mineral.*, **94** [5-6] 777–784 (2009).

[21] P. McMillan, "Structural studies of silicate glasses and melts—applications and limitations of Raman spectroscopy," *Am. Mineral.*, **69** [7-8] 622–644 (1984).

[22] G. Padmaja and P. Kistaiah, "Infrared and raman spectroscopic studies on alkali borate glasses: Evidence of mixed alkali effect," *J. Phys. Chem. A*, **113** [11] 2397–2404 (2009).

[23] R. Akagi, N. Ohtori, and N. Umesaki, "Raman spectra of K_2O–B_2O_3 glasses and melts," *J. Non-Cryst. Solids*, **293-295** [1] 471–476 (2001).

[24] A.A. Osipov, L.M. Osipova, and V.E. Eremyashev, "Structure of alkali borosilicate glasses and melts according to Raman spectroscopy data," *Glass Phys. Chem.*, **39** [2] 105–112 (2013).

[25] M. Sakamoto, Y. Yanaba, H. Yamamura, and K. Morita, "Relationship between Structure and Thermodynamic Properties in the CaO–SiO_2–$BO_{1.5}$ Slag System," *ISIJ Int.*, **53** [7] 1143–1151 (2013).

[26] F. Angeli, T. Charpentier, D. De Ligny, and C. Cailleteau, "Boron Speciation in Soda-Lime Borosilicate Glasses Containing Zirconium," *J. Am. Ceram. Soc.*, **93** [9] 2693–2704 (2010).

[27] B.O. Mysen and P. Richet, *Silicate Glasses and Melts*, 1st ed. Elsevier, Amsterdam, 2005.

[28] Y. Kang and K. Morita, "Thermal conductivity of the CaO-Al_2O_3-SiO_2 system," *ISIJ Int.*, **46** [3] 420–426 (2006).

[29] G.H. Kim and I. Sohn, "Role of B_2O_3 on the Viscosity and Structure in the CaO-Al_2O_3-Na_2O-Based System," *Metall. Mater. Trans. B*, **45** 86–95 (2013).

Chapter VI

Thermal Conductivity of the Alkali-Borate Glass

6.1 Background

In the previous chapters, thermal conductivity of the molten in the various borate and borosilicate system was measured along with structure investigation. According to previous researches, temperature dependence of thermal conductivity in the oxide system shows distinct characteristic, compared to simple temperature dependence of thermal conductivity in the metal system. In the silicate system, positive temperature dependence in the solid state but negative temperature dependence in the glass state were observed. However, thorough investigation for the conflicting temperature dependence of thermal conductivity in the glass and molten borate system has not been reported.

Considering that thermal conductivity is a function of heat capacity and no structural change below glass transition temperature, such positive temperature dependence of thermal conductivity results from the change of heat capacity. On the other hands, at high temperature, when the heat capacity is kept constant, it seems that other variables become dominant resulting in opposite temperature dependence.

Therefore, in this chapter, temperature dependence of thermal conductivity was investigated in the varying temperature range; from room temperature to 1273 K. In addition, the temperature showing maximum thermal conductivity will be discussed. The effect of not only the borate structure change, but also specific heat capacity will be considered in order to explain the thermal conductivity change with different temperature. Finally, cation effect on thermal conductivity in the alkali borate glass system will be studied.

6.2 Experiment Procedure

6.2.1. Sample Preparation

The R_2O-B_2O_3 (R = Li, Na, and K) sample was prepared from the reagent grade of R_2CO_3 and B_2O_3. After ground in the agate mortar for 30 min, the powder mixture was transferred into Pt crucible and melted at 1373 K. After 1 h, the molten sample was quenched on copper plate and then, finely crushed in order to obtain homogeneous mixture. The crushed powder was re-melted in the Pt crucible at 1373 K. After 30 min, the molten glass was poured into the hole in the copper plate. In the copper plate, rectangular groove for hot-wire and cylinder shape hole for glass sample were carved. The hot-wire (0.15mmϕ Pt-13% Rh wire) welded with 0.15mmϕ Pt wire and 0. 5mmϕ Pt wire was placed on the rectangular-groove, in advance. Detailed description of the copper plate can be found in Fig. 6-1. During cooling, in order to reduce the thermal stress, copper plate was heated placing on the hot-plate maintained at 603 K. The glass sample was transferred into alumina brick. Due to the viscous flow of glass sample over the glass transition temperature, the alumina brick has hole same size to glass sample, playing a role of sample holder. Finally, the alumina brick placed on the alumina plate hanging on the long alumina lance equipped with Pt wires for thermal conductivity measurement. The schematic diagram of thermal conductivity measurement apparatus is shown in Fig 6-2.

6.2.2. Thermal Conductivity Measurement

In order to measure the thermal conductivity of glass sample, hot-wire method was adopted. The glass sample was inserted into electric resistance furnace equipped with SiC heating element. During the measurement, using a PID (proportional integral differential) controller and calibrated K-type thermocouple, sample temperature was controlled.

Thermal conductivity was measured at 100 K intervals from room temperature to the liquidus temperature. Using a galvanostat, a constant current of 1.3–1.5 A was supplied to a 0.15mmϕ Pt-13%Rh hot-wire, and any voltage change between the two terminals of the wire was monitored by a digital multimeter. A linear relationship between ΔV and ln$t$ was obtained within 0.8–2.0 seconds, and the thermal conductivity, λ ($Wm^{-1}K^{-1}$), was calculated by the equation (1-18). During the measurement, to ensure the thermal equilibrium of the system, the furnace temperature was increased at a rate of 3 K/min and held for 15 minutes at the target temperature. To confirm the reproducibility of the results, the measurement was repeated three times at the same temperature, with a 5-minutes interval between one

measurement and the following one.

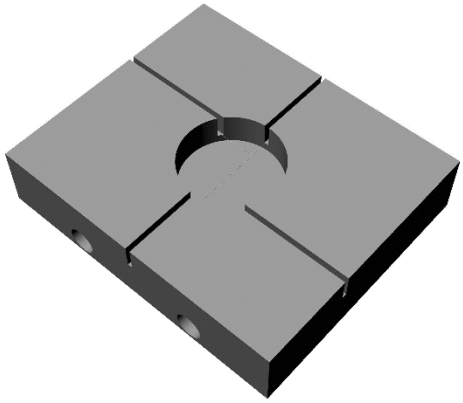

Fig. 6-1. Schematic diagram of the copper plate carved with four rectangular-grooves and cylinder-shape hole.

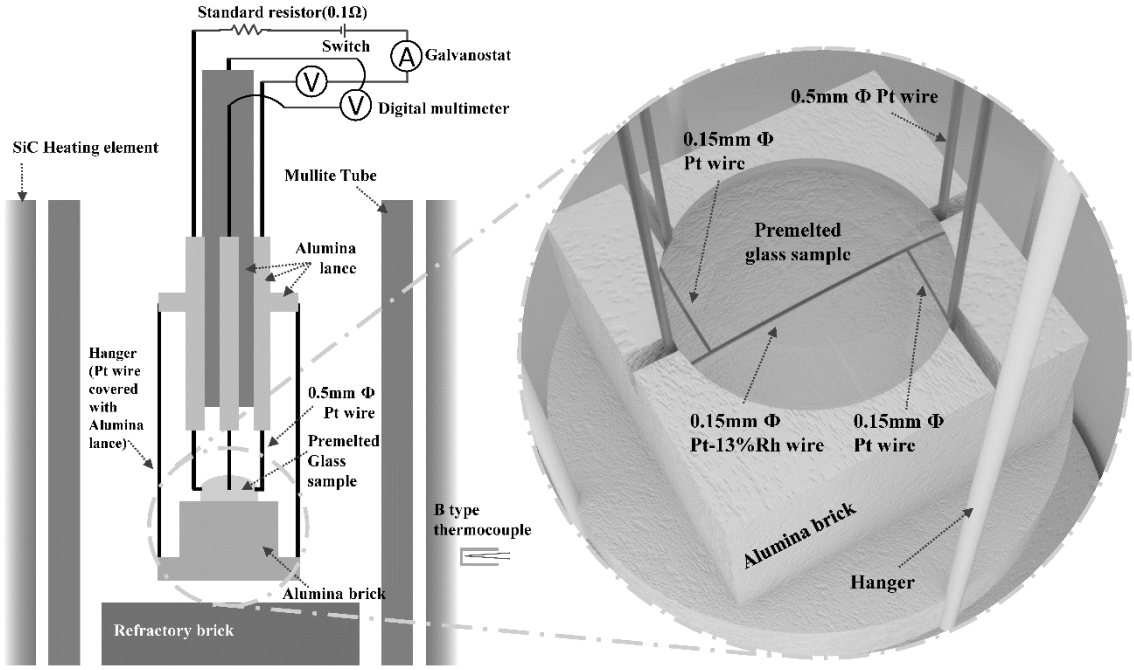

Fig. 6-2. Schematic diagram of the thermal conductivity measurement apparatus for the glass sample.

6.2.3. Analytical Procedures

6.2.3.1. Determination of the boron, lithium, sodium and potassium concentration in the sample

Following the measurement of thermal conductivity by the hot-wire method, the sample was ground and sieved using a 100 μmϕ mesh. In order to evaluate the chemical composition, approximately 0.01 g of the ground sample was transferred into 100 ml of beaker. Following the addition of acid-solution (10 ml of distilled water + 15 ml of HCl + 5 ml of HNO_3), the beaker was placed on the hot-plate covered with watch glass, and then heated at 493 K for several hours. When the almost of the acid solution was evaporated, approximately 5 ml of $HClO_4$ was added, and kept on heating until white smoke appeared.

The heated beaker was cooled down at room temperature. The solution was filtered using a filter paper (ash contents 0.1 mg/circle) attached on glass funnel, and transferred into 100 or 500 ml of volumetric flask. After rinsing the beaker and filter paper several times by distilled water, the final volume was made. In order to obtain the homogeneous concentration across the solution, the volumetric flask was kept for 24 hours.

Using the inductively coupled plasma atomic emission spectroscopy (ICP-AES; SPS7700, SII NanoTechnology, Japan), final concentration of boron was determined. Diluting the 1000 ppm of boron standard solution (Kanto chemical, Tokyo, Japan), 10, 20, 50 and 100 ppm of boron standard solution was prepared. Using the four standard solutions, calibration line was drawn from 0 to 100 ppm showing larger than 0.999 of correlation coefficient. During the analysis, 249.773 nm, 670.784 nm, 588.995 nm and 766.490 nm of wavelength were chosen for boron, lithium, sodium and potassium as analytical wavelength.

Table 6-1 shows the final composition the present work.

Table 6-1. Initial and final composition of the present experiment.

	Initial Compositions (mol %)				**Final Compositions (mol %)**			
	B_2O_3	**Li_2O**	**Na_2O**	**K_2O**	**B_2O_3**	**Li_2O**	**Na_2O**	**K_2O**
1	90	10	-	-	90.8	9.2	-	-
2	80	20	-	-	81.4	18.6	-	-
3	90	-	10	-	90.5	-	9.5	-
4	80	-	20	-	81.4	-	18.6	-
5	90	-	-	10	90.9	-	-	9.1
6	80	-	-	20	82.0	-	-	18.0

6.2.3.2. Determination of the crystalline phase

Above the glass transition temperature, formation of the crystalline phase was observed and it results in a drastic increase in thermal conductivity. After the thermal conductivity measurement, the crystalline phase was confirmed using X-ray Diffraction (XRD; RINT 2500, Rigaku, Japan). The background subtraction and peak search were carried out using "MDI Jade (ver. 4.0)" software. In the case of the $Li_2B_8O_{13}$ crystalline phase, XRD peak was obtained using "Mecury (ver. 3.5.1)" crystal structure visualization software based on the reported crystal structure information. Figure 6-3 shows the XRD pattern of the K_2O-B_2O_3 and Li_2O-B_2O_3 system where mole percent of K_2O and Li_2O is 10 mol%. On the other hands, no crystalline phase was observed in the sodium borate system containing 10 mol% Na_2O.

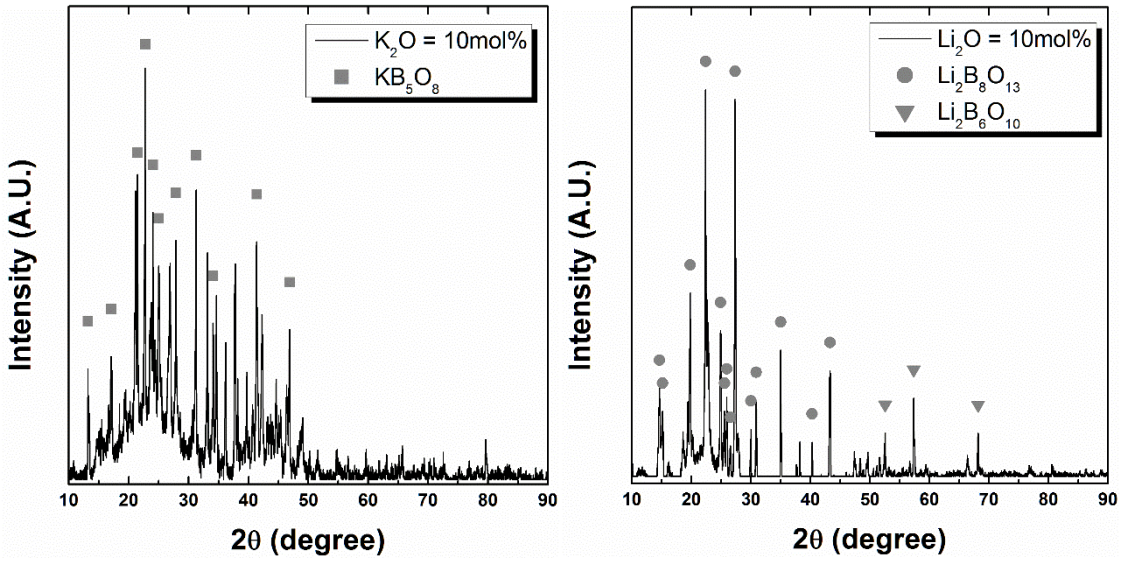

Fig. 6-3. X-ray diffraction pattern of crystalline phase in the **(a)** K_2O-B_2O_3 and **(b)** Li_2O-B_2O_3 system.

6.2.4. Determination of the Glass Transition Temperature and Crystallization Temperature

In order to find the glass transition temperature and crystallization temperature, differential thermal analysis (DTA) was carried out using TG-DTA (Thermo plus TG 8120, Rigaku, Tokyo, Japan). Approximately 0.02 g of powdered sample was filled in the platinum pan (ID: 5 mm; OD: 5.05 mm; height: 2.5 mm) and placed on the platinum plate at the end of ceramic rod. A similar quantity of reference sample (Al_2O_3) was filled in the same size of platinum

pan and placed on the platinum plate at the end of another ceramic rod. Under the argon atmosphere, the samples were heated up from room temperature to the liquidus temperature at a rate of 5 K/min. The differential thermocouple temperature was recorded as function of time. After it reaches target temperature, the sample was cooled down at a rate of 20 K/min. The glass transition temperature was determined from the heating curve by standard test method (E1356-08) proposed by American Society for Testing Materials (ASTM).[1] In addition, crystallization temperature was determined as the temperature showing maximum heat flow at the distinct sharp peak. Figure 6-4 shows the DTA thermal curve for the present K_2O-B_2O_3 system where K_2O = 10 mol%.

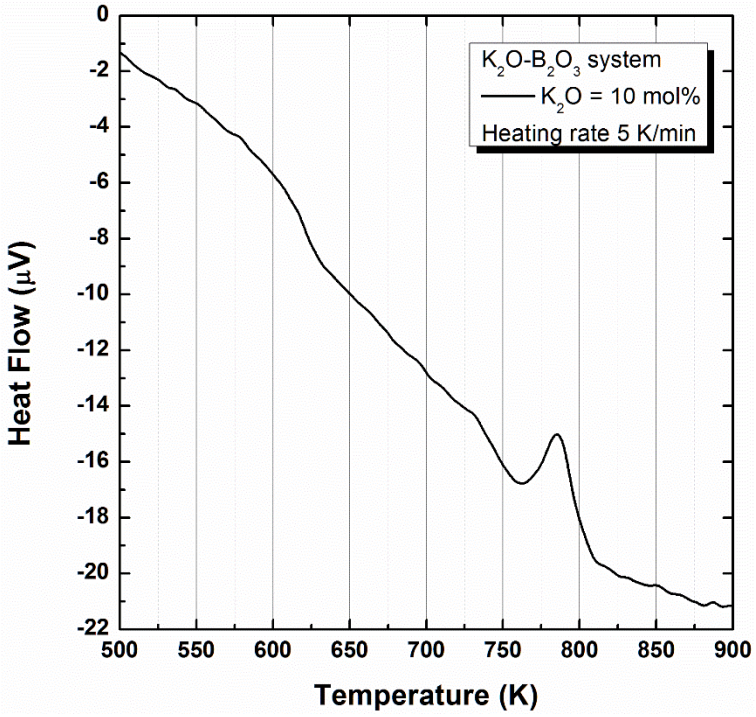

Fig. 6-4. The DTA thermal curve for the K_2O-B_2O_3 glass sample.

6.3 Results and Discussion

6.3.1. Temperature Dependence of the Thermal Conductivity in the Glass and Molten R_2O-B_2O_3 System

Figure 6-5, 6-6 and 6-7 show the temperature dependence of thermal conductivity in the various R_2O-B_2O_3 systems. In the figures, measured glass transition temperature (T_g) and calculated one-dimensional Debye temperature (Θ_{D1}) are marked as black arrow. In addition, the thermal conductivity measured above crystallization temperature is shown as open rectangle and these points were not considered. In Table 6-2, measured glass transition temperature and crystallization temperature are summarized.

It can be commonly observed that thermal conductivity of glass sample gradually increases with higher temperature. After it reaches maximum, thermal conductivity is kept constant within short temperature range, and then decreases with higher temperature. Similar temperature dependence of thermal conductivity was reported by Nagata and Goto[2] who measured thermal conductivity in the CaO-SiO_2-Al_2O_3 system. Although their study has some limitation; the crystalline phase would be formed due to the continuous thermal conductivity measurement from molten to solid state, present results; which were carried out separately, successfully show that thermal conductivity of oxide glass system has maximum thermal conductivity.

It is interesting that the temperature where the maximum thermal conductivity is observed, is excellent in accordance with one-dimensional Debye temperature. According to Debye model, it can be inferred that thermal conductivity below one-dimensional Debye temperature, heat capacity is the dominant factor affecting thermal conductivity. However, above one-dimensional Debye temperature, other factors, such as phonon mean free path or sound velocity would become dominant. Although there is a drastic increasing of heat capacity at glass transition temperature, thermal conductivity gradually increases without showing any sudden change.

It should be noted that in the molten K_2O-B_2O_3 and Li_2O-B_2O_3 system, drastic decrease in thermal conductivity was observed. In the previous chapter, the change of intermediate range order borate structure would result in a sudden decreasing of thermal conductivity. However, in this chapter, the sudden decrease in thermal conductivity near the liquidus temperature was not considered.

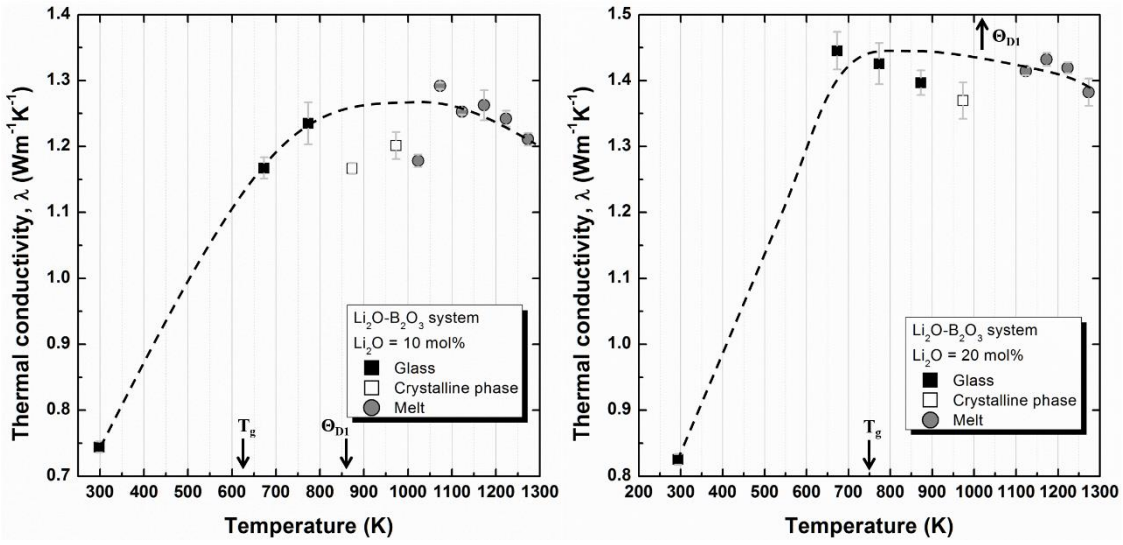

(a) **(b)**

Fig. 6-5. The relationship between thermal conductivity and temperature in the Li_2O-B_2O_3 system at **(a)** Li_2O = 10 mol% and **(b)** Li_2O = 20 mol%. (The black dashed line has been drawn as a guide)

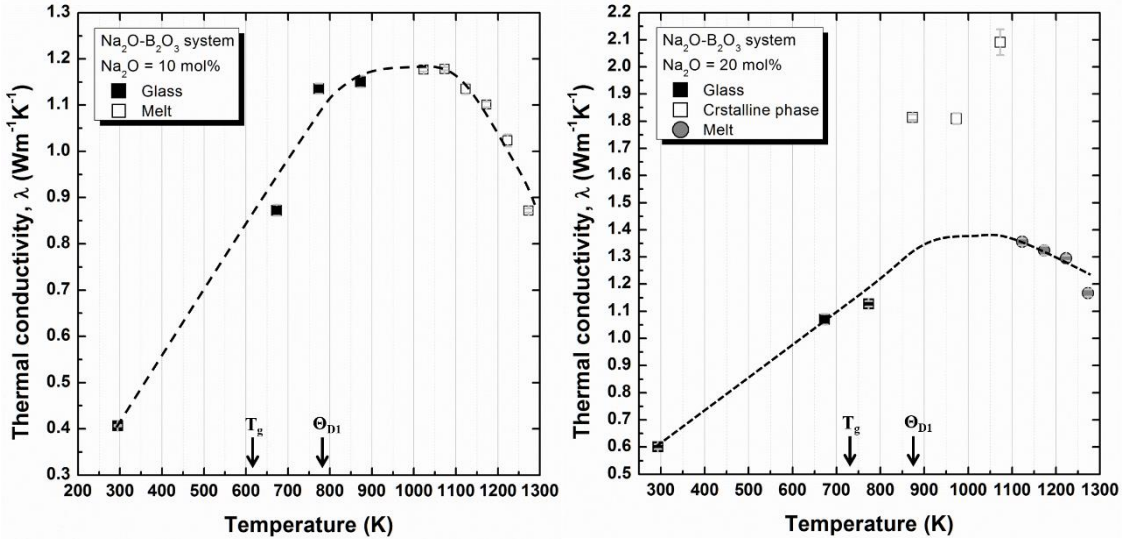

(a) **(b)**

Fig. 6-6. The relationship between thermal conductivity and temperature in the Na_2O-B_2O_3 system at **(a)** Na_2O = 10 mol% and **(b)** Na_2O = 20 mol%. (The black dashed line has been drawn as a guide)

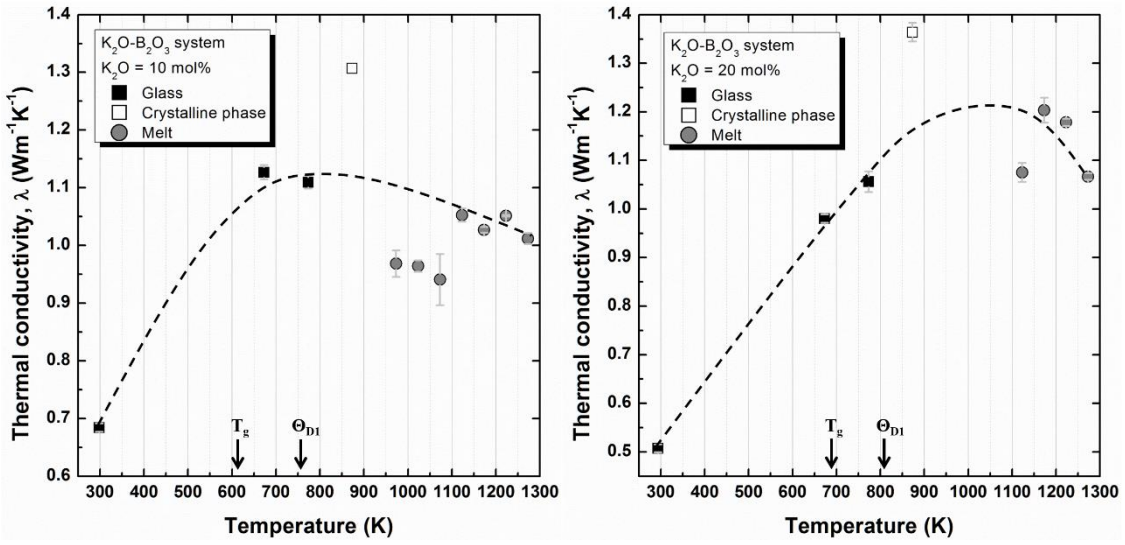

(a) **(b)**

Fig. 6-7. The relationship between thermal conductivity and temperature in the K_2O-B_2O_3 system at **(a)** K_2O = 10 mol% and **(b)** K_2O = 20 mol%. (The black dashed line has been drawn as a guide)

Table 6-2. Glass transition temperature (T_g), crystallization temperature (T_C) and the dominant crystalline phase in the present R_2O-B_2O_3 system.

		Glass transition temperature (T_g)	**Crystallization temperature (T_C)**	**Dominant Crystalline phase**
Li_2O-B_2O_3 system	**Li_2O=10 mol%**	628 K	796 K	$Li_2B_8O_{13}$
	Li_2O=20 mol%	749 K	881 K	$Li_2B_8O_{13}$
Na_2O-B_2O_3 system	**Na_2O=10 mol%**	618 K	-	-
	Na_2O=20 mol%	736 K	873 K	$Na_2B_6O_{13}$
K_2O-B_2O_3 system	**K_2O=10 mol%**	619 K	785 K	KB_5O_8
	K_2O=20 mol%	692 K	814 K	$K_5B_{19}O_{31}$, KB_5O_8

6.3.2. Effect of Heat Capacity and Cation Type on Thermal Conductivity in the Alkali Borate Glass

Figure 6-8 shows the change of thermal conductivity with varying cation types. At the room temperature, Yano et al.[3], and Osipov and Osipova[4] reported almost same relative fraction of 4 coordinated boron in the same R_2O concentration, regardless of the cation type; 10 mol% R_2O system has the relative fraction of 4-coordinate boron of 0.11, and 20 mol% R_2O system has the relative fraction of 4-coordinate boron of 0.25, approximately.

In the R_2O-$4B_2O_3$ system at the room temperature, different thermal conductivity can be found with varying cation type, in spite of the almost same relative fraction of 4-coordinated boron. In addition, thermal conductivity increases with higher temperature.

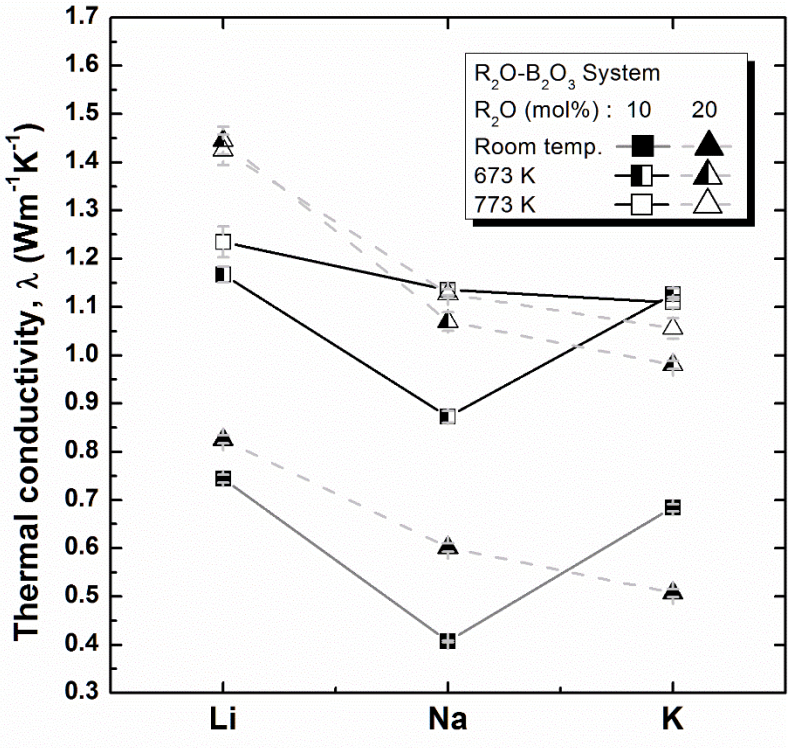

Fig. 6-8. The relationship between thermal conductivity and type of cation in the R_2O-B_2O_3 system. The rectangular and triangular points represent 10 mol% and 20 mol% R_2O system, respectively.

As mentioned in the previous chapter, due to the change of the intermediate range order borate structure along with increasing of disorder, linear relationship between thermal conductivity and the relative fraction of 4-coordinated boron couldn't be observed in the 10 mol% R_2O system. Such an intermediate range order structure change is different depending

on the cation type. As a result, in the 10 mol% R_2O system, different thermal conductivity is observed among three R_2O-B_2O_3 system, in spite of the almost same relative fraction of 4-cooridnated boron. However, thermal conductivity also increases with higher temperature.

Figure 6-9 shows the temperature dependence of the specific heat and thermal conductivity in the R_2O-$4B_2O_3$ system. Similar temperature dependence between specific heat capacity and thermal conductivity can be observed. According to DTA results, glass transition temperature was determined above 690 K for all experiment compositions. Considering that there is no borate structure change below glass transition temperature, it can be inferred that the increase in thermal conductivity from 273 K to 673 K results from the increase in specific heat capacity.

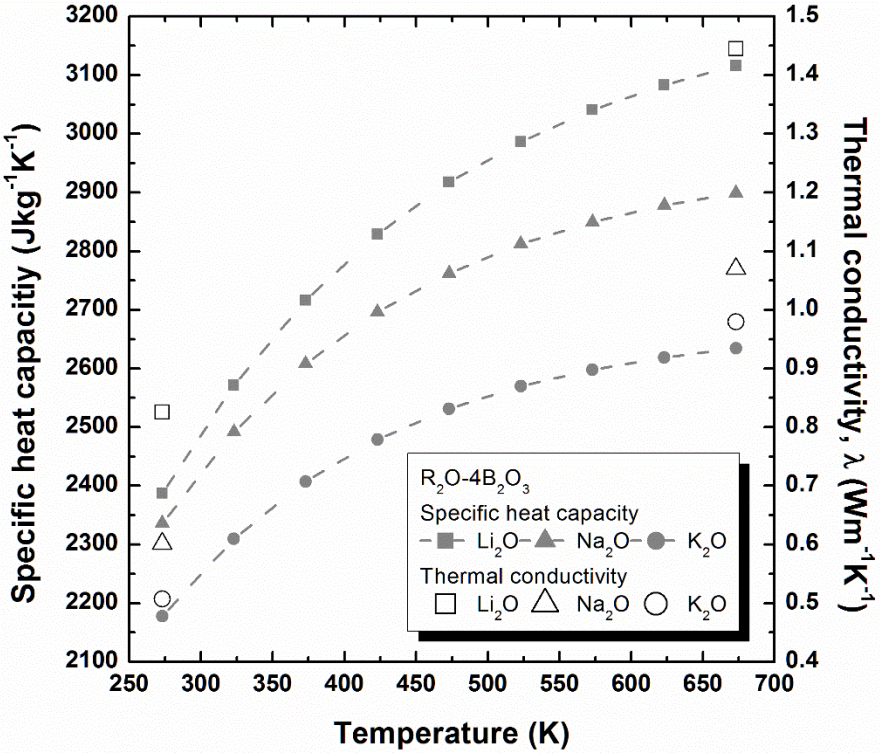

Fig. 6-9. Change of specific heat capacity and thermal conductivity with varying temperature in the R_2O-$4B_2O_3$ system.

In order to see the cation effect, thermal conductivity was plotted as a function of ionization potential in the R_2O-$4B_2O_3$ system. In Fig. 6-10, similar to 1273 K, the effect of cation on thermal conductivity can be found. The slope between thermal conductivity and ionization potential is excellent in accordance with each other. As reported in the previous chapter, the relative fraction of 4-coordinated boron is approximately 0.17 in the R_2O-$4B_2O_3$ system at 1273 K. In spite of the lower relative fraction of 4-coordinated boron at 1273 K, higher

thermal conductivity can be observed. The calculated heat capacity using equation (3-11) is 2387, 2336, 2177 $Jkg^{-1}K^{-1}$ at room temperature, and 3229, 2961, 2676 $JKg^{-1}K^{-1}$ at 1273 K for Li_2O-$4B_2O_3$, Na_2O-$4B_2O_3$, and K_2O-$4B_2O_3$ system, respectively. Therefore, it can be also inferred that the thermal conductivity difference between room temperature and 1273 K results from the heat capacity change.

However, at a fixed temperature of 1273 K, in spite of difference of heat capacity among three systems, the effect of heat capacity can be hardly observed. It would indicate that other variables become more dominant at higher temperature region.

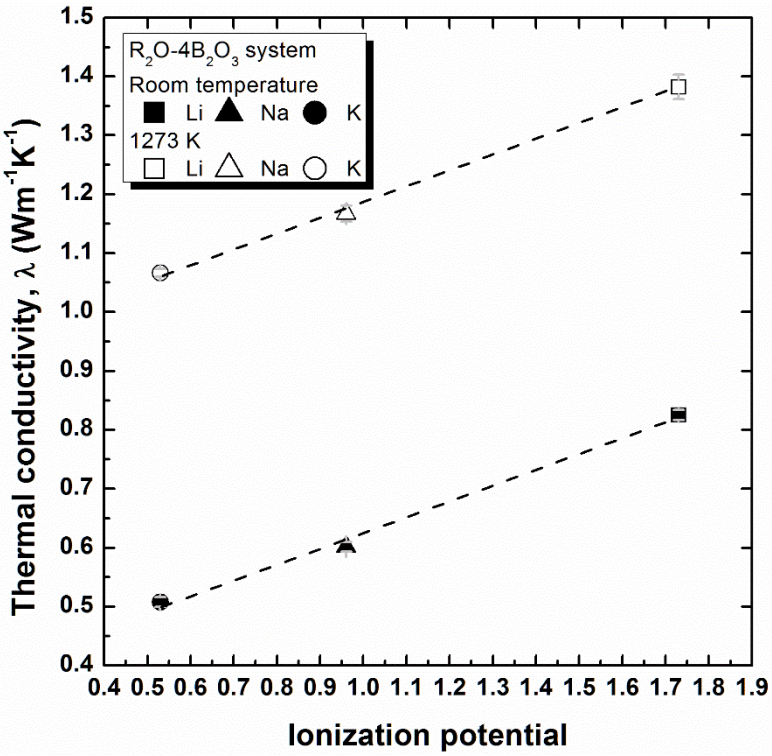

Fig. 6-10. The relationship between thermal conductivity and ionization potential in the R_2O-B_2O_3 system at room temperature and 1273 K.

6.4 Short Summary

In this chapter, temperature dependence of thermal conductivity was considered from glass to molten alkali borate system. Thermal conductivity initially increases with higher temperature at the glass state. After it reaches maximum, decrease in thermal conductivity was observed at the liquid state. The temperature where thermal conductivity shows maximum is well in accordance with the one-dimensional Debye temperature. According to Debye model, it can be inferred that thermal conductivity increases with higher temperature due to the increasing of heat capacity along with small structural change. However, above one-dimensional Debye temperature, other variables dominantly effect on the thermal conductivity as a result of constant heat capacity. Increasing of thermal conductivity below glass transition temperature; where is no borate structural change, supports that the change of specific heat capacity determines the thermal conductivity change at low temperature region.

The cation effect on thermal conductivity was evaluated as a function of ionization potential. The linear slope between thermal conductivity and ionization potential obtained at room temperature is excellent in accordance with that obtained at 1273 K. However, in spite of the higher relative fraction of 4-coordinated boron at room temperature, lower thermal conductivity was observed at room temperature. Considering the significant difference of heat capacity, it can be inferred that higher thermal conductivity at 1273 K would result from the higher heat capacity.

References

[1] ASTM E1356-08, *Standard Test Method for Assignment of the Glass Transition Temperatures by Differential Scanning Calorimetry*. West Conshohocken, PA, 2014.

[2] K. Nagata and K.S. Goto, "Heat Conductivity and Mean Free Path of Phonons in Metallurgical Slags;" pp. 875–889 in *Second Int. Symp. Metall. Slags Fluxes*. Edited by H.A. Fine and D.R. Gaskell. The Metallurgical Society of AIME, Warrendale, Pa., 1984.

[3] T. Yano, N. Kunimine, S. Shibata, and M. Yamane, "Structural investigation of sodium borate glasses and melts by Raman spectroscopy. II. Conversion between BO_4 and BO_2O^- units at high temperature," *J. Non-Cryst. Solids*, **321** [3] 147–156 (2003).

[4] A.A. Osipov and L.M. Osipova, "Raman study of binary alkali borate glasses and melts in wide temperature range;" pp. 121–142 in *Prop. Struct. Oxide Glas.* Edited by V.P. Klyuev and B.Z. Pevzner. Research Signpost, Kerala, 2010.

Chapter VII

Discussion

7.1 Background

In the previous chapters, thermal conductivity in the various borate and borosilicate system was investigated from the structural viewpoint and several variables affecting on the thermal conductivity were revealed.

During the continuous casting process, thermal conduction through mold flux is closely related to the quality of final products and operation conditions. For this reason, optimization of thermal conductivity has been importance issue for mold flux design. However, during the process, mold flux forms various phases; liquid, crystalline, and glass phases, along with different thermal conductivity. As a result, complicated thermal conductivity profile in the mold flux layer is observed depending on the position from copper mold.

Although understanding of thermal conductivity with different temperature is important, measurement of thermal conductivity of molten oxide system is challenging owing to tremendous radiation and convection effect at high temperature. Therefore, development of thermal conductivity prediction model is highly in demand. Although, few thermal conductivity models has been proposed in the molten salt and oxide system, these prediction models cannot cover various composition and temperature region. In addition, many models focused on the silicate based system. Compared to the simple silicate system, borate structure is affected by not only the short-range order structure, but also the intermediate range order structure. In addition, the structural mixture of various intermediate range order structure results in the drastic decreasing of thermal conductivity. Unfortunately, such a mixing of several intermediate range order structure is hard to be evaluated, quantitatively. For these reasons, development of the thermal conductivity model in the borate based system is challenging.

Therefore, in this chapter, thermal conductivity prediction model will be developed based on the Debye model.

7.2 Thermal Conductivity Prediction Model for Oxide System

7.2.1. Practical Importance of Development of Thermal Conductivity Prediction Model

As reviewed in *Introduction*, mold flux exists between molten steel and copper mold playing significant roles during the continuous casting process. Especially, thermal conduction property of mold flux is closely related with various defects.

Uneven heat transfer through mold flux and large shrinkage coefficient between δ and γ phases of steel cause the longitudinal crack.[1] It has been reported that the longitudinal crack can be reduced by use of mold flux having low heat transfer.[2–4] In general, crystalline phase formation in the mold flux can decrease in heat transfer by i) scattering the radiation heat transfer, and ii) formation of thick air-gap between copper mold and mold flux by transformed from glass into more dense crystalline phase. The radiative heat flux to total heat flux accounts for approximately 30 % and formation of air-gap can provide high thermal resistance.[5] For these reasons, formation of crystalline phase in mold flux layer has been paid attention for the purpose of lowering thermal conductivity.

On the other hands, sticker breakout; another significant defect occurred during the continuous casting process, can be improved by increasing of horizontal heat transfer. Higher horizontal heat flux reduces sticker breakout by forming thicker and stronger steel shell.[6] It has been reported that the high horizontal heat transfer can be achieved by the formation of thin and glass mold flux film.[5]

It can be found that the remedy for reducing longitudinal crack and sticker breakout requires opposite thermal conductivity property. Therefore, optimization of the heat transfer through mold flux is significant in order to control the operational conditions and quality of final products.

According to Mills and Fox,[5] the resistance to thermal transfer; thickness over thermal conductivity, can be expressed as the summation of each layer's resistance to thermal transfer;

$$R^*_{total} = R^*_{Cu/mold} + (d/k)_l + (d/k)_{gl} + (d/k)_{cry} \quad (7\text{-}1)$$

where, R^*_{total} is the overall thermal resistance, $R^*_{Cu/mold}$ is the interfacial resistance between copper mold and mold flux film. $(d/k)_l$, $(d/k)_{gl}$, and $(d/k)_{cry}$ represents the thickness over thermal conductivity of liquid, glass and crystalline layers, respectively. Figure 7-1 shows the typical temperature profile in the mold flux[2] along with thermal conductivity distribution of

the Na_2O-B_2O_3 system. The thermal conductivity of the Na_2O-B_2O_3 was determined based on the temperature at each position. As shown in the figure, thermal conductivity changes with varying temperature and phases within the mold flux layer.

Therefore, in order to design the mold flux system, understanding of the thermal conductivity from glass to molten state is practically importance. However, direct measurement of thermal conductivity is difficult due to the tremendous radiation and convection effect. For this reason, development of thermal conductivity prediction model is highly in demand.

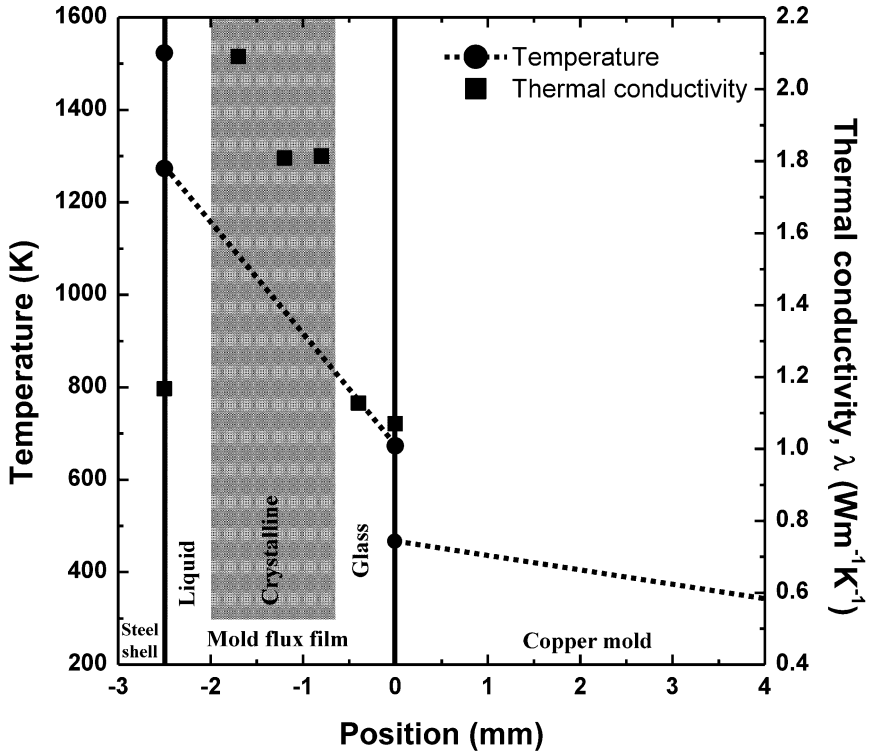

Fig. 7-1. Typical temperature profile observed between steel shell and copper mold along with thermal conductivity change in the Na_2O-B_2O_3 system with varying temperature.

7.2.2. Thermal Conduction Mechanism in the Glass and Molten Oxide System

Ziman[7] explained the transport of heat in terms of collective model instead of individual particle vibrating. Namely, thermal energy is the distribution of normal modes of vibration. Owing to the collective model, the excitations can be considered as the movement of particles in a gas resulting in a possibility of adopting kinetic theory. In the case of glass and ceramic system, since there is no regular lattice, determination of a single Brillouin zone is impossible. For this reason, not Umklapp scattering but irregular structure determines the phonon

scattering in the glass system. Kingery[8] reported that the phonon interaction by discrete lattice is equivalent to random scattering in the ceramic and glass system. For convenience, he adopted mean free concept and expressed thermal conductivity by phonon as the transport of energy by particle. As a result, thermal conductivity has been explained by the Debye model; equation (2-15), in the various glass and ceramic systems.[9–11]

However, the heat transfer mechanism in the liquid and molten oxide system is still controversial. In order to develop the thermal conductivity prediction model, the thermal conductivity mechanism should be defined, in advance. In the liquid state, Zwanzig[12] proposed the collective dynamical variables having the similar characteristic of longitudinal and transverse phonon. The frequency of the elementary excitation is defined as approximate eigenvalue by an eigenfunction of the Liouville operator. In addition, he also calculated the lifetimes of elementary excitations showing that it is determined by the elastic moduli and viscosities. As a result, in the molten oxide system which has enough viscosity coefficients, an elementary excitation has physical meaning. Recently, using the *ab initio* molecular dynamics simulations, Iwashita et al.[13] showed that the local configurational excitations in the atomic connectivity network is the elementary excitations in molten metal at high temperature.

Turnbull[14] found that thermal conduction mechanism in the molten salts system is similar to the solid state. Due to the similar ionic spacing of salt system in the solid and liquid state along with the relatively small heat fusion, he assumed that thermal motion would be similar in liquid and solid. In addition, according to his calculation, the diffusional contribution to thermal conductivity of liquids does not exceed 4 %, indicating the major role of vibrational conduction in heat transfer. Similar to molten salt system, it can be concluded that although there is no phonon in liquid state, heat is mainly transferred by vibrational excitations in the molten oxide system.

7.2.3. Previous Thermal Conductivity Prediction Model

In the glass system, several thermal conductivity model was developed based on the empirical relationship. The empirical equation considered total thermal conductivity as the summation of thermal conductivity of each components or summation of thermal conductivity factor of each components.[15–17] For instance, Primenko[17] proposed the thermal conductivity prediction model by the following equation;

$$\lambda_t = \lambda_{1,t} P_1 + \lambda_{2,t} P_2 + \cdots + \lambda_{i,t} P_i \tag{7-2}$$

where λ_t is the thermal conductivity at temperature t ($Wm^{-1}\,{}^oC^{-1}$), P_i is the wt% of i-th oxide, and $\lambda_{i,t}$ is the partial coefficient of thermal conductivity of i-th oxide in the glass at temperature t ($Wm^{-1}\,{}^oC^{-1}$). Although he provided various partial coefficients of thermal conductivity at different temperatures, their partial coefficient of thermal conductivity does not consider the any mixing effect of each component. In the previous chapters, the various structure change of boron oxide and its complicated effect on thermal conductivity has been discussed. Considering the complicated borate structure change in the oxide system, such empirical relationship does not work in the complex system.

Van der Tempel[18] proposed temperature dependence thermal conductivity prediction model for glass system as a function of density and specific heat.

$$\lambda(T) = 1.68\left(\frac{C_P(T)}{\rho(T)}\right)^{0.38} \tag{7-3}$$

From the various thermal conductivity data of commercial glass system, coefficient and exponent were determined; 1.68 and 0.38, respectively. At higher temperature, heat capacity becomes constant. In addition, phonon-phonon interaction by thermal energy would increase with higher temperature shortening phonon mean free path collisions. Therefore, although heat capacity and density can reflect the effect of network structure, Van der Tempel's equation would not be adopted at high temperature.

Recently, a thermal conductivity prediction model was suggested in the $CaO\text{-}SiO_2$ system. Inose et al.[19] proposed equation based on the relative fraction of Si-O bonding along with the ionic bonding between cation and non-bridging oxygen (NBO);

$$\lambda = \lambda_B\left(1 + \frac{f}{\frac{1-f}{3} + \frac{\lambda_B}{\lambda_N + \lambda_B}}\right) \tag{7-4}$$

where λ is the total thermal conductivity, λ_B is the thermal conductivity through bridging oxygen (BO), λ_N is the thermal conductivity through NBO, and f is the relative fraction of NBO. The thermal conductivity through the bonding between NBO and basic oxide is calculated by the following equation;

$$\lambda_N = \sum_i \frac{\sum_i n_i \lambda_i}{\sum_i n_i} \quad (7\text{-}5)$$

where λ_i is the thermal conductivity through *i*-th basic oxide(such as Na^+ or Ca^{2+}) in the oxide melts and n_i is the mole fraction of *i*-th basic oxide. However, in spite of silicate network structure change with varying temperature,[20] their experimental results are independent from temperature change.[19] In addition, above equation could not reflect the effect of heat capacity change. Considering that heat capacity change results in significant difference of thermal conductivity between glass and molten oxide system, above equation could not explain the temperature dependence of thermal conductivity. In the case of borate structure, the drastic decrease in thermal conductivity was observed resulting from the increasing of disorder by the change of intermediate range order structure. Such an effect cannot be explained by thermal conductivity through BO or NBO bond. Therefore, more fundamental thermal conductivity prediction model is needed in order to explain temperature dependence of thermal conductivity along with various structure change at the intermediate range order.

According to Bridgeman-type equation[21], thermal conductivity (λ) in the liquid can be expressed by the function of speed of sound (v) and inter-particle distance (l); similar to the kinetic theory of gases.

$$\lambda = 2\alpha v l^{-2} \quad (7\text{-}6)$$

where α is the gas constant (2.02×10^{-16}). From the above equation based on the kinetic theory of gases, several thermal conductivity prediction models were proposed. Kincaid and Erying[22] revised above equation and proposed following equation;

$$\lambda = \left(\frac{0.931}{\gamma^{1/2}}\right) 3k \left(\frac{nN_A}{V}\right)^{2/3} v \quad (7\text{-}7)$$

where λ is thermal conductivity, γ is the ratio of the heat capacity at constant pressure to that at constant volume, k is Boltzmann's constant, n is the number of ions per liquid molecule, N_A is Avogadro's number, V is the molar volume and v is the speed of sound.

In the last chapter, the validity of Debye model for entire temperature range of alkali borate system was confirmed. Not only the structure change, but also the variables of heat capacity and sound velocity would provide better prediction of thermal conductivity across the wide

temperature range; from glass to molten state. Therefore, similar to above equations for liquid system, thermal conductivity of the molten oxide system could be expressed by the kinetic theory of gases.

7.2.4. Thermal Conduction Prediction Model

Based on the Debye model, thermal conductivity for oxide system is expressed by following equation;

$$\lambda = \frac{1}{3} C v d l^{*} \tag{7-8}$$

where λ is thermal conductivity, C is specific heat capacity, v is speed of sound; especially speed of the longitudinal wave, d is density, and l^{*} is the modified phonon mean free path.

Determination of phonon mean free path is challenging. Therefore, during the calculation, phonon mean free path was assumed to be proportional to the molar volume of oxide system. According to Kang and Morita,[23] the number of thermally broken bond is inversely proportional to the phonon mean free path showing the Arrhenius type relationship. Higher temperature results in more phonons. In addition, above the Debye temperature, all vibrational frequencies are performed by the lattice waves. It was assumed that phonon-phonon interaction is proportional to the temperature difference with one-dimensional Debye temperature.

Based on the above assumption, the modified phonon mean free path is expressed by the following equation;

$$l^{*} = \left(\frac{V}{N_A} \right)^{1/3} X^{(T - \Theta_{D1})} \tag{7-9}$$

$$X = \exp\left(\frac{A}{RT} \right) \tag{7-10}$$

where V is molar volume, N_A is Avogadro's number, T is temperature, Θ_{D1} is one-dimensional Debye temperature, R is gas constant, A is adjustable parameter. The adjustable parameters (A) were determined by the thermal conductivity at 1273 K; showing 0, 4.47 and 13.43 for the Li_2O-B_2O_3, Na_2O-B_2O_3, and K_2O-B_2O_3 system, respectively. In addition, it should be noted that, at the high temperature, due to the short phonon mean free path, only

longitudinal sound velocity was considered. However, at the low temperature, not only longitudinal sound velocity (v_l), but also transverse sound velocity (v_t) should be considered. Assuming that transverse sound velocity of 1.5 km/s in the glass system, the average sound velocity (v_{av}) was calculated using the following equation.[24]

$$v_{av}^2 = \frac{1}{3}\left(v_l^2 + 2v_t^2\right) \tag{7-11}$$

The thermally broken bond term; the second-term in equation (7-9) was ignored below the melting temperature. The calculated thermal conductivity along with measured one is shown in Fig. 7-2.

The present equation can successfully explain the different temperature dependence of thermal conductivity; showing the maximum thermal conductivity point. However, the calculated thermal conductivity in the solid state shows significant discrepancy with measured thermal conductivity. It should be noted that during the calculation, heat capacity was calculated by equation (3-11). In addition, density and sound velocity were obtained from the selected references.[25–28] However, data of density and sound velocity in the glass system were limited. For this reason, sound velocity and density of the solid state were assumed to be same for all temperature range. Such an assumption would be the one of the reason causing significant error in the solid state. For the better results, more accurate data; sound velocity and density, should be needed.

Instead of the complicated assumption for phonon mean free path, the following equation would be suggested for prediction of thermal conductivity.

$$\lambda = \frac{1}{3}Cv^2\tau \tag{7-12}$$

where C is specific heat capacity, v is sound velocity, and τ is relaxation time. Considering that phonon-like vibrational excitation results from the local atomic connectivity,[13] the thermal conductivity would be closed related to the structure of molten oxide system. In addition, relaxation time is the function of viscosity and shear modulus providing the linear relationship between thermal conductivity and viscosity. Unfortunately, relaxation time for molten oxide system is hard to be obtained. More investigations; such as wave transfer in the molten oxide and bonding lifetime, should be paired with thermal conductivity study.

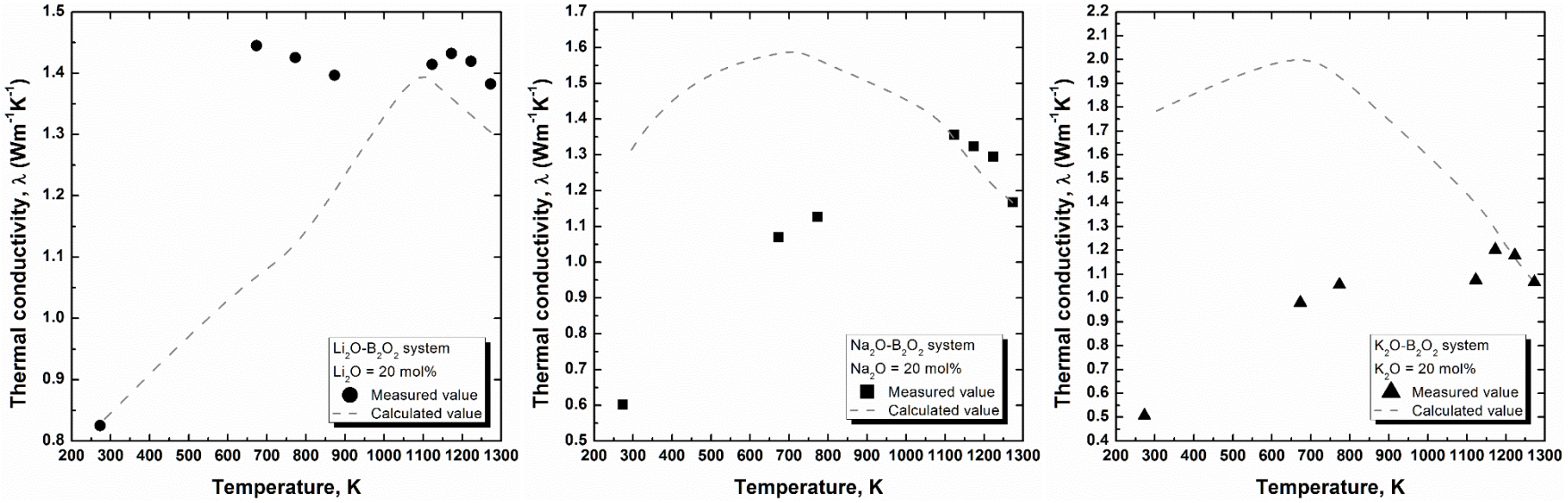

(a) **(b)** **(c)**

Fig. 7-2. Measured (black solid dot) and calculated (grey dashed line) thermal conductivity in the **(a)** Li_2O-B_2O_3, **(b)** Na_2O-B_2O_3, and **(c)** K_2O-B_2O_3 systems.

7.3 Short Summary

In this chapter, thermal conductivity prediction model was considered in the glass and molten alkali-borate system.

During the continuous casting process, understanding of thermal conductivity is practically important for the purpose of controlling products quality and operational condition. In order to reduce the longitudinal crack and sticker breakout, lower or higher thermal conductivity is required, respectively. As a result, optimization of thermal conductivity is significant. However, the mold flux layer formed between steel and copper mold accounts for various phases due to the drastic temperature change. It results in complicated thermal conductivity profile. Therefore, development of thermal conductivity prediction model is practically important.

The limitation of previously reported thermal conductivity prediction model was reviewed. Based on the findings of previous chapters, thermal conductivity prediction model was proposed; modified Debye model. The mean free path was calculated from the molar volume and modification factor was considered. The prediction model works well at high temperature region, but shows discrepancy at the glass state region. Instead of using phonon mean free path variable; which is hardly determined, Debye model including relaxation time variable would provide the better result. However, more accurate physical properties are needed for the better understanding and prediction of the thermal conductivity in the glass and molten oxide system.

References

[1] L.Y. Chen, G.H. Wen, C.L. Yang, F. Mei, C.Y. Shi, and P. Tang, "Development of low-fluoride and titanium-bearing mould fluxes for medium carbon peritectic steel slab casting," *Ironmak. Steelmak.*, **42** [2] 105–111 (2015).

[2] D. Stone and B. Thomas, "Measurement and modeling of heat transfer across interfacial mold flux layers," *Can. Metall. Q.*, **38** [5] 363–375 (1999).

[3] Y. Kobayashi, R. Maehashi, R. Endo, and M. Susa, "Effects of Valence Control of Iron Ions on Radiative Heat Transfer in Mould Flux," *ISIJ Int.*, **53** [10] 1725–1731 (2013).

[4] M. Kawamoto, Y. Tsukaguchi, N. Nishida, T. Kanazawa, and S. Hiraki, "Improvement of the Initial Stage of Solidification by Using Mild Cooling Mold Powder," *ISIJ Int.*, **37** [2] 134–139 (1997).

[5] K.C. Mills and A.B. Fox, "The Role of Mould Fluxes in Continuous Casting-So Simple Yet So Complex," *ISIJ Int.*, **43** [10] 1479–1486 (2003).

[6] K.C. Mills, A.B. Fox, R.P. Thackray, and Z. Li, "The Performance and properties of mould fluxes;" pp. 713–722 in *VII Int. Conf. Molten Slags Fluxes Salts*. The South African Institute of Mining and Metallurgy, Johannesburg, South Africa, 2004.

[7] J.M. Ziman, *Electrons and Phonons : The theory of transport phenomena in solids*. Oxford University Press, London, 1960.

[8] W.D. Kingery, *Introduction to ceramics*. John Wiley & Sons, New York, 1967.

[9] M. Tohmori, T. Sugawara, S. Yoshida, and J. Matsuoka, "Thermal conductivity of sodium borate glasses at low temperature," *Phys. Chem. Glas. Eur. J. Glas. Sci. Technol. Part B*, **50** [6] 358–360 (2009).

[10] R. Zeller and R. Pohl, "Thermal conductivity and specific heat of noncrystalline solids," *Phys. Rev. B*, **4** [6] 2029–2041 (1971).

[11] C. Kittel, "Interpretation of the thermal conductivity of glasses," *Phys. Rev.*, **75** [6] 972–974 (1949).

[12] R. Zwanzig, "Elementary Excitations in Classical Liquids," *Phys. Rev.*, **156** [1] 190–195 (1967).

[13] T. Iwashita, D.M. Nicholson, and T. Egami, "Elementary excitations and crossover phenomenon in liquids," *Phys. Rev. Lett.*, **110** [20] 205504 (2013).

[14] A.G. Turnbull, "The thermal conductivity of molten salts II. Theory and results for pure salts," *Aust. J. Appl. Sci.*, **12** 324–329 (1961).

[15] M.M. Ammar, M.M. Halawa, N.A. Ghoneim, A.F. Abbas, and H.A. El Batal, "Thermal Conductivity of Lead Borate Glasses," *J. Am. Ceram. Soc.*, **65** [10] c174–c175 (1982).

[16] M.M. Ammar, S. a. Gharib, M.M. Halawa, H. a. El-Batal, and K. El-Badry, "Thermal Conductivity of Silicate and Borate Glasses," *J. Am. Ceram. Soc.*, **66** [5] C–76–C–77 (1983).

[17] V. Primenko, "Theoretical method of determining the temperature dependence of the thermal conductivity of glasses," *Glass Ceram.*, **3** [5] 240–242 (1980).

[18] L. Van der Tempel, "Thermal conductivity of a glass: II. The empirical model," *Glass Phys. Chem.*, **28** [3] 147–152 (2002).

[19] T. Inose, J. Ojima, T. Maesono, S. Sukenaga, H. Shibata, and H. Ohta, "Relationship between Thermal Conductivities and Viscosities of CaO-SiO_2-Al_2O_3-R_2O (R=Na, K, Li) Melts;" pp. 843–845 in *6th Int. Congr. Sci. Technol. Steelmak.* Edited by X. Wang. China Machine Press, Beijing, China, 2015.

[20] T. Yano, S. Shibata, and T. Maehara, "Structural Equilibria in Silicate Glass Melts Investigated by Raman Spectroscopy," *J. Am. Ceram. Soc.*, **89** [1] 89–95 (2006).

[21] P.W. Bridgman, "The Thermal Conductivity of Liquids.," *Proc. Natl. Acad. Sci. U. S. A.*, **9** [10] 341–345 (1923).

[22] J.F. Kincaid and H. Eyring, "Free Volumes and Free Angle Ratios of Molecules in Liquids," *J. Chem. Phys.*, **6** [10] 620–629 (1938).

[23] Y. Kang and K. Morita, "Thermal conductivity of the CaO-Al_2O_3-SiO_2 system," *ISIJ Int.*, **46** [3] 420–426 (2006).

[24] M. Kishimoto, M. Maeda, K. Mori, and Y. Kawai, "Thermal conductivity and specific heat of metallurgical slags;" pp. 891–905 in *Second Int. Symp. Metall. Slags Fluxes*. Edited by H.A. Fine and D.R. Gaskell. The Metallurgical Society of AIME, Warrendale, Pa., 1984.

[25] O.V. Mazurin, M.V. Streltsina, and T.P. Shvaiko-Shvaikovskaya, *Handbook of glass data part B: Single-component and binary non-silicate oxide glasses*. Elsevier, New York, NY, 1985.

[26] M. Kawashima, Y. Matsuda, S. Aramomi, and S. Kojima, "High Temperature Brillouin Scattering of Potassium Borate Glasses," *Japanese J. Appl. Phys.*, **49** [7] 07HB02 (2010).

[27] J.O. Bockris and E. Kojonen, "The Compressibilities of Certain Molten Alkali Silicates and Borates," *J. Am. Chem. Soc.*, **82** [17] 4493–4497 (1960).

[28] K. Nagata, K. Ohira, H. Yamada, and K.S. Goto, "Velocity and absorption coefficient of ultrasonic waves in molten and glassy silicates and borates," *Metall. Trans. B*, **18** [3] 549–555 (1987).

Chapter VIII

Conclusions

In order to understand the relationship between physical properties and borate structure, thermal conductivity was studied using a transient hot-wire method along with the structural investigation by MAS-NMR and Raman spectroscopy. Addition to the experiments, thermal conductivity prediction model was considered based on the various variables.

In *Chapter 1*, the importance of B_2O_3 bearing oxide system was reviewed in terms of industrial and academic viewpoint. Owing to the increase in demand for Al_2O_3 bearing high-strength and low weight steel along with strict environmental regulation, B_2O_3 bearing mold flux system has been paid attention. In addition, due to its various applications, understanding of the physical properties of borate based glass system becomes significant. Since physical property of oxide system is closely related with its structure, the borate structure change was reviewed in the various alkali and alkali-earth bearing system. Following the literature survey of borate structure, the importance of thermal conduction property in the glassmaking and pyro-metallurgy processes was reviewed. It was found out that thermal conductivity of the molten borate system has not been fully understood in spite of the practical importance. Consequently, the aim of present study was established. In addition, various structural investigation methods were reviewed. Considering the challenging experiment conditions; effect of radiation and convection, appropriate thermal conductivity measurement method was chosen; a transient hot-wire method.

In *Chapter 2*, thermal conductivity in the pure B_2O_3 melts and molten B_2O_3-SiO_2 was investigated along with the structure studies by MAS-NMR and Raman spectroscopy. Due to the temperature dependence of B_2O_3 structure; which is denoted as *double bond-switching mechanism*, increasing of thermal conductivity was observed even at high temperature region. However, above 1400 K where such structure change terminates, decrease in thermal conductivity was observed resulting from the increase in thermally broken bond along with shortening phonon mean free path. In the B_2O_3-SiO_2 binary melt, much lower thermal conductivity than weighted average was found. By an aid of structural investigation using ^{11}B MAS-NMR, 3Q-MAS and ^{29}Si MAS-NMR, short range order borate structure was determined. Along with the Raman spectroscopy result; which provides intermediate-range order structure, the oxide structure in the B_2O_3-SiO_2 system was evaluated. Finding shows that the formation of boroxol ring cluster results in the lowering thermal conductivity due to the increasing of thermal resistance. The basic idea was obtained that not only the short-range

order borate structure but also intermediate range order borate structure can effect on thermal conductivity, significantly.

In *Chapter 3*, thermal conductivity of the various alkali-borate systems was investigated. In addition, based on the thermal conductivity in the molten Na_2O-SiO_2 system, different effect between borate and silicate structure was compared. Phonon mean free path was evaluated using Debye model. In the alkali-borate system, the linear relationship between thermal conductivity and relative fraction of 4-coordinated boron was observed at the tetraborate- and diborate-unit dominant region indicating the positive effect of three-dimensional network structure on thermal conductivity. The drastic decrease in thermal conductivity was observed below 10 mol% alkali oxide; where both tetraborate and boroxol ring structures coexist. The change of intermediate range order structure results in an increasing of disorder along with shortening phonon mean free path. However, in the Na_2O-SiO_2 system, only simple linear relationship between thermal conductivity and relative fraction of Q^4 unit was observed. It was suggested that in order to evaluate the effect of short-range order borate structure change on physical property, understanding of the intermediate range order borate structure has to be preceded. The cation effect of various alkali ion was evaluated using the ionization potential. The linear relationship between thermal conductivity and ionization potential indicates that phonon can be transferred through ionic bond between cation and non-bridging oxygen.

In *Chapter 4*, in order to compare the effect of borate and silicate structure on thermal conductivity, thermal conductivity was investigated in the sodium borosilicate ternary system. ^{11}B and ^{29}Si MAS-NMR results showed that thermal conductivity is affected by formation of the relative fraction of 4-coodinated boron and depolymerization of borate, silicate network. The Raman spectroscopy result showed that formation of 4-coordinated boron results in the increasing of tetraborate unit along with increase in thermal conductivity. The effect of K ratio (SiO_2/B_2O_3) was evaluated. The increase in thermal conductivity with higher K ratio indicates that better thermal conduction through silicate structure than borate network.

In the mold flux system, due to the high CaO concentration, almost boron oxide exists as asymmetric 3-coorindated boron. In *Chapter 5*, the effect of asymmetric borate structure on thermal conductivity was evaluated along with structural investigation using Raman spectroscopy. The experiment was carried out at high CaO/SiO_2 and low $BO_{1.5}$ concentration of 5, 15, and 25 mol%. The conflicting effect of B_2O_3 on thermal conductivity was observed depending on the CaO/SiO_2 ratio. According to the activity coefficient change of B_2O_3, it was found that B_2O_3 is incorporated into silicate network structure at the low basicity region. Lowering thermal conductivity with higher B_2O_3 concentration was observed as a result of change of the nature of network structure along with disrupting phonon transfer. On the other

hands, due to the polymerization of both borate and silicate network structure, thermal conductivity increases with higher B_2O_3 concentration at CaO/SiO_2 ratio of 1.15 and 1.38. In addition, despite of increase in asymmetric 3-coordinated boron, increasing of thermal conductivity was observed as a result of the formation of chain-type metaborate structure. From *Chapter 2* to *Chapter 5*, the variables affecting the thermal conductivity in the molten borate system were determined; relative fraction of 4-coordinated boron, intermediate range order borate structure, temperature and cation type.

In *Chapter 6*, thermal conductivity was measured in the alkali borate glass system. From the room temperature, thermal conductivity initially increases with higher temperature and reaches maximum around one-dimensional Debye temperature. After that, thermal conductivity gradually decreases as increasing of temperature. In spite of decreasing of relative fraction of 4-coordianted boron with higher temperature, increasing of thermal conductivity was observed indicating the effect of heat capacity on thermal conductivity. In addition, the same relationship between ionization potential and thermal conductivity was obtained at room temperature and 1273 K.

Finally, in *Chapter 7*, thermal conductivity prediction model for mold flux system was considered along with literature survey about thermal conduction mechanism in the molten oxide system. Based on the finding; conflicting temperature dependence of thermal conductivity along with maximum thermal conductivity at one-dimensional Debye temperature, the thermal conductivity prediction model was suggested based on the Debye model. Considering the thermal effect on the phonon mean free path, modification factor was considered based on the Arrhenius type relationship. The proposed model well worked at higher temperature region.